Titre: Title:	Experimental Study of Choking Flow of Water at Supercritical Conditions
Auteur: Author:	Altan Muftuoglu
Date:	2014
Type:	Mémoire ou thèse / Dissertation or Thesis
Référence: Citation:	Muftuoglu, A. (2014). Experimental Study of Choking Flow of Water at Supercritical Conditions [Ph.D. thesis, École Polytechnique de Montréal]. PolyPublie. https://publications.polymtl.ca/1431/

UNIVERSITÉ DE MONTRÉAL

EXPERIMENTAL STUDY OF CHOKING FLOW OF WATER AT SUPERCRITICAL CONDITIONS

ALTAN MUFTUOGLU

DÉPARTEMENT DE GÉNIE PHYSIQUE

ÉCOLE POLYTECHNIQUE DE MONTRÉAL

THÈSE PRÉSENTÉE EN VUE DE L'OBTENTION

DU DIPLÔME DE PHILOSOPHIÆ DOCTOR

(GÉNIE NUCLÉAIRE)

MAI 2014

UNIVERSITÉ DE MONTRÉAL

ÉCOLE POLYTECHNIQUE DE MONTRÉAL

Cette thèse intitulée:

EXPERIMENTAL STUDY OF CHOKING FLOW OF WATER AT SUPERCRITICAL CONDITIONS

présentée par : MUFTUOGLU Altan

en vue de l'obtention du diplôme de : Philosophiæ Doctor

a été dûment acceptée par le jury d'examen constitué de :

M. KOCLAS Jean, Ph. D., président

M. TEYSSEDOU Alberto, Ph. D., membre et directeur de recherche

M. BALAZINSKI Marek, Docteur ès sciences, membre

M. HARVEL Glenn, Ph. D., membre

DEDICATION

This thesis is dedicated to Tibet and my family

ACKNOWLEDGMENTS

It is impossible to acknowledge all the individuals who helped me during this study; the following individuals are specifically appreciated.

Foremost, I would like to express my sincere gratitude to Professor Alberto Teyssedou, my director, for his guidance throughout this project. His ceaseless energy, inventiveness and insightful criticism guided me to complete a rigorous work. Without his experience and patience, it would be impossible to complete this research program.

I would like to take this opportunity to thank Professor Altan Tapucu, for his excellent guidance and encouragement throughout my time in Ph.D. program at École Polytechnique de Montreal. I have benefited greatly from his generosity and expertise.

I also would like to thank Professor Andrei Olekhnovitch, my former co-supervisor, for his help getting me started in thermal-hydraulics laboratory.

I owe special gratitude to all the members of nuclear engineering institute, fellow graduate students and friends. The participation of Thierry Lafrance (Ing.), Stephen Schneller (Ing.), Cyril Koclas (Associate Researcher) and Jean-Claude Juneau (Technician) are greatly appreciated. Without them the realization of this research program should be impossible. The recognition and continuous support of Dr. Laurence Leung from AECL is largely appreciated.

I also would like to thank all jury members, Professor Glenn Harvel, Professor Jean Koclas, Professor Marek Balazinski and Professor Saydy Lahcen for their support and helpful suggestions.

Finally, I would like to thank my parents for providing me unconditional support. Special thanks are due to my wife for her support, patience, love and understanding throughout the several years of my doctoral work.

The work presented in this thesis was possible due to the financial support of the Gen-IV CRD research program granted by the Natural Sciences and Engineering Research Council of Canada (NSERC), National Resources Canada, Atomic Energy of Canada Limited, Hydro-Québec and Alexander Graham Bell Canada Graduate Scholarship granted by NSERC.

RÉSUMÉ

Les prochaines générations de réacteurs nucléaires vont opérer avec un fluide de refroidissement dont la pression sera près de 25 *MPa* et dont la température de sortie sera de 500°*C* à 625°*C*, selon le type de réacteur. En conséquence, l'enthalpie du flux de sortie de ces futurs réacteurs à eau supercritique, SCWR, «Supercritical Water-Cooled Reactors» sera beaucoup plus élevée que celle des réacteurs actuels. Cela permettra à l'efficacité des centrales nucléaires de passer d'environ 30-33% aujourd'hui jusqu'à 48%. Cependant, le comportement thermo-hydraulique de l'eau supercritique n'est pas encore bien compris sous de telles conditions d'écoulement, notamment en ce qui concerne par exemple les chutes de pression, la convection forcée, la détérioration du transfert de chaleur et le flux massique critique. Jusqu'à maintenant, seul un nombre très limité de recherches ont été effectuées utilisant des fluides en conditions supercritiques. De plus, ces recherches n'ont pas été effectuées dans des conditions représentatives des SCWR. Aussi, les données existantes au sujet du flux massique critique ont été recueillies lors d'expériences dont la pression de décharge était celle de l'atmosphère ambiante, et dans la plupart des cas en utilisant des fluides autres que l'eau. Il est à noter que la compréhension de l'écoulement critique des fluides supercritiques est essentielle pour effectuer les analyses de sûreté des futurs réacteurs nucléaires et pour concevoir leurs principaux composants mécaniques, par exemple, les valves de contrôle et les vannes de sûreté. Ainsi donc, une installation d'eau supercritique a été construite à l'École Polytechnique de Montréal pour effectuer des recherches sur le débit critique. Ce montage expérimental consiste en deux boucles fonctionnant en parallèle, servant à déterminer les conditions d'écoulement qui déclenchent le débit critique de l'eau supercritique. Cette installation est également en mesure d'effectuer des expériences de transfert de chaleur et de perte de pression utilisant de l'eau en conditions supercritiques.

Dans cette thèse, seront présentés les résultats obtenus grâce à cette installation avec l'utilisation d'une section d'essais munie d'un orifice de 1 *mm* de diamètre interne et de 3,17 *mm* de longueur, et dont les rebords sont acérés. Ainsi, 545 points de données de flux massique critique ont été obtenus en conditions supercritiques, pour des pressions d'écoulement allant de 22,1 *MPa* à 32,1 *MPa*, et à des températures d'écoulement allant de 50°*C* à 502°*C*, et ce pour des pressions

de décharges 0,1 *MPa* à 3,6 *MPa*. Les données obtenues sont comparées avec celles provenant de la littérature pour l'eau et même pour le dioxyde de carbone en conditions supercritiques.

Il est également très important de mentionner que les modèles actuels utilisés pour prédire les flux massiques critiques ont été développés pour des fluides en conditions sous-critiques. Même si aucun de ces modèles n'a été développé spécifiquement pour gérer l'expansion des fluides supercritiques, les prédictions des quelques-uns de ces modèles ont été comparées avec les données obtenues expérimentalement en conditions supercritiques. De plus, un simple modèle polytropique est proposé pour estimer les flux massiques critiques. Les résultats de cette comparaison aideront les concepteurs des futurs réacteurs à choisir correctement les dispositifs de sécurité nucléaire.

Dans la littérature, la différence entre la température du fluide et la valeur de la température pseudo-critique (DT_{pc}) est utilisée pour traiter les données de débit massique critique. À cette fin, il doit être mentionné qu'une nouvelle relation est proposée pour estimer les températures pseudo-critiques de l'eau et du dioxyde de carbone. En particulier, pour des températures d'écoulement moindres que leurs valeurs pseudo-critiques, les flux critiques semblent se produire dans une région très limitée. Près de la température pseudo-critique, nos expériences fournissent des données dans une région où les données des recherches antérieures ont été très rares.

En général, un excellent accord est observé avec les expériences effectuées par d'autres chercheurs, mais avec une précision supérieure. Le flux massique diminue alors que la température en amont de l'orifice augmente. En particulier, le montage expérimental permet de contrôler les paramètres d'opération avec perfection. En outre, un faible gradient de pression se produisant en amont de l'orifice est systématiquement mesuré. Il est aussi observé que près de la température pseudo-critique, le coefficient de transfert de chaleur change très rapidement, ce qui affecte la différence entre la température de la surface intérieure du tube et celle du liquide de refroidissement. Ces variations rapides associées à la variation correspondante de la densité du fluide rendent très difficile le contrôle et le maintien des conditions d'écoulement à proximité de l'état critique.

On a trouvé que le facteur dominant sur le débit massique critique est la température en amont de l'orifice. L'augmentation de cette température entraine toujours la diminution du débit massique. Pour des températures bien inférieures à la température critique (ou de la température pseudo-

critique si la pression est différente de la pression critique), le taux de cette diminution est faible. Toutefois, lorsque la température du fluide en amont se rapproche de la température critique, le taux de la diminution du débit massique augmente significativement en raison de la baisse drastique de la densité du fluide. Après avoir dépassé la température critique, la densité du fluide change lentement et donc le taux de diminution du débit massique redevient faible. Enfin, en utilisant des prédictions obtenues par les modelés HEM «Homogeneous Equilibrium Model», M-HEM «Modified-Homogeneous Equilibrium Model», par l'équation de Bernoulli, ainsi que par l'équation polytropique, les prédictions de ces modèles sont comparées avec les données expérimentales. En général, pour les écoulements dans des conditions de températures sous-critiques, on observe que l'équation de Bernoulli avec coefficient de débit de 0,7 est satisfaisante pour prédire l'évolution expérimentale. D'autre part, à des températures supercritiques et autour des températures pseudo-critiques, M-HEM est le plus approprié pour prédire les débits massiques. Cependant, l'équation de Bernoulli peut aussi être utilisée dans une certaine mesure avec un coefficient de débit de 0,4 pour les températures supercritiques et de 0,7 pour les températures sous-critiques.

Le projet présenté dans cette thèse a fait l'objet de deux présentations lors de conférences internationales, d'une séance d'affichage et d'une publication dans un journal scientifique.

- ✓ A. Muftuoglu and A. Teyssedou, Design of a supercritical choking flow facility, UNENE R&D Workshop 2011, Toronto, Ontario, Canada, 12-13 December 2011.
- ✓ A. Hidouche, A. Muftuoglu and A. Teyssedou, Comparative study of different flow models used to predict critical flow conditions of supercritical fluids, The 5th International Symposium of SCWR (ISSCWR-5), Vancouver, British Columbia, Canada, March 13-16, 2011.
- ✓ A. Muftuoglu and A. Teyssedou, Experimental study of water flow at supercritical pressures, 34th Annual Conference of Canadian Nuclear Society/ 37th Annual CNS/CNA Student Conference, Toronto, Ontario, Canada, 9-12 June 2013.
- ✓ A. Muftuoglu and A. Teyssedou, Experimental Study of Abrupt Discharge of Water at Supercritical Conditions, Experimental Thermal and Fluid Science, Volume 55, February 2014, Pages 12-20.

ABSTRACT

Future nuclear reactors will operate at a coolant pressure close to 25 *MPa* and at outlet temperatures ranging from $500^{o}C$ to 625°*C*. As a result, the outlet flow enthalpy in future Supercritical Water-Cooled Reactors (SCWR) will be much higher than those of actual ones which can increase overall nuclear plant efficiencies up to 48%. However, under such flow conditions, the thermal-hydraulic behavior of supercritical water is not fully known, e.g., pressure drop, forced convection and heat transfer deterioration, critical and blowdown flow rate, etc. Up to now, only a very limited number of studies have been performed under supercritical conditions. Moreover, these studies are conducted at conditions that are not representative of future SCWRs. In addition, existing choked flow data have been collected from experiments at atmospheric discharge pressure conditions and in most cases by using working fluids different than water which constrain researchers to analyze the data correctly. In particular, the knowledge of critical (choked) discharge of supercritical fluids is mandatory to perform nuclear reactor safety analyses and to design key mechanical components (e.g., control and safety relief valves, etc.). Hence, an experimental supercritical water facility has been built at École Polytechnique de Montréal which allows researchers to perform choking flow experiments under supercritical conditions. The facility can also be used to carry out heat transfer and pressure drop experiments under supercritical conditions. In this thesis, we present the results obtained at this facility using a test section that contains a 1 *mm* inside diameter, 3.17 *mm* long orifice plate with sharp edges. Thus, 545 choking flow of water data points are obtained under supercritical conditions for flow pressures ranging from 22.1 *MPa* to 32.1 *MPa*, flow temperatures ranging from 50°*C* to 502°*C* and for discharge pressures from 0.1 *MPa* to 3.6 *MPa*. Obtained data are compared with the data given in the literature including those collected with fluids other than water.

It is also important to mention that present models used to predict supercritical choking flows have been developed for fluids under subcritical conditions. Even though none of these models were developed to handle the expansion of supercritical fluids, we tested some of the models (Homogenous Equilibrium Model, Modified-Homogeneous Equilibrium Model and Bernoulli equation) under supercritical conditions and compared their predictions with our data and those of other researchers, available in the literature. In addition, a simple polytropic model is proposed to estimate the critical flow rate of water. It is found that the Modified Homogeneous Equilibrium

Model is the most appropriate model to estimate the discharge flow rate of water under supercritical conditions. Results of the model comparison must help SCWR designer to choose safety devices correctly.

As a common practice, the difference between the fluid temperatures with respect to the pseudo-critical value (*DTpc*) is used to treat the data. To this aim, it must be mentioned that a new relationship is proposed to estimate the pseudo-critical temperature of water and carbon dioxide. In particular, for flow temperatures lower than pseudo-critical values, choking flow seems to occur within a very limited region. Close to the pseudo-critical temperature, our experiments provide data in a region where up to now, are very scarce.

In general, an excellent agreement with experiments carried out by other researchers is obtained. It is observed that the mass flux decreases with increasing the flow temperature upstream of the orifice. In particular, the proposed experimental arrangement (i.e., use of two loops running in parallel) permitted us to determine flow conditions that trigger supercritical water choking flow. Furthermore, a small pressure gradient occurring upstream of the orifice is systematically measured. It is also observed that close to the pseudo-critical point, the heat transfer coefficient changes very rapidly which affects the difference between the inner tube surface and coolant temperatures. These fast variations combined with the corresponding change in fluid density make it very difficult to control and maintain flow conditions in the proximity of the critical point.

The research work presented in this thesis has been the subject of two presentations at international conferences, a poster session and a publication in a scientific journal.

- ✓ A. Muftuoglu and A. Teyssedou, Design of a supercritical choking flow facility, UNENE R&D Workshop 2011, Toronto, Ontario, Canada, 12-13 December 2011.
- ✓ A. Hidouche, A. Muftuoglu and A. Teyssedou, Comparative study of different flow models used to predict critical flow conditions of supercritical fluids, The 5th International Symposium of SCWR (ISSCWR-5), Vancouver, British Columbia, Canada, March 13-16, 2011.
- ✓ A. Muftuoglu and A. Teyssedou, Experimental study of water flow at supercritical pressures, 34th Annual Conference of Canadian Nuclear Society/ 37th Annual CNS/CNA Student Conference, Toronto, Ontario, Canada, 9-12 June 2013.

- ✓ A. Muftuoglu and A. Teyssedou, Experimental Study of Abrupt Discharge of Water at Supercritical Conditions, Experimental Thermal and Fluid Science, Volume 55, February 2014, Pages 12-20.

TABLE OF CONTENTS

LIST OF TABLES

LIST OF FIGURES

LIST OF SYMBOLS AND ABBREVIATIONS

Symbols

a	Wave velocity (m/s)
A	Cross sectional flow area (m^2)
C	Sound velocity (m/s)
C_d	Discharge coefficient
c_p	Specific heat at constant pressure (kJ/kg.K)
c_v	Specific heat at constant volume (kJ/kg.K)
DT_{pc}	Temperature difference between the fluid with respect to the pseudo-critical value
FTr	Flow rate transmitter (*L*/s)
g	Gravity (m/s^2)
G	Mass flux ($kg/m^2.s$)
Gr	Grashof number
h	Convective heat transfer coefficient ($W/m^2.K$)
I	Current (A)
k	Specific heat ratio, thermal conductivity (W/m.K)
L	Characteristic length (m)
$\dot{m}$	Mass flow rate (kg/s)
Ma	Mach number
Nu	Nusselt number
P	Pressure (MPa)
Pr	Prandtl number
PTr	Pressure transducer (MPa)
Q	Power (kW)

R	Electrical resistance (Ω)
Re	Reynolds number
s	Entropy (kJ/kg.K)
T	Temperature (°C)
TTr	Temperature transducer (°C)
u	Average flow velocity (m/s)
ν	Specific volume (m^3/kg)
V	Fluid velocity (m/s)
x	Thermodynamic quality
ΔG	Mass flux difference (kg/m^2.s)
Δh	Enthalpy difference (kJ/kg), elevation difference (m)
Δs	Entropy difference (kJ/kg.K)
α	Void fraction coefficient
ε	Surface roughness (μm)
γ	Isentropic expansion coefficient
ρ	Specific mass (kg/m^3), electrical resistivity (Ω·m)
ξ	Pressure drop coefficient
Ψ	Correction factor

Subscripts and superscripts

acc	acceleration
amb	ambient
o	stagnation
b	bulk fluid
c	critical

C	sonic
d	discharge
el	electrical
E	equilibrium
f	fluid
fr	friction
g	gas
grav	gravitation
in	inlet
l	liquid
n	polytropic expansion coefficient
pc	pseudo-critical
r	ratio
sur	surface
t	throat (critical plane)
tp	triple point
x	reference temperature

Abbreviations and acronyms

AECL	Atomic Energy of Canada Limited
AO	Analog Output
ASME	American Society of Mechanical Engineers
BV	Block Valve
BWR	Boiling Water Reactor
CANDU	Canada Deuterium Uranium

CHF	Critical Heat Flux
CV	Control Valve
DAS	Data Acquisition System
DC	Direct Current
EDM	Electro Discharge Method
FFPP	Fossil Fuel Power Plant
FM	Frequency Modulated
FPGA	Field-Programmable Gate Array
GIF	Generation International Forum
GFR	Gas-Cooled Fast Reactor System
HEM	Homogeneous Equilibrium Model
HP	High Pressure
ID	Inside Diameter
IEA	International Energy Agency
I/O	Input/output
LFR	Lead-Cooled Fast Reactor System
LOCA	Loss of Coolant Accident
LPF	Low Pass Filter
M-HEM	Modified Homogeneous Equilibrium Model
MSR	Molten Salt Reactor System
NI	National Instrument
NIST	National Institute of Standards and Technology
NPP	Nuclear Power Plant
NPS	National Pipe Standard

OD	Outside Diameter
PWR	Pressurized Water Reactor
RBQ	Régie du Bâtiment du Québec
R&D	Research and Development
RMS	Root Mean Square
RPM	Revolutions Per Minute
SCH	Schedule
SCR	Silicon Controlled Rectifier
SCWR	Supercritical Water-Cooled Reactor
SFR	Sodium-Cooled Fast Reactor System
SS	Stainless Steel
VHTR	Very-High-Temperature Reactor System
QA	Quality Assurance

LIST OF APPENDIXES

INTRODUCTION

For years, world energy needs are continuously increasing. Hence, the International Energy Agency (IEA) has stipulated that by the year 2040, world energy requirements will increase by 56% [1]. Therefore, to assure a worldwide good economic growth, as well as adequate social standards in a relatively short term, new energy-conversion technologies are mandatory. In that respect, nuclear industry may play an important role to overcome these requirements. In particular, like most of the developed countries, Canada has largely contributed in different research and development (R&D) programs that permitted the national nuclear industry to continue growing. To this aim, Canada has signed the Generation IV International Forum (GIF) agreement in July 2001 to develop new technologies for the future. Thus, GIF members have selected the development of six new generations of nuclear power reactors to replace present technologies such as: Gas-Cooled Fast Reactor System (GFR), Lead-Cooled Fast Reactor System (LFR), Molten Salt Reactor System (MSR), Sodium-Cooled Fast Reactor System (SFR), Supercritical Water-Cooled Reactor System (SCWR), Very-High-Temperature Reactor System (VHTR). The principal goals of these power reactors among others are economic competitiveness, sustainability, safety, reliability and resistance to proliferation. In addition to these advantages, these reactors must also permit other energy applications, such as hydrogen production, seawater desalination and petroleum extraction [2].

Within this framework, from these six different nuclear reactors that will be developed by GIF members, Canada has oriented the R&D towards the design of a Supercritical Water-Cooled Reactor (SCWR), which up to now is the only proposed water-cooled nuclear reactor design. According to preliminary design criteria of these concepts, future supercritical reactors will use water as coolant at severe operating conditions. The working pressure will be 25 MPa and reactor coolant inlet/outlet temperature will be around $280°C$ / $510°C$ – $625°C$, respectively depending on the proposed design [3]. Since the operating pressure is higher than the critical pressure of water (22.06 MPa), boiling phenomena will not occur in SCWRs and complex two-phase problems will be significantly reduced. It is very important to mention that even though there will be no boiling in SCWRs, the density, as well as other thermo-physical properties will change rapidly close to the critical temperature of water ($373.95°C$). As an example, Figure I-1 shows the change of fluid density between inlet and outlet of the reactor coolant at two different pressures

covering the critical temperature zone. This figure shows that the density between the inlet and the outlet of the reactor core will change by a factor of 11.5 times even though no subcritical type boiling flow occurs. It must be mentioned that the thermo-physical properties of water presented in this study are obtained using NIST Standard Reference Database 23 [4].

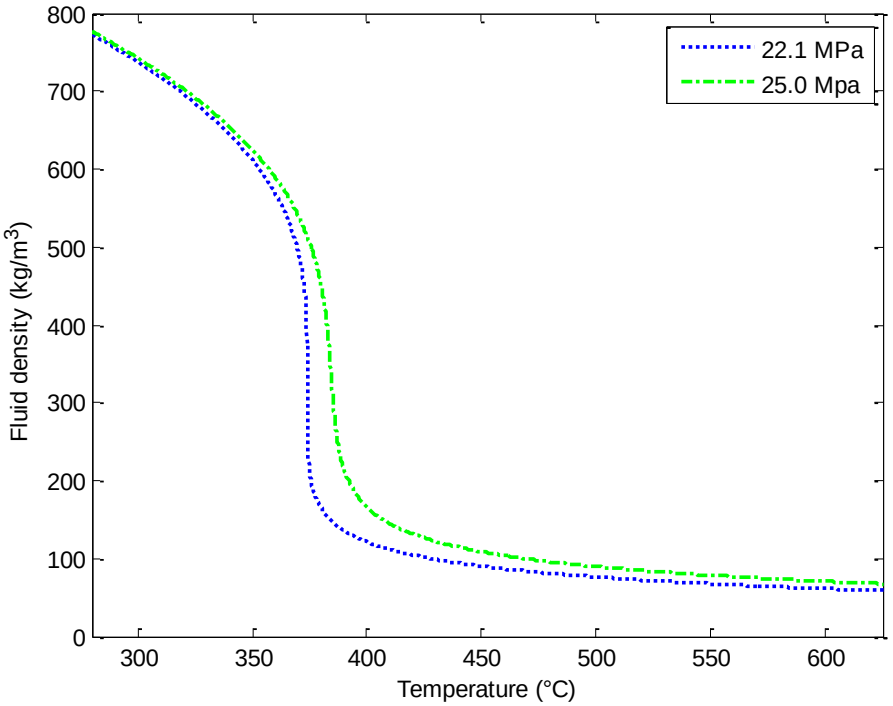

Figure I.1 Change of density as a function of temperature at critical pressure and SCWR's operating pressure.

Moreover, in future nuclear power plants, not only the chance of Critical Heat Flux (CHF) phenomena will be reduced, but also the use of single-phase flow in the reactor will eliminate several equipments, such as: pressurizers, steam generators and steam separators that are used in Pressurized Water Reactors (PWR) and Boiling Water Reactors (BWR). Also, having high outlet fluid temperatures will increase the coolant outlet enthalpy and decrease its density; therefore for a given thermal power much less coolant mass flow rate will be required. Consequently, the water inventory of SCWRs will be low and will require less pump power as compared to actual reactors which will make the reactor more compact. All these advantages, among others, will improve net thermal efficiency of the reactor up to 44-50% as compared to about 30% efficiency for existing nuclear power plants. Furthermore, compactness of the nuclear reactor including

plant simplifications will reduce the capital cost of the reactor which is very high for nuclear power plants (NPP) comparing to other types of power plants [3].

SCWRs will be built based on a similar technology used for supercritical fossil fuel power reactors (FFP), BWRs and PWRs. BWRs, PWRs and several supercritical FFPs are already in operation since 1950s [5, 6]. This valuable engineering knowledge, combined with the actual know-how of supercritical water fossil-fired power plants, could be implemented together for designing future SCWRs. Hence, SCWR appears as the foremost candidate of future nuclear power plants to be built by the year 2040. Consequently, it is expected that in the near future, SCWR technology will replace actual Generation III or advanced Canada Deuterium Uranium (CANDU) reactors. Even though Canada has more than 56 years of experience in the construction and operation of nuclear power plants, it is obvious that designing future SCWRs will be impossible without performing extensive experimental and theoretical studies of complex thermal-hydraulics processes that will occur in supercritical fluids. Although the power industry has more than 60 years of experience working with fossil-fuelled supercritical boilers, the available technical information in the open literature is still quite limited [7]. Consequently, the appropriate design and the safety analyses of SCWRs will require fundamental research to be accomplished. Recently, the European Nuclear Commission and the University of Tokyo have jointly studied the feasibility of a high performance supercritical light water reactor [8]. This study was based on several years of European experience in operating fossil-fuelled supercritical once-through boilers. From this work, some recommendations that involve fundamental research and data collection required for performing design and safety analyses of future SCWRs are:

a) To develop coupled neutronic/thermal-hydraulics calculations.

b) To develop advanced thermal-hydraulics models to handle subcritical to supercritical flow transition conditions.

c) To perform out-of-pile heat transfer and pressure drop experiments using supercritical water flows.

d) To study supercritical water choking flow phenomena in orifices and breaks.

In particular, it has been argued that the amount of data in the open literature concerning the last two subjects is very scarce [2, 3, 5, 6, 8, 9]. It must be pointed out that up to now, most studies were intended to investigate choking flow phenomenon under subcritical conditions for

applications related to PWR. In these systems, Loss of Coolant Accident (LOCA) provokes a reactor vessel depressurization that brings about a deterioration of the cooling conditions of the fuel, leading to very high fuel temperatures that compromise integrity of the reactor. Therefore, the prediction of the leaking flow rate is of prime importance to perform safety analyses. Moreover, the "critical" flow rate is limited by choking flow phenomenon which depends on the operating reactor conditions, as well as the geometry and the location of the break in the system. Even though a significant number of works were conducted using carbon dioxide and other fluids that have low values of critical pressure, many physical phenomena inherent to the thermal-hydraulic behavior of supercritical coolant, in particular for water, are not clearly known yet. For instance, under supercritical pressure and high heat flux conditions, deterioration of the heat transfer coefficient (similar to CHF) occurs [5, 10-12]. Further, for a given supercritical pressure, the speed of sound exhibits a minimum at a pseudo-critical temperature. This behavior must considerably affect choking flow conditions that can occur during a LOCA in SCWRs.

It is apparent that fundamental research in this field is essential to generate new knowledge for specified target designs of future nuclear power plants. Furthermore, supercritical water choking flow phenomenon has been identified as one of SCWR safety research activities in the Technology Roadmap for Gen-IV Nuclear Energy System. Understanding critical flow would improve the design of the reactor, while improving reactor safety, which is one of four technology goals of the Gen-IV Nuclear Energy Systems. Thus, the objectives of the present thesis consist of designing, manufacturing and studying experimentally choking flows using water at supercritical conditions. In addition, the results obtained from this research project are submitted as Canadian contribution to GIF.

This thesis is organized as follows: Chapter 1 describes the phenomenological description of choking flow and thermo-physical properties of water at supercritical conditions. Moreover, an extensive literature review is presented in this chapter. Chapter 2 presents the supercritical water flow facility built at École Polytechnique de Montréal thermal-hydraulic laboratory to perform choking flow experiments. Chapter 3 introduces the experimental procedure and the methodology applied along the present study. Chapters 4 and 5 present the results of the experiments and as well as the comparison of the results with predictions obtained with analytical models.

The contributions of this thesis are finally summarized and topics for future studies are recommended.

The part of the project presented in this thesis has been the subject of two presentations at international conferences, a poster session and a publication in a scientific journal [13-16].

- ✓ A. Muftuoglu and A. Teyssedou, Design of a supercritical choking flow facility, UNENE R&D Workshop 2011, Toronto, Ontario, Canada, 12-13 December 2011.
- ✓ A. Hidouche, A. Muftuoglu and A. Teyssedou, Comparative study of different flow models used to predict critical flow conditions of supercritical fluids, The 5th International Symposium of SCWR (ISSCWR-5), Vancouver, British Columbia, Canada, March 13-16, 2011.
- ✓ A. Muftuoglu and A. Teyssedou, Experimental study of water flow at supercritical pressures, 34th Annual Conference of Canadian Nuclear Society/ 37th Annual CNS/CNA Student Conference, Toronto, Ontario, Canada, 9-12 June 2013.
- ✓ A. Muftuoglu and A. Teyssedou, Experimental Study of Abrupt Discharge of Water at Supercritical Conditions, Experimental Thermal and Fluid Science, Volume 55, February 2014, Pages 12-20.

CHAPTER 1 LITERATURE REVIEW

In pressurized water reactors, a loss of coolant accident will provoke a reactor vessel depressurization that can bring about the core voiding. Therefore, the accurate knowledge of the coolant loss rate through an eventual pipe break is important to predict the time limit until the core will be partially uncovered. In turn, a rapid change in the system pressure can trigger a transient boiling process from partial nucleate boiling to film boiling on the heated fuel rods. It is apparent that the resulting deterioration on fuel element cooling conditions may lead to very high fuel temperatures that may compromise integrity of the reactor. Hence, the precise prediction of the coolant loss is of prime importance for carrying out nuclear reactor safety analyses as well as for choosing the reactor safety components [2, 9]. In particular, it is important to remark that the coolant leaking flow rate during a LOCA may be considerably limited by critical or choking flow conditions that depend, among others on: the operating reactor conditions just before the LOCA occurs, the geometry and the location of the break in the thermal-hydraulic system. Under choking flow, the maximum discharge flow rate is limited by the speed of sound that is determined by the flow conditions prevailing at the throat. Thus, the knowledge of the choking flow condition may help maintaining the reactor pressure during an eventual LOCA.

1.1 Phenomenological description of choking flow

When compressible fluid passes through an opening, choking flow (sometimes referred to as critical flow) phenomena happens if the fluid velocity reaches the local speed of sound in the medium. After this moment, a further decrease in the back (discharge) flow pressure doesn’t affect the mass flow rate because the disturbance in the flow at the discharge section cannot propagate to the upstream region of the opening (nozzle or pipe break) [17].

In several different applications we can encounter choking flow. For example, in a long straight pipe, friction causes pressure drop, hence, density, temperature and other parameters of the fluid change and the flow starts to accelerate. After a given point, flow velocity can reach the local speed of sound. At this location, flow cannot accelerate anymore and it becomes choked. We can see the same effect in a heated pipe where the temperature of the fluid increases while flowing inside the channel and density of the flow decreases. If enough heat is added to the fluid from the pipe, the fluid accelerates until the flow becomes choked. We can also see choking flow

conditions with two component mixtures (such as steam and air) fluid flows. We can give more examples of choking flow, but here choking flow of converging nozzles are studied since this type of situation is the closest situation to LOCA scenario which is seen in NPPs.

To better understand the choking flow phenomena, a schematic of rounded converging nozzle, commonly used to perform critical flow experiments, is given in Figure 1.1. In this figure, P_o, P_c, P_d are the stagnation pressure, critical flow pressure and discharge pressure, respectively while T_o, T_c, T_d are the stagnation temperature, critical flow temperature and discharge temperature, respectively. If there is no pressure difference along the nozzle, there will be no flow across the nozzle. This situation is given by the point 'P1' in Figure 1.2 and by line 'L1' in Figure 1.3. While keeping upstream conditions of the nozzle (P_o and T_o) always constant, if the discharge pressure P_d is decreased, the flow will start passing through the nozzle and there will be a pressure drop across the nozzle as shown in Figure 1.2 and Figure 1.3 by 'P2' and 'L2', respectively. If we continue to decrease the back pressure, more flow will pass through the nozzle (see 'P3' and 'L3') and more steep pressure profile will be obtained. Up to this moment, even though the flow rate is increased with decreasing the discharge pressure, the flow is still subsonic. Decreasing the back pressure increases the mass flow rate until the flow velocity reaches the speed of sound at the throat of the nozzle. At this condition, the mass flow rate doesn't increase with decreasing P_d and the flow becomes chocked. This situation is shown by 'P4' in Figure 1.2 and by line 'L4' in Figure 1.3. Since the speed of sound is reached in the throat, a further decrease in the back pressure cannot propagate upstream of the nozzle and the pressure in the throat stays constant at P_c as shown in Figure 1.2 and Figure 1.3. One objective of this research work consists of obtaining 'P5', 'P6', 'L5' and 'L6' experimentally; the results will be presented later.

It is important to pay attention to the terminology because the critical pressure condition of the water has a different meaning than the "critical flow pressure". In fact, the critical pressure of water is 22.06 MPa, i.e., its thermodynamic property [4, 5]. However, critical flow pressure is not a thermo-physical property, it depends on the flow conditions prevailing upstream of the nozzle. Thus, the critical flow pressure corresponds to the pressure in the nozzle where the flow velocity reaches the sonic value. Note that the same terminology applies to the critical temperature of the water which is always 373.95°C according to the NIST Standard Reference Database 23 [4, 5]

whereas the critical flow temperature is the temperature of the flow where it reaches the speed of sound in the medium.

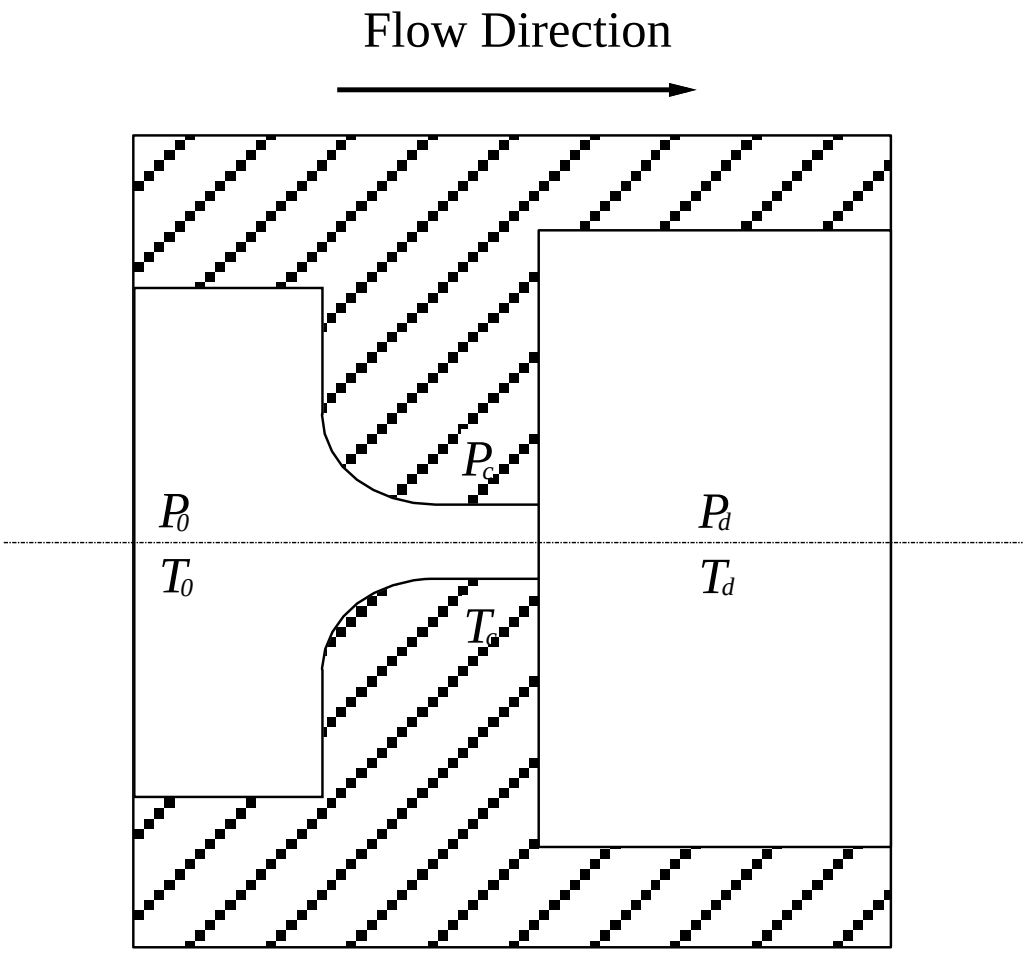

Figure 1.1 Schematic of round edged nozzle.

If we try to better understand the physics of choked flow in compressible fluids, we must look how the fluid particles communicate with each other. When the pressure is reduced at the discharge, this information is transferred to the upstream of the nozzle by waves propagating at the speed of sound. The velocity of the wave passing through the nozzle can be expressed in a very simple way as follows [18]:

$$a = C - V \tag{1.1}$$

where a is the wave velocity, C is the speed of sound and V is the fluid velocity.

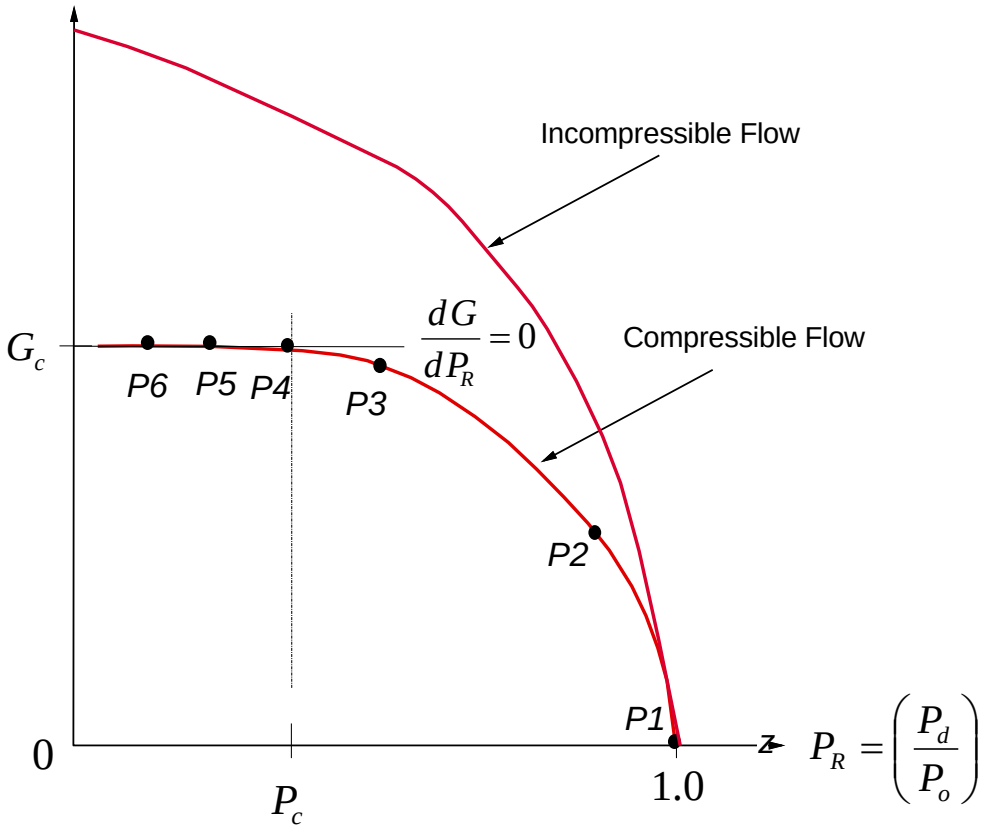

Figure 1.2 Mass flux (G) as a function of pressure ratio (P_d / P_o).

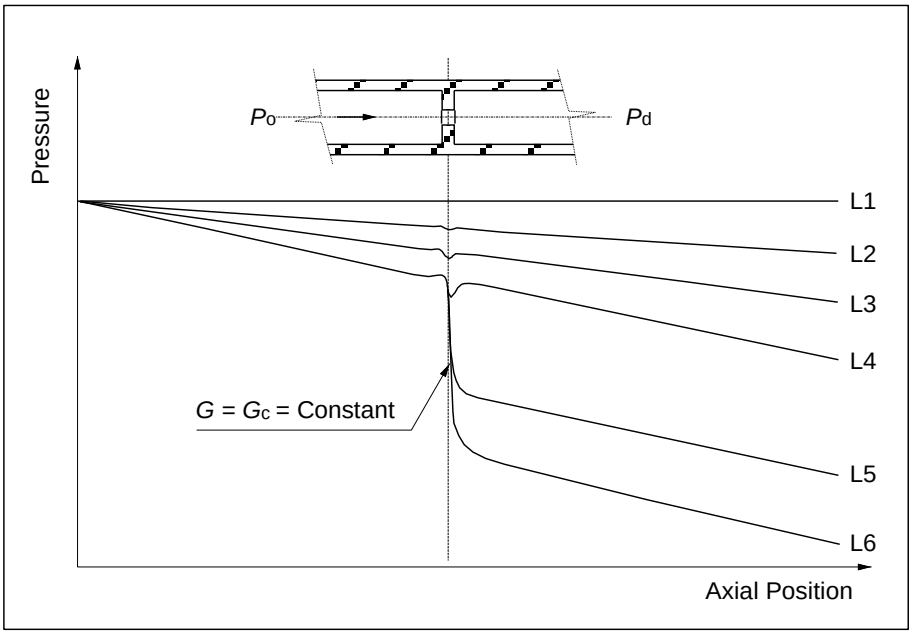

Figure 1.3 Pressure distribution in the nozzle for different back pressure values.

So, we can consider that when $P_o = P_d$, fluid particles communicate each other with the sound velocity, C, because the V is equal to zero when the fluid is at rest. Small changes in back pressure creates a flow in the nozzle and since the velocity of the fluid is still relatively small comparing to the speed of sound, this signal is transferred to upstream of the nozzle very fast. Thus, small changes in back pressure result in a huge increase on the flow rate and the flow velocity; see the slope of the line at point 'P2' in Figure 1.2. When the back pressure of the nozzle decreases, the mass flow rate continues to increase until the flow velocity reaches the speed of sound. However, if we examine Figure 1.2 closely, we see that the slope of the mass flux decreases with increasing the mass velocity. Hence, the system cannot react to the changes fast, because the transfer velocity of signal wave a decreases with increasing the flow velocity (i.e., reducing the back pressure). When flow is choked, the flow velocity, V becomes equal to the speed of sound C and absolute velocity of the wave a becomes zero. After this moment, any acoustic signal cannot propagate to the upstream of the nozzle and a further reduction on the back pressure does not affect the upstream flow conditions [18, 19]. The behaviour cannot be seen in incompressible flows, because tremendous pressure differences are necessary to reach sonic flow velocities through nozzles; therefore, one can say that in practice, choking flow phenomena do not exist in incompressible flows. As a result, decrease in back pressure always results in increase in mass flow rate as shown in Figure 1.2 [17].

1.2 The speed of sound and behaviour of ideal gas

In several engineering applications compressible fluid moves at high velocities [18] and sometimes it reaches the speed of sound in the medium. If the fluid velocity is less than sonic velocity in the medium, the flow is called sub-sonic; if the fluid velocity reaches sonic velocity in the medium then the flow is called sonic and finally, if the fluid velocity is higher than the sonic velocity in the medium, the flow is called super-sonic flow. The ratio between the fluid velocity and sonic velocity is defined as the Mach number (Ma) in the literature which is also the dimensionless quantity of compressibility of the fluid [20]:

$$Ma = \frac{V}{C} \tag{1.2}$$

where V and C are the flow velocity and speed of sound of the fluid, respectively.

Several classifications (or ranges) are given for the Mach number in the literature [18, 21-23]. In this work, since we are working with only the internal flows at nozzles, the flow will be considered sonic for $Ma = 1$ and sub-sonic for $Ma < 1$ [21].

The speed of sound can be derived from either continuity and momentum conservation or continuity and energy conservation equations. Both methods give the same result which is given by [20, 22]:

$$C = \sqrt{\frac{\delta p}{\delta \rho}} \tag{1.3}$$

where P is the flow pressure and ρ is the fluid density.

If we assume that there is no heat and energy transfer between the nozzle and the fluid (i.e., adiabatic flow) as well as no friction, the flow is considered reversible (i.e., isentropic). It is important to remember that isentropic flow is impossible since there are always frictional losses in the flow, but, for a short nozzle, this approximation gives satisfactory results for the calculation of the speed of sound. Since the flow is so fast, there is no time for the energy transfer between nozzle and the flow. In isentropic flow, entropy of the fluid does not change and the speed of sound for this case is given by [21]:

$$C = \sqrt{\left(\frac{\partial p}{\partial \rho}\right)_s} \tag{1.4}$$

where s is used to express that the partial derivation must be taken at constant entropy.

For the isentropic (frictionless adiabatic flow) expansion of an ideal gas, which means that the entropy does not change during the expansion process, the equation of state is given as:

$$p\rho^{-\gamma} = pv^{\gamma} = constant \tag{1.5}$$

where $\gamma = c_p/c_v$ is the specific heat ratio with c_p (specific heat at constant pressure) and c_v (specific heat at constant volume) values as constants, so the derivation of equation (1.5) gives:

$$\frac{dp}{d\rho} = \frac{\gamma p}{\rho} \tag{1.6}$$

By combining (1.4), (1.5) and (1.6), the speed of sound for an ideal gas can be written as [20]:

$$C = \sqrt{\gamma RT} \tag{1.7}$$

where $R = c_p - c_v$ is the gas constant and T is the absolute temperature. As we see from this equation, the speed of sound only depends on the absolute temperature of the gas. This approximation is quite true for most common gases including steam at high temperatures since γ doesn't change significantly with temperature [21]. Figure 1.4 shows the change of the speed of sound at different pressures for temperatures up to 800°*C*.

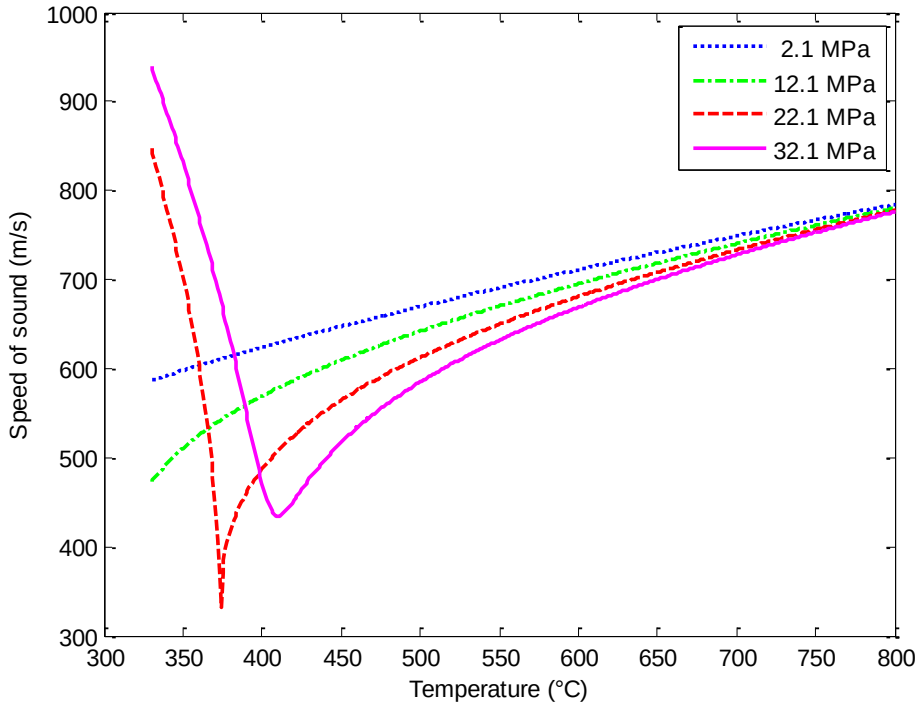

Figure 1.4 Speed of sound vs. temperature at constant pressures.

It is clearly seen that for both subcritical and supercritical pressures, the difference between the speed of sound lines decreases with increasing the fluid temperature. In this figure, even though the pressure differences between the lines are huge (10 *MPa*), the change on the speed of sound

at high temperatures increases with lower pace with pressure. Since the work presented in this thesis is related with the expansion of supercritical water, it is important to show how supercritical fluid behaves almost like an ideal gas at high temperatures. Since, in this study the supercritical water is used as a fluid, in the following section, the thermo-physical properties of the supercritical water are presented.

1.3 Thermodynamics and thermo-physical properties of supercritical fluids

A system of a pure substance may be encountered at single state phase or it may consist of one-component but two phases coexisting at the same time. If there is more than one phase, it is called two-phase system, such as; ice and water or water and steam. These phases are expressed in the thermodynamic phase diagram shown in Figure 1.5. In this diagram, all the solid lines are called phase curves. On these lines, more than one phase can co-exist. For example, on the saturation line (blue line), we may have only vapor or liquid or both of them at the same time. In particular, for the triple point all three phases co-exist.

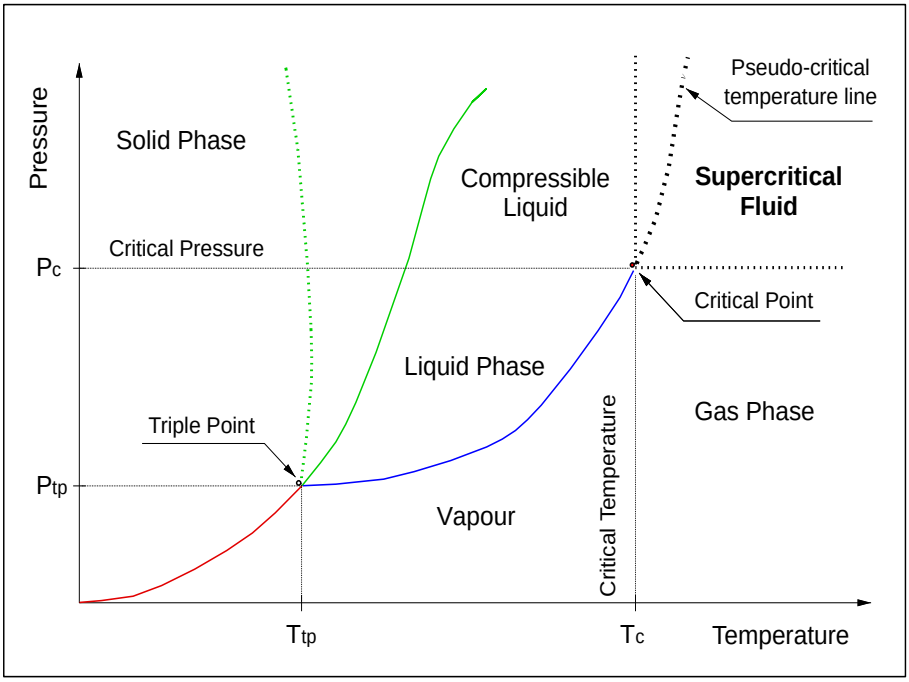

Figure 1.5 Pressure-temperature phase diagram for water.

In Figure 1.5, we will be mostly interested in the supercritical region, but other regions are also shown to complete the diagram. A supercritical fluid is defined as a thermodynamic state where the fluid pressure and temperature are higher than the critical values.

As shown in Figure 1.5, at supercritical pressures, no matter what the temperature is, there will be no gaseous phase. However, the fluid may transform to compressed liquid and finally to solid depending on how much the temperature is decreased. Critical temperature can be defined as no matter how much the fluid is compressed, there will be no liquid phase, but over critical temperature, supercritical fluid may transform into gaseous phase depending on the pressure.

As clearly seen in the figure, in supercritical region, there is no co-existence of phase separation line since there are no phase changes above these thermodynamic conditions. This can be explained by the fact that when the pressure and temperature of the system on the blue boiling curve increase, the density of the fluid decreases and the density of the gas increases. At the critical point, these two densities become equal and the phase boundary between gas and liquid disappears [24]. Instead, we can define a new term in this region. This new curve shown in Figure 1.5 with dashed lines in the supercritical region is called the 'pseudo-critical temperature line'. Pseudo-critical temperature line passes from pseudo-critical temperature points of corresponding pressure at supercritical region where the pseudo-critical temperature can be defined as the temperature that corresponds to the maximum value of the specific heat at a given pressure (i.e., at constant pressure). As shown in Figure 1.6, each supercritical pressure has its own pseudo-critical temperature. Moreover, as already mentioned, pseudo-critical temperature points altogether create a locus of pseudo-critical states as presented in Figure 1.6 (i.e., the specific heat as a function of temperature [25]). It is important to mention that while passing through this pseudo-critical line, even though there are no phase changes, other thermo-physical properties may change quite fast.

From Figure 1.7 to Figure 1.13, the change of thermo-physical properties as a function of temperature is shown for three different constant pressures. Since the change of thermo-physical properties at critical temperature is very important, the first pressure shown in these figures corresponds to the critical pressure of water (i.e, 22.1 *MPa*). Other pressure is the isobar of 25 *MPa* because most of the future nuclear reactor concepts will operate under this pressure [3, 5]. Finally, 32 *MPa* is also selected because it is the maximum operating pressure of the supercritical

loop of École Polytechnique de Montreal, described in Chapter 2. In Figure 1.7 to Figure 1.13, the vertical solid lines show the position of pseudo-critical temperature point for each corresponding pressure.

At critical pressure, the specific heat theoretically goes to infinite (Figure 1.6) and the speed of sound decreases by 3.5 times (Figure 1.7) with increasing the temperature from 300°*C* to 374°*C* (i.e., critical temperature) and then starts increasing, but much slowly.

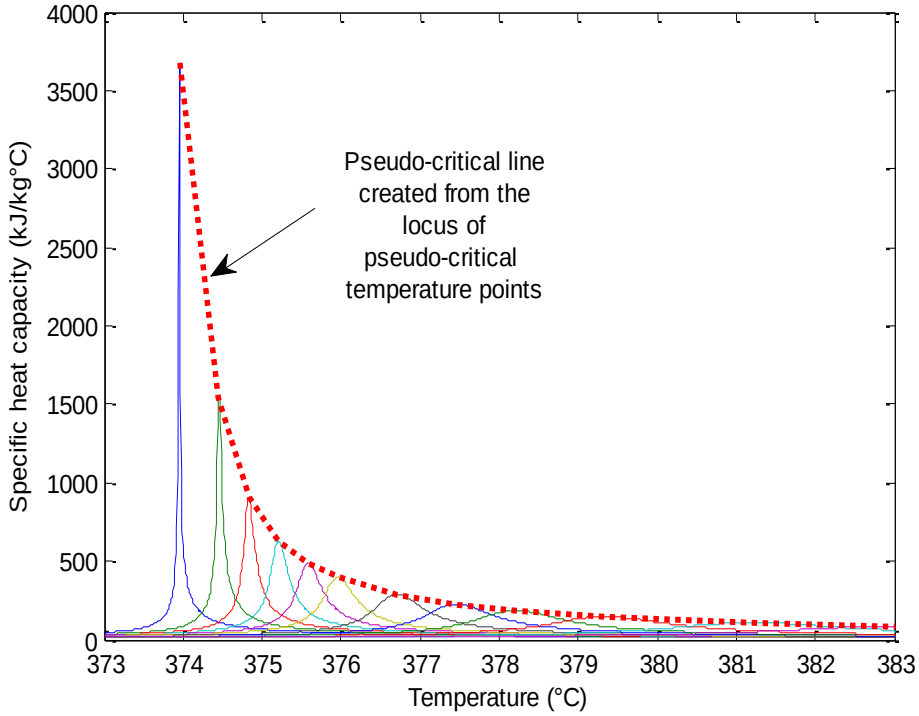

Figure 1.6 Specific heat capacity vs. fluid temperature for different constant pressures.

Within a temperature range of 300°*C* to 500°*C* the density decreases by a factor of 8 (Figure 1.8). The viscosity of the water decreases 3 times with increasing the temperature from 300°*C* to 374°*C*, then it stays almost constant (Figure 1.10). At higher pressures, these variations maintain almost the same ratios, but the slopes of the changes are much smaller.

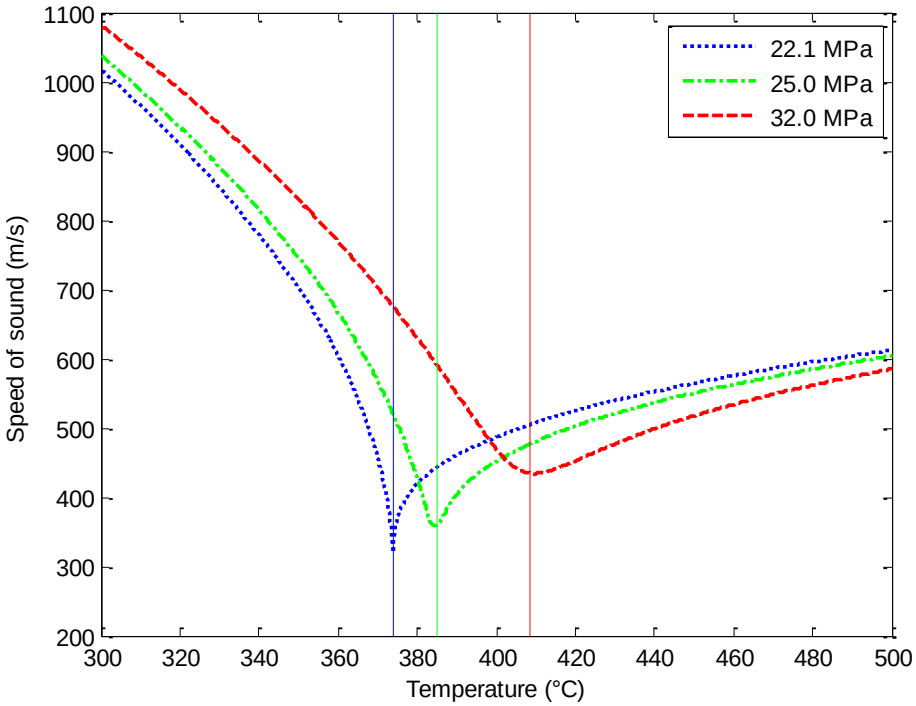

Figure 1.7 Change of speed of sound as a function of temperature.

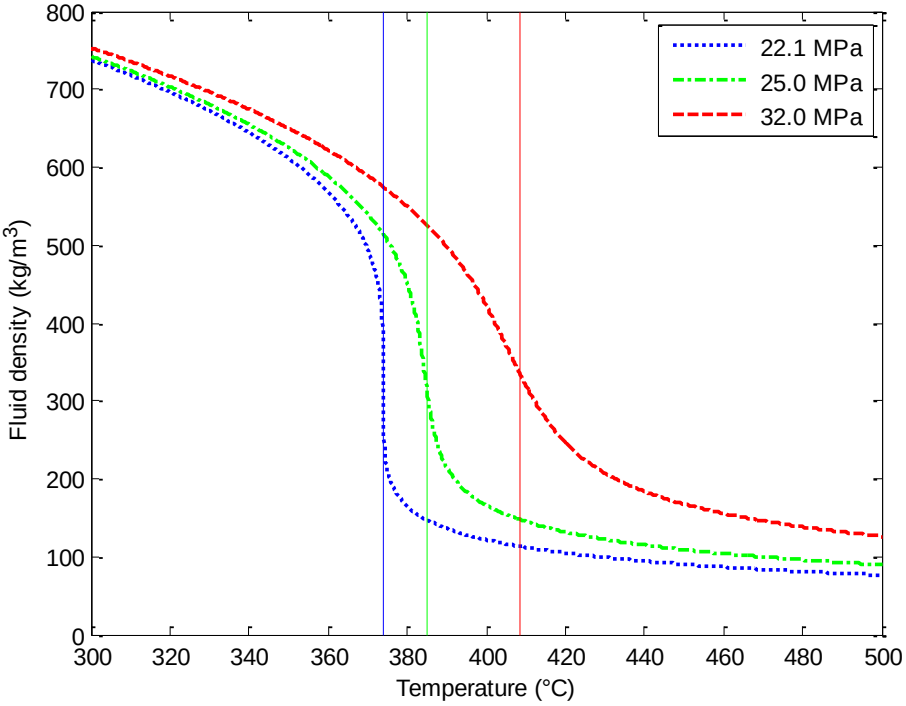

Figure 1.8 Change of density as a function of temperature.

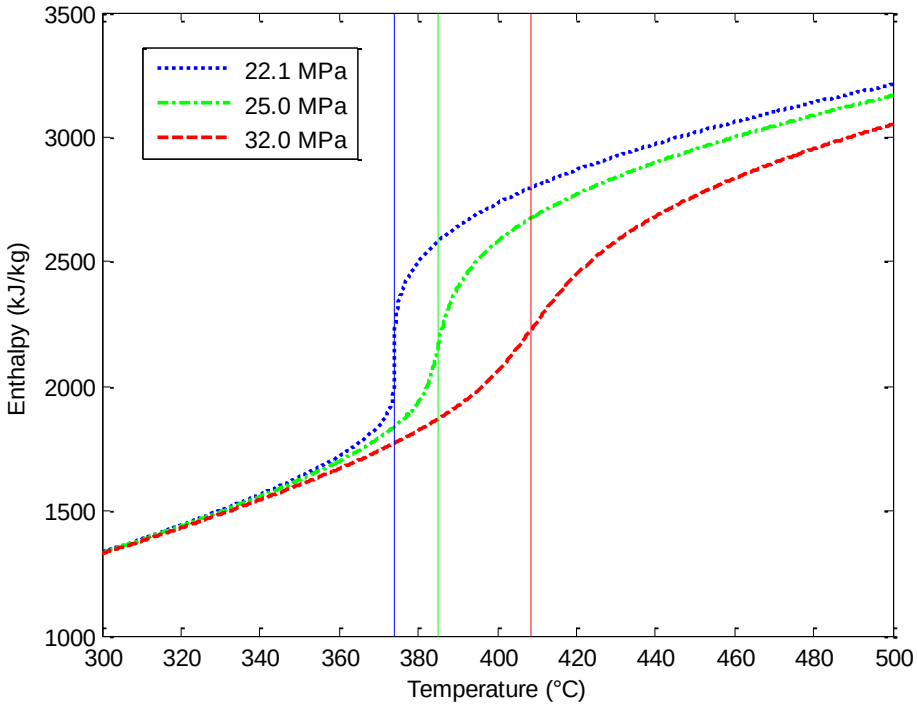

Figure 1.9 Change of enthalpy as a function of temperature.

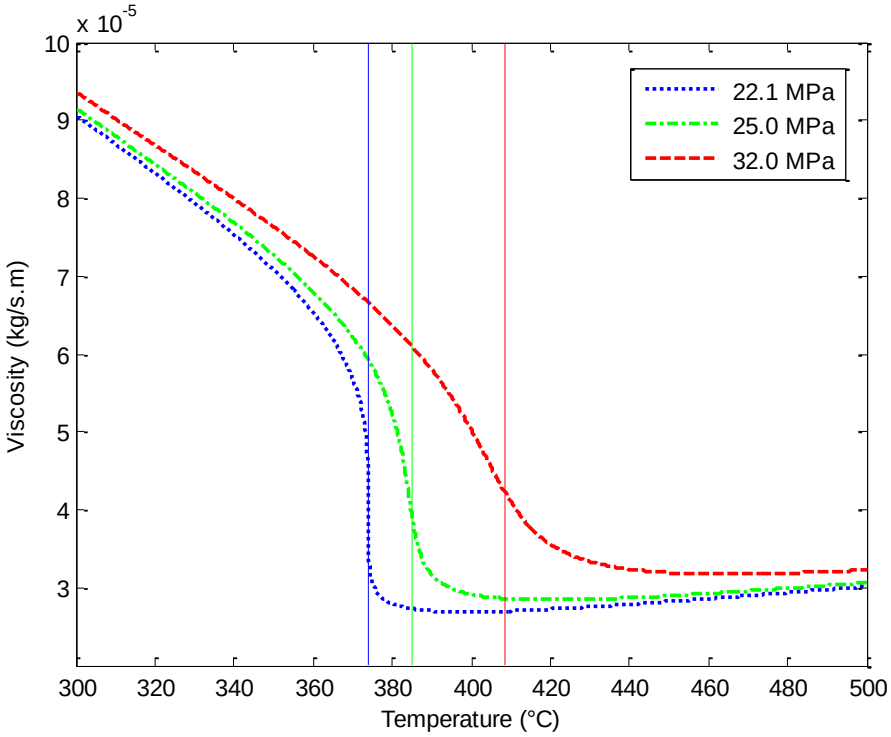

Figure 1.10 Change of viscosity as a function of temperature.

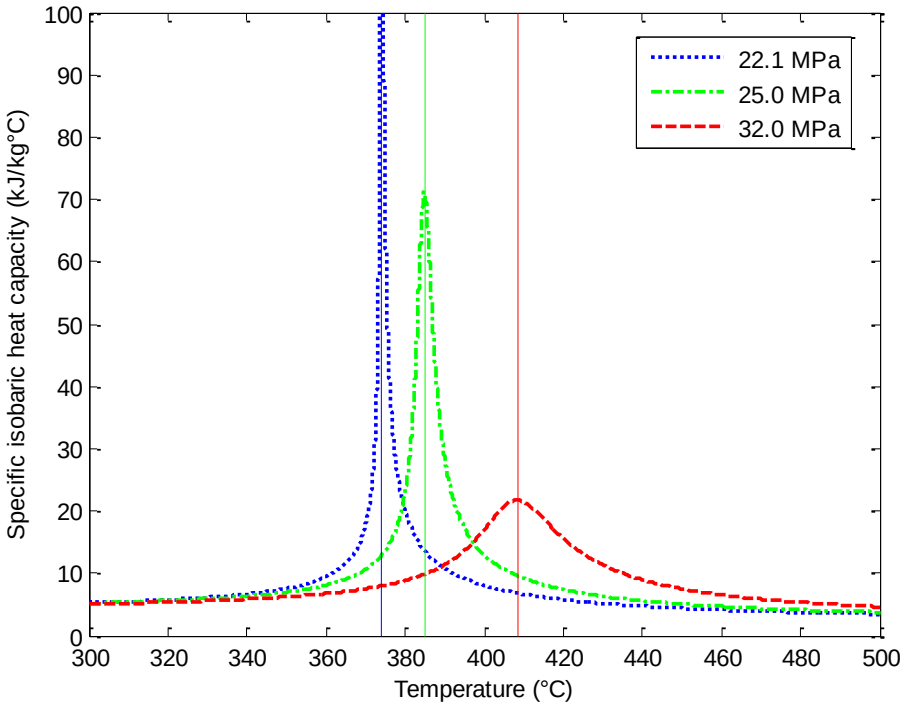

Figure 1.11 Change of specific isobaric heat capacity as a function of temperature.

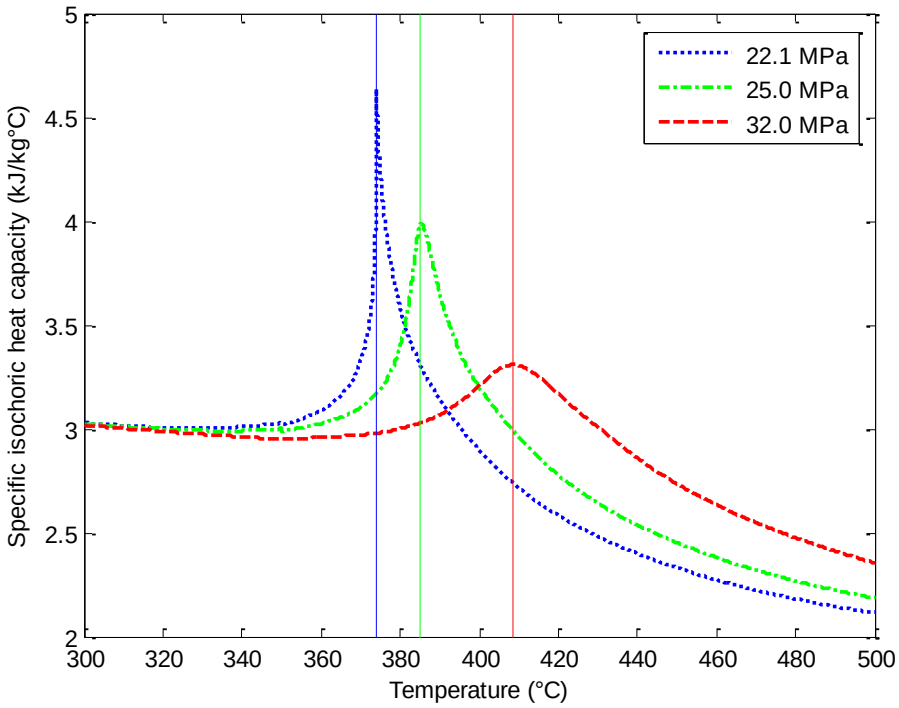

Figure 1.12 Change of specific isochoric heat capacity as a function of temperature.

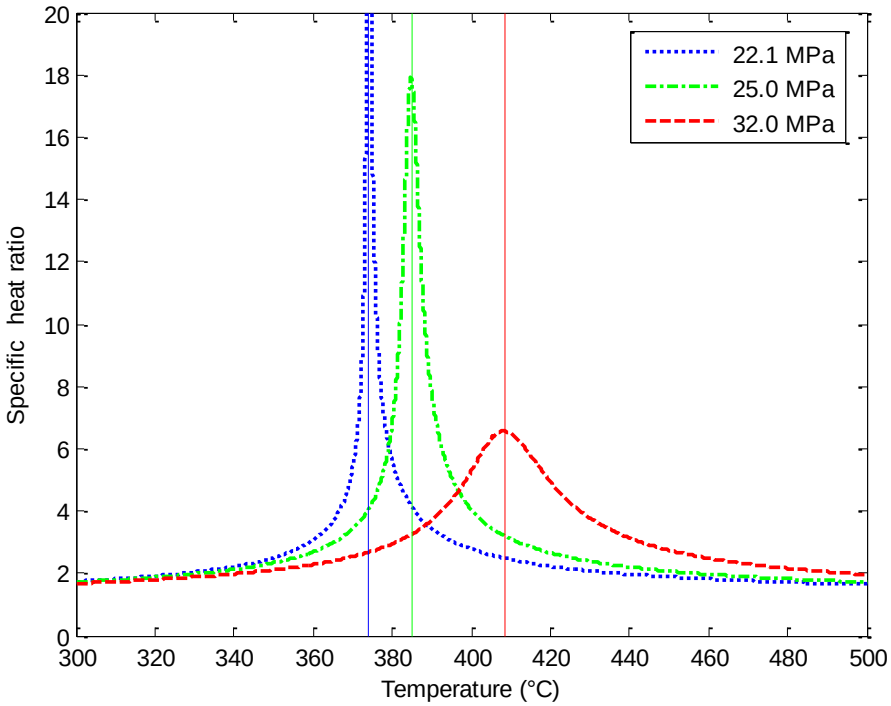

Figure 1.13 Specific heat ratio as a function of temperature.

For all thermo-physical properties, it is very important to mention that their variations close to pseudo-critical temperature are very drastic. However, for temperatures far away from the pseudo-critical value, variations in the thermo-physical properties become less significant. Also, as shown in from Figure 1.7 to Figure 1.13, when the pressure increases, the changes in the thermo-physical properties become smoother. For instance, if the pressure is increased over 50 *MPa*, the peak of the property widens a lot and it makes almost impossible to determine the exact location of pseudo-critical temperature. For some fluid properties, this peak becomes almost flat.

Since several safety calculations such as; depressurization rate, selection of safety valve, heat transfer are dependent on these thermo-physical parameters, it is very important to know the behaviour of the fluid at supercritical conditions. For example, the convection heat transfer coefficient will be highly influenced by the change of specific isobaric heat capacity. If pressure changes during a LOCA or even close to normal operation conditions, the integrity of the fuel may be affected due to a sudden increase of rod bundle surface temperatures. On the other hand,

if the critical discharge flow rate at these pressures is unknown, it will be impossible to control the cooling conditions safely during an eventual LOCA.

The critical pressure and temperature of water are very aggressive in terms of magnitude, which makes it difficult to perform experiments with water compared to the ones with other fluids. As a result, carbon dioxide, helium and freon also are widely used at supercritical conditions [5, 26]; their critical conditions are given in Table 1.1 for comparison.

Actually, it is known that supercritical fluids exist in nature since the universe was formed but scientists discovered them in the late 1800s and they have been used in industrial applications only during the last 50-60 years mostly for food extraction, dry-cleaning, cleaning, cutting of high precision materials and coal fired boilers. Recently, the nuclear industry is also aimed to use supercritical fluids to increase the efficiency of the nuclear power reactors [27, 28].

Table 1.1 Critical parameters of fluids [5].

Fluid	P_c **(*MPa*)**	T_c **(°*C*)**
Carbon dioxide	7.38	30.98
Freon-134a	4.06	101.06
Helium	0.2275	-267.95
Water	22.06	373.95

As a result, the high interest of using supercritical fluids for industrial applications, in particular by the power industry in the last few years, increased the number of the research works in this area. Within this frame work, researchers have investigated the thermo-physical properties of fluid at supercritical conditions and the existence of a pseudo-critical line. Imre et al. [29] have studied the thermo-physical properties of water at supercritical conditions for pressures up to 50 *MPa*. They determined a pseudo-critical line identified as the ‘Widom line’. Since for a given pressure the maxima or minima for every thermo-physical property do not occur at the same temperature, for each fluid there is a collection of lines. Thus, there are several Widom lines instead of a single one. This set of lines delimits a zone called the Widom region. As a result, for any thermo-physical property, there is a Widom line that connects their maximum or minimum. However, there is only one pseudo-critical line [5] that corresponds to the locus of maxima of the

isobaric heat capacity at different constant pressures. Close to critical point the Widom lines approach each other and become almost identical to the pseudo-critical one. For the operation range of SCWR (about 25 *MPa*) the difference between these two definitions can be neglected. Researchers have also separated the supercritical region into two parts called liquid-like SCW and gas-like SCW [28], because a drastic change of thermo-physical properties occur, passing through one region to another. The liquid-like region is represented by triangle limited by the pseudo-critical temperature line and the constant critical temperature line at supercritical pressures. The gas-like region is delimited by a constant pressure line at supercritical temperatures and the pseudo-critical temperature line as shown in Figure 1.14.

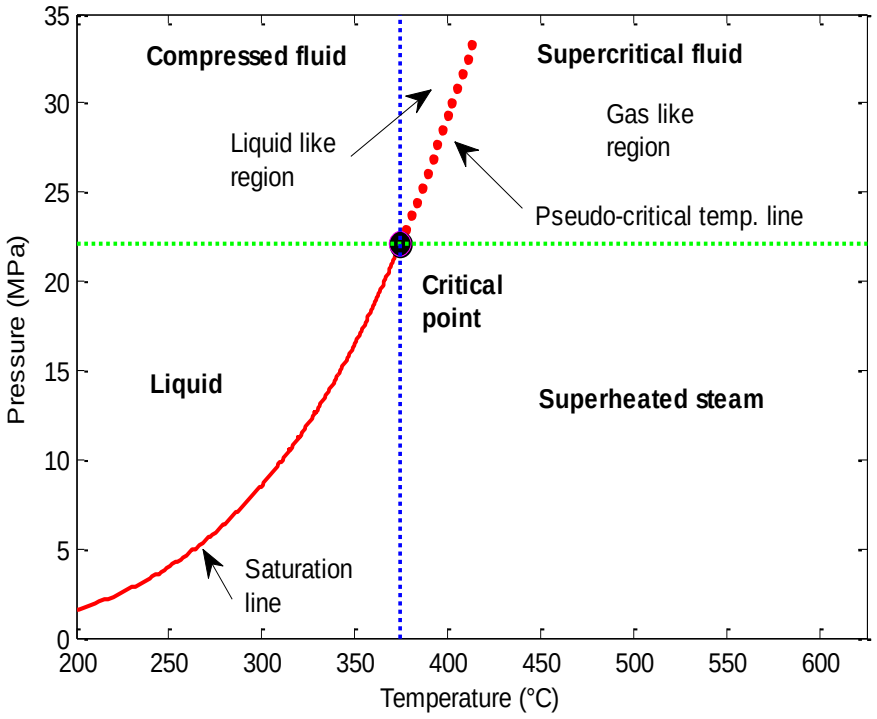

Figure 1.14 Pressure-temperature diagram for water and liquid-like and gas-like supercritical regions.

Brazhkin et al. [30-32] have also separated the supercritical region into two zones, calling them solid-like and gas-like regions or rigid and non-rigid liquids. They used shear resistance parameter to define the crossover zone and introduced the gas-like region where the shear resistance disappears for any vibrational frequencies where significant changes in thermo-physical properties occur. They call this line as ‘Frenkel line’ in honor of Frenkel’s contributions

in the area of viscoelastic theory of fluid flows [33]. The differences between the Frenkel line and Widom lines (i.e., pseudo-critical temperature line) can be explained by the fact that the Frenkel line exists even for the fluids where the pseudo-critical temperature or Widom lines practically do not exist. Brazhkin and Ryzhov [34] also found that Widom lines merge into a single line for $T < 1.1 \times T_c$ and $P < 1.5 \times P_c$.

Finally, Kurganov et al. [35] have studied the importance of the precise knowledge of the thermo-physical properties of a working fluid near the pseudo-critical region, especially in performing experiments, where small measurement errors may create huge discrepancies. For example, since the carbon dioxide may contain traces of other elements (such as water, air, oil), it is very difficult to achieve its critical conditions accurately; therefore, most data are extrapolated near critical and pseudo-critical conditions. Moreover, the existence of gas mixtures not only shifts the location of the maximum values of thermo-physical properties but also changes their values. In the case of SCWR, the nuclear reaction may generate gases (nitrogen, hydrogen) inside the working fluid (water) which can affect the physical properties enormously. Even though several fluids are currently used to perform experiments at supercritical pressures, most available data were collected using water, carbon dioxide and helium. Therefore, reliable trustworthy thermo-physical values for these fluids exist in the literature near pseudo-critical temperatures.

1.4 Pressure drop in supercritical fluids

Even though there is no phase change in supercritical fluids, drastic thermo-physical property changes will occur in future power plants. Moreover, for many years, researchers have tried to apply subcritical pressure drop correlations to estimate the pressure drop in supercritical fluids; however, because of the fast change in density and other thermo-physical properties near the pseudo-critical point, they did not obtain satisfactory results [5, 36]. Therefore, these large property variations should be considered to develop new correlations and models to estimate the pressure drop in supercritical fluids.

The knowledge of appropriate pressure drop correlations to handle supercritical conditions is essential for design engineers to choose the right size of equipment to be used in SCWRs (i.e., valves, pipes, pumps, etc.). Because of the high specific enthalpy (around 2500-3500 *kJ/kg*) of water at supercritical conditions, the coolant mass flow rate is expected to be 5-10 times less than

the actual PWRs for the same power. Accordingly, tighter fuel bundles can be used in SCWRs; in return, the pressure drop will increase. Commonly, pressure drop along a pipe is calculated as independent contributions of four terms: frictional pressure drop, acceleration pressure drop, gravitational pressure drop and irreversible pressure losses. In the open literature, most experiments are concerned with the estimation of the heat transfer coefficient in supercritical fluids, but only few works are devoted to pressure drop in tubes using coolants at supercritical conditions. In addition, pressure drop given in the literature corresponds to the total pressure drop that includes all the components. In general, the gravitational pressure drop and the acceleration pressure drop are neglected which creates huge discrepancies. However, considering that the density of fluid changes drastically, the acceleration pressure drop can play an important role in the total pressure drop. As a result, assuming only the frictional pressure drop in the calculations could be not appropriate. Even though, a complete range of flow parameters are not always given by the researchers, Pioro and Duffey [5], and Kurganov et al. [36] have summarized and categorized vertical and horizontal supercritical water and carbon dioxide flows for most available pressure drop experiments. All of these studies have been conducted between 1969 and 1986; according to Kurganov et al. [36] the quality of these data is questionable. Moreover, only one of these studies [37] was performed with fuel bundles. Also the pressure drop in rod bundles strongly depends on the geometry, spacers, end plates, cross flow area, etc. Hence, they can only be used as preliminary calculations for designing the SCWRs. In most of these studies, the frictional pressure drop coefficients found during the experiments were lower than those predicted by using subcritical pressure drop correlations such as one given by Filonenko [38], that is expressed as:

$$\xi_{fr} = \frac{1}{(1.82\ Log_{10}Re - 1.64)^2} \tag{1.8}$$

This correlation is valid for Reynolds number, $4.10^3 \leq Re \leq 10^{12}$.

It must be pointed out that recently Zoghlami [39] performed an extensive literature review about supercritical fluid pressure loss correlations. She has compared the predictions of pressure drop with the available data; thus, for SCWR she has recommended the use of Garimella's correlation. Like other researchers in the literature, she has also argued that even though some correlations to estimate the pressure drop for supercritical fluids are available for circular tubes and in particular

for fuel bundles, there is no satisfactory correlation to estimate the pressure drop in nuclear systems and complex fuel bundles [5, 36, 37, 40]. Therefore, in the near future, pressure drop has to be studied in more detail in order to provide more appropriate design tools as required by the SCWR nuclear industry.

1.5 Convective heat transfer in supercritical fluids

Even though the heat transfer is one of the most studied areas in supercritical fluids, the number of the works related to fuel bundles in the literature is very limited. Most of the studies are conducted using circular tubes [5, 40]. In this section, only some of these studies are presented to understand the problems about heat transfer in fluids at supercritical conditions. As in the case of pressure drop, due to the fast changes in the fluid properties particular attention must be given to develop correlations and models for estimating the convective heat transfer coefficient in fluids at supercritical pressures and temperatures [24].

Heat transfer in fluids at supercritical pressures is divided into the following three regimes: i) deteriorated heat transfer regime, ii) normal heat transfer regime and iii) improved (or enhanced) heat transfer regime [5, 10, 41]. Even though it is almost impossible to clearly identify distinctive limits between these heat transfer regimes, Cheng and Schulenberg [25] simply explained them using the well-known Dittus-Boelter equation, despite the fact that this correlation is more appropriate for handling internal turbulent flows in circular tubes. This relationship is given as:

$$Nu = 0.023 \times Re^{0.8} \times Pr^{1/3} \tag{1.9}$$

where *Nu* is the Nusselt number and *Pr* is the Prandtl number.

Since the thermo-physical properties change significantly with temperature, as already shown in Figure 1.7 to Figure 1.13, the heat transfer coefficient is affected enormously near pseudo-critical temperatures. Currently, the following three phenomena [40] affect the heat transfer in supercritical fluids:

- Drastic change of thermo-physical parameters of the coolant with temperature,
- Flow acceleration due to the change in the density of the coolant,

- Property differences through the cross section of the flow, especially density changes which create natural convection as a result of buoyancy forces.

Although it is known that the Dittus-Boelter equation and conventional heat transfer coefficient correlations do not give satisfactory result near pseudo-critical temperatures [42, 43], when they are used to determine heat transfer regimes at a pressure higher than the critical value, in particular it is used to determine the three heat transfer regimes. These regimes can be summarized as follows: for fluid temperatures increasing from 280°*C* (i.e., the anticipated inlet temperature of SCWR) to 360°*C* ± 5°*C* there is normal heat transfer regime, between 360°*C* ± 5°*C* and 425°*C* ± 15°*C* there is an improved heat transfer regime and for temperatures higher than 425°*C* ± 15°*C* there is deteriorated heat transfer regime. It must be pointed out that the forced convection heat transfer coefficient profile has the same trend as the specific isobaric heat capacity shown in Figure 1.11; thus, the heat transfer coefficient reaches its maximum value at the maxima of the fluid specific heat capacity [43].

1.5.1 Experimental heat transfer studies at supercritical pressures

As already mentioned in the previous sections, future nuclear reactors will operate at higher outlet coolant temperatures [3]. It is obvious that the increase in the outlet fluid temperature should affect heat transfer conditions, because the fluid properties significantly change between the inlet and outlet of the reactor core. Therefore, for the safe operation of future nuclear power reactors, one must be able to precisely calculate the convective heat transfer coefficient for each heat transfer regime for the entire range of reactor operation conditions. Since supercritical fossil fueled power plants are working at the conditions close to future SCWRs', several experimental studies were already performed during 1950s to understand the behaviour of the convective heat transfer at supercritical pressures and temperatures [25, 42-44].

Most of these experimental heat transfer studies were performed using water and carbon dioxide [10, 12, 25, 43]. It is important to mention that using water at supercritical conditions is not only costly but also a difficult task. Several precautions have to be taken since the operating conditions are extremely severe. It is not the subject of the present study to explain all of these experimental works, but some of them are focused in this chapter only for reference purposes. Several heat transfer studies based on the use of supercritical cryogen fluids such as hydrogen, helium and

Freon-12 for specific applications can also be found in the open literature. In this section, these studies are not presented since their range of application is far from the operating conditions of future nuclear power plants.

Swenson et al. [42] performed supercritical water heat transfer experiments using stainless steel (SS304) test section smooth bore tubes with 9.4 *mm* inside diameter (ID) and 1.83 *m* heated length. The test section also contained two unheated lengths, one upstream of the heated zone for the development of fluid and one downstream of the heated region for flow discharge purposes. Their experimental parameters were as follows: pressures from 22.8 *MPa* to 41.4 *MPa*, heat fluxes from 205 kW/m^2 to 1823 kW/m^2, mass velocities from 542 kg/m^2s to 2149 kg/m^2s, fluid temperatures from 75°*C* to 575°*C*. They studied the effect of each flow parameter separately to develop a correlation to estimate the convective heat transfer coefficient in upward water flows. The experiments were carried out in such a way that one parameter was varied while the others were maintained constant. They found that the heat transfer regimes in the first half (inlet zone) of the heated tube were different than in the second half (outlet zone). This effect is observed to be more dominant near or above critical temperature of the fluid. They also found that the inlet flow effect decreases the heat transfer coefficient regardless of the inlet flow temperature. Afterwards, the convective heat transfer coefficient increases up to a bit over pseudo-critical temperatures of fluid and then the heat transfer coefficient starts decreasing. Swenson et al. found that the convective heat transfer decreases with increasing the fluid pressure. Furthermore, they have also observed that near pseudo-critical temperatures the maximum heat transfer decreases with increasing heat flux. It is observed that this observation should serve engineers to perform better equipment design depending on required pressures and heat fluxes.

Yamagata et al. [43] studied experimentally the heat transfer of supercritical water in horizontal and vertical tubes for both upward and downward flows. The following flow conditions were applied during the experiments: pressures ranging from 22.6 *MPa* to 29.4 *MPa*, fluid temperatures from 230°*C* to 540°*C*, heat fluxes from 116 kW/m^2 to 930 kW/m^2 and mass velocities from 310 kg/m^2s to 1830 kg/m^2s. They used 7.5 *mm* and 10 *mm* ID test sections (SS316) with 1500 *mm* and 2000 *mm* heated lengths. Similar to Swenson et al. [42], they also found that near the pseudo-critical region, the heat transfer coefficient reaches a maximum value and then starts decreasing for both horizontal and vertical flows. The increase in the heat transfer coefficient occurs very rapidly with the fluid temperature approaching the pseudo-critical value

as well as with the tube wall temperatures higher than pseudo-critical ones. Moreover, this effect is more dominant for low heat fluxes and at flow pressures close to the critical value. The maximum value of the convective heat transfer coefficient decreases with increasing the applied heat flux and/or the flow pressure. These results are coherent with those discussed in Section 1.3. Yamagata et al. [43] have also observed that the increase in heat flux triggers a deteriorated heat transfer regime close to the pseudo-critical regions. According to the literature this observation is not well understood; therefore, it should be studied more in detail for designing future SCWRs. At low heat flux conditions, no differences in the heat transfer between horizontal and vertical flows are observed. In turn, at high heat fluxes, the heat transfer coefficient loses its uniform shape and decreases in the upper section of the heated tube. However, it is much higher in the bottom section of horizontal tubes; for the vertical flows the value of the heat transfer coefficient are between these two limits. For reference purposes, they found the maximum heat transfer coefficient to be about 80 $kW/m^2°C$ at a pressure of 24.5 *MPa*, for a mass velocity of 1830 kg/m^2s and heat flux less than 233 kW/m^2.

Vikrev and Lokshin [45] studied convective heat transfer using 6 *mm* ID steam-generating horizontal tubes at supercritical flow pressures. Their working parameters were: pressures ranging from 22.6 *MPa* to 29.4 *MPa*, heat fluxes from 349 kW/m^2 to 699 kW/m^2 and mass velocities from 400 kg/m^2s to 1000 kg/m^2s. They observed that similar heat transfer deteriorations occur in steam generation tubes as those observed in boiling water plants. They explained this deterioration by the fact that at supercritical pressures the fluid does not have an isothermal temperature profile in the cross section of the tube. Thus, the fluid close to wall surface reaches the maximum heat capacity before the rest of the fluid and as a result, the heat transfer rate decreases towards the center. During their experiments, the heat transfer deterioration starts just before the average bulk fluid temperature reaches the pseudo-critical temperature, which occurs a couple of degrees Celsius earlier than that reported by other studies. They have also observed that the maximum heat transfer coefficient decreases with increasing the pressure. This behaviour is coherent with similar works found in the literature. For the flow working range, they observed deterioration on the heat transfer coefficient for all the experiments. However, the upper region of the vertical test section indicates slightly higher heat transfer coefficients than the lower zone; which is due to the buoyancy effect. Even though the authors did not provide enough

information, they proposed a new correlation to predict convection heat transfer which is not based on Dittus-Boelter equation.

Adebiyi and Hall [46] performed experiments at subcritical and supercritical pressures with carbon dioxide in 22.14 *mm* ID horizontal tube having 2.44 *m* heated length. They applied uniform heat flux at a pressure of 7.586 *MPa*. The ranges of the experimental parameters were: inlet temperatures from 10°*C* to 31°*C*, mass flow rates from 0.035 *kg/s* to 0.15 *kg/s* and heat fluxes from 5 kW/m^2 to 40 kW/m^2. The fluid temperature was increased just up to the pseudo-critical value; therefore, the experimental range was very limited. Both axial and angular temperature distributions were determined using several thermocouples installed on the external wall of the tube. To obtain angular temperature profile information, at each axial location four thermocouples were placed 90° apart. The authors found that temperature at the bottom of the tube was lower than the upper part. Consequently, these results show that the heat transfer at the bottom seems to be enhanced by a buoyancy effect. Obviously, the opposite behaviour occurs at the upper part of the tube (i.e., buoyancy tends to reduce convective heat transfer). Same observations were also reported by Vikrev and Lokshin [45].

To better understand the effect of buoyancy on heat transfer in supercritical water flows, Bazargan et al. [47] have studied experimentally its effect in horizontal round tubes. Their experiments cover the following flow conditions: pressures were varied from 23 *MPa* to 27 *MPa*, mass fluxes from 330 kg/m^2s to 1230 kg/m^2s for a single uniform heat flux of 310 kW/m^2. They found that for some experimental ranges, buoyancy effect is so important that non-uniform flow distribution exists in the cross section of the tube. Nevertheless, Petukhov et al. [48] have established a criterion to be used for determining when the buoyancy effect should be considered in horizontal heated tubes. Hence, they have proposed a correlation that later was extensively validated among others by Bazargan et al. [47].

Litch et al. [49] performed supercritical water heat transfer experiments in annular channels having circular and square geometries. They kept the outlet pressure constant at 25 *MPa* while the mass velocity was changed from 350 kg/m^2s to up to 1425 kg/m^2s for heat flux varying from 250 kW/m^2 to 1.0 MW/m^2 and inlet fluid temperatures from 300°*C* to 400°*C*. For low flow mass velocities, the heat fluxes were changed from 125 kW/m^2 to up to 650 kW/m^2. Even though they had 3.3 *m* total heated length, only 76 *cm* in the center portion of the heater rod was used as a test

section. They equally located 16 thermocouples on the inner cladding of the central heated length. Six supports were used to keep the heater centered while enough distance was maintained between them and the wall to avoid any perturbation on the flow structure. An E-type thermocouple was used for measuring the inlet flow temperature and type-K thermocouples were used for measuring the inner cladding temperatures. The maximum allowable temperature measurement was limited to 600°*C*. Even though the researchers found that the Dittus-Boelter correlation is able to produce good heat transfer predictions, (79% of the values were within 25% accuracy) their results have shown that this correlation is not able to predict correctly the heat transfer close to pseudo-critical temperatures. They compared also other Nusselt based correlations such as those proposed by Jackson [50], Watts [51] and Krasnoshchekov [52]. They achieved 25% of accuracy for 86% of the data with the Jackson's correlation which is much lower than what was found by Jackson himself. The discrepancies between the estimations obtained with Jackson's correlation and the work of Litch et al. may be related to the coaxial geometry of the test section (e.g., Jackson used a circular tubular geometry). Moreover, according to Litch et al. [49] the correlations proposed by Watts and Krasnoshchekov were not able to predict Litch et al.'s results satisfactorily. In general, these two correlations were not able to provide good predictions of the convective heat transfer coefficient for supercritical fluids.

Litch et al. [53] have also investigated integral heat transfer measurements only for upward flow in a square annular channel (i.e., they modified the test section as required). These modifications permitted them to have an optical view to the heater rod as well as the flow cross sectional area. During these experiments the applied heat fluxes were varied to up to 440 kW/m^2, the inlet flow temperature was changed from 175°*C* to 400°*C* and the mass velocity was changed from 300 kg/m^2s to 1000 kg/m^2s. All experiments were carried out at a constant outlet pressure of 25 *MPa*. Their previous research [49] has shown that the variations in supercritical fluid properties affect the heat transfer conditions. In fact, the radial density gradient induces buoyancy effects while the axial density differences create fluid acceleration effects. These two mechanisms tend to reduce the heat transfer due to important changes that they provoke in the wall shear stress and consequently in the flow velocity profile. From this point of view, Litch et al. [53] have found that at low mass velocities, mixed heat transfer conditions occur. This phenomenon is due to buoyancy effects, however most Nusselt based correlations are not able to foresee huge wall temperature changes. At high mass velocities (i.e., the buoyancy criterion is

given by $Gr_b/Re_b^{2.7}<10^{-5}$ where subscript *b* denotes thermo-physical properties evaluated at the bulk fluid temperature and *Gr* stands for Grashof number) forced convection heat transfer dominates; therefore, Nusselt based correlation can better predict the measured wall temperatures. They have also observed that the heat transfer coefficient increases near the pseudo-critical temperature conditions and the amount of this increase depends on the applied heat flux.

Recently, Yang et al. [54] studied heat transfer of supercritical water flowing in vertical channels having spacers for both upward and downward flows. They covered the following flow conditions: flow pressures ranging from 23 *MPa* to 25 *MPa*, mass fluxes of 700 kg/m^2s and 1000 kg/m^2s and uniform heat fluxes from 200 kW/m^2 to 1000 kW/m^2. They observed that spacers improve the heat transfer in both upward and downward flows. Moreover, for some cases (especially at low heat flux conditions) spacers diminished the buoyancy effect. They also observed that the increase in the heat flux decreases convective heat transfer, as was shown in the literature by other researchers. In turn, they found that near the pseudo-critical point, the convective heat transfer is considerably enhanced. The heat transfer in downward flows was generally higher than that obtained for upward flows but the difference was reduced at low heat fluxes. This can be explained by the buoyancy effect which becomes more important at high heat fluxes for upward flows. They also compared four different correlations to estimate the convective heat transfer where Swenson's [42] correlation was the closest one to predict their experimental data.

Up to now, we have focused on the literature review of experimental heat transfer studies performed using mostly circular channels. This is due to the lack of experimental studies based on the use of full scale heated rod bundles. There are only two heat transfer studies in the literature that used supercritical water in simplified rod bundles [37, 55]. Xi'an Jiaotong University has a research program to study heat transfer in 4-rod bundle test section using water at supercritical pressures, but no data has been published yet. In Canada, the University of Ottawa jointly with Atomic Energy of Canada Limited (AECL) is building a carbon dioxide heat transfer loop to perform heat transfer experiments in rod bundles [56].

Dyadyakin and Popov [37] performed supercritical water experiments using 7-element helically finned rod bundles with different cross section flow areas and hydraulic diameters; six rods were

in the corners of hexagon and the seventh one in the center of the flow channel. The ranges of experimental flow conditions covered bulk fluid temperatures from 90°*C* to 540°*C*, mass velocities from 500 kg/m^2s to 4000 kg/m^2s, pressure at 24.5 *MPa* and heat flux less than 4.7 MW/m^2. During the experiments, at high heat fluxes, they observed huge pressure oscillations (5 *MPa*) for mass fluxes over 2000 kg/m^2s.

Silin et al. [55] studied also heat transfer in supercritical water using large bundles at the Russian Scientific Center Kurchatov Institute. Their experimental flow parameter were: flow pressures of 23.5 *MPa* and 29.4 *MPa*, mass velocities from 350 kg/m^2s to 5000 kg/m^2s, bulk water enthalpies from 1.0 *MJ/kg* to 3.0 *MJ/kg* and heat fluxes from 0.18 MW/m^2 to 4.5 MW/m^2. The most important outcome of this study concerns the fact that they were not able to observe heat transfer deterioration in multi rod bundles, while heat transfer deterioration is usually observed in circular tubes for the same range of flow parameters. However, this does not mean that deteriorated heat transfer regimes do not exist in rod bundles. In fact, Richards et al. [57] have studied data for a 7-element rod bundle cooled with supercritical Freon-12 where they have observed the occurrence of deteriorated heat transfer regimes.

Recently Pioro and Duffey [5, 10, 12] presented an excellent literature survey of experimental heat transfer under supercritical conditions both for water and carbon dioxide. Unfortunately, not all data sets given in this reference are available; they are either lost or inaccessible. Groeneveld et al. [56] have created a data set of experimental studies of supercritical water heat transfer. As it is already mentioned, most of these studies are related to circular geometries not for fuel bundles. Hence, while using these data sets, one must be very conservative since in fuel bundles the actual heat transfer coefficients may substantially change.

1.5.2 Empirical convective heat transfer studies at supercritical flow pressures

Almost all heat transfer correlations given in the literature have been derived based on experimental data obtained from circular tubes. In general, they are modified forms of the Dittus-Boelter equation where correction factors are added to include fluid property changes by using appropriate dimensionless number. Most of these studies are categorized as a function of working fluids, geometries, flow direction and a convenient reference temperature (i.e., bulk fluid

temperature, wall temperature or pseudo-critical temperature) [5, 10, 12, 25, 42, 43, 58]. Most of these correlations can be given under the following version of the modified form of the Dittus-Boelter relationship:

$$Nu = \frac{h.d}{k} = a.(Re_x)^b (Pr_x)^c.\ \Psi \tag{1.10}$$

where *x* corresponds to the reference temperature, the coefficient *a* and the exponents *b* and *c* are adjusted to fit the predictions with experimental data. The function Ψ is used as a correction factor that takes into account the important changes of fluid's thermo-physical properties at supercritical conditions.

Swenson et al. [42] have performed studies to find the empirical convective heat transfer coefficient at supercritical conditions where fluid thermo-physical properties change drastically. They observed that the best fit is achieved when a ratio of specific volumes at bulk temperature and inner wall surface temperature is taken into account. It is important to mention that, in 1965, when Swenson et al. conducted their experiments, only water properties were measured precisely at supercritical conditions. They used 2657 data points collected from the second half of a complex test section [42]. These experimental data were used to obtain appropriate values of the fluid required by the Dittus-Boelter equation (*a*, *b*, *c* and Ψ) at the inner wall temperatures. Later, the authors included the effect of viscosity and thermal conductivity into dimensionless number; thus, they were able to fit 94.9% of the data within ±15% error. Afterwards, they added 294 data points obtained at a flow pressure of 41.4 *MPa*. This experimental information permitted them to improve the previous correlation (i.e., the error band was reduced to 11.8%.)

Swenson et al. [42] have also compared the prediction of their correlation with similar ones obtained with the standard Dittus-Boelter correlation for inside wall surface temperatures lower than 371°*C*. At these conditions, Dittus-Boelter correlation gives relatively acceptable results since the thermo-physical properties do not change too fast. Nevertheless, Swenson et al. [42] have also found that their correlation behaved better. However, the Dittus-Boelter correlation can be considerably improved if the exponent of Reynolds number is increased from 0.80 to 0.89 as has also been suggested by McAdams [59]. Moreover, Swenson et al. [42] applied their correlation to predict some of the carbon dioxide data where they obtained a maximum deviation of ±20 %.

Bishop et al. [44] have also studied convective heat transfer at supercritical conditions. They have developed a correlation based on the modified Dittus-Boelter equation. The methodology used and the form of the correlations proposed were very similar to those used by Swenson's et al. [42].

In 1971, Yamagata et al. [43] collected supercritical water upward flow data using a 10 *mm* ID tubular test section. For a wide range of flow conditions, they correlated the data with the Dittus-Boelter relation. It must be mentioned that this work has not included data obtained at high heat fluxes. In fact, under such conditions the thermo-physical properties of the water close to the heated wall change quite abruptly which triggers a deteriorated convective heat transfer regime. It is apparent that original form of the Dittus-Boelter correlation is not able to handle fluid property changes at the neighbourhoods of the heated wall. Therefore, Yamagata et al. included these thermo-physical property variations into the Prandtl number. The modified correlation was able to predict the data within an error band of ±20%.

Yang and Khartabil [60] proposed a convective heat transfer correlation valid for both carbon dioxide and water flow at supercritical pressures. Their correlation was based on the previous relation proposed by Petukhov et al. [52] used to predict convection heat transfer in supercritical carbon dioxide flows. They compared the new correlation with carbon dioxide upward flow data collected using an 8 *mm* ID tube at supercritical pressures given in Pioro and Khartabil [61]. The convection heat transfer was divided into two different regimes; i.e., normal and deteriorated heat transfer regions. Later on, the same correlation was applied to estimate the convection heat transfer in supercritical water flows. For the normal heat transfer region, 1416 data points obtained by Yamagata et al. [43] and for the deteriorated heat transfer region 1172 data points obtained by Shitsman [62] were used. The results of this study have shown that the correlation is able to predict the data with an average error of -0.17% and an RMS of ±11.7% for the normal heat transfer conditions, and an average error of -0.53% and an RMS of ±6.65% for the deteriorated heat transfer conditions. Yang and Khartabil [60] have also shown that close to the pseudo-critical temperature and at low heat fluxes, the heat transfer coefficient reaches a maximum value and it decreases with increasing heat flux.

Petukhov and Polyakov [63], and Petukhov et. al. [64], Yamagata [43], Grabezhnaya and Kirillov [40, 65] have also experimentally studied the location of the deteriorated heat transfer regimes in

upward and horizontal flows. The objectives of these studies were to understand the reason of the heat transfer deterioration and its boundaries. The deterioration was then explained as follows: when the fluid temperature close to the heated wall approaches to the critical value, the local coolant density decreases very fast, even though the bulk fluid density is still high. Therefore, on the heated surface a gas-like phase develops while in the center of the channel the coolant has fluid-like behaviour. In such a case, close to the wall, a deterioration in turbulent convective heat transfer occurs which consequently decreases the heat transfer coefficient. This phenomenon is sometimes called as "pseudo-boiling" process. The boundaries where convective heat transfer becomes deteriorated are also estimated with correlations for different types of fluids.

Recently, the research group of Professor Pioro were involved in finding the best heat transfer correlation that fits water and carbon dioxide data [66, 67]. As a result of these works, Mokry et al. [67] have developed an empirical convective heat transfer correlation based on the data obtained with 10 *mm* ID and 4 *m* long vertical bare tube for upward supercritical water flows. They have studied only normal convective heat transfer and improved convective heat transfer regimes. The data at deteriorated heat transfer regime conditions as well as those associated to the entrance of the tube were not taken into account for developing their model. They have also verified the performance of some existing models (Dittus-Boelter, Bishop, etc.) and none of them were able to produce satisfactory results, especially near the pseudo-critical region. Their proposed model provides the best fit for the data that were used for the correlation and has ±25% uncertainty to calculate convective heat transfer coefficient. Since the correlation was developed for circular tube data, one must be very attentive and conservative while using it to estimate convective heat transfer rate in rod bundles. Moreover, Zoghlami [39] performed an extensive literature review on convective heat transfer coefficient of water at supercritical pressures and compared the predictions of these correlations with experimental data. She also found that the Mokry et al. [67] correlation has the minimum standard deviation.

Gupta et al. [66] have used experimental data set of 4600 points obtained at Chalk River Laboratories in 8 *mm* ID, 2.208 *m* long Inconel-600 tubular vertical test section to develop convective heat transfer correlations for carbon dioxide. They tested existing heat transfer correlations that were developed for supercritical water, but the results were not satisfactory due to the fast change of the thermo-physical properties. Consequently, three different correlations to estimate the convection heat transfer coefficient for carbon dioxide were proposed by Gupta et al.

which are based on the previous work of Mokry et al. [68]. Gupta et al. have also observed three convective heat transfer regimes as given by other researchers (i.e., deteriorated, normal and enhanced heat transfer regimes). However, they removed deteriorated heat transfer points from the data set and correlated the new equation only for the other two heat transfer regimes. Actually, the three proposed correlations have similar structures except for the reference temperature used to calculate the thermo-physical properties of carbon dioxide. The first two correlations use the wall surface temperature [42] and the bulk fluid temperature values [43] as reference temperatures which are already used by others in the open literature. The third correlation uses the average value of these two temperatures. They have concluded that taking the wall temperature as a reference provides the best results; it allows the convective heat transfer coefficient to be estimated within an error band of ±30%.

Up to now, only one correlation exists in the open literature to estimate the convective heat transfer coefficient for water in rod bundles. Dyadyakin and Popov [37] have developed a heat transfer correlation for 7-element helically finned rod bundle based on their experimental results. Nevertheless, the convective heat transfer coefficient is very sensitive to flow geometry (type of fuel bundles, rod diameter, etc.); therefore, this correlation cannot be extended to other types of fuel bundles. However, since it is the only known correlation for rod bundles, it may be a good start point to develop new ones for more specific nuclear fuels.

Other than empirical correlations, Loewenberg et al. [69] created a convective heat transfer look-up table for fully upward developed supercritical flows in tubes. They used experimental data collected from 12 different studies. Loewenberg et al., however, have applied the buoyancy effect criterion proposed by Jackson [70] to remove data points that correspond to the deteriorated convection heat transfer regime. Thus, their look-up table contains a total of 7120 data points. Since all the experimental data were obtained using only vertical tubes, they proposed a look-up table that has five dimensional parameters. Ranges of these parameters were given as mass fluxes from 700 kg/m^2s to 3500 kg/m^2s, heat fluxes from 300 kW/m^2 to 1600 kW/m^2 and pressures from 22.5 *MPa* to 25 *MPa.* The look-up table is useful for tube IDs of 8 *mm* to up to 20 *mm* and bulk fluid enthalpies from 1200 *kJ/kg* to 2700 *kJ/kg*. Loewenberg et al. have also compared their results with the predictions obtained by using different correlations. Thus, they were able to show that the look-up table is able to predict inner wall temperatures with an average error of -1.7% and a standard deviation of ±10.2%.

The open literature also contains information about convective heat transfer correlations for fluids other than carbon dioxide and water. For example, Locke and Landrum [71] made a detailed literature survey of heat transfer correlations for hydrogen at supercritical conditions; they have also studied their range of applicability. They have tested some other relationships that were developed for other fluids, but couldn't obtain good predictions for supercritical hydrogen flows. The uncertainty analysis has shown that the uncertainty on the values of the thermo-physical properties affects the heat transfer predictions; however, these effects are not necessarily the main contributors to the total error.

Finally, it is observed that the convective heat transfer coefficient is strongly dependent on the physical properties of the fluid under supercritical conditions. Close to the pseudo-critical temperatures it increases and reaches a maximum at the pseudo-critical value and then, it decreases with increasing the fluid temperature. This effect is more dominant at pressures close to critical pressures and less dominant at high heat fluxes. Similar observations for carbon dioxide flows have been reported by Petukhov et al. [52].

It is important to mention that the literature review presented in Sections 1.4 and 1.5 permitted us to select the most appropriate supercritical water correlations. These relationships are then used to design some key components of the loop as well as to simulate flow conditions required to determine the loop safety operational limits. More information about these items is given in the next Chapter.

1.6 Studies on choked (critical) flows

Choking flow corresponds to the maximum flow rate that can pass through a restriction, i.e., orifices, nozzles, etc., for a given stagnation condition. Single and two-phase (one component) critical flow are important for performing safety analysis of nuclear power plants as well as for many other industrial applications such as; boilers, turbines, heat pipes and refrigerators. From a nuclear safety view point, LOCA or any accidental condition that can bring about the depressurization from supercritical flow conditions in future SCWRs can consequently compromise the reactors integrity; therefore, it is important to know leakage flow rate at supercritical conditions and thus, adapt the response time of safety equipment during such a

transient. At the moment, the estimation of this critical flow rate is calculated using empirical models which take fluid pressure, temperature and phase velocity changes into consideration.

Even though choking flow of gases at subcritical conditions is a very well-known phenomenon, the critical discharge of two-phase flows and in particular supercritical flows are not well understood, yet. Up to now, several studies at subcritical conditions were conducted using especially carbon dioxide and water; nevertheless, only few choking flow studies were performed using fluids at supercritical conditions. Moreover, in most supercritical fluid cases, data were collected under conditions that are not representative of future SCWR (i.e., at low fluid temperatures or with fluids other than water). In addition, present models used to predict supercritical choking flows have been developed for fluids under subcritical conditions. None of these models were developed to handle the expansion of supercritical fluids. Due to the complexity of the flow phenomena, even under subcritical flow conditions, the models are able to predict the experimental trends only for limited cases [72]. Most of these models can be classified under the following three categories: homogeneous equilibrium, slip flow and disequilibrium. In some of them a thermal disequilibrium is empirically introduced. The Homogeneous Equilibrium Model (HEM) assumes that during the flow expansion, the supercritical fluid enters into the liquid-vapor mixture zone with the two-phases coexisting as a homogeneous pseudo-fluid [73]. Furthermore, it is assumed that along the expansion a strong coupling between the phases exists; thus, mechanical and thermal dissipation between the phases are neglected (i.e., the phases are considered both in mechanical and thermal equilibrium). In addition, the expansion is assumed to be isentropic starting from the initial supercritical thermodynamic state up to the end of the process (i.e., low pressure reservoir). However, this sounds as a contradiction from thermodynamics point of view.

In some models a thermal disequilibrium is more or less empirically introduced. If a total thermal disequilibrium is taken into account, then the Homogeneous Frozen Model is obtained [74]. Instead, if only a fraction of thermal disequilibrium is introduced, a well-known Henry-Fauske model is obtained [75]. In general, non-homogeneous models, where thermal disequilibrium is considered, have been developed based on the homogeneous one [72, 74, 76-78]. A non-homogenous disequilibrium formulation was proposed and applied by Trapp & Ransom [79] to simulate the discharge of two-phase flows.

The literature review presented in this section will be based not only on experimental studies but also on different modeling approaches to estimate the choking flow rate at subcritical and supercritical conditions [13, 26, 72-75, 79-113]. Moreover, some of these modeling approaches are going to be briefly presented. Furthermore, it is important to mention that none of these models have been completely validated for fluids under supercritical conditions.

1.6.1 Choking flow models

In this section, four choking flow models are briefly presented and some of them are compared in Chapter 5 with our own data. The first model is the well-known Henry-Fauske equation widely used to predict critical discharges in boiling water nuclear power reactors. The second one is the HEM which is developed by assuming an expansion of homogeneous two-phase flow mixtures. It must be pointed out that this model has also been applied to simulate the critical discharge of supercritical fluids [96-98]. The third approach that is also commonly used for treating supercritical fluids is the Bernoulli's equation [97]. Finally, we have proposed a simple analytical polytropic equation that will be also discussed in this section [13].

a) The Henry-Fauske model

The thermal non-equilibrium model developed by Henry and Fauske [75] assumes that the entropy does not change while the steam phase behaves as an ideal gas during the expansion process. This hypothesis was used to develop a model for predicting choking mass fluxes. Using this assumption, for isentropic flow conditions (i.e., ideal adiabatic, frictionless flows), the critical mass flux at the throat is written as:

$$G_c^2 = \left[\frac{x_o v_g}{n P} + \left(v_g - v_{lo}\right) \left\{ \frac{\left(1-x_o\right)N}{s_{gE} - s_{lE}} \cdot \frac{ds_{lE}}{dP} - \frac{x_o c_{pg}\left(1/n - 1/\gamma\right)}{P\left(s_{go} - s_{lo}\right)} \right\} \right]_{throat}^{-1} \tag{1.11}$$

where η is the pressure ratio calculated by:

$$\eta = \frac{P_t}{P_0} = \left[\frac{\frac{1-\alpha_0}{\alpha_0}(1-\eta) + \frac{\gamma}{\gamma-1}}{\frac{1}{2\beta\alpha_t^2} + \frac{\gamma}{\gamma-1}} \right]^{\frac{\gamma}{\gamma-1}} \tag{1.12}$$

and

$$\beta = \left[\frac{1}{n} + \left(1 - \frac{v_{lo}}{v_g}\right) \left[\frac{(1-x_o)NP}{x_o(s_{gE} - s_{lE})} \cdot \frac{ds_{lE}}{dP} \right] - \frac{c_{pg}(1/n - 1/\gamma)}{(s_{go} - s_{lo})} \right]_{throat} \tag{1.13}$$

In these equations c_{pg} corresponds to the specific heat of the gas phase at constant pressure, P is the flow pressure, s is the specific entropy, v is the specific volume, x is the thermodynamic quality, n is the thermal equilibrium polytropic coefficient, α_0 and α_t are the stagnation and throat averaged void fractions, respectively, and γ is the isentropic expansion coefficient for the steam. The subscripts *E*, *g*, *l*, and *o* represent equilibrium, vapor, liquid and stagnation flow conditions, respectively. The variable *N* in this equation is used to account for partial phase change occurring in the throat. Henry and Fauske have correlated the value of *N* as a function of a throat equilibrium quality [114]. This model as well a similar one proposed by Moody [78] are largely used by the nuclear industry to perform nuclear power reactor safety analyses, but their applicability to supercritical fluid is not necessarily a straightforward task.

b) The Homogeneous Equilibrium Model (HEM)

The HEM is also a frequently used model to calculate choking flow rates, especially for liquid-vapour mixtures [96-98]. In this model, it is assumed that the two phases are strongly coupled thermally and mechanically; thus, velocities, temperatures and pressures acting on the phases are equal [73]. Therefore, it must be pointed out that this model has been developed to treat the critical discharge of two-phase flow mixtures by assuming that there is no slip between the phases and that both heat and mass transfer between them are negligible. Hence, the critical mass flux given by this model is expressed as:

$$G_c = \frac{\left[2\left(h_o - (1-x_E)h_{lE} - x_E h_{gE}\right)\right]^{1/2}}{(1-x_E)v_{lE} + x_E v_{gE}} \tag{1.14}$$

where h_o is the stagnation specific enthalpy, x_E is the thermodynamics equilibrium quality, g and l represents vapor and liquid conditions at the plane where choking flow occurs, respectively. According to the open literature, this model provides better results for high stagnation pressures and qualities (i.e., when the two-phase flow condition approaches saturation vapour conditions). Moreover, it is observed that increasing the residence time of the fluid in the channel (i.e., higher length to diameter ratios) increases the accuracy of the HEM, which is coherent with the assumption of thermal equilibrium [88].

c) The Bernoulli model

The critical flow rate of frictionless, single-phase flows can be estimated by using Bernoulli's equation which is written as [97]:

$$G_c = C_d \sqrt{2\rho\left(P_o - P_d\right)} \tag{1.15}$$

where P_d is the discharge pressure, C_d is the discharge coefficient, ρ is the fluid density determined at stagnation conditions (P_o, T_o) and P_o is the stagnation pressure prevailing in the reservoir before the expansion. Even though this formulation is straightforward (i.e., conversion of potential into kinetic energy), it is included in this document to compare its predictions with supercritical water choking flow data. Furthermore, this equation is largely used by the nuclear industry by optimizing discharge coefficient C_d .

d) A Proposed polytropic expansion approach

Within the framework of this research, we have developed a simple polytrophic equation [13] to estimate choking flow rates. Assuming that the supercritical fluid behaves like a gas inside an ideal nozzle, we can write the following polytropic expansion equation [22];

$$Pv^n = \text{constant} \tag{1.16}$$

where *P* is the pressure, *v* is the specific volume, *n* is a polytropic expansion coefficient.

Differentiating this equation and rearranging the terms result in:

$$Pnv^{n-1}\left(\frac{dv}{dP}\right) = -v^n \tag{1.17}$$

From this equation, we can write:

$$\left(\frac{dv}{dP}\right) = -\frac{v}{nP} \tag{1.18}$$

For a two-phase mixture flow, the momentum conservation equation under steady state conditions can be written as:

$$\frac{d}{dz}\left(\frac{\dot{m}_g^2}{\rho_g A_g} + \frac{\dot{m}_l^2}{\rho_l A_l}\right) = -A\frac{dP}{dz} - f_{fr} \tag{1.19}$$

where the mass flow rates for the gas and the liquid are given, respectively by:

$$\dot{m}_g = \rho_g u_g A_g \qquad \text{and} \qquad \dot{m}_l = \rho_l u_l A_l \tag{1.20}$$

and the flow quality can be expressed as:

$$x = \frac{\dot{m}_g}{\dot{m}_g + \dot{m}_l} = \frac{\rho_g u_g A_g}{\rho_g u_g A_g + \rho_l u_l A_l} \tag{1.21}$$

In these equations, ρ_g, ρ_l are the specific masses and u_g, u_l are the average flow velocities for the gas and the liquid, respectively. A_g and A_l represent the cross-sectional flow area occupied by the gas and the liquid, respectively.

Assuming a single phase flow (i.e., gas), the flow quality should be equal to 1 (x=1). Then we can write $\rho_g = \rho, u_g = u$, $u_l = 0$ and $A_g = A$. Using these new definitions, the mass flow rate in equation (1.20) can be rewritten as:

$$\dot{m} = \rho A u \tag{1.22}$$

This mass flow rate is then used in the axial momentum conservation equation, equation (1.19), neglecting the effect of the frictional forces; thus it yields:

$$\frac{d}{dz}(\rho A u^2) = -A\frac{dP}{dz} \tag{1.23}$$

Since mass is conserved along the process, this equation can be rewritten as:

$$\dot{m}d(u) = -AdP \tag{1.24}$$

Introducing the mass flux, $G = \dot{m}/A$, we obtain :

$$G = -\frac{dP}{du} \tag{1.25}$$

As already explained in Section 1.1, when choking flow conditions are achieved, the following condition must be satisfied:

$$\frac{dG}{dP} = 0 = \frac{d(\rho u)}{dP} \tag{1.26}$$

Expanding this derivative yields:

$$\frac{dG}{dp} = \rho\frac{du}{dP} + u\frac{d\rho}{dP} = 0 \tag{1.27}$$

Using the definition of the mass flux and rearranging terms allow us to write:

$$Gu = \rho\left(\frac{dP}{d\rho}\right) \tag{1.28}$$

Multiplying both sides of this equation by the density yields:

$$G^2 = \rho^2 \left(\frac{dP}{d\rho} \right) \tag{1.29}$$

where this equation can be rewritten as:

$$G^2 = \rho^2 \left(\frac{dP}{dv} \right) \left(\frac{dv}{d\rho} \right) \tag{1.30}$$

Inserting equation (1.18) into this equation and since $v = 1/\rho$, we have:

$$G^2 = \rho^2 \left(-\frac{nP}{v} \right) \left(-\frac{1}{\rho^2} \right) \tag{1.31}$$

After rearranging, this equation becomes:

$$G_c{}^2 = \frac{n\ P}{v} \tag{1.32}$$

where P is the pressure at the throat, n is a polytropic expansion coefficient and v is the specific volume determined at critical plane flow conditions. Thus, we have proposed to use this relationship to estimate the critical mass flux for choked flows at supercritical conditions. Herewith, it is assumed that the flow can expand within a full range of thermodynamic conditions, i.e., complete thermal equilibrium fully irreversible (n=1) or fully out of equilibrium and completely isentropic ($n=\gamma$). Notice that these two extreme cases can easily be controlled by a single correlation parameter (n). When the flow expands isentropically (i.e., out of equilibrium), the isentropic expansion coefficient γ is considered constant during the whole process. It is calculated from small changes of the pressure and the temperature around the critical point, by keeping the entropy constant. The comparison of this model with the experimental data is presented and discussed in detail in Chapter 5.

1.6.2 Choking flow studies at supercritical conditions

In this section, most available critical flow studies performed with fluids at supercritical conditions will be presented. It is important to mention that only very few studies of this kind

exist in the open literature. In addition, most of them have been performed using carbon dioxide instead of water. Therefore, this lack of experimental information emphasizes the original work presented in this thesis.

One of the first studies related to the steady depressurization of supercritical water was performed by Lee and Swinnerton [96] where two objectives were established to perform the experiments. The first objective was to obtain choking flow data required to test the applicability of existing models (HEM, Burnell, Henry-Fauske Model and Bernoulli's equation). To this aim, they applied flow pressures from 3.44 *MPa* to up to 31.0 *MPa* to simple nozzle geometries (i.e., sharp, rounded and baffled edged nozzles made from FV520B material) by using three piston positive displacement high pressure pump. The second objective was to obtain heat transfer data to validate some of the existing convective heat transfer correlations (Section 1.5.2). It is important to mention that, since the Henry-Fauske and Burnell's models are not applicable for fluids at supercritical conditions, they were not tested at above critical conditions of water. Only, the HEM and the Bernoulli equation were tested at supercritical water flow conditions.

Lee and Swinnerton performed 283 tests both at subcritical and supercritical conditions using four different nozzles. Only 124 of 283 tests were performed at supercritical pressures and only 43 of 124 tests were performed slightly above the critical temperature of water (i.e., between 374°*C* and 402°*C*) which is far below from the operating conditions of future's SCWRs. Moreover, only 13 of 43 tests were performed above pseudo-critical temperatures of water (in the gas-like region) for the corresponding flow pressures. It must be pointed out that all the experiments were performed by maintaining the discharge pressure at atmospheric pressure conditions. They considered that the flows were choked along the experiments without varying the discharge pressure. They have argued that choking flow occurs in all the cases, because the pressure difference between the upstream and downstream of the orifice was very high. They found that the results for all nozzles follow the same trends but the critical mass flux is up to 30% higher for round edged nozzles than sharp edged nozzles, depending on the stagnation conditions. They have not observed the effect of the nozzle diameter on mass fluxes for pressure less than 13.7 *MPa* where different diameter size flow data are available in the open literature. In general, the comparison of mass flux data has shown good agreement with the data obtained in the literature (i.e., about 10% difference).

Lee and Swinnerton [96] proposed, by the first time, a correlation to estimate the pseudo-critical temperature of water only by using the stagnation flow pressure. They presented critical mass flux data versus DT_{pc} both in graphical and tabular form (DT_{pc} is given as the difference between pseudo-critical temperature already discussed in Section 1.3 and the fluid temperature at a corresponding fluid pressure). This definition can be considered similar to the subcooled temperature concept used for boiling fluids at subcritical pressures. It must be pointed out that negative DT_{pc} values represent temperatures higher than pseudo-critical temperatures in contrast to subcooled temperatures where negative values represent the temperatures lower than saturation temperatures. The representation of choking flow based on DT_{pc} was later used by Chen et al. [97-100].

Table 1.2 shows the dimensions and the geometries of each nozzle used by Lee and Swinnerton [96]. Temperatures at the inlet of the nozzles were from 204°*C* up to 400°*C* at supercritical pressures. To achieve supercritical water conditions, Lee and Swinnerton have used a heater element made of a coil tube heated by Joule effect.

Table 1.2 Nozzle dimensions and shapes used by Lee and Swinnerton [96].

Nozzle type	**Diameter (*mm*)**	**Length (*mm*)**	**Inlet rounding (*mm*)**	**Baffle spacing (*mm*)**
Nozzle A	1.8	1.65	Sharp nozzle	-
Nozzle B	1.8	6.43	0.89	-
Nozzle C	2.54	8.84	1.27	0.30
Nozzle D	2.5	8.84	1.27	-

When models were compared, under subcritical conditions (remember that only HEM and Bernoulli's equation at supercritical pressures have been tested) Lee and Swinnerton [96] have found that HEM model predicts choking flow rates quite satisfactorily for the high DT_{pc} temperatures (over 37.8°*C*) but fails to predict for the low DT_{pc} conditions, while other models (i.e., Burnell and Henry-Fauske) perform better than HEM for all flow regions. Bernoulli's equation also performed quite well when the C_d coefficient is adjusted depending on the nozzle

type at high sub-coolings (0.75 for sharp and 0.60 for rounded edged nozzle). However, at low DT_{pc} temperatures and high pressures this value must be as low as 0.30.

Gebbeken and Eggers [101] performed the first blowdown type experiments cited in the literature, by using pure carbon dioxide at initially supercritical conditions. Main objective of their work consisted of studying the pressure and temperature transient flow behaviour of a discharge from a vessel, as well as to obtain void fraction and phase distribution along the axis of a 50 *L* reservoir using a gamma densitometer technique. The collected data were useful for designing chemical processing equipment. To obtain the data, they have mechanically connected exchangeable diameter orifices to a venting pipe open to the atmospheric pressure. Initial pressures in the vessel were varied from 15 *MPa* to 30 *MPa,* above the critical pressure of carbon dioxide, (i.e., is 7.38 *MPa*) for fluid temperatures ranging from 24.85°*C* to up to 31.05°*C* (i.e., the critical temperature of carbon dioxide is 30.98°*C*). Their operating flow parameters have shown that they were always in the liquid-like region of the pseudo-critical temperature line, where the stagnation entropy is always smaller than the pseudo-critical temperature entropy for the same pressure. They observed that the expansion from the vessel was almost isentropic both at supercritical and subcritical section of the depressurization, $s_o < s_{pc}$; consequently, flow flashing was observed when the fluid conditions reach saturation conditions. Unfortunately, the values of the choking flow rate were not given by the authors; this lack of information prevents further analysis of their results to be considered.

Mignot et al. [102] have used the HEM model to create a blowdown flow map for the sudden depressurization of water from supercritical conditions (i.e., for flow pressures varied from 25 *MPa* to 37 *MPa* and for temperatures from 400°*C* to 600°*C*). They proposed three flow regions which are shown in Figure 1.15 where it is very difficult to determine the exact path of the boundaries between flow regions.

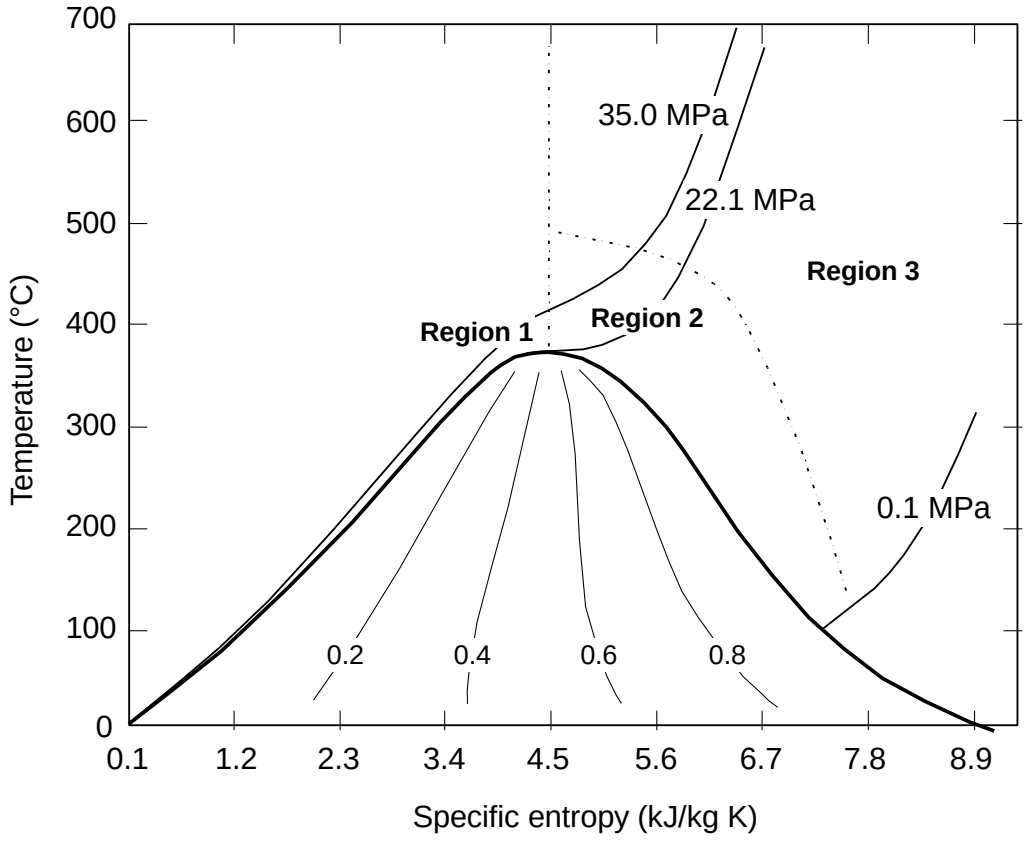

Figure 1.15 Blowdown map of water's depressurization from supercritical conditions.

Depending on the initial flow conditions, they have determined that the fluid (water in this case) can pass through different flow conditions after the depressurization. Under depressurizations in Region 1, the fluid starting from supercritical conditions undergoes a transformation to superheated steam conditions; in Region 2, the fluid starting from supercritical conditions goes to superheated steam conditions first and then, when the saturation line is reached, steam condensation takes place. In the Region 3, supercritical fluid conditions go through compressed liquid conditions before the saturation line is reached; only afterwards liquid spontaneous vaporization may occur (i.e., flashing). Since all the three regions can occur during an eventual LOCA in NPPs, all these processes are studied by the author in the present thesis. Results from these experiments are presented in Chapter 4 and Chapter 5.

Lee and Swinnerton [96] have compared their experimental data with the exception of those obtained using nozzle C (see Table 1.2) under supercritical pressures and temperatures with the predictions produced using the HEM and RETRAN (also based on HEM) code. They have found

that at high mass fluxes, predictions obtained by these two models do not give satisfactory results. They overestimated by up to 40% of the experimental data. Lee and Swinnerton have also studied experimentally the depressurization time required for the fluid to reach the subcritical pressures starting from supercritical initial conditions. They measured that the real depressurization time is much higher than what can be estimated by HEM which considers that the expansion is isentropic. This can be explained by the fact that the HEM does not take into account the effect due to friction. However, no critical mass flow rate data are presented in this part of Lee and Swinnerton`s study.

Mignot et al. [103] have also conducted transient critical flow blowdown experiments using carbon dioxide and water. Since the supercritical water loop was initially constructed for performing heat transfer and corrosion studies, only few data on choking flow were obtained at a pressure of 24.4 *MPa* and for temperatures ranging from 479°*C* to up to 511°*C*. They used a test section made from a 0.28 *m* long smooth sapphire tube with 1.59 *mm* ID. They have obtained 7 data points and since the initial flow conditions for all the data points were almost the same, the results are superposed within a very small region. However, due to technical difficulties, Mignot et al. [103] have continued their experimental studies mainly on carbon dioxide flows. In this case, they have used a fast opening valve (i.e., the same used for water critical flow experiments) at the exit of the 0.125 m^3 pressure vessel. Choking flow rates were calculated by using a weighing scale with a 5 *g* resolution. For each experiment, they collected 10 samples of weight per second; data obtained during the first 5 *s* and the last seconds were removed from the measurements since they were affected by the opening and closing of fast acting ball valve. Furthermore, a 0.335 *m* long 2 *mm* ID rounded inlet quartz tube having surface roughness of 0.007 μm was used at 10 *MPa* constant pressure for stagnation temperatures from 40°*C* to 95°*C* to measure the critical flows of carbon dioxide. They compared their experimental data with the predictions obtained with HEM model which included a friction term. They obtained 8% deviation between the predictions and the experiments.

Mignot et al. [104] have also performed additional carbon dioxide (industrial grade) critical flow experiments to study the effect of the length to diameter ratio and the surface roughness of the nozzle more in detail. Table 1.3 gives information about the tubes that have been used to perform the experiments.

Table 1.3 Nozzle dimensions and geometries used by Mignot et al. [104].

Material	**Inside surface roughness (μm)**	**Length (mm)**	**Tube inside diameter (mm)**	**Entrance geometry**
Stainless Steel	1.5	334.5	7	Sharp edged
Stainless Steel	4.3	338.1	3.715	Sharp edged
Stainless Steel	3.8	338.1	2	Sharp edged
Stainless Steel	3.8	337.3	2	Round edged
Quartz	0.007	338.1	2	Round edged

Mignot et al. [104] have performed the experiments by using the same pressure vessel system that was used previously [103]. Moreover, they have also used the same measurement techniques and data acquisition system (DAS). However, they have replaced the fast acting ball valve by fast acting pneumatic one. This modification permitted them to reduce the effect of opening and closing the valve on the measurements.

Mignot et al. have also proposed blowdown maps for the depressurization of carbon dioxide; as they have previously discussed for water [102]. These additional experiments were performed at a fluid pressure of 10 MPa for temperatures ranging from 35°C to up to 130°C. They have found that the entrance effect decreases with increasing the tube diameter. They have observed that the surface roughness may affect the choking flow rate by almost 15%; this can be explained by the increase in pressure drop. They found that the effect due to the presence of a sharp edge nozzle was about 7%. This can be explained by the effect of the formation of a vena-contracta. Mignot et al. were able to show that the HEM model that takes into account friction predicts their experimental data within ±5% for a smooth quartz tube and within 10% for stainless steel tubes. However, it is important to mention that their published results show the opposite trends. They have also observed that for a given flow pressure, the choking flow rate decreases with increasing the flow temperature for all tubes.

Chen et al. [97, 98] have studied choking flows of water both at subcritical and supercritical pressures under steady-state conditions. Since in the framework of this thesis we are only interested in the behaviour of the water at supercritical pressures, studies performed at subcritical

pressures are not discussed. Chen et al. have covered a wide range of flow parameters; such as the flow pressures from 22.1 *MPa* to 26.8 *MPa* and temperatures from 38°*C* to 474°*C*. To perform the experiments, they have used a rounded nozzle having a 1.41 *mm* ID and 4.35 *mm* length. Deionized water in upward flows was used as working fluid, driven by a three-head piston pump. Downstream the nozzle the fluid pressure was kept constant at 0.1 *MPa* for all the experiments. Different than Mignot et al. [103] they used a flowmeter to measure the flow rates; the thermal power was supplied by a 1100 *kW* DC power supply.

Similar to the work of Lee and Swinnerton [96], Chen et al. [97, 98] have used *DTpc* temperature difference to represent the experimental mass flux data. They observed that beyond certain temperature, choking flow does not occur. Nevertheless, this is a challenging problem to be understood without changing the back flow pressure. To this aim, the arguments of Chen et al. are questionable, because they have not changed the downstream flow pressure to assure the detection on the occurrence of choking flow. Afterwards, Chen et al. compared their data with the predictions obtained with Bernoulli's equation, the HEM and the choking flow model (proposed by Trapp and Ransom [79]) implemented in RELAP5/MOD3.3 nuclear reactor safety analysis code. They have concluded that the HEM overpredicted the experimental data by about 15% for flow temperatures higher than the pseudo-critical values and in the same region, where they have observed flow thermal equilibrium. They have also tried to estimate the flow pressure at the critical plane close to pseudo-critical flow temperatures for upstream flow pressures of 24 *MPa*. The pressure at the critical plane was estimated using HEM to be between 15 *MPa* and 19 *MPa*. When the inlet flow temperature was decreased, the prediction of the HEM becomes less accurate; for flow temperatures approximately less than 170°*C*, the deviation becomes almost +50%. The authors explained this deviation by arguing that choking flow does not occur at these flow conditions. However, in this region, Bernoulli's equation estimated the mass fluxes reasonably well (note that this equation is valid for single phase flows). In turn, Bernoulli's equation was not able to predict the experimental trends at supercritical flow temperatures; the predictions deviate by almost +50% near pseudo-critical temperatures. The predictions given by the RELAP5 code were also compared with experimental data using two different settings in the code (considering the flow choked or not-choked for all temperatures). They have shown that this code is not appropriate to estimate choking flow rate at supercritical temperatures.

Recently, Chen et al. [99, 100] performed new choking flow experiments using sharp edged orifice having 1.41 *mm* ID and 4.35 *mm* length with the setup previously explained [97, 98]. These new experiments were performed for flow pressures from 22.1 *MPa* to 29.1 *MPa* and temperatures from 263°*C* to 454°*C;* more than 200 data points were obtained using two nozzles [97-100]. Their data (especially for the sharp edged nozzle) show a huge scattering around pseudo-critical temperatures, in particular at high flow pressures. In general, they have reported the same observation obtained in their previous study [97, 98], (i.e., below certain flow temperature choking flow does not occur). Similar to their previous work, the same DT_{pc} variable is also used to compare sharp edged data with rounded edged data. They have found that the mass flux increases with increasing DT_{pc}. As has already been observed, close to DT_{pc} = 0°*C*, the mass flux changes at higher pace. It is important to mention that these two trends are expected because the density of the fluid increases with increasing DT_{pc}, especially close to the pseudo-critical temperature.

Chen et al. also proposed a new correlation to estimate the mass flow rate at choking conditions, given as:

$$G_c = \left[\frac{2\left(h_0 - (1-x_E)h_{lE} - x_E h_{gE}\right)}{\frac{C}{\bar{\rho}^2} + \left((1-x_E)v_{lE} + x_E v_{gE}\right)^2} \right]^{1/2} \tag{1.33}$$

where C is a local flow resistance coefficient and $\bar{\rho}$ is the average fluid density evaluated at the inlet of the nozzle.

This relationship obviously corresponds to a modified version of the HEM where the authors have taken into account local flow resistance. They proposed to use C=0.2 for rounded edged nozzles and C=0.6 for sharp edged nozzles for estimating flow rates at fluid temperatures where the flow is considered to be choked. They have also suggested using Bernoulli's equation with C_d=0.61 for other flow conditions. In general, these two equations are used to estimate the critical flow rates for fluid temperatures close to the values where choking flow occurs, because the exact location where this phenomenon takes place inside the nozzle is not known. Chen et al. have considered the minimum value produced by these two equations to fit their experimental data; this method permitted them to estimate the mass flux data within ±15% for mass fluxes lower

than 45000 kg/m^2s. Nevertheless, at high mass fluxes, the huge scattering in the sharp edged nozzle data could not allow them to obtain satisfactory results. However, rounded edged nozzle data were predicted more satisfactorily.

In summary, the review of the literature clearly shows that choking flows of water under supercritical conditions still require to be studied. In particular, a methodology must be implemented to determine unambiguously when choking flow occurs. Within this framework, the present work is intended to fulfill this gap by producing choking flow of water at supercritical conditions by rigorously controlling all flow variables that may affect the phenomenon, i.e., upstream and downstream flow pressures.

CHAPTER 2 SUPERCRITICAL WATER FLOW TEST FACILITY

As mentioned in Chapter 1, only a limited number of studies exist about choking flow of supercritical water, therefore, an experimental facility was constructed at the Thermal-hydraulics Laboratory of École Polytechnique de Montreal to perform research work on this subject. This chapter presents technical details of the facility and its principal mechanical components. Since the experimental system consists of a medium pressure steam-water loop connected in parallel to a supercritical one, a brief description of the former facility is also given. Note that for the experiments included in this thesis, the medium pressure steam-water loop serves as a low-pressure controlled reservoir in such a way that the discharge flow pressure of the test section can be changed independently of the upstream flow pressure. The way these two loops operate is discussed in the methodology section.

It is obvious that the design and construction of a very complex supercritical water loop requires the participation of several high qualified personal. Nevertheless, I have extensively contributed among other by providing new ideas based on the literature review, I have also simulated the thermal-hydraulics of key complements and thus, I have determined not only loop operational conditions but also established the safety limits used to propose a great number of alarm trip thresholds.

2.1 The medium pressure steam-water loop

The Nuclear Engineering Institute of École Polytechnique has a steam-water loop with a total installed thermal power of 200 *kW*. Originally, this loop had 750 *kW* thermal power, but presently 550 *kW* of this power is used by the new supercritical water loop. The principal operational characteristics of the medium pressure steam-water loop are given in Table 2.1.

Figure 2.1 shows a schematic of this installation which consists mainly of a steam drum, a direct contact condenser, two circulating pumps, a heat exchanger and two preheaters. It must also be mentioned that one of the most important features of this loop is its capability to operate as a stand-alone pressurizer system; therefore, it does not require the presence of a heated test section to produce the steam required to maintain the pressure of the system. This particular configuration permits us to combine this loop with the supercritical water branch as will be explained in the following section.

Table 2.1 Medium pressure loop operational limits.

Variable	Range
Pressure	0.1 - 4.0 *MPa*
Temperature	4 – 250°*C*
Mass flow rate	0.05 – 2.7 *kg/s*
Power	0 - 200 *kW*
Sub-cooling	0 – 100°*C*

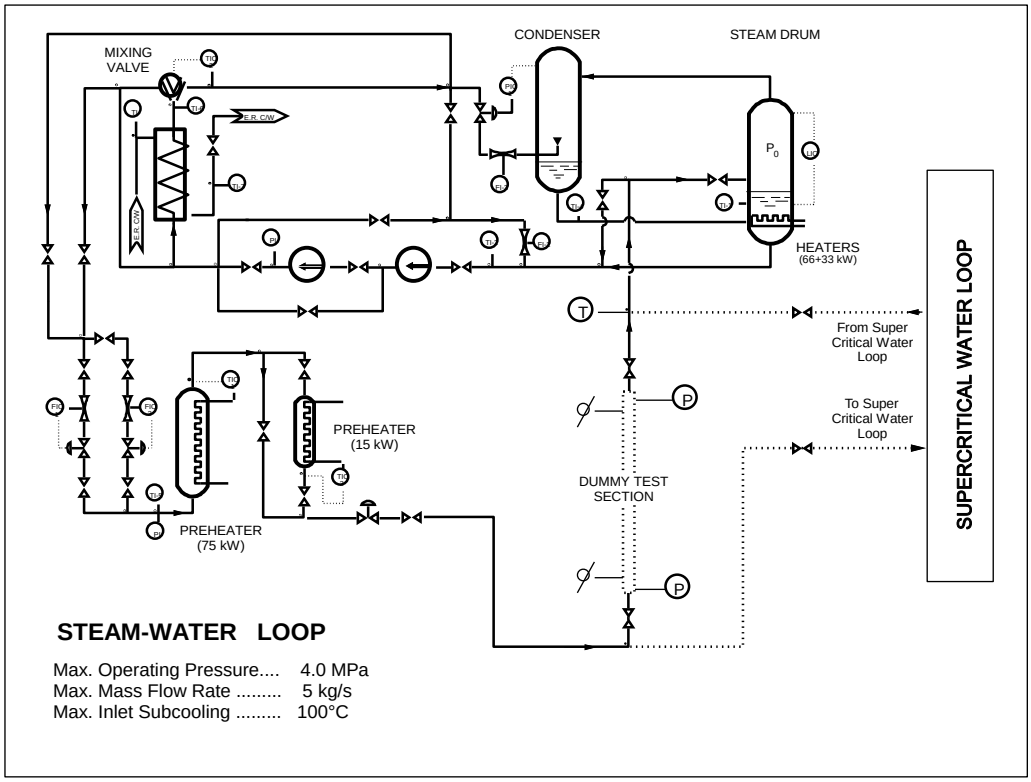

Figure 2.1 Medium pressure steam-water thermal loop.

In order to control the pressure of the system, the heater elements located in the steam drum are used to generate the necessary amount of steam required for operating the direct contact condenser at the desired pressure (see Figure 2.1). In fact, the direct contact condenser allows the system pressure to be controlled within range of ±0.01 *MPa*. The water flow rate is measured at

the inlet side of two preheaters by using a high temperature "Flow Technology®[1]" turbine flow meter having accuracy better than ±1% of the full scale.

Performing supercritical flow experiments has necessitated some modifications of the medium pressure loop to be carried out. These modifications consisted of adding a supplementary branch with the required thermal equipment necessary to control water flow conditions precisely at the entrance of the supercritical branch as well as at the upstream of a test section. In fact, to achieve supercritical water conditions, the medium pressure loop is connected in parallel to the supercritical water thermal components as shown by the dotted lines in Figure 2.1. The following section presents the major equipment and operation conditions of the supercritical pressure water flow loop.

2.2 The supercritical pressure water flow loop

A simplified flow diagram of the supercritical flow loop is given in Figure 2.2, while an isometric view is shown in Figure 2.3. Looking to the flow diagram, demineralised water is supplied by the intermediate pressure loop (not shown in Figure 2.3). The supercritical loop is interconnected to the medium pressure steam-water loop via a test section to be discussed in Section 2.2.5 and in Chapter 3. Thus, the steam-water loop serves as a low-pressure controlled reservoir. This particular flow configuration allows us not only to control the back flow pressure but also to change it from about 0.1 *MPa* to up to 4.0 *MPa* independently of the pressure upstream, i.e., from the throat. Under well-established supercritical water conditions prevailing in a test section, the ability to change the discharge pressure should permit us to rigorously determine whether the flow reaches choking conditions or not. As discussed in Chapter 1, up to now, all experimental studies related to choking flows of supercritical fluids were performed by discharging them into atmospheric pressure conditions without changing the back pressure. This means that the collected data were not validated to determine whether choking flow conditions are unambiguously reached or not (i.e., any change on the downstream back pressure must not affect the flow upstream of the nozzle). Thus, the facility discussed in this thesis, according to the knowledge of the author and the open literature, constitutes the first and unique experimental

[1] Trade mark of Flow Technology, USA

installation in this area. The maximum allowable operating conditions of the supercritical water loop are given in Table 2.2. Key flow parameters used for designing the system will be explained in detail in the following sections.

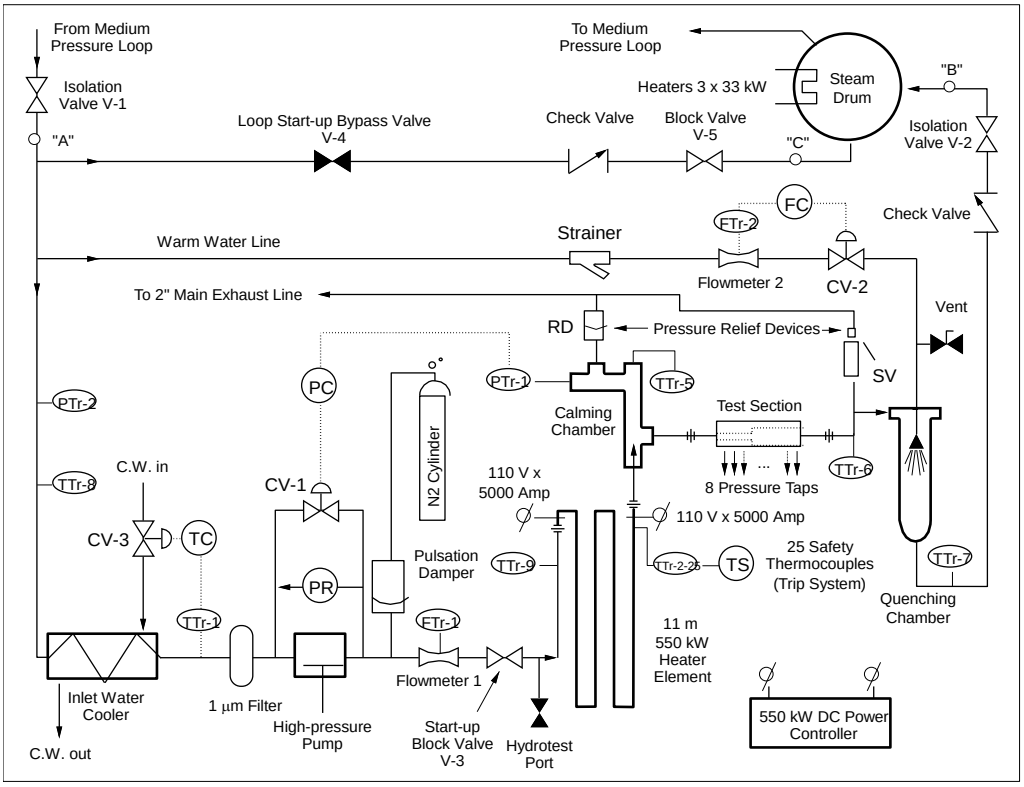

Figure 2.2 The supercritical water experimental facility.

Table 2.2 Supercritical pressure loop operational limits.

Variable	**Range**
Pressure	0.1 – 32.2 *MPa*
Back Pressure	0.1 - 4.0 *MPa*
Temperature	4 – 505°*C*
Mass flow rate	0.001 – 0.18 *kg/s*
Power	2 - 550 *kW*

It is important to mention that the minimum range of operational conditions of the supercritical pressure loop equipment is in general limited by the precision of the corresponding equipment.

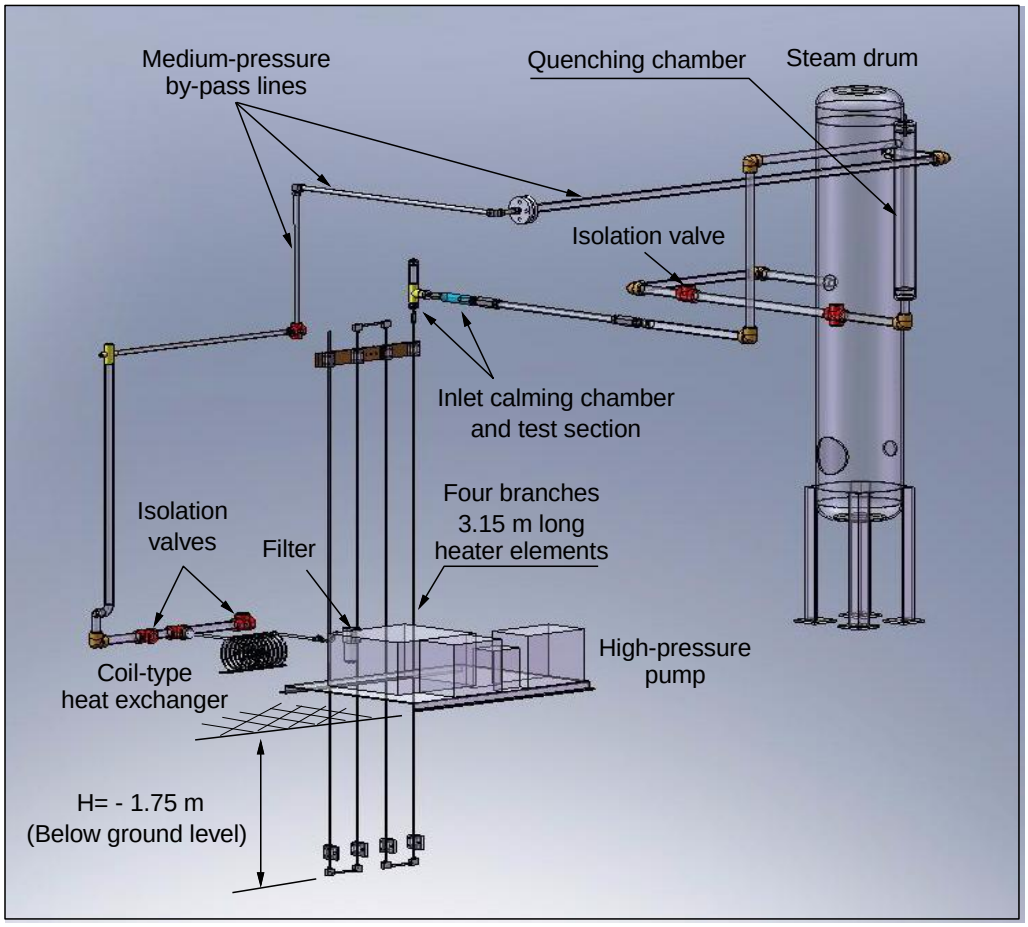

Figure 2.3 Isometric view of the supercritical part of the loop.

Hereafter, a description of each component as well as their working conditions is presented. However, it must be pointed out that after commissioning, the loop was slightly modified (i.e., an additional heat exchanger and some valves were added to the system.

2.2.1 Water cooler and filter

As shown in Figure 2.2 and Figure 2.3, a heat exchanger is located just at the inlet of the supercritical branch. In fact, depending on the operation of the medium pressure steam-water loop (Table 2.1) the inlet flow temperature can be as high as 250°*C*. Note that this value is read by thermocouple TTr-8 shown in Figure 2.2. Nevertheless, such a high value does not satisfy the

maximum allowable water temperature at the inlet of the high pressure (HP) pump (Figure 2.2). Therefore, to cool down the water before entering into the pump, a dual tube heat exchanger manufactured by Sentry®[1] Equipment Co. (model DTC-SSB/SSD-8-1-1) is installed in the loop. As can be observed in the Figure 2.2, a control valve (CV-3) combined to a pneumatic actuator is used to maintain the inlet water temperature below $65°C$ as requested by the HP pump.

Furthermore, to satisfy technical operational characteristics of this pump, a $5\ \mu m$ glass fiber filter is installed in the flow line (see Figure 2.2). This unit prevents solid particles to be transported by water entering into the piston system of the pump. In summary, in this portion of the supercritical water branch, distilled and filtered water at pressures ranging from 0.1 *MPa* to 4.0 *MPa* for flow temperatures lower than $65°C$ is used.

2.2.2 Pump, dampener and flowmeter systems

As shown in Figure 2.2, filtered water enters into a six piston positive displacement pump (McFarland®[2] MAC P-15). According to the specifications of the manufacturer, the maximum operation pressure and volumetric flow rate of this pump are 24.13 *MPa* and 10.23 *l/min*, respectively. Furthermore, as has already been mentioned, the maximum inlet temperature of the pump should not exceed $65°C$. Two systems are used to control the outlet pressure: a bypass valve (CV-1 in Figure 2.2) and a variable electronic speed controller (ABB ACH550®[3]). In addition, the pump also has a pressure relief system connected to a manual high precision needle valve. It is important to mention that the valve CV-1 is pneumatically controlled via a National Instrument®[4] data acquisition and control system that will be discussed in the instrumentation section.

It is well known that, positive displacement pumps tend to produce huge flow and pressure fluctuations. To avoid any undesirable effect during the experiments, a pulsation dampener

---

[1] Trade mark of Sentry Equipment Corp

[2] Trade mark of McFarland-Tritan, LLC

[3] Trade mark of ABB

[4] Trade mark of National Instrument

(Norman 4525TF-B5AN-V®[1]) is installed at the outlet of the pump (Figure 2.2) to damp eventual flow pressure oscillations. According to the manufacturer, this unit must attenuate the pulsations below ±1% of the pump discharge pressure. For its proper operation, the dampener unit requires a counter balance pressure of about 80% of the operational pressure (i.e., about 19.3 *MPa* when the pump is working close to critical pressure of the water). To this purpose, it is filled with nitrogen (see Figure 2.2). To see the effectiveness of the dampener unit, preliminary tests were performed at temperatures of 150°*C* and 230°*C*; the results of these tests are discussed in Chapter 4.

As shown in Figure 2.2, after the pulsation dampener, the compressed water passes through a turbine type flow meter (Flow Technology®, FT6-8NEYW-LEDT1) which is used to measure the flow rate via a frequency to current converter and the data acquisition system. It must be pointed out that all these equipment will work under high pressure, but at quite low temperature (i.e., the working temperature is lower than 65°*C*). Therefore, all fluid pipe connections are carried out using Swagelok®[2]-NPTF SS-304 type fittings. In order to have the possibility of removing the flow meter for periodic cleaning and calibration, special WCO O-Ring face seal unions are used. Both the inlet and outlet sides of the flow meter are symmetric and include at least 10 IDs of hydraulic lengths as suggested by the manufacturer. The outlet of the flow meter is connected to a heater element which is described in the following section. It is important to mention that after the flow meter, all the tubes used in the supercritical loop are made of Hastelloy C-276 alloy (nickel molybdenum - chromium alloy). This material has been selected to be compatible with water at supercritical conditions.

2.2.3 The heater element

The heater element is one of the most important equipment of the supercritical water loop. For the design of the heater, seamless Hastelloy C-276 tubes were selected which have excellent resistance to corrosion, a desired property for supercritical water [115]. In fact, this part of the facility, according to design criteria, should permit us to increase the temperature of the pressurized water from 65°*C* to up to 560°*C*. Hence the heater element is manufactured from

[1] Trade mark of Norman Filter Company, LLC

[2] Trade mark of Swagelok

9.530 *mm* (3/8 inches) outside diameter (OD) and 6.223 *mm* inside diameter (ID) Hastelloy C-276 tube. For safety reasons (i.e., very high flow pressures and temperatures prevailing in this unit), it is partially installed in a 2x2x2 *m* concrete pit. Three major constraints influence the designing of the heater element. The first one takes into account the electrical characteristics of the existing power controller, i.e., maximum values of voltage and current (110 *V* DC x 5000 *A*). It is obvious that, these maximum values impose some limitations to the electrical resistance of the tube to be used as a heater element. The second constraint is imposed by both the electrical resistance and the mechanical strength of the tube, i.e., wall thickness necessary to support high pressure and very high wall temperature conditions. The third and probably the most important one is imposed by the fact that due to the high flow pressure and temperature conditions, it is very difficult if not impossible to use gaskets having both good mechanical and electrical insulation properties. Therefore, an arrangement has been selected in such a way that the ends of the heater element will be connected to ground, i.e., at the same electrical potential as the test section and the rest of the medium pressure steam-water loop. Note that this particular solution permits to eliminate the use of electrically isolated gaskets.

Figure 2.4 shows the heater which consists of four tubes mechanically connected in series but electrically connected in parallel. Since heat is produced by Joule effect, electrical potential is applied to each end of the heated tubes using copper clamps. As explained before, in this design we have used a particular electrical connection which assures that the inlet and the outlet of heater element tubes are at ground potential (i.e., the same as the rest of the loop). To this aim, positive wires of the power supply are connected using separate connectors (see the right bottom corner in Figure 2.4) at the bottom part of the heater element. In turn, a single copper bus bar (see the left top corner in the figure) at the top of the heater element is used for connecting the negative wires, which are grounded.

Moreover, to increase the electrical contact conductivity and resistance to oxidation, the copper bus bars are nickel coated. Also as shown in Figure 2.5, 0.1 *mm* thick 99.9% metal basis silver foils are placed between the electrical clamps and all along the perimeter of the heater tubes to guarantee high contact conductivity between the clamps and the section of the heated tubes.

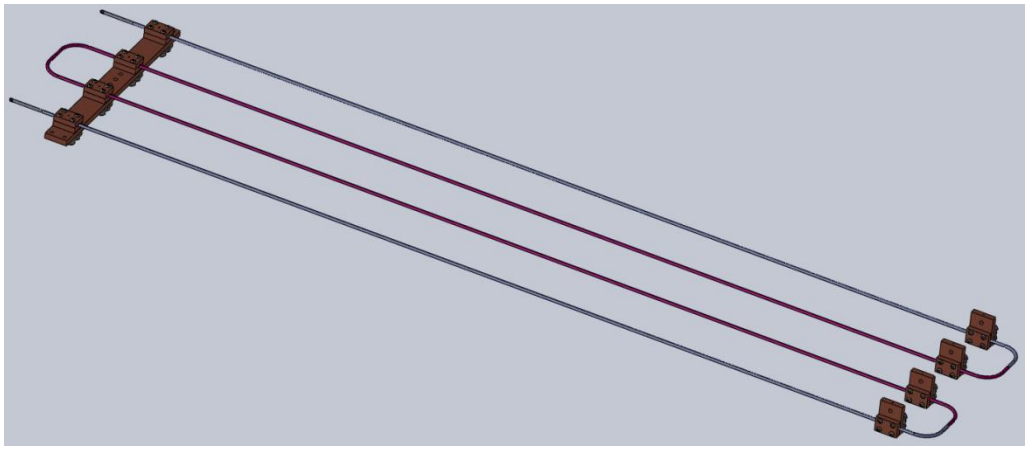

Figure 2.4 Heater element with electrical connections.

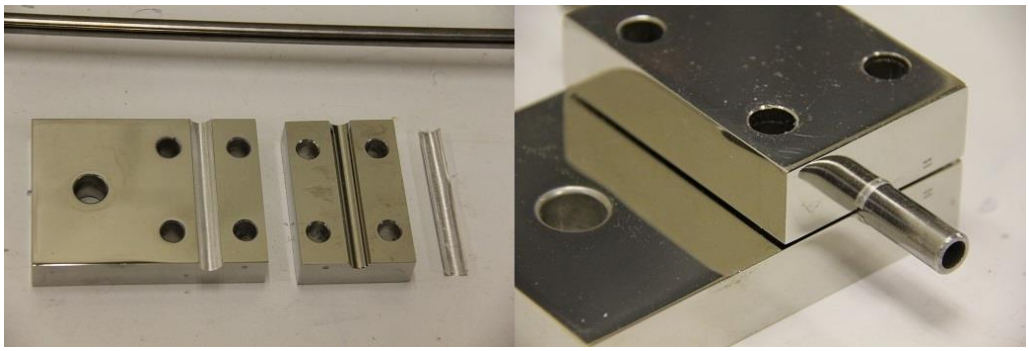

Figure 2.5 Silver foil between heater tubes and copper clamps.

Several spot welded ungrounded thermocouples on the heater external wall surface have been installed; more information about them will be provided in the instrumentation section (Section 2.3). Furthermore, the heater element is thermally insulated not only to reduce heat losses but also to insure an appropriate mechanical rigidity. To this aim, two different layers of insulation material are used. A first layer, 25.4 *mm* thick of Superwool®[1] fibre is used which is relatively flexible and resilient. It has an excellent thermal insulation performance even at high temperatures, up to 1250°*C* (see Figure 2.6). At the outside layer, thermal rigid Foamglass®[2] with 66.3 *mm* thickness is used as a second layer insulation material as shown in Figure 2.7. This

[1] Trade mark of Morgan Advanced Materials

[2] Trade mark of Pittsburgh Corning

arrangement allows us to reduce heat losses and maintain the mechanical rigidity of quite long heater elements.

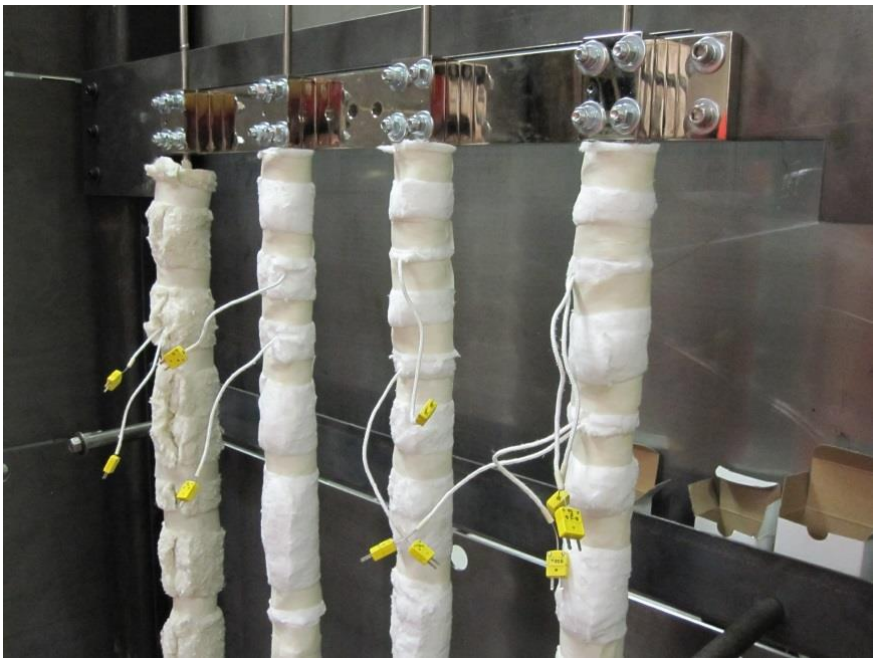

Figure 2.6 Heater element with Superwool® insulation.

During the preliminary design of the heater element, Autoclave®[1] high pressure elbows were selected to connect the tubes to each other and a straight Autoclave coupling to connect the outlet to the rest of the loop. However, due to safety concerns, we decided to reduce the number of mechanical connections (i.e., couplings) to a minimum. For this reason, it was determined to replace Autoclave® elbows by custom made ones directly welded to the tubes. Thus, instead of using six Autoclave elbows, the heater element tubes were welded to custom elbows made of the same material (i.e., Hastelloy® C276 tube) at three different locations. It is worth to mention that these locations correspond to the outside region of the heated part of this element. Hence, eliminating mechanical connections not only ensured us a better loop safety but also simplified the design. However, to manufacture these new parts (i.e., curved heater element branches) one would have checked the wall thickness variation of the tubing due to material deformation caused

[1] Trademark of Parker Autoclave Engineers.

by the manufacturing process. To this purpose, a tube made from Hastelloy C276 having the same wall thickness was slowly bended along a radius of 25 *mm* and cut at five different places, as shown in Figure 2.8, to perform further mechanical analysis.

Figure 2.7 Heater element with Foamglass® solid thermal insulation.

The distribution of the wall thickness was carefully analyzed for each of these five axial cuts and for eight angular locations (i.e., every 45°) using a digital calliper (Mitutoyo Model CD-8" P) with a precision higher than ± 0.005 *mm*. Figure 2.8 shows the schematic of the bended tube including the locations where the tube has been cut to perform mechanical analyses.

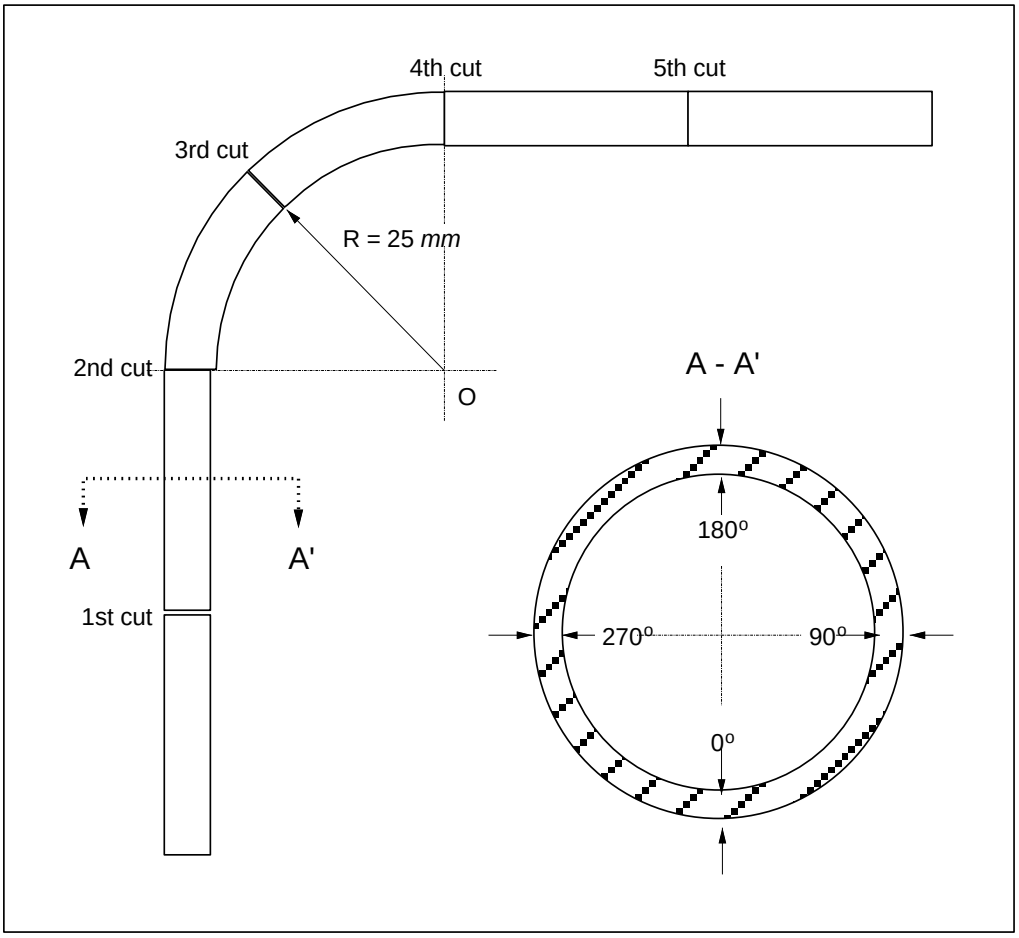

Figure 2.8 Schematic of a bended tube used to perform mechanical analyses.

As it can be seen in Figure 2.9, due to the manufacturing process the maximum wall thickness decreased by about 7%. After calculating the minimum wall thickness as required by the American Society of Mechanical Engineers (ASME) Pressure Vessel Code, the allowable pressure at the maximum tube skin temperature would be over 4300 *psi* which is well above the operating pressure of 3500 *psi* (note that in the ASME Pressure Vessel Code pressures are given in *psi*, therefore for convenience, the maximum operating pressure is given using the same unit). This mechanical study permitted us to confirm that custom made bended tubes were acceptable for replacing Autoclave elbows without compromising safety design criteria used for the high pressure loop.

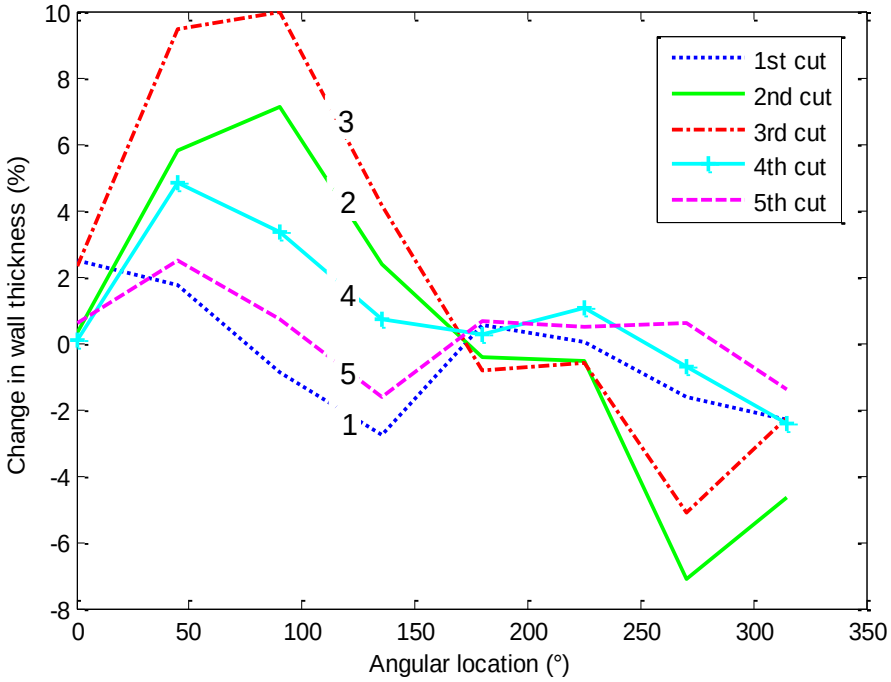

Figure 2.9 Bending analysis of a Hastelloy C-276 0.065" thick tube.

Another important parameter used to design the heater element is the maximum flow rate that can be obtained from the high pressure pump, at a maximum working pressure of 24.23 *MPa* and a maximum outlet temperature of 501°*C*. Note that these values are selected to study choking flow of water at conditions that represent future NPPs. As already mentioned, the tube of the heater element has 9.53 *mm* (3/8 *in*) outside diameter (OD) x 1.65 *mm* (0.065 *in*) wall thickness. It is good to mention that the tube length, wall thickness and material are chosen to provide the necessary heat to increase the water temperature from 65°*C* to up to 501°*C* for the maximum flow rate that the pump is able to deliver (i.e., as given by the pump manufacturer). However, on the other hand, the wall thickness of the tube must also satisfy the maximum allowable working pressure as well. Since the heat is generated by Joule effect, the design of the heater element must also satisfy the electrical resistance that must be compatible with the power controller.

Thus, in order to complete the design of the heater element, a very important criterion, the electrical resistance of the unit must be compatible with the properties of the power controller. In fact, this controller can deliver up to 550 *kW* (i.e., maximum 110 *V DC* at 5000 *A*, which corresponds to a maximum acceptable electrical resistance of 0.022 Ω). However, we have

considered a more conservative approach by limiting the power to 450 *kW* for outlet fluid temperatures of 501°*C*, by assuming that the pump operates at its maximum pressure. Hence, the maximum flow rate is calculated from the following enthalpy balance equation where heat losses are neglected:

$$\dot{m} = \frac{Q}{h_o - h_{65°C}} \quad \xrightarrow{yields} \quad \dot{m} = 9.335 \frac{kg}{\min} \quad \text{or} \quad \dot{m} = 0.156 \frac{kg}{s} \tag{2.1}$$

where *Q* is the power, $h_{65°C}$ and h_o are the enthalpies of the fluid at 65°*C* and 501°*C*, respectively for a flow pressure of 24.23 *MPa*. Since this value is smaller than the maximum flow rate that can be delivered by the pump (10.13 *kg/min*), it is obvious that the use of a correct dimension for the nozzle should permit us to reach a convenient flow rate. Assuming that at these conditions the flow is choked while the critical mass flux is determined experimentally (i.e., estimated to be around 22000 kg/m^2s), then the maximum allowable diameter of the nozzle is calculated to be around 3 *mm* to design future test sections.

Following the same approach and taking 450 *kW* as the maximum applied power to the heater element, the required length of the heater element is calculated by considering it as a single long tube. Nevertheless, the final design (serpent shape) shown in Figure 2.4, is arranged as four branches connected in parallel. This topology allows us to fit the overall size of this equipment to the available laboratory space and avoid the use of high pressure electrically insulated gaskets. Since the same electrical current is assumed to pass through each branch of the heater element, the thermal power produced by Joule effect is calculated as:

$$\left(\frac{I}{4}\right)^2 \times \frac{R}{4} = \frac{Q}{4} \tag{2.2}$$

For an electrical potential of 106 *V*, with Q = 450 *kW*, and I = 4500 *A*; the electrical resistance must be R = 0.356 Ω. Taking into account an average value for electrical resistivity of Hastelloy C276 of ρ_{el} = 1.3 $\mu\Omega$-*m* [116] and assuming that the electrical resistance is constant along the heater element (i.e., independent of its temperature), the length is calculated as:

$$L = \frac{R \times A_{wall}}{\rho_{el}} \tag{2.3}$$

which yields to a total effective length of L = 11.17 *m* where *A* is the cross sectional area of the tube. Consequently, the total heated length is given by four lengths of 2.79 *m* (110 *in*) each in such a way to obtain a total required value of 11.17 *m* (36.67 *feet*).

In reality, since the four branches of heater element are electrically connected in parallel, for the same electrical potential, the electrical current passing from each tube will change in time due to the change of resistance according to its average temperature. It is important to remember that fluid temperature increases along the heater element; therefore, the resistivity of each branch will be slightly different (resistivity of the tubes will increase in the fluid direction since the average tube temperature will also increase). A similar trend will occur for the elongation of each branch; nevertheless the maximum elongation will be seen in the fourth branch due to the maximum temperature difference (average tube temperature difference when the electrical potential is applied with respect to the room temperature). Knowing the electrical resistivity of the tube at a given temperature, the electrical resistance of each branch is estimated as:

$$R = \frac{\rho_{el} \times L/4}{A_{wall}} \tag{2.4}$$

To better understand the effect of temperature differences on electrical parameters of each branch, it is assumed that 106 *V* of electrical potential is applied to the entire heater element. Using equation (2.4) and Ohm's law ($V = I \times R$), the electrical resistivity and current passing on each branch are calculated; the results are given in Table 2.3. The fact that each branch will have uneven electrical current for the same electrical potential; different thermal power will be produced. In turn, the tube wall temperature will be controlled by the convective heat transfer coefficients prevailing in the fluid. To this aim, it is important to mention that close to the supercritical temperature conditions convective heat transfer changes significantly as explained in Section 1.5 of the literature review. Consequently, this will affect the average tube temperature and the electrical resistance as well. As a result, the values given in Table 2.3 must be considered

as rough estimations necessary for design purposes. The real values will be available only after performing the commissioning tests of the whole system.

Furthermore, it is important to mention that as a result of material limitations, for the supercritical portion of the heater element, the tube outside wall temperature must also be limited to a maximum value of 621°*C*. To verify this limitations, the preliminary simulations are performed with a convective heat transfer coefficient given in [5]. This calculation permitted us to estimate the temperature distribution along the heater element.

Table 2.3 Preliminary electrical calculations of each heater element branch at 106 *V*.

Heater element	**Electrical resistance (Ω)**	**Current (*A*)**
Branch 1	0.0966	1104
Branch 2	0.1005	1061
Branch 3	0.1026	1039
Branch 4	0.1047	1018
Total	0.0253	4223

Preliminary calculated temperature differences between the fluid and the inside wall of the tube and between the inside wall and the external surface of the tube are around 40°*C* and 75°*C*, respectively. Figure 2.10 shows the estimated temperature distributions along the heater element for a mass flow rate of 0.156 *kg/s* and an applied thermal power of 450 *kW*. Note that along these simulations, the unheated portions of the heater element are not considered in the calculations.

The same power is then applied to estimate the fluid outlet temperatures as a function of the mass flow rates; the results are plotted in Figure 2.11. It is important to mention that for flow rates lower than 0.156 *kg/s*, the required thermal power decreases with decreasing the flow rate, necessary to increase fluid outlet temperature over 500°*C*. However, for flow rates higher than 0.167 *kg/s*, the fluid outlet temperature cannot go up to 500°*C* and the maximum fluid outlet temperature is limited to around 450°*C*.

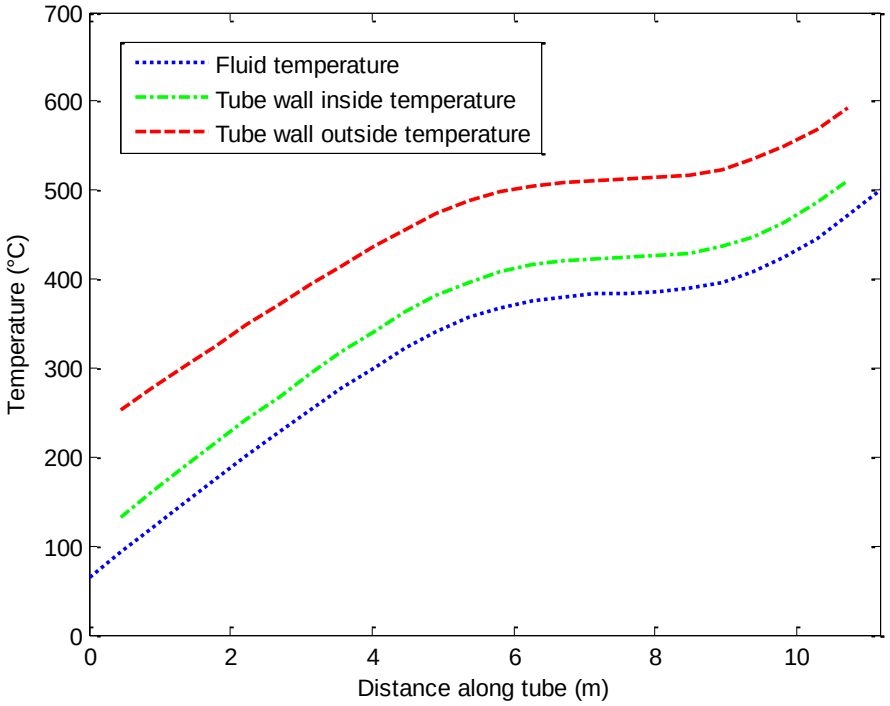

Figure 2.10 Estimated temperature distributions along the heater tube.

Another important thermal-hydraulic parameter required for designing the loop is the pressure drop that will be introduced in the loop, in particular between the calming chamber and the test section (see Figure 2.2 and Figure 2.3). The estimation of this pressure drop is necessary not only for the safety of the supercritical loop but also for the accuracy of the experimental parameters. Since temperatures and pressures are measured just after the heater element, the pressure drop between the calming chamber and the orifice plate (i.e. test section, shown in Section 2.2.5) should be considered to estimate upstream thermo-physical fluid conditions. As has been discussed in Section 1.4, the total pressure drop can be calculated as a function of four terms: frictional, acceleration, gravitational and irreversible pressure drops. Irreversible pressure losses due to sudden geometry changes are neglected. Since the calming chamber and the test section have the same elevation, gravitational pressure drop does not exist. However, even though the change of fluid density is too low, the acceleration pressure drop has to be estimated because the tube diameter changes in this same region. Thus, we must consider the contribution of acceleration and frictional pressure drops.

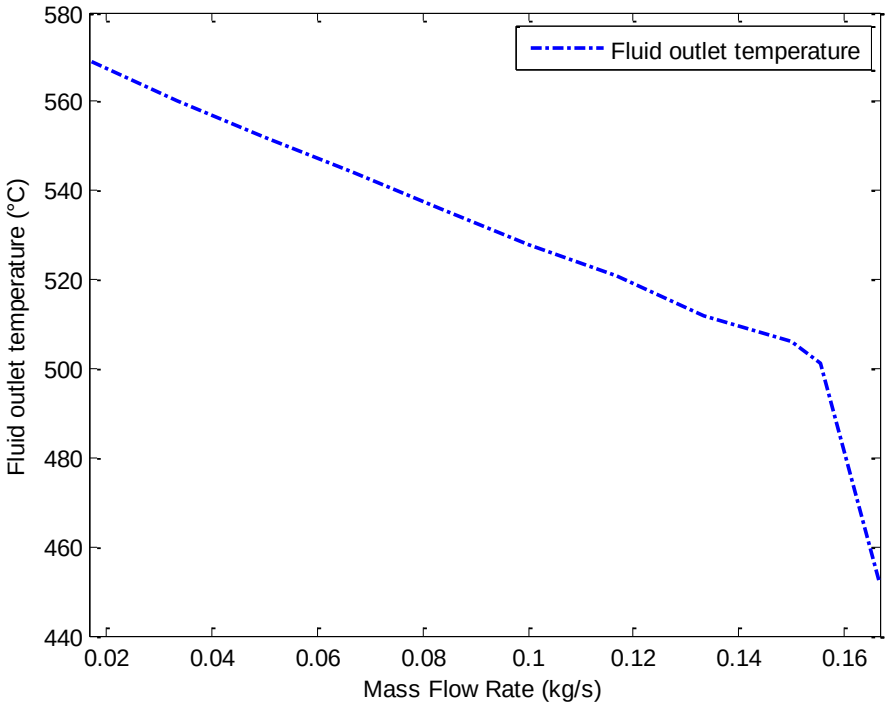

Figure 2.11 Fluid outlet temperature as a function of heater mass flow rate.

The acceleration pressure drop between the calming chamber and the test section is estimated as [117] :

$$(\Delta P)_{acc} = \rho_1 V_1^2 - \rho_2 V_2^2 \tag{2.5}$$

The acceleration pressure drop, at supercritical pressures for a 1 *mm* ID sharp nozzle, is estimated for two extreme cases: at minimum and maximum fluid temperature conditions which correspond to the minimum and maximum mass flow rates. For a minimum mass flow rate of 0.0174 *kg/s* and for a flow pressure of 24 *MPa* and a temperature of 500°*C*, the acceleration pressure drop is estimated to be 0.0116 *MPa*. For a maximum mass flow rate of 0.125 *kg/s* at the same flow pressure and for a fluid temperature of 52°*C*, the acceleration pressure drop between the calming chamber and the test section is estimated to be 0.0503 *MPa*.

The frictional pressure drop (Δp_{fr}), along the same region (between the calming chamber and the test section in Figure 2.3), is estimated by using the equations given in Pioro and Duffey's [5].

Nevertheless, the friction coefficient is taken from the Moody diagram [21] or it is calculated by using Colebrook friction factor equation [20] that is given as:

$$\xi_{fr} = \frac{1}{\left(-2 \times \log\left(\frac{\varepsilon}{3.7 \times D} + \frac{2.51}{\mathrm{Re}\sqrt{\xi_{fr}}} \right) \right)^2} \tag{2.6}$$

where for smooth tubes surface roughness, $\varepsilon = 1.5\text{x}10^{-6}\ m$ [118]; thus, the frictional pressure is drop estimated as:

$$(\Delta P)_{fr} = \xi_{fr} \frac{L}{D} \frac{G^2}{2\rho} \tag{2.7}$$

The two extreme flow cases that were applied before are also used to estimate the frictional pressure drop between the calming chamber and the nozzle. For the minimum flow rate, the frictional pressure drop is about 0.00654 *MPa* and for the maximum flow rate, this value increases up to 0.03390 *MPa*.

Hence, the total estimated pressure drops between the calming chamber and the nozzle as function of upstream flow conditions are given in Table 2.4. The differences between two values can be related to several factors such as different mass flow rates, estimation of friction factor for two different conditions, measurement of the flow conditions, etc. These simple calculations indicate that in the worst case the pressure drop should not be higher than 0.1 *MPa*. However, this estimation is very important for adjusting the RPM of the HP pump during the experiments, because we must satisfy that the upstream pressures are always higher than the critical pressure just at the inlet of the orifice. Even though this section presents design values, some results are presented in Table 2.4 to compare estimated key flow variables with the measurements that will be discussed in detail Chapter 5.

Table 2.4 Comparison of estimated pressure drop vs. measured pressure drop between the calming chamber and the test section.

Flow rate (*kg/s*)	**Upstream pressure (*MPa*)**	**Upstream temperature (°*C*)**	**Estimated ΔP (*MPa*)**	**Measured ΔP (*MPa*)**
0.0174	24	500	0.0181	0.04380
0.1250	24	52	0.0842	0.06494

Having pressures higher than the critical value during the experiments are also very important to protect the heater element from the eventual occurrence of Critical Heat Flux (CHF). Since we have not made a provision for installing pressure transducers at the exit of the pump, achieving a flow pressure in the calming chamber higher than the critical value guarantees us the safe operation of the heater element.

In addition, since the operational maximum outlet pressure of the pump is 24.13 *MPa*, it is also necessary to know the pressure drop in the heater element as well. To this purpose, we must estimate the total pressure drop between the outlet of the pump and the nozzle. Equations (2.5) and (2.7) are used to calculate acceleration and frictional pressure drops, respectively. Moreover, as shown in Figure 2.3, the outlet of the pump and the calming chamber are not at the same elevation, therefore the gravitational pressure drop must be included in the calculations. Gravitational pressure drop is given as:

$$(\Delta P)_{grav} = \rho g \Delta h \tag{2.8}$$

where Δh is the elevation difference between the calming chamber and the outlet of the pump, g is the gravitational force and ρ is the fluid density.

Similar to the former calculations, two cases are considered to determine the gravitational pressure drop component in the heater element. For a minimum mass flow rate with 1 *mm* ID nozzle, gravitational pressure drop is estimated to be 0.00082 *MPa*. Due to the change in temperature (i.e., density), this value increases while increasing the mass flow rate and for the maximum flow rate it is calculated as 0.00978 *MPa*. As shown in Equation (2.5), only the change in the fluid density and flow velocity affects acceleration pressure drop. Therefore, when the fluid

temperature is extremely pseudo-subcooled, the density changes can be neglected and the flow velocity does not change along the heater element, for maximum measured flow rate (at 52°*C*), no acceleration pressure drop is expected. For the minimum expected mass flow rate, estimated acceleration pressure drop is calculated as 0.00654 *MPa*. Frictional pressure drop for the minimum and the maximum mass flow rates are estimated as 0.102 *MPa* and 0.323 *MPa*, respectively. Table 2.5 summarizes the total estimated pressure drop in the heater element for these two extreme cases. As one can see comparing Table 2.4 and Table 2.5, the pressure drop in the heater element is a couple of times higher than the pressure drop between the calming chamber and the nozzle.

Table 2.5 Estimated pressure drop in the heater element.

Flow rate (*kg/s*)	**Upstream pressure (*MPa*)**	**Upstream temperature (°*C*)**	**Estimated ΔP (*MPa*)**
0.0174	24	500	0.1097
0.1250	24	52	0.3328

Up to now, expected flow rates with 1 *mm* ID sharp nozzle are used to compare the calculated pressure drops with the estimated ones. In Figure 2.11, fluid temperature at the outlet of the heater element as a function of the mass flow rate is presented. However, one must know that, to obtain these flow rates, the nozzle diameter has to be adapted, in fact, when the flow is choked, the mass flow rate will be determined by the flow itself. For example, with 1 *mm* sharp edged nozzle (which is used in this study to perform the experiments), one cannot obtain flow rates higher than 0.0174 *kg/s* at 23.66 *MPa* and 499.9°*C*, because at these conditions the flow becomes choked.

Figure 2.12 shows the margin over critical pressure if nozzle diameter changes while Figure 2.11 shows the maximum attainable outlet temperature for a specific flow rate. Since mass flow rate increases with increasing the nozzle diameter, consequently the overall pressure drop increases and outlet fluid temperature decreases. Therefore, Figure 2.12 can be used to estimate the maximum pressure that can be achieved at the outlet of the heater element, which is a key flow parameter for the safe operation of the loop.

As a design requirement, the thermal expansions of the tubes and copper bars have also been studied. It is apparent that the temperature on each leg of the heater will be different; therefore, the thermal expansion of the tubes and the copper bars in thermal contact with them will differ as well. To this aim, the thermal expansion between the copper bars and Hastelloy C-276 tubes are calculated. High differences in the thermal expansion of these components may induce important mechanical stresses. To perform the calculation, a mean value of thermal expansion coefficient of Hastelloy C-276 is used. The results have shown that the differences in thermal expansion between the copper bar and Hastelloy C-276 tube are very small. Therefore, they were not considered during the design of the system.

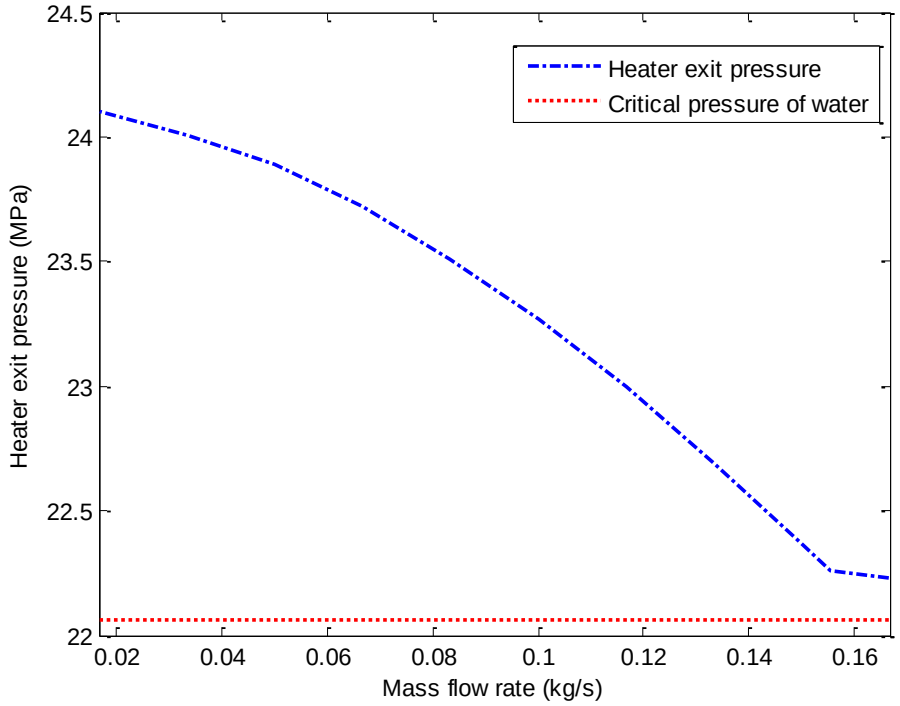

Figure 2.12 Heater exit pressure as a function of mass flow rate.

2.2.4 The calming chamber

Due to relatively high heat fluxes that will be applied to the heater element (i.e., 2 MW/m^2 for 450 kW) and to a relatively low convective heat transfer that seems to be a characteristics of supercritical fluids [5], it is quite possible that a considerably non-uniform temperature flow distribution will occur at the outlet of the heater. To overcome this drawback, a flow stabilization

plenum is installed between the heater outlet and the test section inlet (See Figure 2.2). Furthermore, note that the compressibility of the supercritical fluid contained in this vessel (i.e., designated as calming chamber in Figure 2.2) acts as a supplementary fluid damper and homogenizer before the fluid enters into the test section. The calming chamber is made of three 1- 1/2" SCH 80 Hastelloy C-276 Tees and 1-1/2" SCH 80 pipe welded together as shown in Figure 2.13. It permits the supercritical fluid produced in the heater element to be stirred before entering into the test section. As mentioned before, this process is required to minimize possible flow stratification effects due to density differences within the fluid.

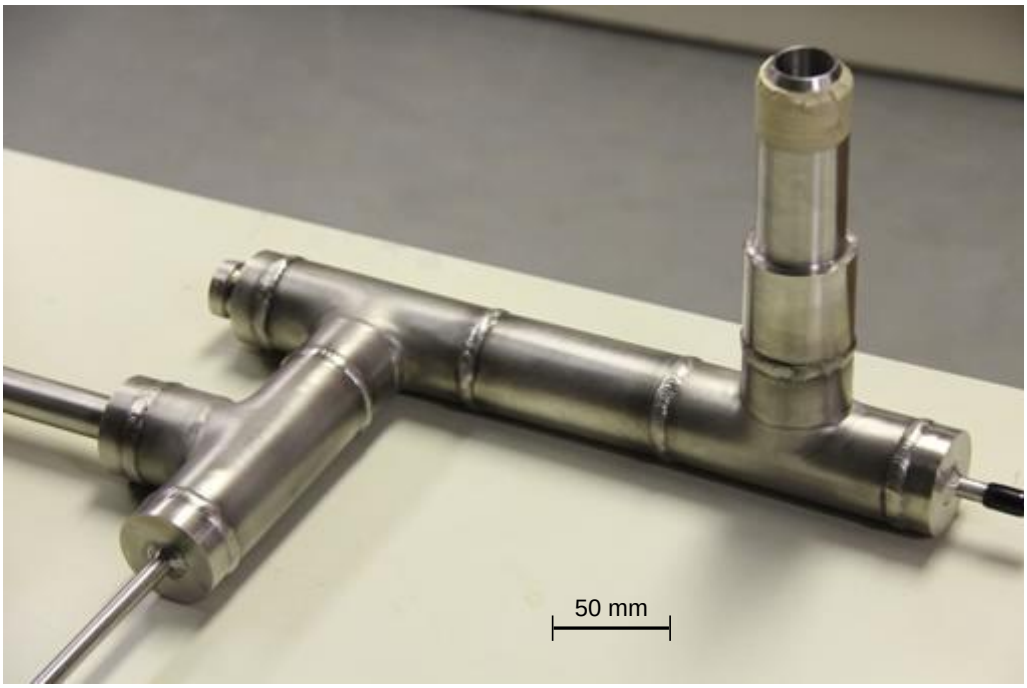

Figure 2.13 Calming chamber.

To satisfy the safety requirements imposed by "Régie du bâtiment du Québec, RBQ[1]", and to protect the loop from undesirable pressure peaks, at the top of the calming chamber, a rupture disc is installed (See Figure 2.2). Moreover, at the same location, the fluid temperature is continuously measured, as it represents a key flow variable necessary for further data analysis.

[1] A copy of the certification of the "Régie du bâtiment du Québec, RBQ" is given Appendix 1.

(Note that this is the last location where the flow temperature is measured before the fluid enters into the test section).

2.2.5 The test section

The test section is manufactured from a Hastelloy C-276 cylindrical bar using Electro Discharge Method (EDM); it is shown in Figure 2.14 and Figure 2.15. As shown in Figure 2.14, the test section is formed by a long straight channel of 4 *mm* ID that interconnects to the calming chamber via a short conical transition piece. At the end of this channel, close to the middle of the test section, 1 *mm* ID sharp edged orifice plate is manufactured with a precision of +0/-0.0002 *in*. The flow discharges from the orifice into a straight channel of 23.8 *mm* ID.

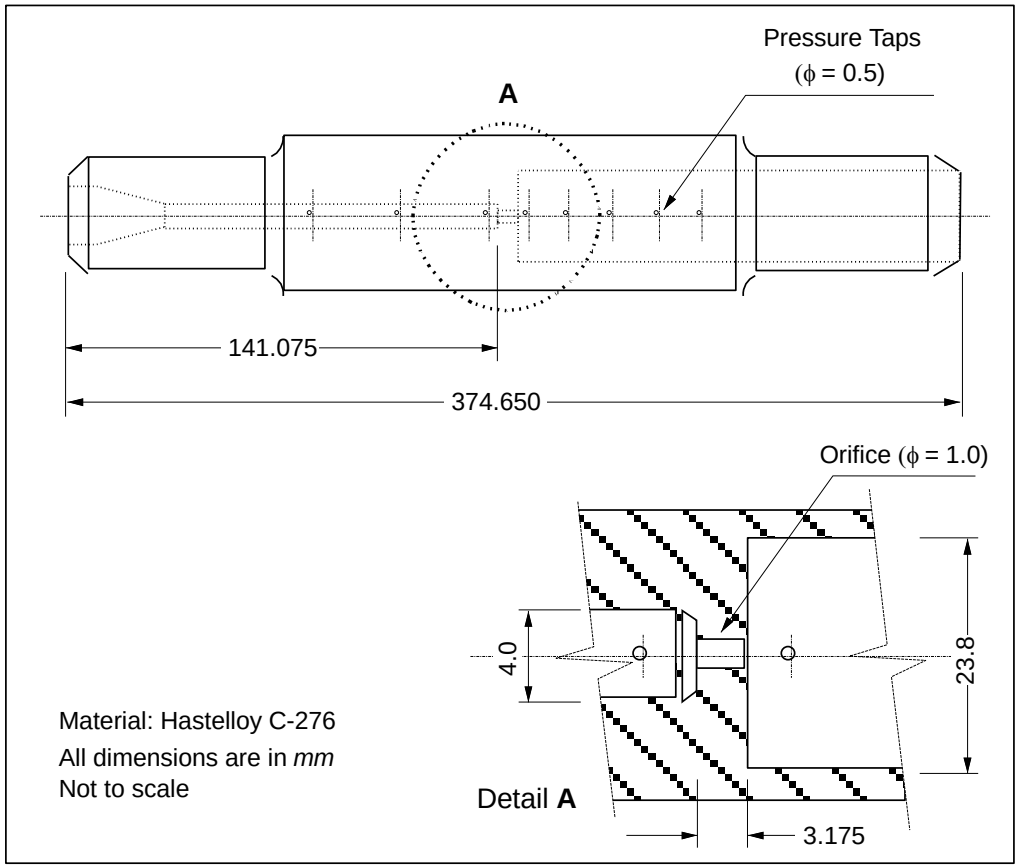

Figure 2.14 Test section with sharp edged orifice.

As shown in Figure 2.14, eight 0.5 *mm* ID pressure taps are manufactured to measure the flow pressure distribution. To guarantee the high manufacturing tolerances required for the nozzle

diameter, making the test section as a one piece was extremely difficult. Therefore, the test section is manufactured from two pieces, welded afterwards as shown in the photo of Figure 2.15. Nevertheless, to this purpose a special attention is given to the location of the welded region not only for safety reasons but also to avoid possible flow effect that it may provoke upstream of the nozzle. Therefore, these pieces are welded on the discharge region, which corresponds to the low pressure side where the flow temperatures are also relatively small, compared to those prevailing in the upstream region.

Figure 2.15 Photo of the test section showing the welded region.

As mentioned before, eight pressure taps (see Figure 2.14 and Figure 2.15) are manufactured to measure the pressure drop along the channel and to determine choking flow pressure profiles around the test section. Three of them are located on the upstream region of the nozzle. They will be used to obtain information on the pressure drop of supercritical water flows in the straight inlet channel. The rest of the pressure taps, located in the downstream region of the nozzle will be used to determine the pressure profile necessary to characterize choking flow conditions.

For safety reasons, the test section and the calming chamber are installed inside a heavy steel enclosure. The upstream and downstream sides of the test section are connected to the high-volume of the calming chamber and to a long discharge pipe, respectively by using Autoclave® fittings where they can support 10000 *psi* (68 *MPa*) at room temperatures. These connectors are not only sealing the test section connections but also they provide extra security to the loop with their special leak relief holes.

® Trademark of Parker Autoclave Engineers

a) The flow expansion in the test section

In this section, we will present the methodology that is used to estimate the critical discharge mass flux as a function of the fluid properties (i.e., flow pressure, flow temperature) to design the supercritical loop. This calculation is essential to determine the maximum experimental conditions that can be eventually covered by the proposed supercritical loop.

For gas flows, frictionless adiabatic isentropic flow or completely isenthalpic conditions cannot be achieved. Figure 2.16 shows two theoretical cases under which a flow can be discharged from a high (supercritical) to a low (subcritical) pressure reservoir. In this figure, blue circle represents one of the flow conditions that could be seen during the anticipated experiment. In Figure 2.16, the flow has the upstream pressure of 23.7 *MPa* and temperature of 500°*C* while the discharge pressure is 0.78 *MPa.* In the figure, the dashed line represents the isentropic expansion and the dotted line represents the isenthalpic expansion. Isobar of 23.7 *MPa*, which passes over the blue circle, is not shown in the figure since it is too close to critical pressure (22.06 *MPa*) isobar, but it is important to mention that it lies between the critical pressure and the 32.1 *MPa* isobars.

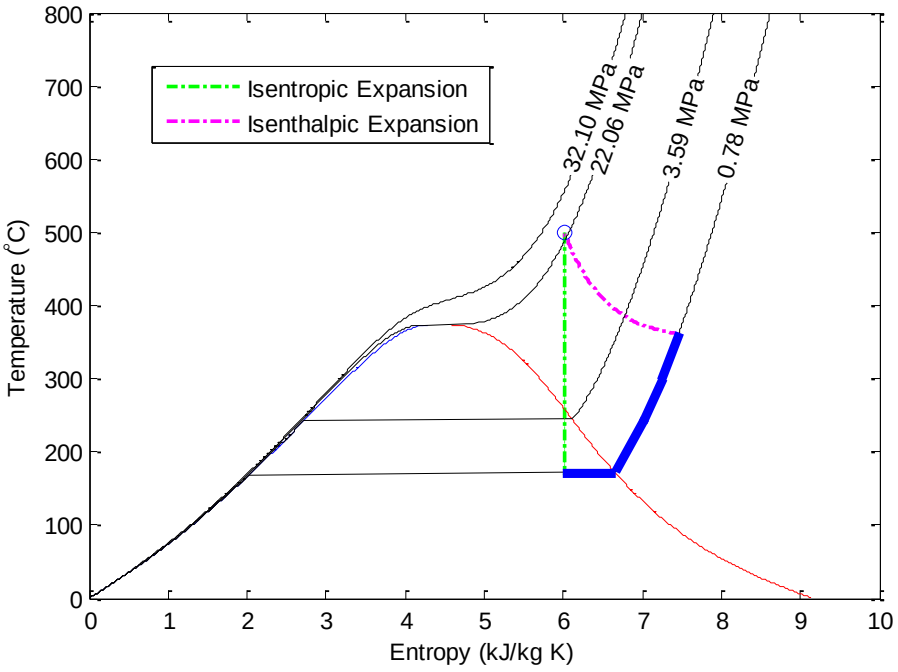

Figure 2.16 Isenthalpic and isentropic expansions from supercritical state.

As mentioned in the literature review in Section 1.6, most of the studies in the literature consider flow expansions as isentropic. However, under real flow conditions this thermodynamic transformation will not occur. As a matter of fact, it is expected that the flow condition after the expansion will be somewhere on the thick blue line. After the experiments that will be performed in this study, the real flow path of the process will be obtained unless the flow expands into two-phase zone. The results will be presented in the following chapters.

In fact, an important aspect necessary for designing the test sections consists of determining the flow conditions that will prevail in the nozzle (i.e., orifice shown in Figure 2.14). For the moment, only upstream and downstream flow conditions are measured on the test section. Therefore, the flow condition in the nozzle itself is predicted using well known equations given in the literature for isentropic expansion of the critical flows. Thus, to perform preliminary calculations of the throat pressure, temperature, fluid density and the critical mass flux, the following equations are used [21, 22]:

$$P_t = P_o \left(\frac{2}{\gamma+1}\right)^{\frac{\gamma}{\gamma-1}} \tag{2.9}$$

$$T_t = (T_o + 273.15°\text{C}) \left(\frac{2}{\gamma+1}\right) \tag{2.10}$$

$$\rho_t = \rho_o \left(\frac{2}{\gamma+1}\right)^{\frac{1}{\gamma-1}} \tag{2.11}$$

$$G_C = \left(\frac{2}{\gamma+1}\right)^{\frac{1}{\gamma-1}} \sqrt{\frac{2\gamma}{\gamma+1}\rho_o P_o} \tag{2.12}$$

where P_o is the stagnation pressure, which in our case corresponds to the pressure prevailing in the calming chamber (Figure 2.2), γ is the isentropic expansion coefficient, ρ_o is the stagnation density, T_o is the stagnation temperature and *t* stands for the throat (critical plane) conditions.

After calculating the mass flux, the pressure, the density and the temperature, one can easily calculate the critical mass flow rate. It is obvious that the real challenge consists of estimating the isentropic expansion coefficient which is not constant during the expansion. As shown in

Figure 2.16, we can expect flow transitions from supercritical to superheated steam and even to two-phase flow conditions. Once the equation (2.12) is solved, the speed of sound and critical mass flow rate are calculated from the following equations:

$$V_C = \frac{G_C}{\rho_t} \tag{2.13}$$

$$\dot{m}_C = G_C A_t \tag{2.14}$$

where *A* is the fluid cross sectional area at the throat. These preliminary calculations have shown that it will be almost impossible to obtain choked flow under supercritical water conditions for a test section having a nozzle (i.e., orifice) diameter larger than 3 *mm*. This limitation is obviously due to the technical characteristics of the pump as well as the specifications of the heater.

2.2.6 The quenching chamber

To satisfy the design criteria of the medium pressure loop, the fluid that comes out from the test section must be cooled down before entering into the steam drum. To this aim, a quenching chamber (shown in Figure 2.17) is designed to cool the outlet flow of the test section to temperature levels compatible with the steam drum.

The quenching chamber is constructed from a carbon steel pipe and its physical dimensions are given in Figure 2.17. It has a flange on top where warm temperature spray nozzle is installed. Moreover, at the upstream of the quenching chamber, a safety valve is used to protect the test section discharge region against accidental closure of the isolating valve or unexpected increase of discharge pressure beyond its maximum limit value. The mass flow rate of the warm water (i.e., at the inlet of the spray nozzle) is adjusted using the valve CV-2 shown in Figure 2.2 and controlled by the response of flow meter FTr-2. Thus, the warm water, derived from the medium pressure loop, is mixed with the flow coming out of the test section in the quenching chamber to reduce the outlet temperature of the test section. Moreover, for the protection of the medium pressure loop, the pipe at the outlet of the quenching chamber is connected to the steam drum via a blocking and check valve.

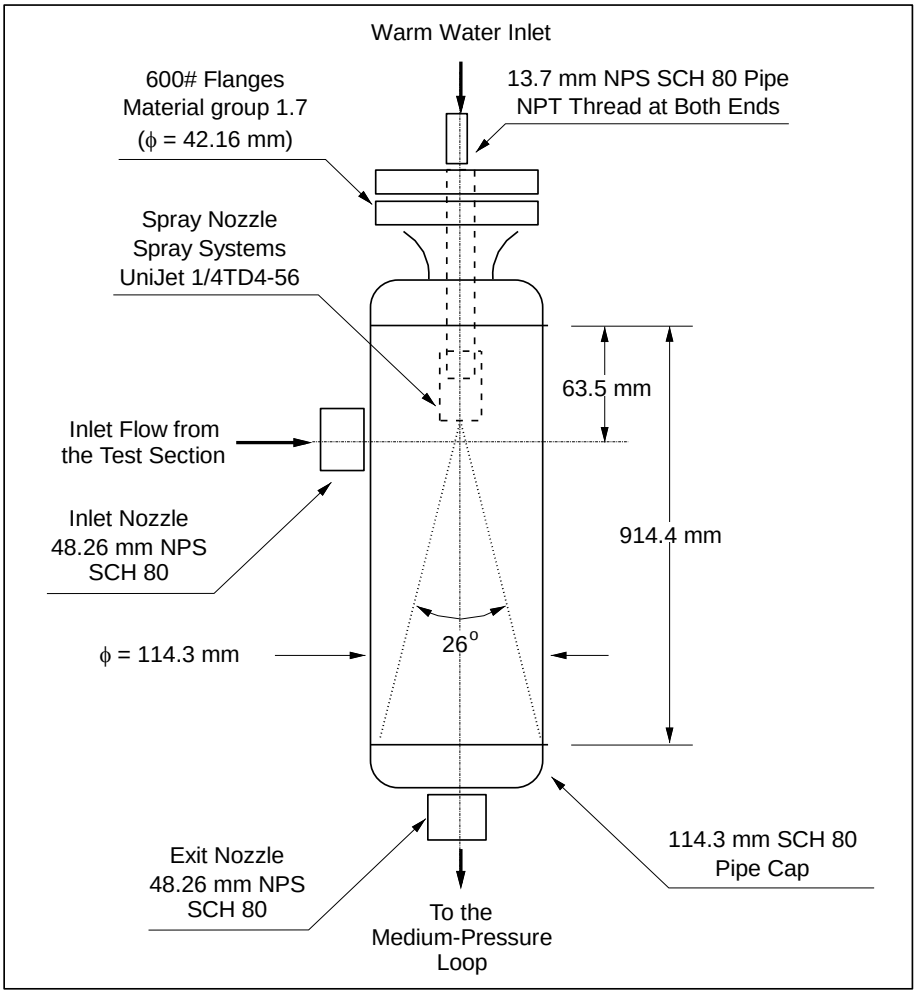

Figure 2.17 Quenching chamber.

2.3 The instrumentation

This section presents the instrumentation used for both controlling the supercritical water loop and collecting data as required by the experiments. All instrumentation and control devices, including electronics, have been verified and/or calibrated by following rigorous protocols. It is important to mention that this is a major requirement to satisfy the Quality Assurance (QA) established by the GEN IV program. Descriptions of calibration and verification tests as well as the results are briefly discussed in the following sections.

2.3.1 The temperature measurement system

Temperatures are measured at several locations by using thermocouples throughout the supercritical water test facility as shown in Figure 2.2. The temperatures at the inlet and outlet of

the high pressure pump are measured using ungrounded type-K immersion thermocouples (Thermoelectric®[1], TTr-1 and TTr-9 in Figure 2.2). A similar instrumentation is also used to determine the coolant temperature at the inlet of the supercritical water loop heat exchangers (TTr-8 in Figure 2.2). All these thermocouples are directly connected to the data acquisition system. It is important to mention that all the temperature measurement devices shown in Figure 2.2 with the designation *TTr* are associated to specific electronic transmitter used to control the loop.

In particular, 31 temperature measurements are implemented using ungrounded 0.8 *mm* type-K thermocouples installed on the heater element (Omega®[2] type U030K). Several of them (i.e., 25 thermocouples) are spot welded to measure wall surface temperatures of the heater element at different critical axial and angular locations as shown in Figure 2.18. This figure shows the exact locations of these thermocouples with their technical designations. Thermocouples identified with *a* and *b* are located on the same axial location but 180 degrees apart. In fact, their locations have been previously selected where the possibility of the occurrence of CHF is high (i.e., close to the elbows where flow reversal may occur and close to the outlet of the heater element). Moreover, they are also located between the heater inlet and the outlet, where possibly fluid phase will change from pressurized liquid to supercritical fluid which can affect the heat transfer. It must be pointed out that all the spot welded thermocouples are used to trip the loop safety system. In particular, they avoid operating the heater element above the maximum allowable wall temperature of $621°C$ as stipulated by the pressure vessel ASME code for Hastelloy C-276 tubes. Thus, it is expected that the thermocouples T46a and T46b located just before the outlet of the heater element, where the maximum surface temperature is supposed to occur, must trigger the safety system. Additional 6 thermocouples on the heater element are used to estimate the heat transfer losses and located in the solid thermal insulation jacket (Foamglass®). Their specific locations will be discussed later.

---

[1] Trade mark of Thermo-Kinetics Company Ltd.

[2] Trade mark OMEGA Engineering inc.

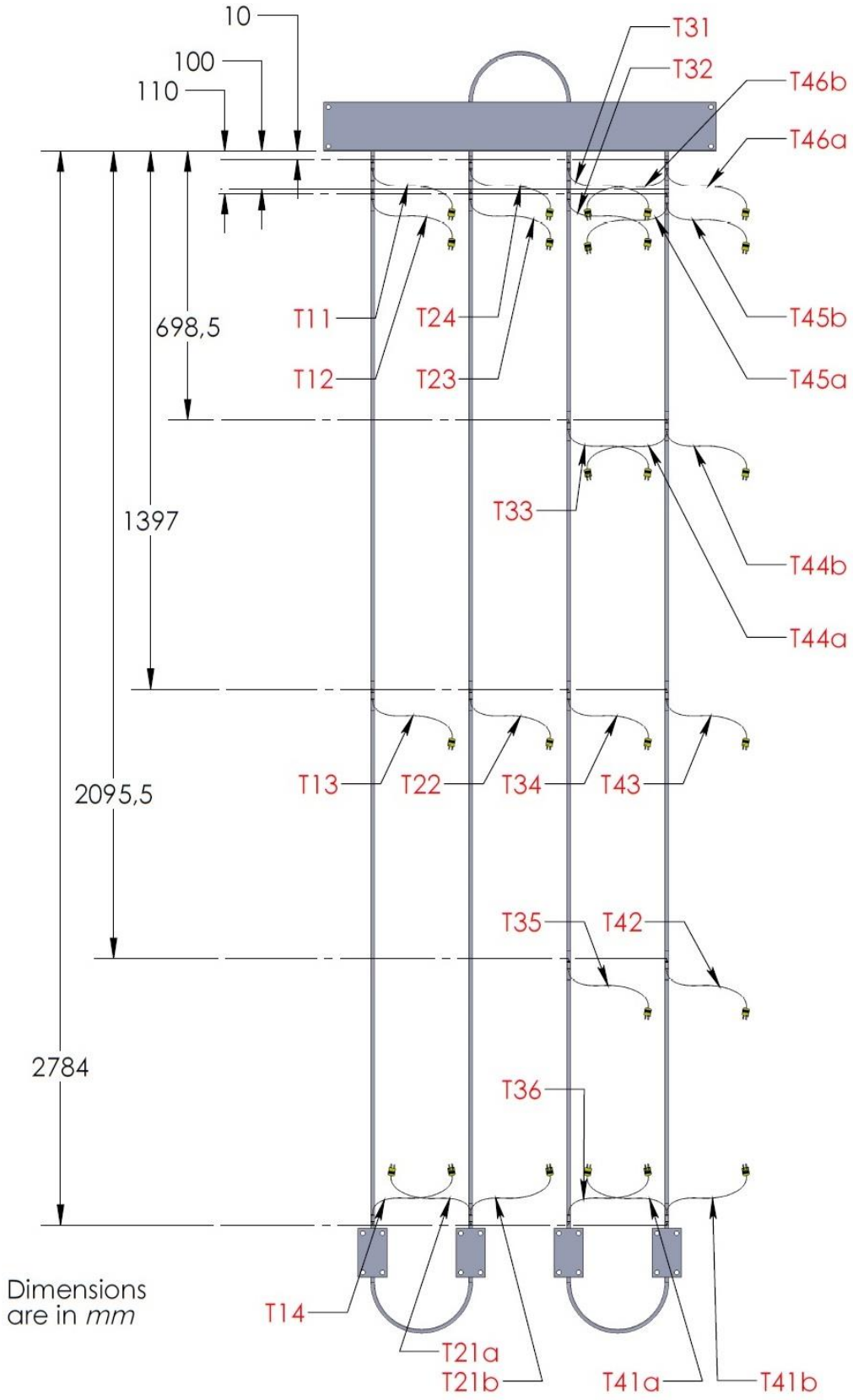

Figure 2.18 Location of spot welded thermocouples on the heater element.

Figure 2.19 and Figure 2.20 show the technique implemented to spot weld the thermocouples on the external surface of the heater element. Spot welding was performed by using UNITEK-125®[1], model 1-163-03 welder machine. Only the tip of the thermocouple was welded using a single pulse of 50 Watts-seconds. As shown in the same figures, each thermocouple was maintained in place by using small ceramic tubes (i.e., 2 *cm* long). They allow thermocouples to be mechanically stable without being in electrical contact with the wall of the heater element tube which under operation is alive. Furthermore, each ceramic tube is fixed in place using metallic strips made from 0.1 *mm* thick Hastelloy C-276 sheet (see Figure 2.19). These strips are also spot welded using 30 Watts-seconds of energy. These energy levels were determined by performing several tests on separate Hastelloy-C276 sampling tubes. Convenient criteria were determined by visual observation, to limit possible damages on both thermocouple tips and the surface of the tube. Note that thermocouple is slightly bended to avoid heat conduction effect on the temperature measurements. Since the heater element will expand with temperature and will create some shear force between the heater tubes and the insulation material, high temperature chemical set cements (Omegabond®[2] 600) are used for final mechanical consolidation.

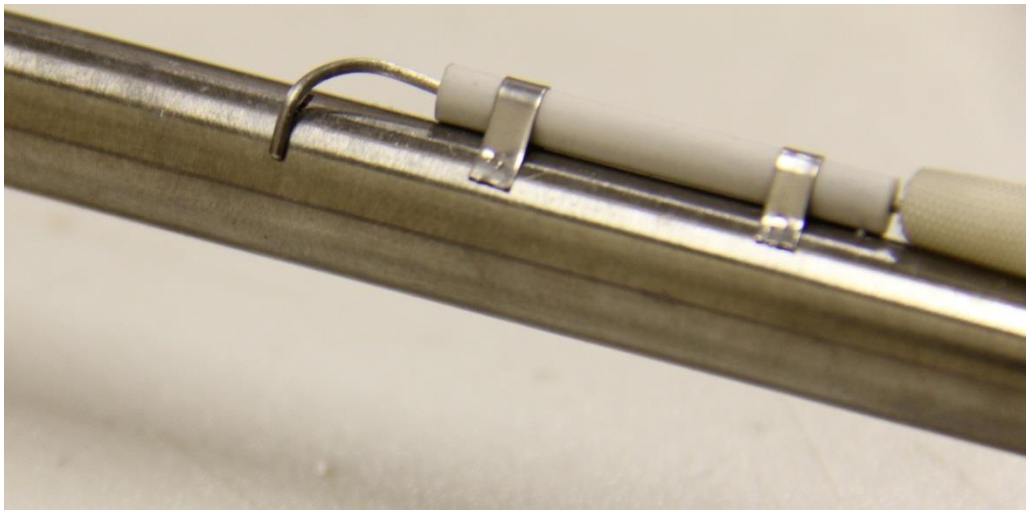

Figure 2.19 A typical spot welded thermocouple on the heater element external surface.

[1] Trade mark of Unitek Corporation.

[2] Trade mark of Omega Engineering Inc.

After thermocouples are installed, their electrical continuities and galvanic isolations are individually tested. A quality criterion of 25 *Ohms* for continuity and more than 10^{12} *Ohms* for electrical isolation is applied to all of them.

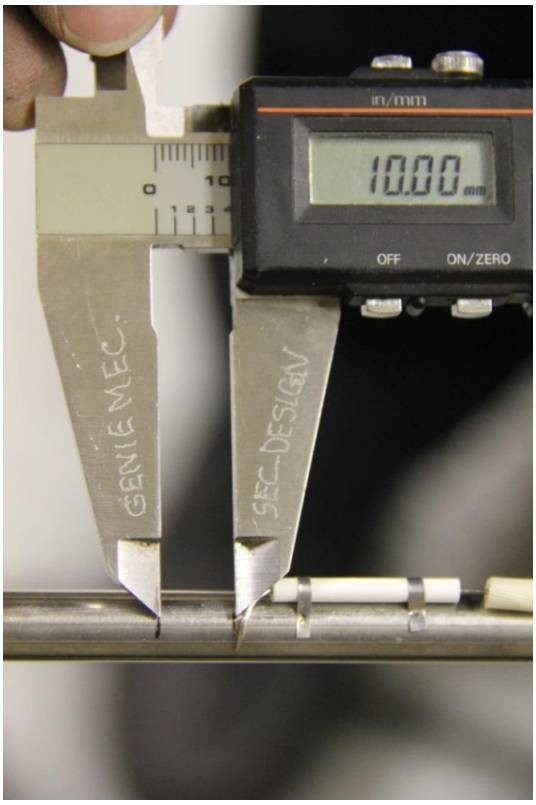

Figure 2.20 Distance measurement between a thermocouple and the copper bus bar.

The distances between the thermocouples that are close to the copper bus bars are determined very accurately using a caliper having a precision of ±0.005 *mm* as shown in Figure 2.20. Longer distances are measured with a tape having a precision better than ±0.5 *mm.* For two different axial locations, close to the outlet of the heater element, similar thermocouples are also installed at different radial positions inside the thermal insulation jacket. As mentioned before, this thermal insulation is made of solid Foamglass® cylinders. These temperature measurement devices are used to estimate heat losses from the heater element to the environment. Figure 2.21 shows the positions of these thermocouples inside the cross section of the heater element assembly; the installation procedures are shown in Figure 2.22 and Figure 2.23. As shown in Figure 2.23, a high temperature chemical cement (Omegabond® 600) is used to keep these devices in place. After installation, their electrical continuity and galvanic isolations are also

tested by applying the same procedure used for spot welded thermocouples. It is important to mention that radial thermocouples T45 R1, T45 R2, and T45 R3 are placed at the same axial position of thermocouples T45a and T45b; the same methodology applies to thermocouples T46 R1, T46 R2, and T46 R3 (see Figure 2.18).

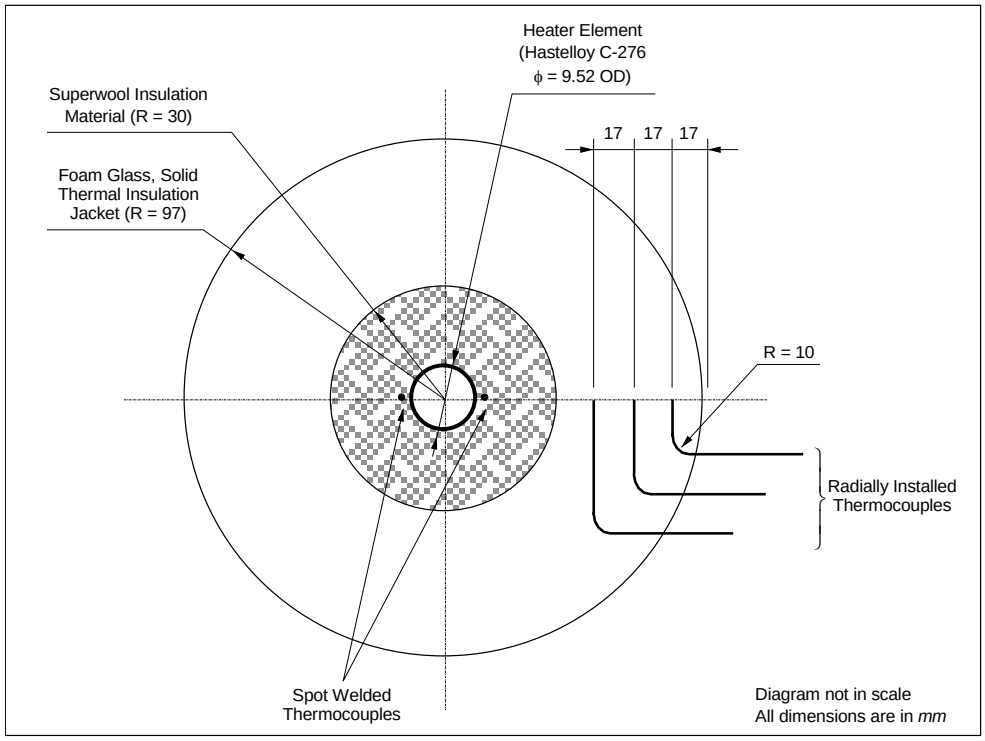

Figure 2.21 Cross-sectional view of the heater element assembly.

Since the heater element is electrically alive and up to 110 *V* DC of potential can be applied to increase the fluid temperature, thermocouples that are spot welded on the external wall of the heater element are subjected to the electrical voltage that will be developed at their respective locations. Thus, their measurement signals must be electrically isolated. This is performed by using Keithley®[1] MB47 thermocouple galvanic isolation amplifier. Hence, each thermocouple is wired to its own galvanic isolation unit before the signal is connected to the data acquisition system. Figure 2.24 shows a photo of this temperature measurement system. Each of these units not only isolates thermocouples but also amplifies and linearizes the signal from *mV* to 0-5 *V*

[1] Trade mark of Keithley Instruments Inc.

levels. Therefore, only the amplified and linearized measurement signals are transferred to the data acquisition system.

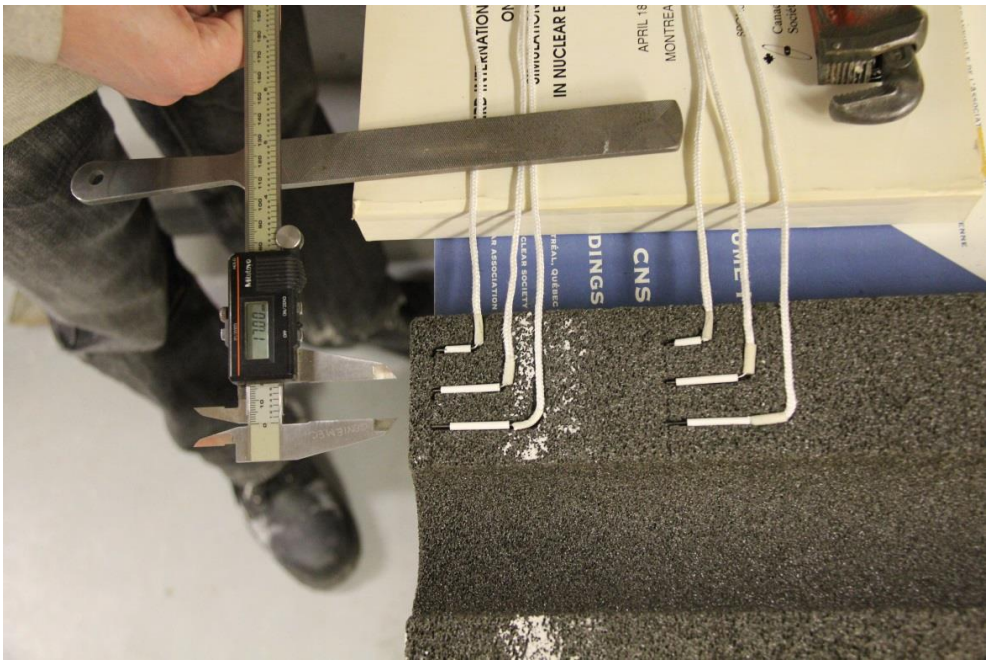

Figure 2.22 Installation procedure of radially positioned thermocouples.

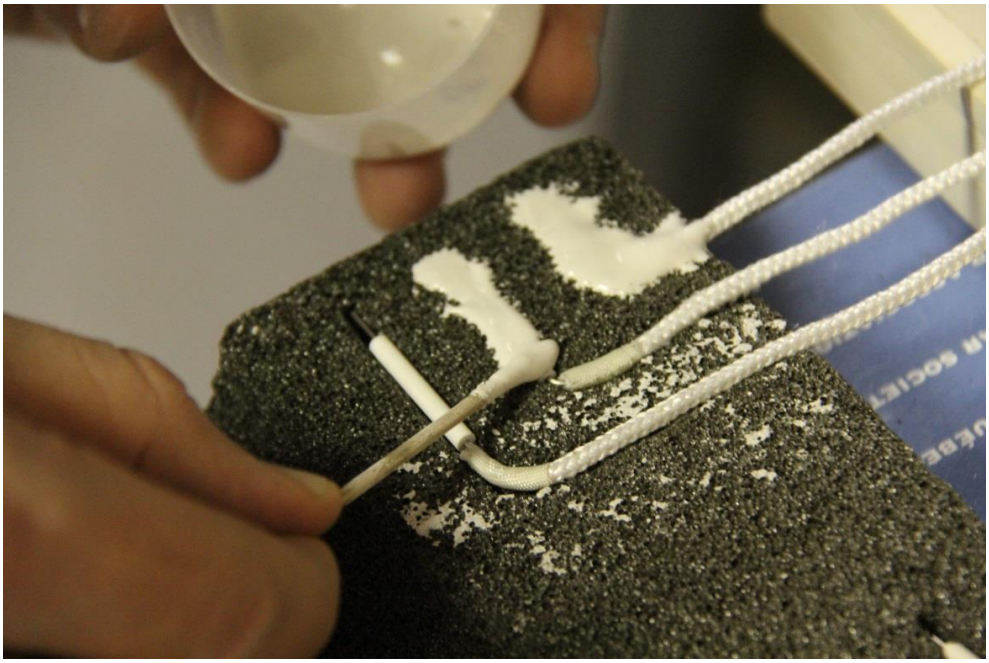

Figure 2.23 Installation procedure of radially positioned thermocouples – application of a chemical cement (Omegabond® 600) fixation layer.

Figure 2.24 Partial view of the temperature measurement panel and the galvanic isolator amplifiers.

a) Calibration of heater element thermocouples

Before installation, all of the thermocouples are calibrated by covering a wide range of temperatures up to 600°*C* by following a special procedure and using a high accuracy thermal calibration block, Thermo-Kinetics® Model TK-3541-HL-FL-LL and an Omega® cold junction S/N 70818533. Multimeter responses are then compared with data given in Type-K Reference Tables, NIST, Monograph 175, Revised ITS-90 [119]. Nevertheless, it is important to mention that, once thermocouples are installed on the heater element, their calibration becomes impossible. Therefore, all the calibration (or verification) of the thermocouples are performed before they are spot welded; typical calibration results for 10 thermocouples are shown in Figure 2.25. As observed in this figure, with the exception of thermocouple #4, for the range of temperature covered, the maximum estimated errors are lower than 2%. These temperature calibration data are then used to determine the correct values of the temperatures required by choking flow experiments. It must be pointed out that higher differences occur only for a calibration temperature of 600°*C*. This high dispersion can be explained by the long period required to achieve the thermal stability of the calibration thermal block. In fact, the higher is the calibration temperature the longer is the time required to obtain thermal steady state conditions.

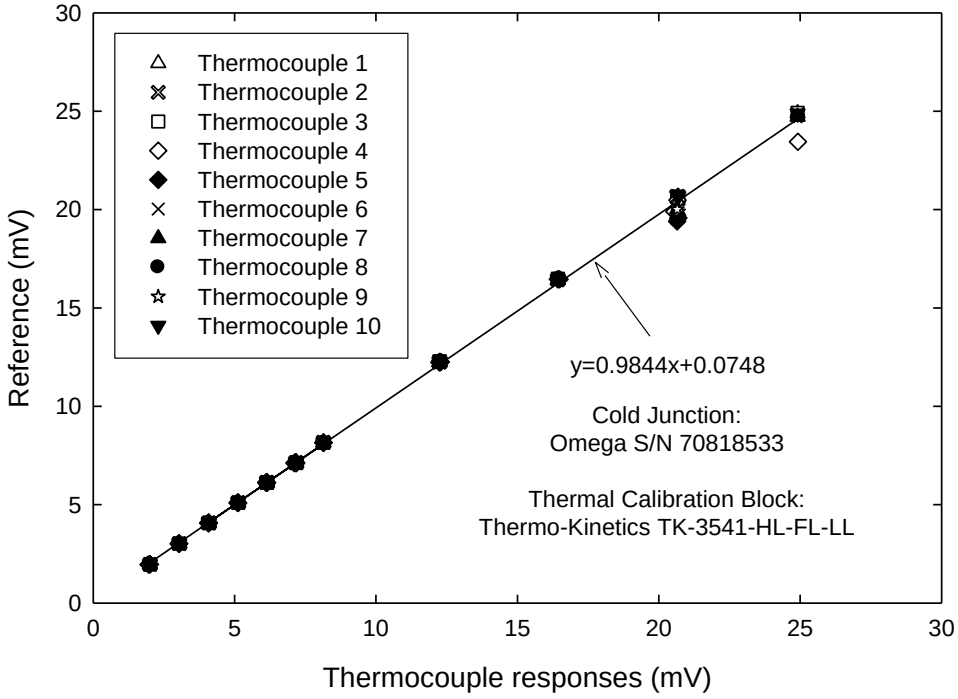

Figure 2.25 Typical calibration of type-K thermocouples used in the heater element.

In Figure 2.25, it is also shown that some thermocouples' responses deviate from the reference list [119]. These thermocouples are replaced with the new ones until all the thermocouples have almost the same (acceptable) responses for the range of experiments. Later, all of the thermocouples responses are obtained using the galvanic isolation amplifiers with all the wire connections up to the data acquisition system keeping the room temperature at $25°C$. Responses obtained from these tests are shown in Figure 2.26 where excellent precision measurements are ensured. This procedure is not only applied to the thermocouples that are used on the heater element, but also to the thermowell and the immersion thermocouples that are used in the rest of the loop. Finally all of the temperature measurement devices are connected to the data acquisition system with the same galvanic amplifiers. Accordingly, almost the same precision is obtained in the whole loop.

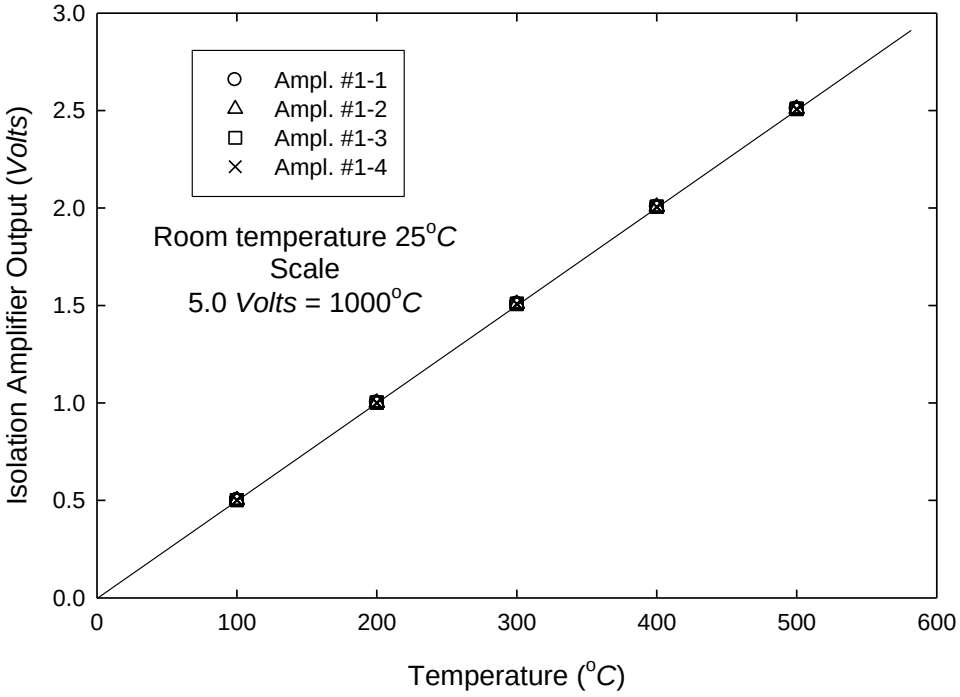

Figure 2.26 Typical responses of the entire temperature measurement chain including thermocouples, wires, galvanic isolation amplifiers and data acquisition system.

b) Calibration of supercritical loop control thermocouples

Several thermowell and immersion thermocouples are simultaneously used to measure process variables that control the loop and to determine key parameters necessary to perform data analyses. As shown in Figure 2.2, most of these devices are installed in loop locations where both high pressure and high temperatures may exist.

These temperature transducers, indicated as TTr-1 and TTr-5 to TTr-9 in Figure 2.2, are also tested by using the same thermal block and control device described in the former section. Because, these devices have high thermal inertia, they were tested up to 600°*C* but using a higher range of temperature increments; the typical calibration results are shown in Figure 2.27. Even though more than 1 *h* of thermal stabilization is applied before collecting each calibration data point, some discrepancies are also observed for high temperature values. In fact, for 600°*C*, the errors are about 1%. The measurements were repeated several times; however they do not appear in the figure because most of these points overlap. The calibration data are used to fit appropriate

polynomials which are then programmed in the data acquisition software. The results obtained using these functions are then considered to provide the most likely temperature values.

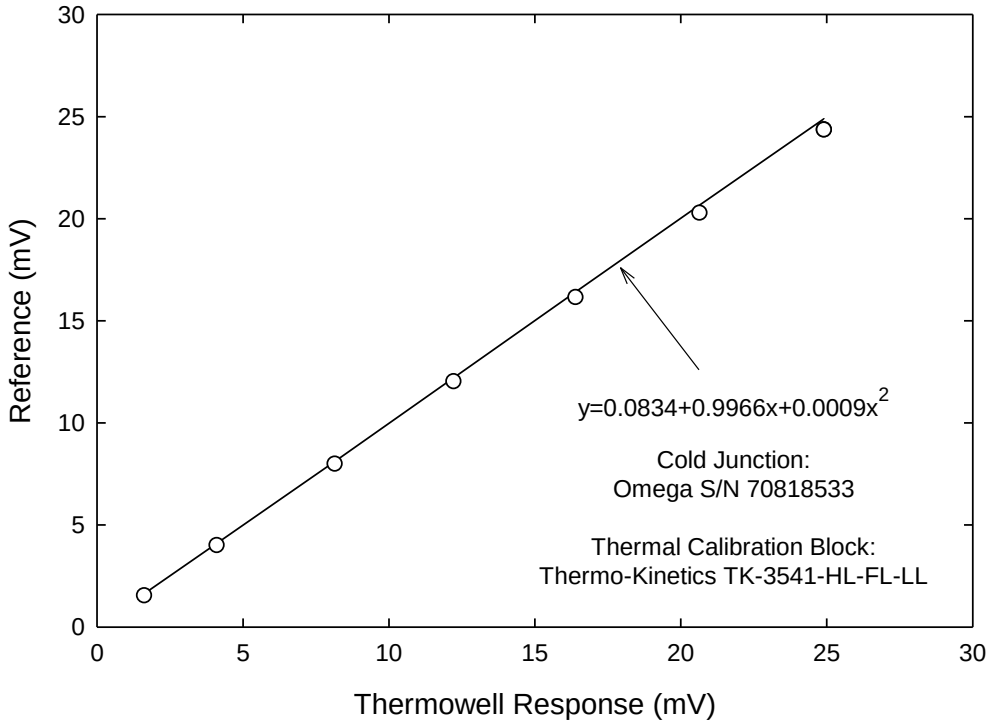

Figure 2.27 Typical calibration data obtained for a Thermowell®.

2.3.2 The flow pressure measurement system

As shown in Figure 2.2, six Sensotec (Honeywell®[1]) absolute pressure transducers are used to measure the pressure at different locations of the supercritical water loop. Pressure at the inlet and outlet of the pump, on the calming chamber and as well as at the discharge section of the loop are measured not only for control purposes but also for the safety of the loop.

The test section is instrumented with eight pressure taps (see Figure 2.28); three of them are located upstream of the nozzle (i.e., orifice) and five downstream. It must be pointed out that due to the high pressure of the fluid and the huge pressure gradient that is expected to occur across

[1] Trade mark of Honeywell International Inc.

the orifice, it is impossible to use pressure-multiplexed devices. Each pressure tap in the test section consists of 0.5 *mm* ID holes manufactured using EDM technique. The size was selected according to manufacturing capabilities, but also as small as possible to avoid any eventual flow perturbations. Each pressure tap is connected to the pressure cells using individual 3 *mm* (1/8 *in*) stainless steel tubing (see the photo in Figure 2.15). Note that the pressure measurement performed in the calming chamber (Figure 2.28) can also be considered as part of the test section pressure measurement system.

Table 2.6 Technical information of the pressure transducers used on the test section.

Identification number	**Pressure transducer serial number**	**Pressure range (*psi*)**	**Full scale precision (*%*)**	**Output signal (*V*)**
PTr-1	AP122 DR / 1371378	0-5000	±0.1	0-5
Px-1	AP122 DR / 1372491	0-5000	±0.1	0-5
Px-2	AP122 DN / 1364591	0-3000	±0.1	0-5
Px-3	TJE/727-22 / 270097	0-750	±0.1	0-5

As can be observed in Figure 2.14 and Figure 2.28, provisions are made to measure the pressure as close as possible to the nozzle (i.e., 1.6 *mm* upstream and 1.6 *mm* downstream) not only for the accuracy of the experimental parameters but also to see if upstream high flow pressure can penetrate to downstream or not. Figure 2.28 shows the schematic of the test section and the calming chamber with pressure lines and the pressure transducers. In this figure, upstream pressure lines are identified by H-1, H-2 and H-3 and downstream pressure lines are identified by L-1 to L-5 where H and L are representing high pressure and low pressure, respectively. In general, lines that are red colored will be used to perform choking flow experiments since they are the ones closest to the inlet and outlet of the nozzle. If pressure drop experiments are to be performed, other lines will also be used according to the experiment. Not all the pressure taps will be connected to pressure cells during the experiments; therefore, Figure 2.28 shows the four Sensotec (Honeywell®) pressure cells that are used to perform the choking flow experiments. Pressure transducers on the test section and the calming chamber let us determine the pressure

profile and see if the flow is choked or not. Table 2.6 provides information about these instruments.

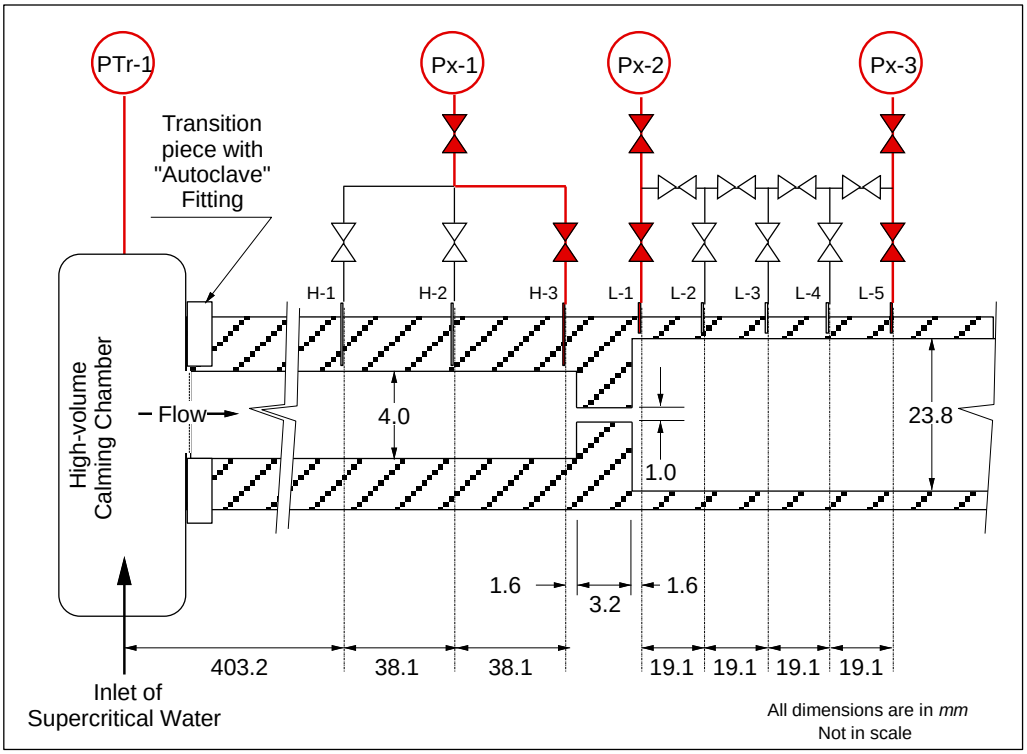

Figure 2.28 Location of pressure taps and pressure lines (in red) used to perform choking flow experiments.

Even though high pressure transducers were already calibrated by the manufacturer, their calibrations are also re-tested and the values are given in Appendix 1. On the other hand, medium pressure transducers are calibrated using Druck Multichannel Pressure Calibrator®[1], Model DPI-602 containing absolute pressure cells with accuracies better than ±0.1% full scale. Furthermore, necessary atmospheric conditions are obtained daily from Environment Canada at Dorval to properly perform these calibrations. Figure 2.29 shows calibration curves obtained for two absolute pressure transducers; comparative tables that present responses of these instruments are given in Appendix 1. For each transducer, the calibration verification test is repeated twice, by

[1] Trade mark of GE Measurement & Control

increasing and decreasing the calibrator pressure. This procedure permits eventual hysteresis effects to be also determined. In general, we have observed that all pressure transducers have accuracies better than ±1% of the readings.

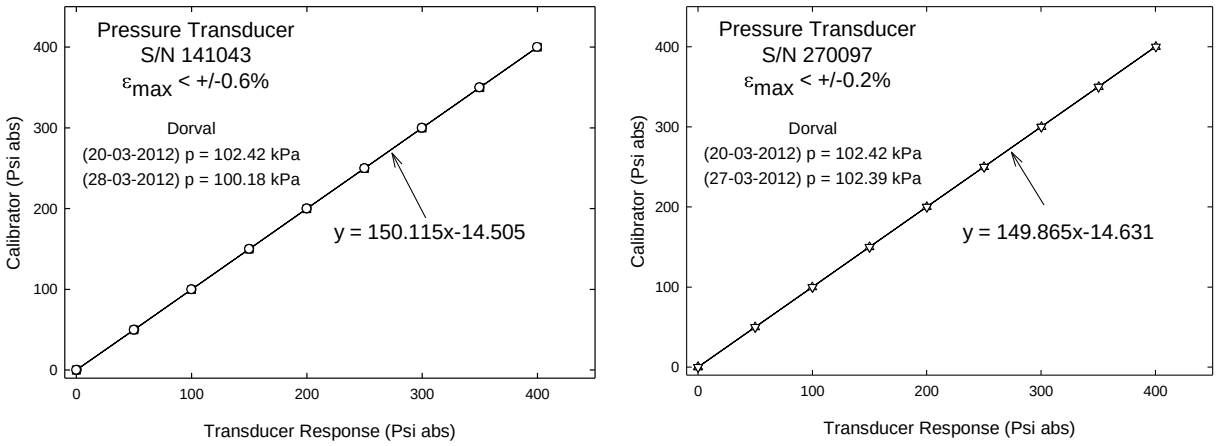

Figure 2.29 Responses of medium pressure transducers.

2.3.3 The control valves

All control valves shown in Figure 2.2 are pneumatically driven through 4-20 *mA* electronic control loops. To validate their correct operation and calibrate their opening or closing positions, a voltage to current converter is manufactured. This circuit configuration permits very accurate and stable control signals to be generated. Thus, the proposed instrument is able to convert voltages from 0 to 5 *V* into 4 *mA* to 20 *mA* with a very good accuracy of +/-0.03 *mA*.

Correct operations of the control valves are essential for the safety of the loop since they are used to control the inlet and outlet key fluid temperatures of the loop; their calibrations are given in Appendix 3.

2.3.4 The flow rate measurement system

As it was already determined in Section 2.2.3, we have estimated the flow rate at choking flow conditions for different orifice sizes. In particular, for a 1 *mm* ID nozzle, which constitutes the first test section to be used to perform the experiments, the mass flow rate will be quite low

(approximately between 0.018 *kg/s* and 0.125 *kg/s* depending on the flow temperature). Moreover, near the pseudo-critical region, while the fluid temperature increases the mass flow rate is expected to decrease quite fast; therefore, an excellent time response is required by the flow meter. To this aim, we have selected a Flow Technology® frequency modulated (FM) type of turbine flow meter that covers a range (extended) of 0.01 to 0.32 *lt/s*, with an uncertainty of ±0.05% at full scale to measure the flow rate that passes through the 1 *mm* ID nozzle. This unit is designated as FTr-1 in Figure 2.2. It must be pointed out that this kind of flow meters is very suitable for measuring very low flow rates with relatively high precision. In fact, it has its own frequency to current converter and electronic linearizer. This unit was already calibrated when purchased and came with its calibration data sheet.

A second flow meter was also necessary to control the flow rate of warm water required by the quenching chamber (see Figure 2.17 and section 2.2.6); it is designated as FTr-2 in Figure 2.2. Previous heat balance calculations have shown that the maximum required flow rate should be approximately 2 *L/s*. Therefore, we have selected standard high temperature turbine type Flow Technology® flow meter. This unit has its own pick-off coil but a separate electronic converter unit. Similar to the former one, the manufacturer provided us its calibration data sheet.

After these flow meters are installed in the supercritical water choked flow loop, their calibration are validated for different flow rate conditions by weighting the water at constant temperature for a relatively long period of time (i.e., longer than 120 *s*). Figure 2.30 shows the data collected for warm water flow meter FTr-2 of the calming chamber.

This figure shows that the response of this unit follows the calibration data provided by the manufacturer and has a linearity better than ±0.1% and accuracy better than ±0.05% of the reading. It must be pointed out that the responses of each unit include the entire electronic chain (i.e, from the instrument up to the data acquisition system).

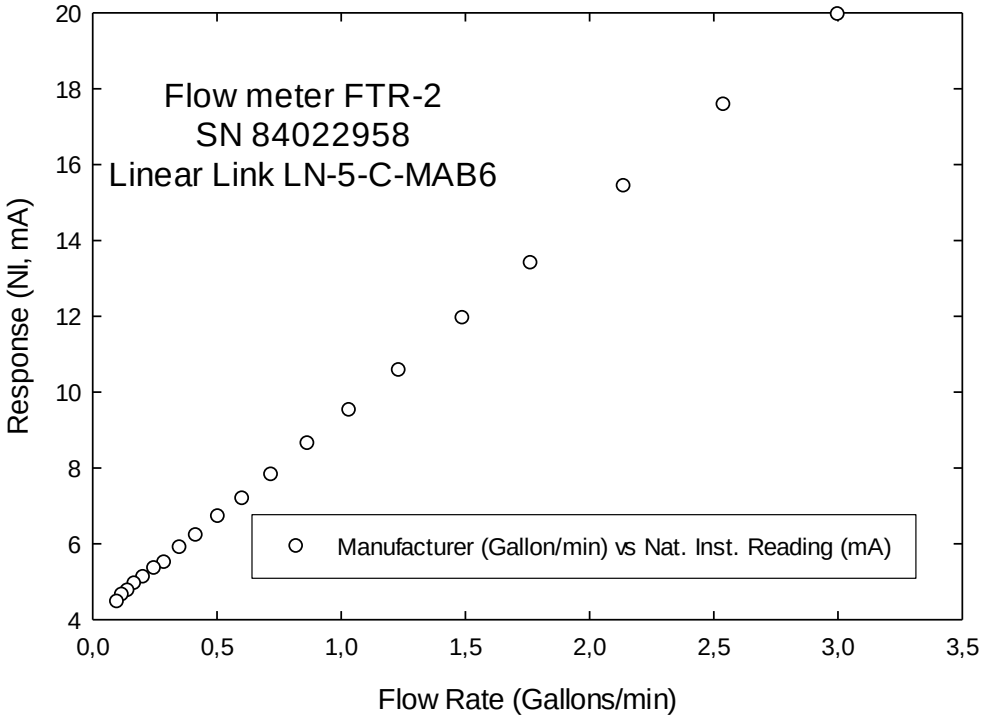

Figure 2.30 Flowmeter (FTr-2) response.

2.3.5 The electrical power measurement system

The thermal power applied to the heater element is determined by using two different set-ups implemented in the power measurement station shown in Figure 2.31. The first system consists of a high precision class 0.5 shunt (Simpson®[1] Model 5000/50 ±0.5%) connected in series with the heater element. As shown in the figure, this unit is also used by the 550 *kW* power controller where the electrical power is determined by the product of response of this shunt (i.e., maximum of 50 *mV* for 5000 *A*) and the DC voltage measured across the point "*A*" and the ground. A second power measurement system is implemented around a Hall Effect electrical current measurement instrument, 5000 LEM shown in the Figure 2.31 and Figure 2.32. In this case, the response of this device (i.e., 15 *V* for 5000 *A*) is multiplied to the same electrical potential

[1] Trade mark of Simpson Electric

difference read between point "*A*" and the electrical ground by the program written in Labview™[1].

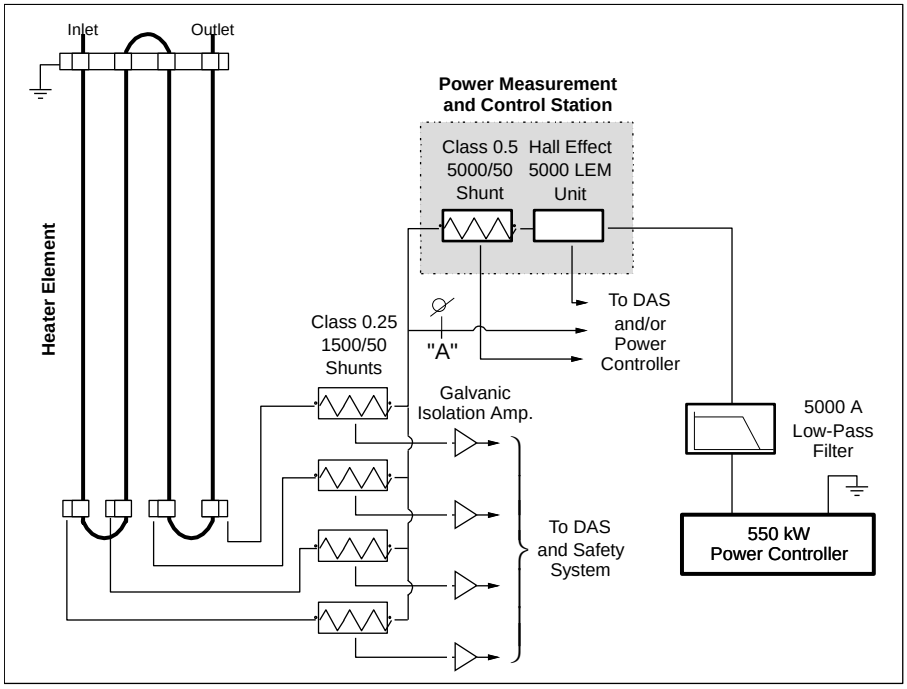

Figure 2.31 Power measurement and control station.

As shown in the Figure 2.31 and Figure 2.32, four high precision electrical shunts (ITM®[2] Model 1500/50 Class 0.25) are used to measure the current passing through each of the heater branches. They are simultaneously read by the DAS via 5 *V* galvanic isolation amplifiers. The principal purpose of these additional shunts is to determine any eventual electrical current unbalance that could be triggered either by electrical resistance difference between the branches (i.e., due to high temperature differences) or by electrical misconnections that could occur in the bus bars. Note that the presence of these shunts introduces an additional electrical potential difference which appears at the measured point "*A*" (see Figure 2.31) with respect to ground. Nevertheless at maximum power conditions, the systematic error they introduce is lower than -0.05%.

[1] Trade mark of National Instrument.

[2] Trade mark of ITM Instruments Inc.

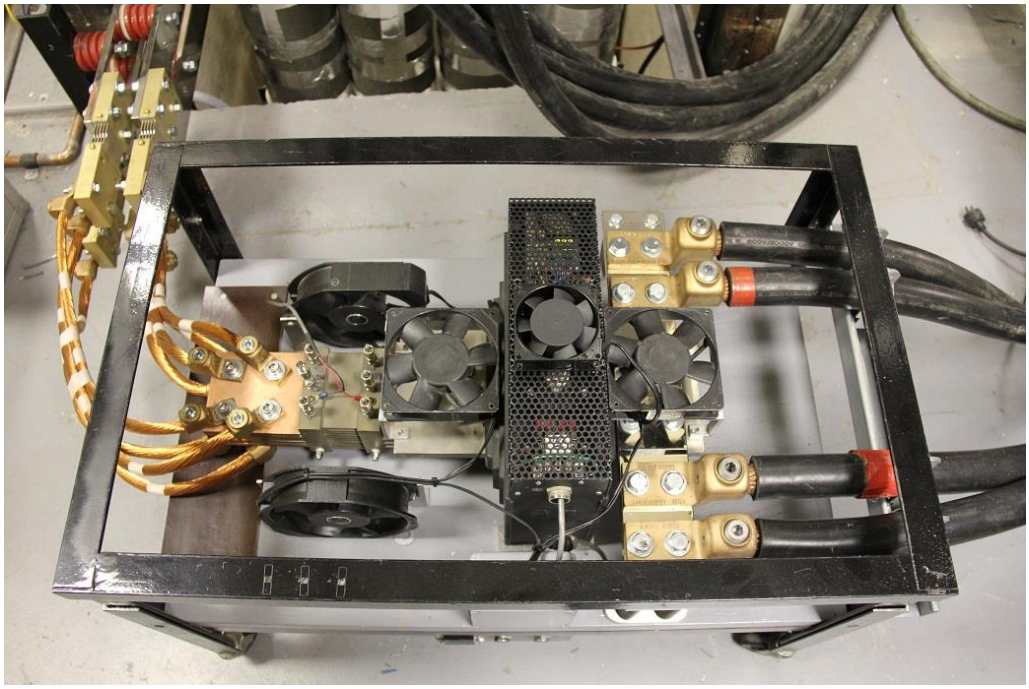

Figure 2.32 Electrical current measurement devices.

As shown in Figure 2.31, the electrical power applied to the heater element is first filtered using a 5000 *A* Low Pass Filter (LPF). In fact, the power controller uses Silicon Controlled Rectifiers (SCR) which tend to generate high frequency electrical noise. Thus, the use of the LPF allows this noise to be alternated by factor higher than 40 *dB* with a corner cut-off frequency at about 150 *Hz*.

Before starting the experiments, the complete power measurements and control set-ups are tested by replacing the heater element by several 110 *V* carbon filament light bulbs connected in parallel. Hence, the performance of the system is completely verified for varying electrical powers within the range of 0-10 *kW*; Figure 2.33 shows a photo of this set-up.

Figure 2.33 Carbon filament light bulb system to commission the electrical power.

2.4 The data acquisition

A stand-alone National Instrument® (CompactRIO NI-9074) data acquisition system (DAS) has been selected to perform both data collection and control of the supercritical water loop. However, since some flow variables of the medium pressure steam water loop are also necessary to treat choking flow, they are collected by the same DAS. As shown in Figure 2.34, the DAS include a wide variety of Input / Output (I/O) modules. Some of them are entirely used for reading the temperatures while others are devoted to handle the 4 *mA* to 20 *mA* signals required for control purposes. Detailed information about the National Instrument® modules used to implement the DAS is given in Table 2.7. As shown in Figure 2.34, the DAS contains its own programmable memory ("Field-Programmable Gate Array", FPGA) which allows to store up to 512 *MB* of data at a maximum collection rate of 8 μs*/sample*. Both, the logic unit and the memory of the DAS can be accessed by an external computer via an Ethernet interface.

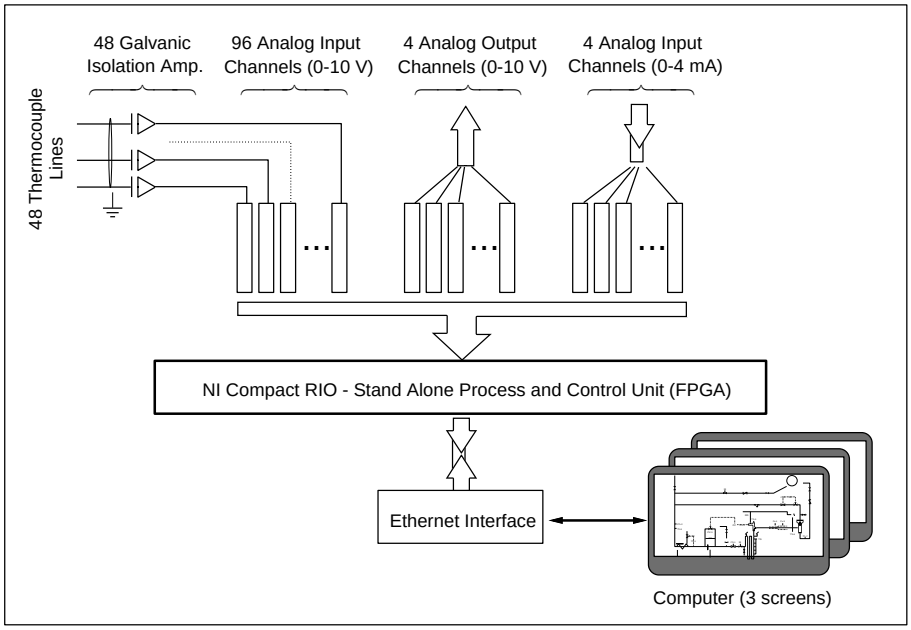

Figure 2.34 Data acquisition system.

The DAS as well as its power supply are installed in a completely shielded (i.e., grounded) separate enclosure. It is interconnected to the computer via a high quality cable. For this unit, we have selected Intel® Core™[1] i7-3820 CPU @ 3.60 *GHz* with 8 *Gb* of RAM and 1 *TB* of hard drive. It has a specialized video card that controls three monitors simultaneously. They are used to have a live view of key flow variables, control units and oscilloscope charts necessary to perform the experiments. Figure 2.35 to Figure 2.37 show screen shots of each of these monitors. To this purpose, the Labview™ software is used to program data acquisition and control process. A copy of the implemented software is given in Appendix 4 and also available upon request.

It is important to mention that in order to avoid slowing down the data collection process and reducing overheat communications between the computer and the DAS, the data presented in the screens are refreshed each 0.75 *s*. Nevertheless, to limit the total amount of data stored along each experiment, the sampling rate is fixed to 100 *ms/sample*. Note that this value is also selected in accordance with the lowest band-pass of the entire instrumentation (i.e., 5 *Hz*). In fact, the selected sampling rate corresponds to the Nyquist frequency, which avoids data aliasing to occur.

[1] Trade mark of Intel

Table 2.7 Technical information of the NI modules used on DAS.

NI module	Function	# of channels	Application
NI 9205 (3 times)	Analog Input (voltage)	96	Temperature, Pressure, Flow rate, Heater voltage, LEM, Heater Shunt, BEEL
NI 9263	Analog Output (voltage)	4	Block Valve and System Trip
NI 9265	Analog Output (current)	4	Control Valve

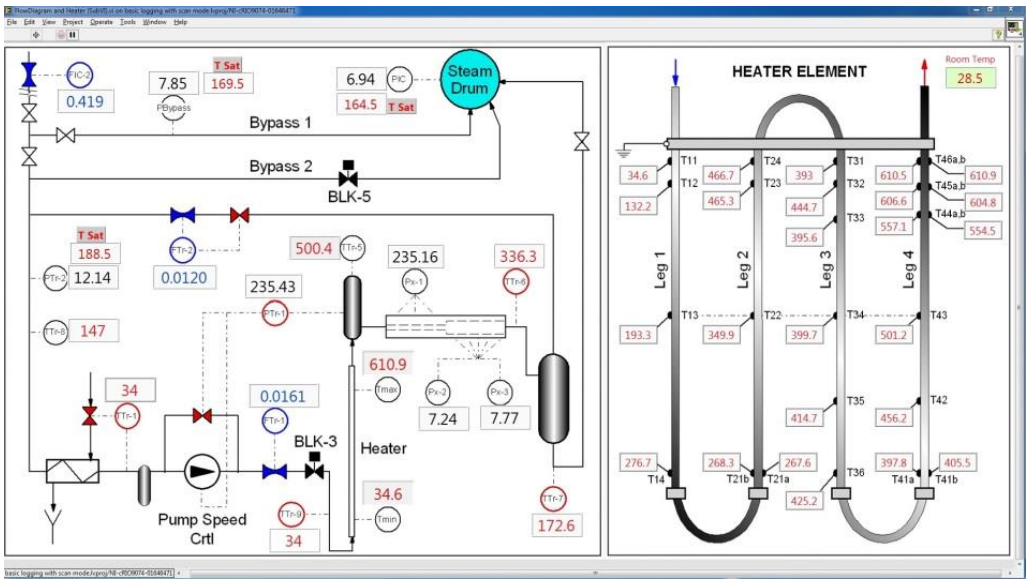

Figure 2.35 Process variables screen shot.

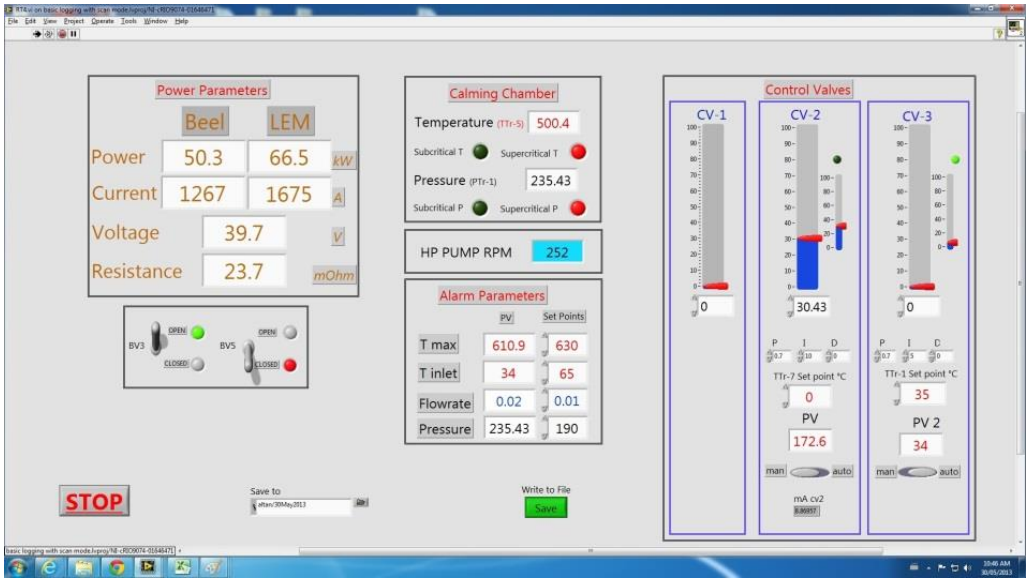

Figure 2.36 Control variables screen shot.

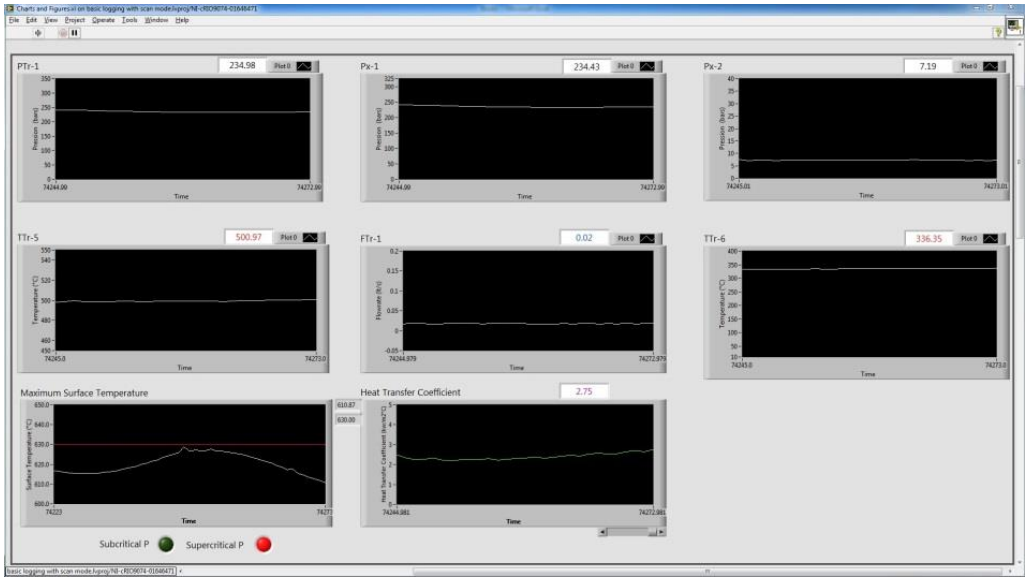

Figure 2.37 Variable charts screen shot.

CHAPTER 3 EXPERIMENTAL METHOD

In this chapter, the methodology to be used for carrying out choking flow experiments is discussed in detail. It is important to mention that the procedures described herewith may necessitate small modifications after performing future experiments.

3.1 Experimental conditions and procedures

The experiments presented in this thesis are intended to characterize choking flow phenomenon of water at supercritical conditions as a function of fluid properties. To this aim, we propose an experimental set-up and a methodology that will permit conditions that bring about choking flow to be determined unambiguously. Therefore, the experiments are performed using two loops running in parallel, as shown in Figure 3.1.

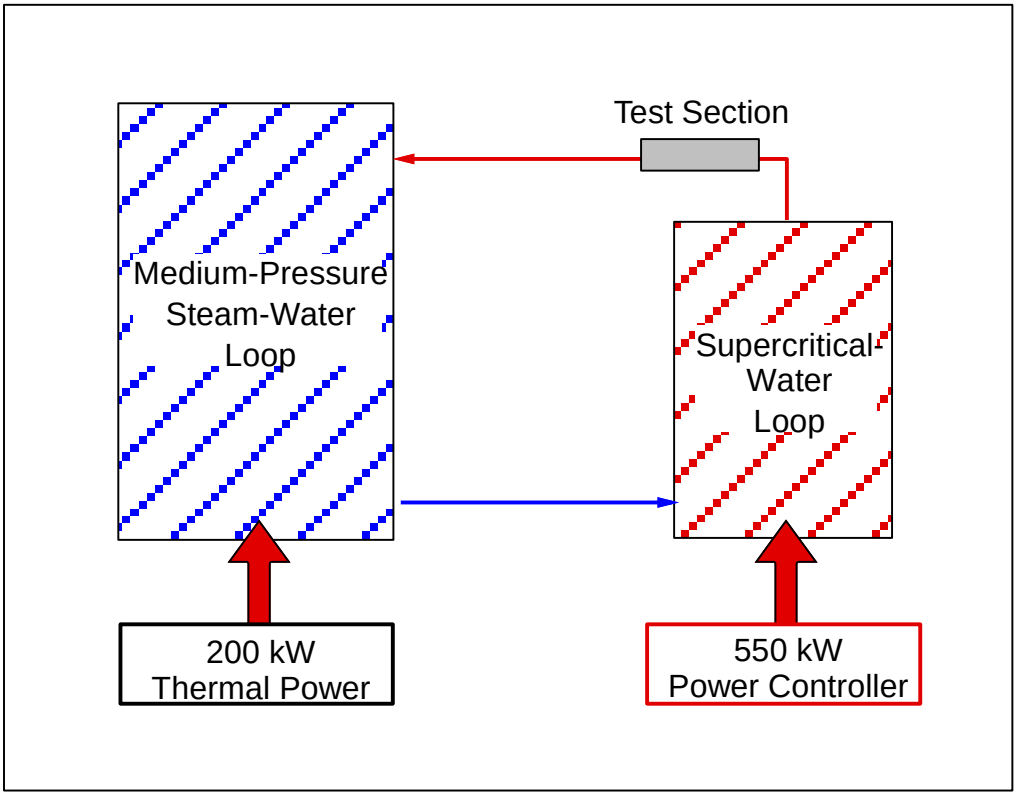

Figure 3.1 Two loops running in parallel.

This particular arrangement allows us to use the medium pressure loop shown in the figure as a low-pressure controlled reservoir. In fact, the outlet flow from the test section discharges into the medium pressure loop where its pressure can be controlled very accurately at will. The test matrix used to perform the experiments is given in Table 3.1.

Table 3.1 Experimental matrix.

Upstream pressure (MPa)	Upstream temperature (^oC)	Discharge pressure (MPa)
22.0 – 23.0	52 – 491	0.1 – 3.6
23.0 – 26.0	52 – 502	0.1 – 3.6
26.0 – 32.1	52 – 456	0.7 – 3.6

It is obvious that this procedure differs from the blowdown type experiments performed by other researchers [102-104]. In blowdown type experiments, the upstream pressure is not kept constant during the experiments and changes during the discharge. Figure 3.2 shows roughly how the typical upstream thermo-physical conditions may change during the blowdown type experiments. As seen, very large temperature and pressure gradients occur in this type of experiments which affect the results. Thus, it is difficult to obtain fruitful information from these types of experiments. Furthermore, downstream discharge pressure (i.e., most of the time it is the atmospheric pressure) cannot be changed. Therefore, it is very difficult, if not impossible, to determine unambiguously whether or not the flow reaches choking conditions. In fact, blowdown experiments should be considered as transient flow behaviour.

On the other hand, steady state condition experiments that will be performed during this study are a lot more complex and costly than blowdown experiments since several flow parameters must be continuously measured and controlled. For example, at steady-state conditions, heat will be continuously added to the flow at one part of the system while it will be removed from another part. Failure to perform this operation may easily cause instabilities in the system and affect other parameters, which will result the loop to be out of control. Another simple example can be given as pressure control in the heater element. For blowdown type experiments, reservoir is

pressurized slowly; when the desirable pressure is reached and afterwards no more heat is added to the system. As a result, having pressure lower than the critical pressure during the experiment will not affect the integrity of the system. However, during the experiments at steady state conditions, CHF can occur in the heater element and may create dangerous situations which can affect the integrity of the heater element.

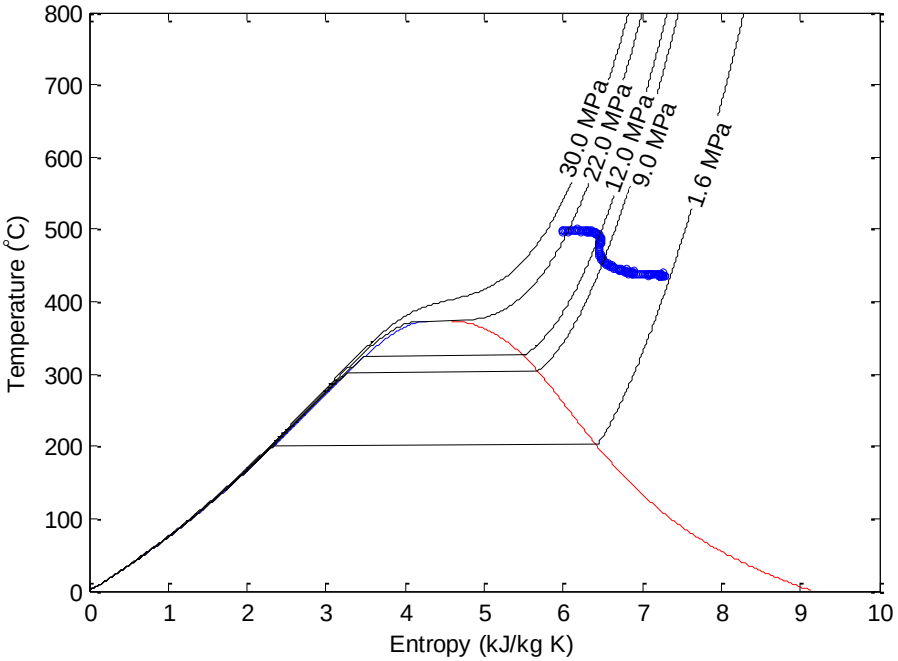

Figure 3.2 Typical change of upstream thermo-physical conditions for blowdown type of experiments.

For the present study, to correctly characterize flow conditions that bring about choking in supercritical water, for a given set of flow pressures and temperatures prevailing upstream of the test section (see Figure 3.1.), the discharge pressure will be changed and maintained constant at a desired value. Since under choking flow conditions, the maximum (critical) flow rate is independent of the discharge pressure, for each set of supercritical inlet flow conditions, i.e., pressure and temperature, the experiments will be repeated by changing the discharge pressure. Then, the critical flow rate will be determined by examining the behavior of the measured flow rate as a function of the discharge pressure. If the flow rate is constant, then the flow will be considered as choked. Thus, the Table 3.2 summarizes the anticipated upstream and downstream flow conditions that will be applied to perform the experiments.

Table 3.2 Experimental conditions.

Upstream pressure (*MPa*)	**Upstream temperature (°*C*)**	**Discharge pressure (*MPa*)**
22-32	50-500	0.6-3.6

The methodology that will be used to carry out the experiments is given as follows:

1. Before starting the experiments, the pressure in the medium pressure loop is gradually increased up to 0.6 *MPa*. This operation is achieved by adding the necessary thermal power into this loop. At this point, the supercritical loop is not in operation, and the bypass line in Figure 2.2 is open.
2. Since the high pressure pump of the supercritical loop cannot support high fluid temperatures (see Section 2.2.2), the inlet temperature of the pump is controlled below 65°*C* before opening the Block Valve 3 (BV-3) shown in Figure 2.2.
3. BV-3 is opened and the pump is put under operation at low speed (i.e., about 400 *RPM*).
4. After reaching a discharge pressure of 0.6 *MPa*, the medium pressure loop is run during a period of about 2 hours. This operation allows non-condensable gases to be completely discharged to the atmosphere before starting the experiments. This procedure is necessary not only for the stability of the loop but also for the accuracy of the measurements, because while not in operation, both of the loops are always filled with nitrogen over atmospheric pressure, to protect them against oxidation.
5. The pressure at the supercritical loop is increased with increasing the speed of the high pressure pump.
6. The pressure at the medium pressure loop is gradually increased up to the desired value. If necessary, the power is gradually applied to the heater element (Figure 2.2) in the supercritical loop to facilitate the increase of pressure in the medium pressure loop. This operation helps to generate the amount of steam required to control the medium pressure loop pressure. Nevertheless, this step must be applied carefully to avoid the occurrence of CHF in the heater element. For example, one must always check the saturation

temperature at the operating pressure and maximum surface temperature of the heater element.

7. After reaching steady discharge flow conditions, the flow pressure at the inlet of the test section is increased above the critical value depending on the desired upstream pressure.
8. After reaching steady flow conditions both at the medium pressure loop and the supercritical pressure loop, the power applied to the heater element is adjusted depending on the desired upstream flow temperature. When all flow parameters are stable at the desired level, the collection of data such as flow rates, temperatures and pressures starts.
9. The pressure in the medium pressure loop is changed to make sure that the flow is choked. It is important to mention that if the flow rate doesn't change while discharge pressure is being changed, that means that the flow is choked.

It is very important to mention that this operation can be difficult to control close to the critical flow conditions. In fact, near pseudo-critical temperatures (see Section 1.3) the thermophysical properties of the water change drastically, this in turn can affect the stability of the loop. During this part of the experiment, the continuous surveillances of both fluid temperature reading obtained from TTr-5 in Figure 2.2 and the maximum wall temperature of heater element tubes are mandatory.

It is important to mention that to satisfy QA requirements of the GEN-IV group; a rigorous check list is completed before running and shutting down the loops. A copy of the checklist is given in the Appendix 6.

CHAPTER 4 ARTICLE 1: EXPERIMENTAL STUDY OF ABRUPT DISCHARGE OF WATER AT SUPERCRITICAL CONDITIONS

Part of the experimental results obtained for choking flows of water at supercritical pressure both for subcritical and supercritical temperatures are presented in this chapter. This part of the thesis is published in a scientific paper in: ″Experimental Thermal and Fluid Science″ [16]. It is important to mention that our publication has been classified as an ″Original Research Article″ by the editor of the journal. The web page of this journal shows that only few number of papers have obtained such a prestigious distinction.

Title: Experimental Study of Abrupt Discharge of Water at Supercritical Conditions

Authors: Altan Muftuoglu & Alberto Teyssedou[1]

Nuclear Engineering Institute, Engineering Physics Department

École Polytechnique de Montréal, Montréal

CANADA

Available online at *Experimental Thermal and Fluid Science* on February 15, 2014. (http://dx.doi.org/10.1016/j.expthermflusci.2014.02.009)

4.1 Abstract

Future SuperCritical Water-cooled nuclear Reactors (SCWRs) will operate at a coolant pressure close to 25 MPa and at outlet temperatures ranging from 500 °C to 625 °C, i.e., above the critical pressure and temperature of the water (22.06 MPa and 373.95 °C, respectively). Coolant pressures higher than critical values will be used to avoid boiling and eventual critical heat flux that may occur. In addition, the outlet flow enthalpy in future supercritical water-cooled nuclear reactors will be much higher than those of actual ones, which can increase overall nuclear plant efficiencies of up to 48%. However, under such flow conditions, thermal–hydraulic behaviors of supercritical water are not fully known, i.e., pressure drop, the deterioration of forced convection

[1] Corresponding author: 2500, chemin de Polytechnique, Montréal, QC., Canada H3T 1J4. E-mail: alberto.teyssedou@polymtl.ca, Tel.: 1 (514) 3404 711, Fax: 1 (514) 340 4192.

heat transfer, critical (choked) flow, blow-down flow rate, etc. In particular, the knowledge of critical discharge of supercritical fluids is mandatory to perform nuclear reactor safety analyses and to design key mechanical components. Nevertheless, existing choked-flow data have been collected from experiments at atmospheric discharge pressure conditions, but in most cases using working fluids different than water. Therefore, a supercritical water facility has been built at the École Polytechnique de Montréal. In this paper, a new database containing 524 data points is obtained using this facility and compared with available information from the open literature.

Keywords: *Supercritical water-cooled reactor, Generation-IV, Supercritical water, Choked-flow, Pseudo-critical temperature.*

Nomenclature

DT_{pc}	temperature difference in Eq. 1 (°C)
G	mass flux (kg $m^{-2}s^{-1}$)
P	pressure (MPa)
PTr	pressure transducer (MPa)
T	temperature (°C)
TTr	temperature transducer (°C)
ΔG	mass flux difference (kg $m^{-2}s^{-1}$)
ΔDT_{pc}	temperature difference calculated from Eq. 1 (°C)
Δs	entropy difference (kJ kg^{-1} K^{-1})

Subscript

pc	pseudo-critical
f	fluid

Abbreviations and acronyms

DC	direct current
ID	inside Diameter
GIF	Generation-IV International Forum
CANDU	CANada Deuterium Uranium
SCWR	Supercritical Water cooled Reactor

4.2 Introduction

During the last 20 years, the world energy needs have been continuously increasing at very high pace. It is obvious that to satisfy future world energy requirements the nuclear industry should play an important role. To this purpose, Canada has largely contributed in different Research and Development (R&D) programs that permitted the national nuclear industry to continue growing. In a long term perspective, Canada has signed the GIF Generation-IV international agreement in July 2001 to participate in the development of nuclear technologies for the future. Different systems were proposed by the Generation-IV International Forum [1, 2]. Within this framework, SCWR appears as the foremost candidate of future nuclear power plants to be built by the year 2040. Consequently it is expected that in the near future, SCWR technology will replace actual Generation III or advanced CANDU reactors. Canada has more than 40 years of experience in the construction and operation of nuclear power reactors. This valuable engineering knowledge, combined with the actual know-how of supercritical water fossil fired power plants, can be implemented together for designing future SCWRs.

Among other advantages such as fuel economy and plant engineering simplifications [3–7], the SCWR technology must also permit the overall thermal efficiency to be increased by up to 15 points of percentage with respect to existing nuclear power plants. Furthermore, for a given thermal power the coolant mass flow rate decreases with increasing the outlet enthalpy; consequently, the water inventory of SCWRs will be low and will require less pump power as compared to actual reactors. Operating above critical water pressure conditions will eliminate phase changes which should simplify reactor's design (i.e., remove steam generators, moisture separators, etc.). However, besides these advantages of SCWRs, some fundamental aspects must be further studied to completely fulfill necessary technical information. For instance, the thermal–hydraulic behavior of future nuclear fuel channels can be very sensitive to both the coolant pressure drop and the heat transfer along fuel bundles. In fact very limited information exists in the open literature concerning supercritical water frictional pressure drop; therefore, additional experiments are mandatory [2]. Moreover, due to the fast change in fluid properties occurring around pseudo-critical conditions, most of the existing correlations are not able to satisfactorily reproduce experimental trends. It has been observed that a significant decrease on fluid thermal capacity occurring beyond the critical point causes the deterioration of forced

convective heat transfer conditions. Consequently, for high heat fluxes, such a situation may compromise the integrity of the nuclear fuel. Since SCWRs will use reduced coolant inventories, the prediction of flow behavior during a loss of coolant accident becomes fundamental for the correct estimation of core depressurization during transients. It is obvious that understanding the physics behind these problems is crucial to perform reactor safety analyses and to design hydraulic components and safety relief mechanisms. From a safety view point, experimental and analytical studies are necessary to estimate the discharge of supercritical water during an anticipated transient without scram event and during the eventual occurrence of pipe breaks. Up to now, existing discharge flow data have been collected from experiments at atmospheric discharge pressure conditions and in some cases by using working fluids different than water [4, 7–9]. It must be pointed out that keeping the discharge pressure at a unique value (i.e., atmospheric pressure) makes it very difficult to determine whether or not the flow reaches the speed of sound (i.e., choked condition). To overcome some of the above drawbacks, in this paper a supercritical water experimental set-up coupled to a medium- pressure steam-water loop has been used to perform choking flow experiments. The facility, designed and constructed at École Polytechnique de Montreal partially shown in Figure 4.1, allows supercritical water flow conditions of up to 32.1 MPa and 570 °C to be achieved. This facility is interconnected to a steam-water medium-pressure loop. This loop, not shown in the figure, permits the back pressure at the discharge of a test section to be varied and kept constant from atmospheric pressure to up to 4.0 MPa. Preliminary results obtained using this experimental set-up, including the conditions where data are very scarce, are presented. The experiments are performed using a test section that consists of a sharp edged orifice plate.

For the sake of completeness, in this paper all data from the open literature concerning choking flow experiments using working fluids under supercritical conditions are compared with the present database [4–7, 9, 10]. Since these experiments are performed using a single type of orifice, possible effects due to the nozzle shape are not addressed in this paper. Nevertheless, data are presented using a common framework that consists of using the mass flux and the pseudo-critical temperature. This representation is quite useful because it permits comparing water and carbon dioxide (CO_2) data altogether.

Figure 4.1 Portion of the supercritical-water experimental facility.

4.3 Experimental facility and instrumentation

A portion of the flow diagram of the supercritical water flow experimental facility is shown in Figure 4.1. It is coupled to a 200 kW medium-pressure steam-water loop not shown in the figure. Both systems use distilled and demineralized water without chemical treatment. The supercritical portion of the facility permits supercritical water conditions to be achieved and carefully controlled. It consists of heat exchangers, a water filter, a six piston reciprocating pump, a pulsating damper, a heater element where supercritical water conditions are achieved, a calming chamber, a test section and a quenching chamber. Other components are also used to measure and control desired flow operation conditions such as pneumatic valves, pressure transducers, thermocouples, and flow meters.

Since the discharge pressure, which can be adjusted between 0.1 MPa – 4.0 MPa, is controlled by the medium-pressure steam-water loop, the water temperature at the inlet of the reciprocating pump can be much higher than the maximum allowable value of 65 °C, as recommended by the pump manufacturer. Therefore, dual tube heat exchangers are used to bring the inlet coolant temperature below the recommended value. Furthermore, to protect the pump from the presence of solid particles larger than 5 μm dispersed in the water, a glass fiber filter is installed at its inlet side.

It is well known that positive displacement pumps tend to produce flow and pressure fluctuations. To damp eventual pressure oscillations and to avoid possible harmful effects during the experiments, a pulsation damper (Flowguard®[1] bladder style HG Series) is installed at the outlet of the pump. The damper uses a counter balance pressure of about 80% of the working pressure (see Figure 4.1). Commissioning tests were carried out at different flow temperature conditions without and with the damper installed in the loop; its performance is clearly shown in Figure 4.2. The use of a damper reduces the pressure pulsations below ±1% of the pump absolute discharge pressure. Just after the pulsation damper, the water passes through a "Flow Technology®" turbine-type flow meter. Its calibration is initially verified by weighing water at constant temperature conditions. The accuracy of the flow measurement system, including the flow meter,

[1] Trader mark of Flowguard USA Inc.

a frequency-to-current converter, an electronic linearizer and the data acquisition system is better than 0.1% of the readings.

Figure 4.2 Commissioning tests of the damper unit.

As shown in Figure 4.1, supercritical-water conditions are reached in an 11.2 m long Hastelloy C-276 tubular heater element heated by Joule effect using a 550 kW DC power supply. The branches of the heater element are connected electrically in parallel and the electrical potential is applied to the end of each tube by using 5000 A nickel plated copper clamps and 0.01 mm thick 99.9% silver foils. The electrical connections are arranged in such a way that both inlet and outlet ends of the heater are at ground electrical potential (i.e., the same as the rest of the loop). The applied thermal power is determined by measuring the electrical potential and the electrical current using two separate instruments, i.e., a 5000 A class 0.5 electrical shunt (Simpson, 5000 A – 50 mV) and a Hall Effect 5000 A current module unit (LEM®[1]). Further, the heater element is instrumented with 25 spot welded type-K thermocouples at different axial and angular locations. Six additional thermocouples are installed at radial and axial locations inside the thermal isolation jacket to estimate heat losses. The instrumentation of the heater element is connected to the data acquisition and control system via galvanic isolation amplifiers. All thermocouples, including their entire electronic chains are calibrated with a precision of ±0.5 °C of the reading, by using a calibration block from Thermoelectric (TK Series Dry Block®[2]).

Since supercritical fluids tend to stratify [11, 12], a calming chamber (see Figure 4.1) is installed just upstream of the test section. Inside the calming chamber the supercritical fluid is previously stirred before entering into the test section. This process avoids flow stratification and permits correct values of the mean fluid temperature and pressure to be measured (*TTr-5* and *PTr-1* respectively shown in Figure 4.1). Before starting the experiments, calibrations of all pressure transducers are verified using a pressure cell from Druck®[3] (DPI 602); in all the cases their

[1] Trade mark of LEM sa, Geneva, Switzerland.

[2] Trade mark of Thermo-Kinetics Company Ltd.

[3] Trade mark General Electric Company.

accuracy is better than 0.1% of the readings. Finally, all measurement and control devices are connected to a NI CompactRIO®[1] data acquisition system.

4.4 The test section

The experiments presented in this paper are carried out using a test section having a 1 mm diameter and 3.175 mm thickness sharp edged orifice plate. Figure 4.3 shows the schematic of the test section manufactured from a solid Hastelloy C-276 cylinder using the electro discharge method. The orifice is carefully measured with a precision higher than ±0.001 mm. As shown in Figure 4.3, the test section is instrumented with three pressure taps located upstream and five located downstream of the orifice. To determine flow pressure profiles upstream and downstream of the orifice, pressure taps are connected to four ‘‘Sensotec’’ 0.1% full scale accuracy absolute pressure transducers. It must be pointed out that the measurement of the downstream pressure is essential to determine whether or not choking flow conditions are achieved during the experiments.

Figure 4.3 Test section with 1 mm orifice plate and pressure taps.

4.5 Experimental conditions and procedures

Experiments were performed by covering a wide range of flow pressure and temperature conditions. Table 4.1 summarizes the experimental matrix applied to collect the data presented in this paper. At supercritical pressures, we are able to cover a wide range of subcritical and supercritical flow temperatures. In particular, subcritical values can be very useful for designing flow valve and nuclear safety components.

As mentioned in the previous section, the medium-pressure steam-water loop serves as a low pressure-controlled reservoir in such a way that the discharge pressure can be changed at will, independently of the flow pressure applied upstream of the orifice. Therefore, most of the

[1] Trademark of National Instruments.

experiments were repeated by changing the discharge pressure while maintaining all other flow parameters constant in the supercritical branch.

Table 4.1 Experimental matrix.

To avoid the presence of incondensable gases, before starting the experiments, the medium-pressure loop is run during 3 h at a pressure of 0.6 MPa. At this set-point, a degassing valve opens to the atmosphere, only afterwards the medium-pressure loop is controlled to a desired pressure. Subsequently, the experiments are performed by increasing slowly the pressure upstream of the orifice. It is important to mention that the pressure in the calming chamber is increased over the critical value before applying thermal power to the heater element. This methodology is necessary to avoid possible occurrence of critical heat flux. For a given fluid pressure, a gradual increase of the power applied to the heater element permits its temperature to be increased at will. The use of two loops allows the discharge pressure to be varied in small steps and thus, to check whether or not choking flow conditions are achieved.

Before collecting the data, flow conditions both upstream and downstream of the orifice are maintained constant for several minutes. At subcritical temperature but supercritical pressure conditions, the pressure is controlled within a band of ±0.02 MPa. For supercritical flow temperatures and pressures the control of the loop is quite complex and cumbersome. These difficulties will be discussed later in the text. Instead, the discharge pressure is always controlled within a band of ±0.005 MPa for the entire range of subcritical and supercritical experimental conditions.

Each experiment is systematically repeated at least three times; each record contains a minimum of 100 measurements at a sampling rate of 100 ms. Performing such complex experiments necessitates the participation of three qualified persons. One person controls the medium-pressure loop, a second one controls both the high-pressure loop and the data acquisition system, and a third person surveys the status of five video cameras. This system permits us to inspect not only the access to the laboratory but also the correct operation of key mechanical components of both loops. This safety installation is connected to its own computer that is able to record any event, automatically triggered by a moving detector algorithm [13].

4.6 Experimental results and analysis

As a common practice, the difference between the pseudo-critical temperature and the fluid temperature as defined in (4.1) is used to treat the data [10].

$$DT_{pc} = T_{pc} - T_f \tag{4.1}$$

where pseudo-critical temperature (T_{pc}) corresponds to the maximum value of the specific heat capacity, c_p, at a given pressure [2]. To this aim, in this paper a new relationship is proposed to estimate the pseudo-critical temperature, T_{pc}, which is given as:

$$\begin{aligned} T_{pc} &= 3.719 \times P + 291.92 \quad 22.1 \le P < 26.0 \\ T_{pc} &= 3.306 \times P + 302.68 \quad 26.0 \le P < 31.1 \end{aligned} \tag{4.2}$$

with the pressure given in MPa. Note that this equation differs from the one proposed earlier by Lee and Swinnerton [10] and recently used by Chen et al. [5, 6]. In fact, it is observed that their correlation does not satisfy the definition of the pseudo-critical temperature [2]. After comparing several thermodynamic libraries, Eq. (4.2) is validated using values from the NIST (National Institute of Standard and Technology) Standard Reference Database 23 [14]. Figure 4.4 shows a comparison between results obtained with Eq. (4.2) and those given in Chen et al. [5, 6].

Figure 4.4. Comparison of results obtained with a new pseudo-critical temperature correlation.

The same methodology is then applied to find a correlation for estimating the pseudo-critical temperature for carbon dioxide as function of the flow pressure. According to our knowledge, such relationship has not been described in the literature yet. Therefore the following equation obtained using carbon dioxide properties given in [15], is proposed:

$$\begin{aligned} T_{pc} &= 5.927 \times P - 12.741 \quad 7.38 \le P < 8.1 \\ T_{pc} &= 5.134 \times P - 6.2834 \quad 8.10 \le P < 10.1 \end{aligned} \tag{4.3}$$

with the pressure given in MPa. Eqs. (4.2) and (4.3) are used to treat water and CO_2 data, respectively; hence, they permit us to apply a single data representation framework valid for both fluids.

The new database (524 data points) of supercritical water presented in this paper are collected for flow pressures ranging from 22.1 MPa to 32.1 MPa, flow temperatures ranging from 50 °C to 502 °C and for discharge pressures from 0.1 MPa to 3.6 MPa. Mass fluxes as a function of *DTpc* are shown in Figure 4.5 which presents the effect of both the upstream pressure and temperature on mass fluxes.

Figure 4.5. École Polytechnique supercritical water data.

Close to the pseudo-critical temperature, our experiments provide data in a region where up to now, they are very scarce. A possible reason that explains this lack of experimental information is due to the fact that performing experiments close to pseudo-critical conditions is not an easy task. In fact, approaching the pseudo-critical point with $DTpc > 0$ °C the water heat capacity increases very rapidly while the mass density decreases. Nevertheless, in this region the forced convective heat transfer increases very rapidly even though the mass flow rate decreases. Consequently, when pseudo-critical conditions are reached, the difference between the inner surface temperature of the heater tube and the fluid temperature decreases noticeably fast. This increase in heat transfer results in a quite fast increase in fluid temperature which triggers an unstable condition because the increase in temperature forces the density to decrease and the pressure to increase. In this region, the reduction in mass flow rate is not able to compensate the increase in the flow pressure. Over passing the pseudo-critical temperature ($DTpc < 0$ °C), the heat capacity decreases quite fast, this condition in turn produces a decrease in the forced convective heat transfer. Therefore, in this region, while the temperature difference between the wall and the fluid increases, the fluid temperature increases and density decreases. This situation makes the control of the desired fluid pressure to be extremely difficult. In parallel, for safety reasons, the maximum allowable surface temperature of heater tubes must be respected along this process. Due to the difficulties encountered to control flow conditions close to the pseudo-critical temperature point, we have determined that measured fluid pressures may increase by about 20% with respect to the desired values only for few seconds. It is important to mention that the

maximum allowable working pressure of the loop (i.e., 34.5 MPa) is limited by the burst pressure of the rupture disk shown in Figure 4.1. But for *DTpc* ≤ 30 °C, i.e., fluid temperatures over 400 °C, the control of the fluid pressure and the temperature are excellent (±1.2%). This fact can also explain the much higher data dispersion observed close to *DTpc* = 0 °C. Despite this inconvenience, experimental results shown in Figure 4.5 clearly indicate that the mass flux decreases with increasing the fluid temperature. For *DTpc* from 100 °C to 0 °C the decrease in mass flux occurs at a very high pace. In fact for *DTpc* from 350 °C to 120 °C, $\Delta G/\Delta DT_{pc} \approx$ 160 kg $m^{-2}s^{-1}$ $°C^{-1}$ for DT_{pc} from 100 °C to 0 °C this change is about 9 times higher. The apparent data dispersion observed for *DTpc* > 120 °C is due to the variation of the discharge pressure (i.e., reservoir pressure) as indicated in Table 4.1. However, while *DTpc* is decreasing mass flux tends to collapse around *DTpc* ≈ 65 °C. This provides us a good indication that for $DT_{pc} \geq 65$ °C the flow is not choked. In fact, for flow temperatures lower than pseudo-critical values, choking flow seems to occur within a very limited region.

For DTpc < 0 °C the mass flux continues to decrease with increasing the fluid temperature, but at a much lower pace. Nevertheless, in this region data points do not present any apparent correlation with the discharge pressure. Therefore, in this zone we can confirm that the supercritical water flow reaches choking flow conditions; these flow behaviors are discussed in more detail in Section 4.6.1.

Observations discussed above have been also reported by other researchers under both subcritical and supercritical water conditions. To this aim, Figure 4.6 shows a comparison of our experimental results with sharp nozzle data given in [4–7, 9, 10]. However, in these studies a limited number of experimental points are presented and only one of them provides data slightly above the critical temperature, with most of the points collected below the critical temperature. In particular, other data given in [4, 9] are collected using CO_2 with blow down type experiments where both fluid pressures and temperatures upstream from the nozzles change during the experiment. Furthermore, the upstream fluid pressure is assumed the same for all data points; therefore, it is almost impossible to determine whether or not this pressure affects choking flows of CO_2. Moreover, it is arbitrarily considered that the flow is choked (i.e., there is no control of the discharge pressure). Also, it is not known at what temperature the flow becomes choked.

Figure 4.6. Comparison of École Polytechnique data with those given in the literature.

According to the previous discussion, the apparent discrepancy in the data can be explained by the difference in orifice length, surface roughness and procedures used to perform the experiments. It is clear, however, that the present experimental data cover a wider range of both fluid temperatures and pressures, with a much lower scattering. In general, all data points present trends similar to those given in the literature. Figure 4.7 shows a comparison of École Polytechnique water data with CO_2 data collected by Mignot et al. [7, 9] using three different inside diameter (ID) sharp nozzles manufactured from stainless steel, having ID of 2 mm, 3.175 mm and 7 mm and almost the same length of 338 mm. To this aim, Eq. (3) is used to calculate the difference between pseudo-critical (T_{pc}) and fluid temperatures for CO_2. It is interesting to remark that the use of DT_{pc} permits data collected with different fluids to be represented and compared in the same diagram.

Figure 4.7. Comparison of École Polytechnique data with CO_2 data from Mignot et al. [7,9].

In particular, it is observed that the inside diameter of nozzles does not affect the mass flux. Moreover, both supercritical water and CO_2 data follow the same behavior, i.e., the mass flux decreases with decreasing DT_{pc}. Moreover, in our case the discharge takes place in a 2500 mm long, 24.3 mm ID straight pipe under different discharge pressure as detailed in Table 4.1. Despite the difference in the experimental conditions, set-ups and fluid properties, in general the observed discrepancy between supercritical water and CO_2 data is almost constant with CO_2 mass fluxes lower by 25% with respect to those of water.

4.6.1 Supercritical water choking flow experiments

Figure 4.8 shows the pressure distribution and the mass flux of a typical supercritical water flow experiment where the discharge pressure has been changed and carefully controlled from 0.7 MPa to up to 3.5 MPa. Data presented in this figure cover two different values of supercritical water pressures. For each flow conditions more than three values were collected at different time intervals; note that some of them appear superimposed in the figure. Upstream of the orifice Fig. 8a shows a small pressure drop. Even though a dispersion of about ±0.4 MPa is observed in the

data, the aforementioned reduction in pressure has been observed systematically during all supercritical water experiments. Downstream of the orifice a systematic small increase in the pressure profile occurs. It is quite possible that these changes are due to a partial recovery of the reversible component of the pressure drop in this region [16]. It is important to remark that the fluid pressure upstream of the orifice is not affected by the change of the downstream pressure. This observation provides a good indication that the flow is choked, i.e., it reaches the speed of sound and confirms the general flow behavior discussed in the previous section.

Fig. 8 (a)

Fig. 8 (b)

Figure 4.8 a) Pressure distribution along the test section vs. discharge pressure, b) Mass flux vs. discharge pressure at different temperatures.

Figure 4.8b shows the mass flux obtained by maintaining the upstream conditions almost constant and by increasing the discharge pressure from 0.7 MPa up to 3.5 MPa. It is apparent that for temperatures higher than approximately 307 °C, the increase on the discharge pressure does not affect the mass flux; thus, under specified flow conditions choking flow seems to be clearly achieved. Note that 307 °C corresponds to $DT_{pc} \approx 67^{o}$C. However, at lower fluid temperatures ($DT_{pc} > 67$ °C), it is seen that the change in the back pressure affects the mass flux, as indicated by the positive slope in Fig. 8b and the apparent data dispersion shown in Figure 4.6.

As it is mentioned in the previous section, the mass flux decreases quite sharply with increasing the fluid temperature (i.e., decreasing DT_{pc} in Figure 4.5). In this region, the fluid density and the speed of sound, both of which determine the mass flux, vary very rapidly. In fact, Figure 4.9 shows the variation of these two Thermophysical properties as a function of the fluid temperature, for a given fluid pressure. It is obvious that the fluid velocity increases with decreasing density, i.e., increasing the fluid temperature. In turn, within the region close to $DT_{pc} = 0$ °C in Figure 4.5, the thermodynamically defined speed of sound, decreases with increasing the fluid temperature, clearly shown in Figure 4.9. Therefore, in this region the fluid velocity reaches quite rapidly the speed of sound. Since both the fluid density and the speed of sound decrease with temperature, the rapid decrease on the mass flux is observed for $70\ °C \leq DT_{pc} < 0$ °C in Figure 4.5. Then, for $DT_{pc} \leq 0$ °C, Figure 4.9 shows that the speed of

sound increases at a much lower pace while the fluid density continues to decrease very slowly with increasing the fluid temperature, where choking flow conditions are well established. This explains the experimental trend shown in Figure 4.5.

Figure 4.9 Variations of density and speed of sound for water at supercritical pressure.

The above analyses, nevertheless, are based on the fact that the speed of sound is correctly established from thermodynamic principles (i.e., assuming isentropic discharge flows). Figure 4.10 shows the entire set containing 524 data points that we have collected with water at supercritical pressure conditions. It also shows an arbitrary data point, P1 which thermodynamic state is experimentally determined. Assuming both isentropic and isenthalpic expansions, however, do not correspond to the measured fluid temperature and pressure shown by P1' in the same figure. It must be pointed out that similar results are obtained for the entire data set presented in this figure. This particular experimental fact provides strong foundations that sudden expansion of supercritical water flows through a sharp edged orifice follow a process that is neither completely reversible nor completely irreversible.

To reinforce the data analyses presented in the previous paragraph, a more rigorous determination of the speed of sound should be studied. In particular, if supercritical flows tend to form fluid agglomerations as already described in [11, 12], then it could be quite possible that the speed of sound will be conditioned by the nature and the relaxation time of different processes occurring in the fluid [17–19]. However, such supercritical water speed of sound characterization necessitates additional experimental and theoretical work to be performed.

Figure 4.10 Experimental data represented on the T-s diagram.

4.7 Error analysis

The accuracy of the instrumentation used to perform the experiments has been discussed in Section 4.3. Due to the number of data points and the complex nature of supercritical water phenomena, the error analysis is not straightforward. Nevertheless, to simplify this task, the data

shown in Figure 4.2 have been subdivided into three distinct regions: Region I for $DT_{pc} <$ -50 °C, Region II for -50 °C $\leq DT_{pc} \leq$ 50 °C and Region III for 50 °C $> DT_{pc}$. Within each of these regions the precision of the measurements for fluid temperature, pressure and mass flux, as well as for the applied power are analysed. Figure 4.11 shows the distributions of fluid variables measured in Region I; it can be observed that in all cases most of the collected values are within the 95% confidence range.

Figure 4.11 Precision of the measurements for Region I ($DT_{pc} <$ -50 °C).

Further, since this work concerns choking flow conditions determined from measured mass fluxes, Figure 4.11c shows that the dispersion of these values is relatively low which seems to be not the case for similar data obtained for sharp nozzles given in the literature (see Figure 4.6). For the entire temperature range the precisions of collected data are summarized in Table 4.2.

As shown in this table, the precision is higher in Regions I and III. In fact as already explained in Section 4.6, for flow conditions corresponding to Region II the control of the system is cumbersome. In fact, in this region the coupling between fluid properties as a function of temperature and pressure is very strong. Small changes of these variables considerably affect the mass flux (see Figure 4.5). Nevertheless, Figure 4.5, Figure 4.8 and Figure 4.11, jointly with the values given in Table 4.2, confirm that choking flow under supercritical water flow conditions have been determined with satisfactory precision.

Table 4.2 Precision of measurements in three different experimental regions.

4.8 Conclusion

Even though the boiler industry has more than 50 years of experience working with water at supercritical conditions, a review of the recent literature shows that the thermal–hydraulic behavior of supercritical water is not completely known yet. In particular, experimental data are very scarce due to the complexity and risks involved in experiments. Therefore, most of the studies have been performed either using fluid different than water or far from operation

conditions of SCWRs. To partially fulfill this lack of information, a supercritical water experimental facility constructed at École Polytechnique de Montréal is presented.

The supercritical water set-up is used to perform choking flow experiments by covering a wide range of flow conditions. A test section having 1 mm diameter sharp edged orifice is used to collect the data presented in this paper. The results are compared with the study of Mignot et al. [4, 7, 9], Chen et al. [5, 6], and Lee and Swinnerton [10]. In general, an excellent agreement with experiments carried out by other researchers is observed. In particular, the proposed experimental arrangement (i.e., use of two-loops running in parallel) permits us to verify if the choking flow conditions are reached or not. Furthermore, a small pressure gradient occurring upstream of the orifice is systematically measured. We observed that close to the pseudo-critical point, the forced convective heat transfer coefficient changes very rapidly which affects the difference between the inner tube surface and fluid temperature. These fast variations combined with the corresponding change in fluid density, makes it very difficult to control and maintain flow conditions in the proximity of the critical point.

The new data set is compared with similar studies given in the open literature. For this purpose, the differences between pseudo-critical temperatures and fluid temperatures ($DT_{pc} = T_{pc} - T_f$) are used to represent the data. To estimate DT_{pc}, new relationships are presented to calculate the pseudo-critical temperatures. It is observed that mass flux decreases with increasing the fluid temperature. Close to the fluid pseudo-critical temperature, these changes become very important. This decrease becomes less apparent for fluid temperature higher than the pseudo-critical temperature. Furthermore, the use of a framework representation based on DT_{pc} permits us to compare the mass flux behavior of water and CO_2. For $DT_{pc} < 0$ °C it is observed that both fluids follow similar trends with almost a constant difference of about 25%.

In addition, we are able to determine a water temperature limit below which the fluid cannot reach the speed of sound. In fact, it seems that supercritical water becomes choked only for fluid temperatures higher than 307 °C ± 5 °C. Measured values of discharge fluid temperatures and pressures provide indications that the discharge through sharp edged orifices are neither isentropic nor isenthalpic.

4.9 Acknowledgements

The work presented in this paper was possible due to the financial support of the Gen-IV CRD research program granted by the Natural Sciences and Engineering Research Council of Canada (NSERC), National Resources Canada, Atomic Energy of Canada Limited, Hydro-Québec and Alexander Graham Bell Canada Graduate Scholarship granted by NSERC. The participation of Thierry Lafrance (Ing.), Stepehen Schneller (Ing.), Cyril Koclas (Associate Researcher) and Jean-Claude Juneau (Technician) are greatly appreciated, without them the realization of this research program should be impossible.

4.10 References

1. Boyle, K. P., Brady, D., Guzonas, D., Khartabil, H., Leung, L., Lo, J., Quinn, S., Suppiah, S. and W. Zheng , Canada's generation IV national program - overview, in 4th International Symposium on Supercritical Water-Cooled Reactors (2009), Heidelberg, Germany.
2. Pioro, I.L. and R.B. Duffey, Heat Transfer and Hydraulic Resistance at Supercritical Pressures in Power Engineering Applications. ASME Press (American Society of Mechanical Engineers), ISBN 0791802523, (2007).
3. Chatharaju, M., Computational study of critical flow discharge in supercritical water cooled reactors, in Engineering Physics (2011), McMaster University: Hamilton, Ontario, Canada, p. 114.
4. Mignot, G., M. Anderson, and M. Corradini, Critical flow experiment and analysis for supercritical fluid. Nuclear Engineering and Technology, (2008), 40 (2), pp. 133-138.
5. Chen, Y., Yang, C., Zhang, S., Zhao, M., Du, K. and X. Cheng, (2009). Experimental Study of Critical Flow of Water at Supercritical Pressure. Frontiers of Energy and Power Engineering in China, 3 (2), pp. 175-180.
6. Chen, Y., Zhao, M., Yang, C., Bi, K., Du, K. and S. Zhang, Research on critical flow of water under supercritical pressures in nozzles. Journal of Energy and Power Engineering, (2012), 6, pp. 201-208.
7. Mignot, G.P., M.H. Anderson and M.L. Corradini, Measurement of supercritical CO2 critical flow: Effects of L/D and surface roughness. Nuclear Engineering and Design, (2009), 239 (5), pp. 949-955.
8. Gebbeken, B. and R. Eggers, Blowdown of carbon dioxide from initially supercritical conditions. Journal of Loss Prevention in the Process Industries, (1996), 9 (4), pp. 285-293.
9. Mignot, G.P.H., Experimental investigation of critical flow of supercritical carbon dioxide, (2008), The University of Wisconsin - Madison: United States - Wisconsin, p. 196.
10. Lee, D.H. and D. Swinnerton, Evaluation of critical flow for supercritical steam-water, (1983), United Kingdom Atomic Energy Authority United Kingdom, Report NP-3086.

11. Ota, J., Okamoto, K., Sakurai, K. and H. Madarame, Measurement of transient supercritical fluid velocity using infrared pulse laser with high-speed camera, in: 11th Int. Symp. App. Laser Tech. Fluid Mech. (2002), Lisbon, Portugal.

12. Sakurai, K., KO, H.S., Okamoto, K. and H. Madarame, Visualization Study for Pseudo-Boiling in Supercritical Carbon Dioxide under Forced Convection in Rectangular Channel. Journal of the School of Engineering, the University of Tokyo, (2001), 48, pp. 49-57.

13. Teyssedou, A., A. Muftuoglu and C. Koclas, Choking flow in supercritical fluids – preliminary commissioning experiments, in Report IGE-334-R12012, Submitted to: NSERC/NRCan/AECL, IGN, École Polytechnique de Montréal.

14. Lemmon, E., M.L. Huber and M.O. McLinden, NIST Standard Reference Database 23: Reference Fluid Thermodynamic and Transport Properties - REFPROP, (2010).

15. Span, R. and W. Wagner, A new equation of state for carbon dioxide covering the fluid region from the triple-point temperature to 1100 K at pressures up to 800 MPa, J. Phys. Chem. Ref. Data, 25 (1996).

16. Tapucu, A., A. Teyssedou, M. Geçkinli and M. Merilo, Axial pressure distribution in two laterally interconnected channels with blockages. International Journal of Multiphase Flow, (1990), 16 (3), pp. 461-479.

17. Radovskii, I.S., Speed of sound in two-phase vapor-liquid systems. Journal of Applied Mechanics and Technical Physics, (1970), 11 (5), pp. 778-784.

18. Olekhnovitch, A., A. Teyssedou and P. Tye, Critical heat flux under choking flow conditions. Part II - maximum values of flow parameters attained under choking flow conditions. Nuclear Engineering and Design, (2001), 205 (1-2), pp. 175-190.

19. Olekhnovitch, A., Teyssedou, A., Tye P. and P. Champagne, Critical heat flux under choking flow conditions. Part I - outlet pressure fluctuations. Nuclear Engineering and Design, (2001), 205 (1-2), pp. 159-173.

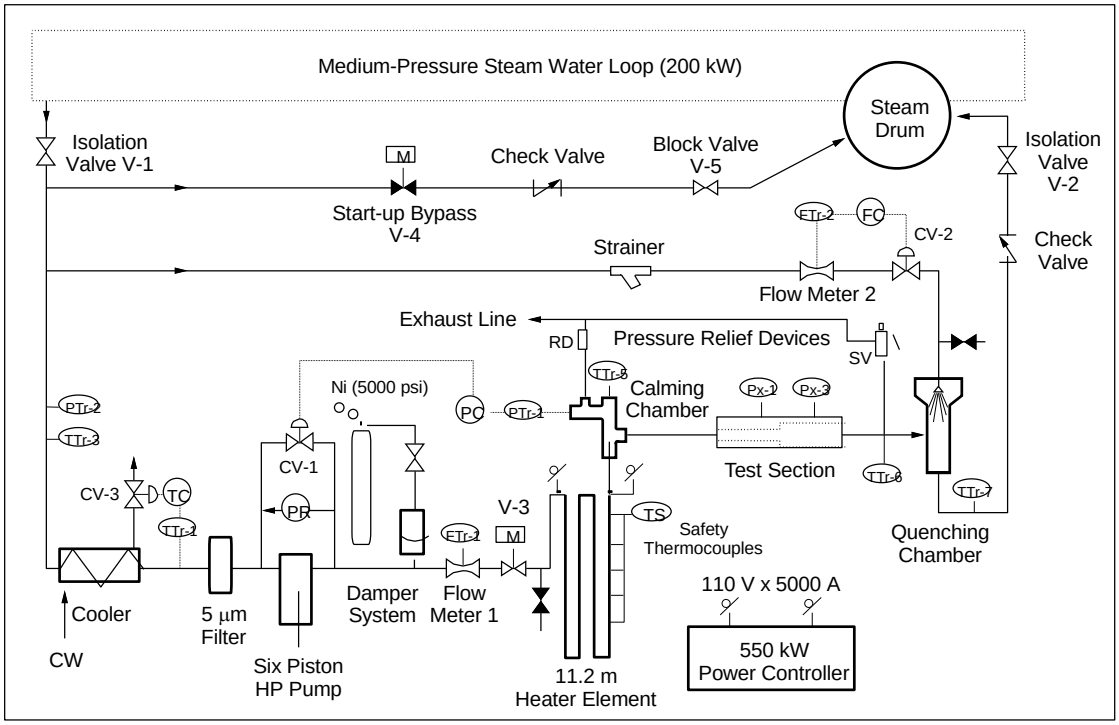

Figure 4.1 Portion of the supercritical-water experimental facility.

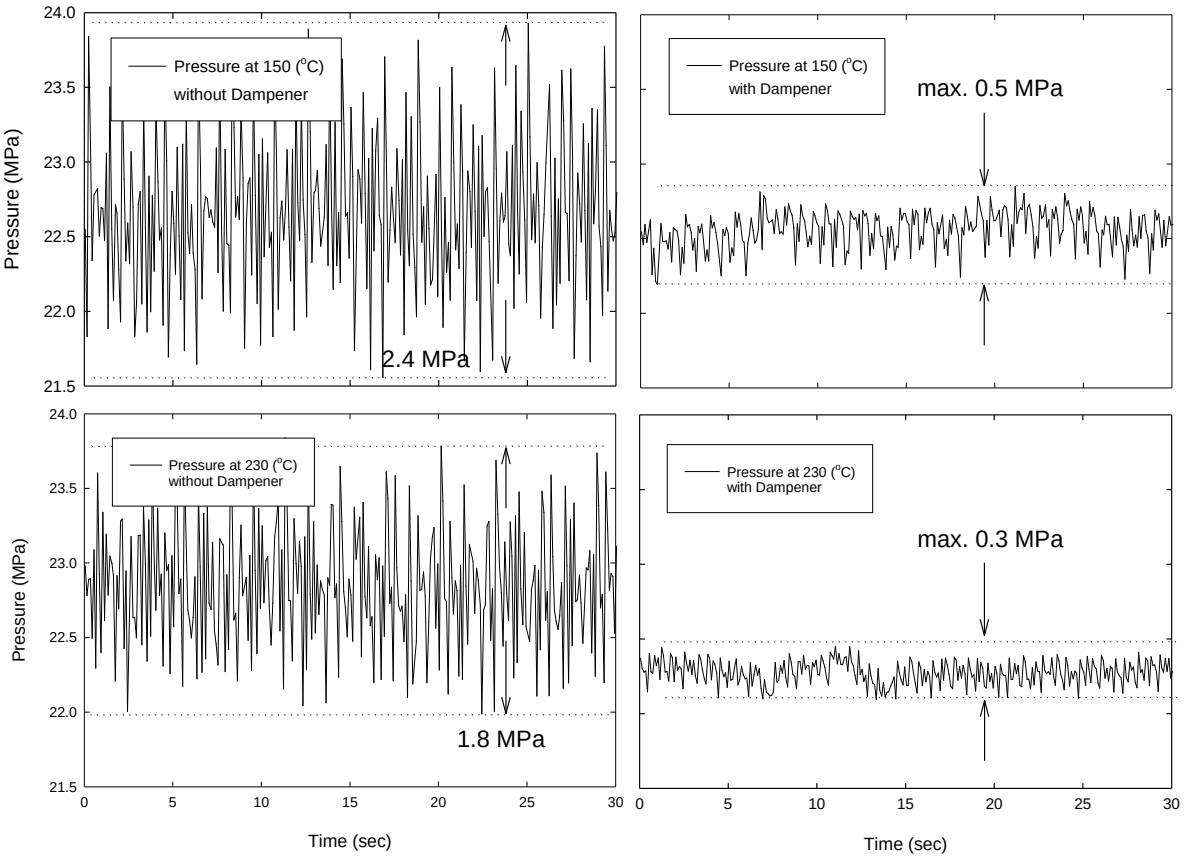

Figure 4.2 Commissioning tests of a damper unit.

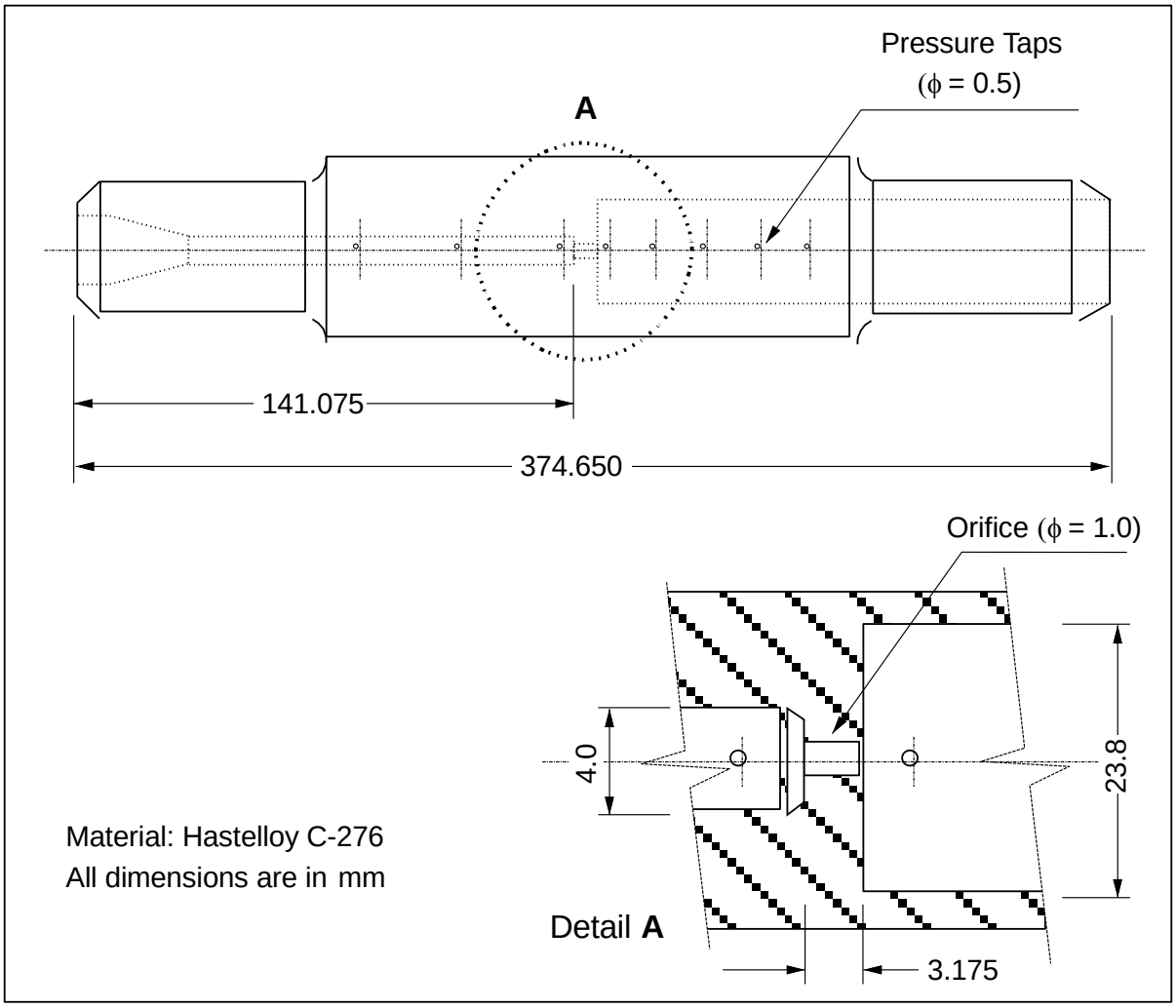

Figure 4.3 Test section with 1 mm orifice plate and pressure taps.

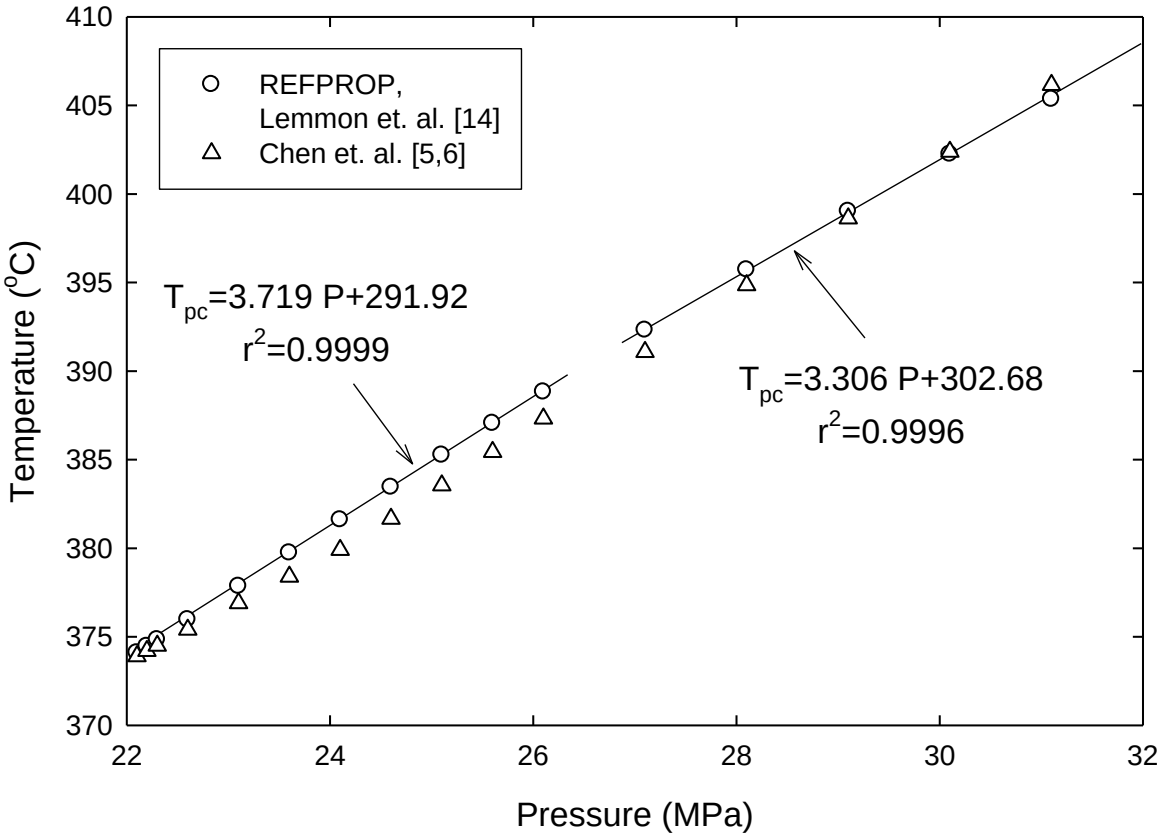

Figure 4.4 Comparison of results obtained with a new pseudo-critical temperature correlation.

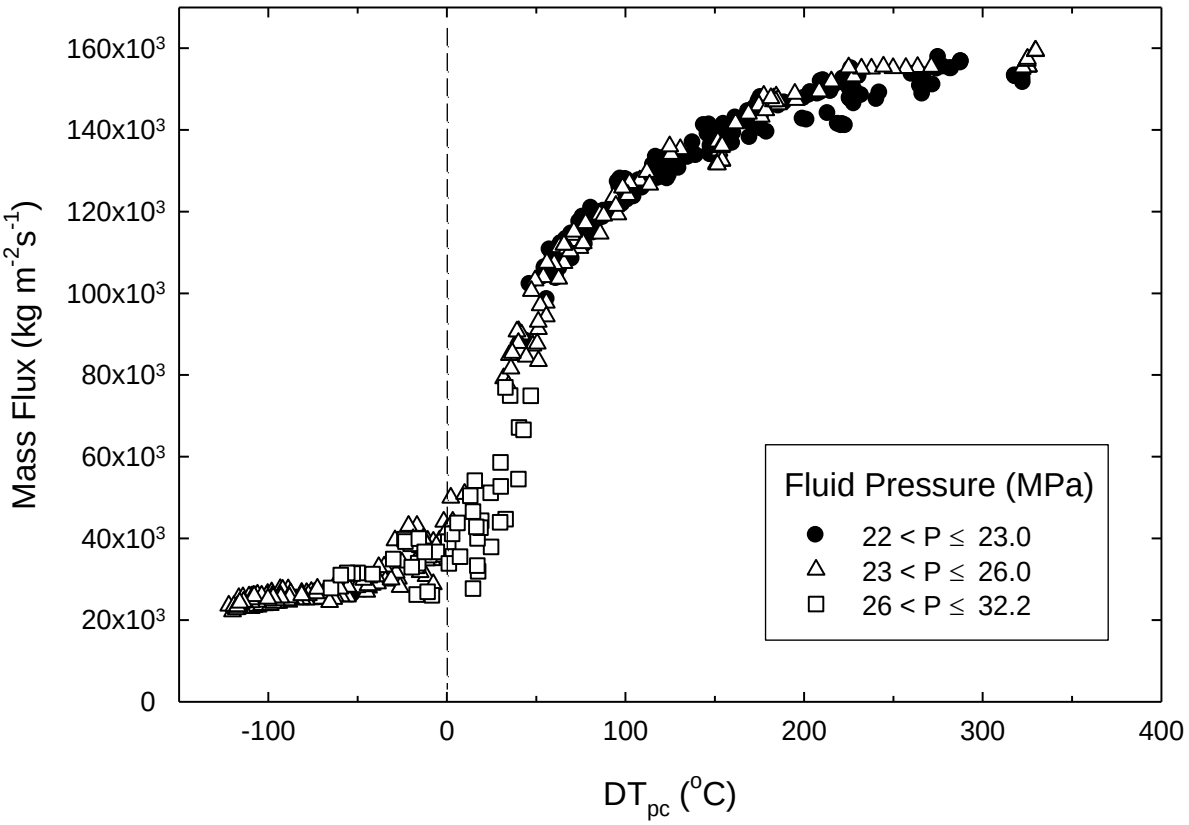

Figure 4.5 École Polytechnique supercritical water data.

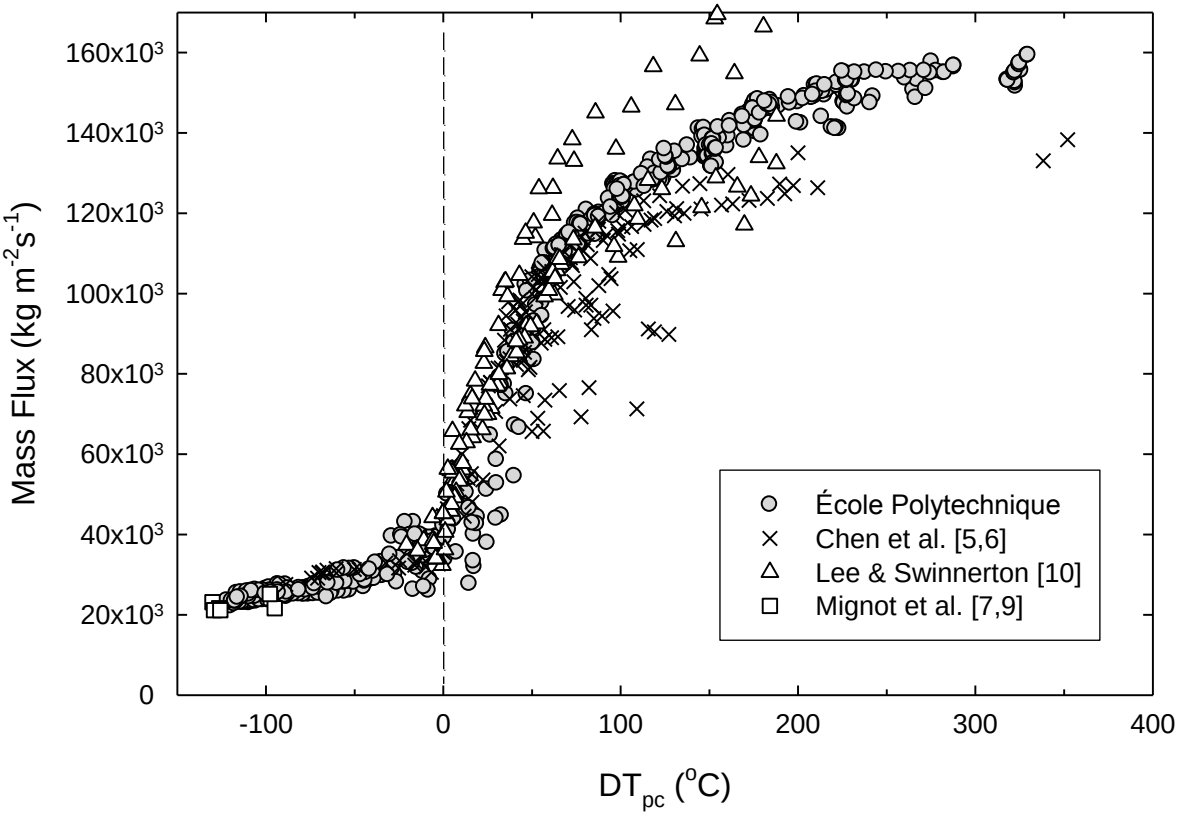

Figure 4.6 Comparison of École Polytechnique data with those given in the literature.

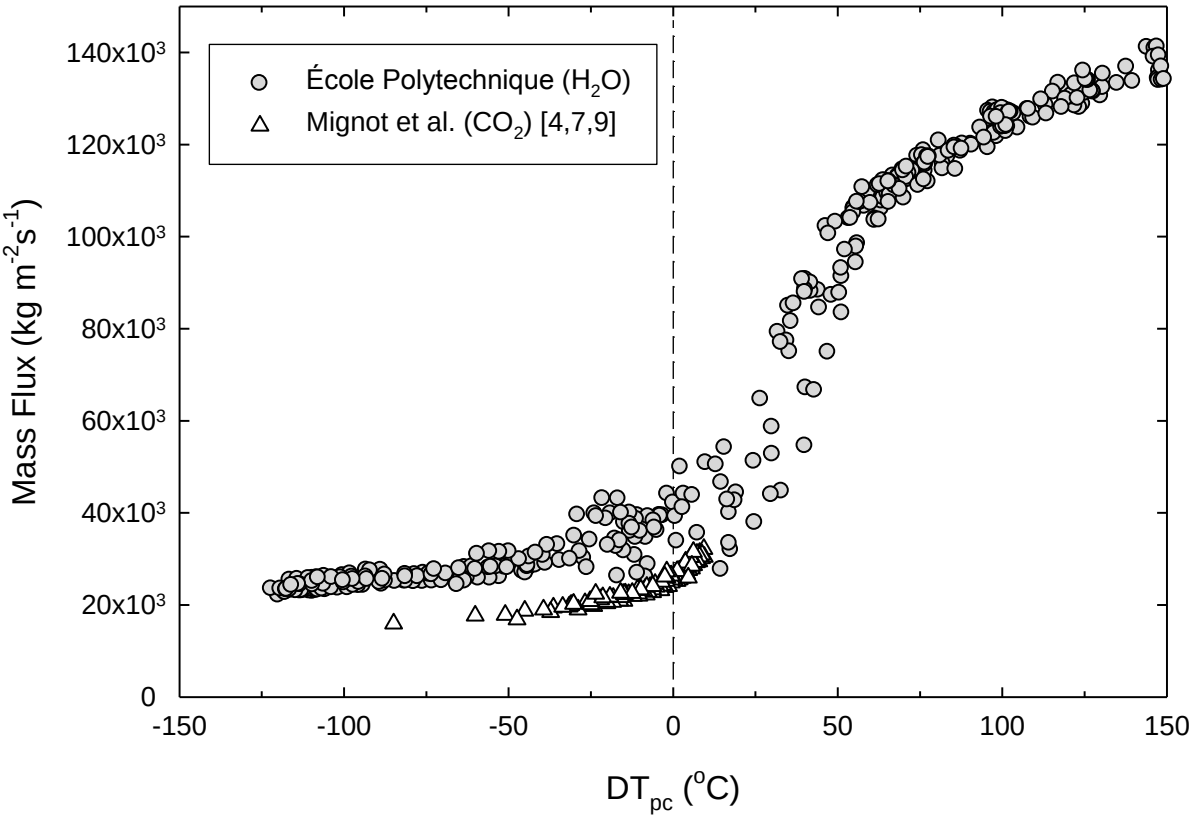

Figure 4.7 Comparison of École Polytechnique data with CO_2 data from Mignot et al. [4,7,9].

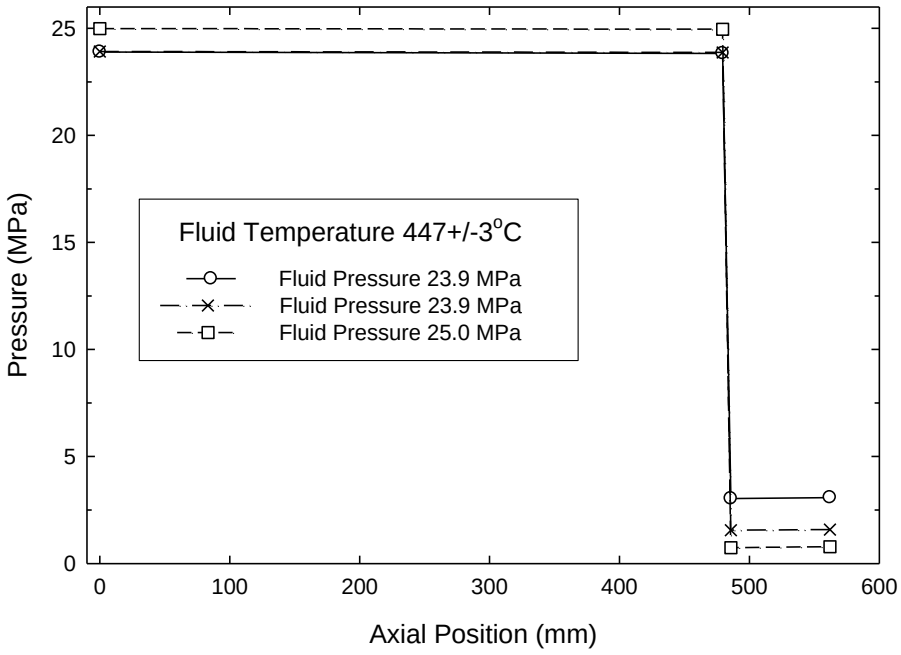

(a)

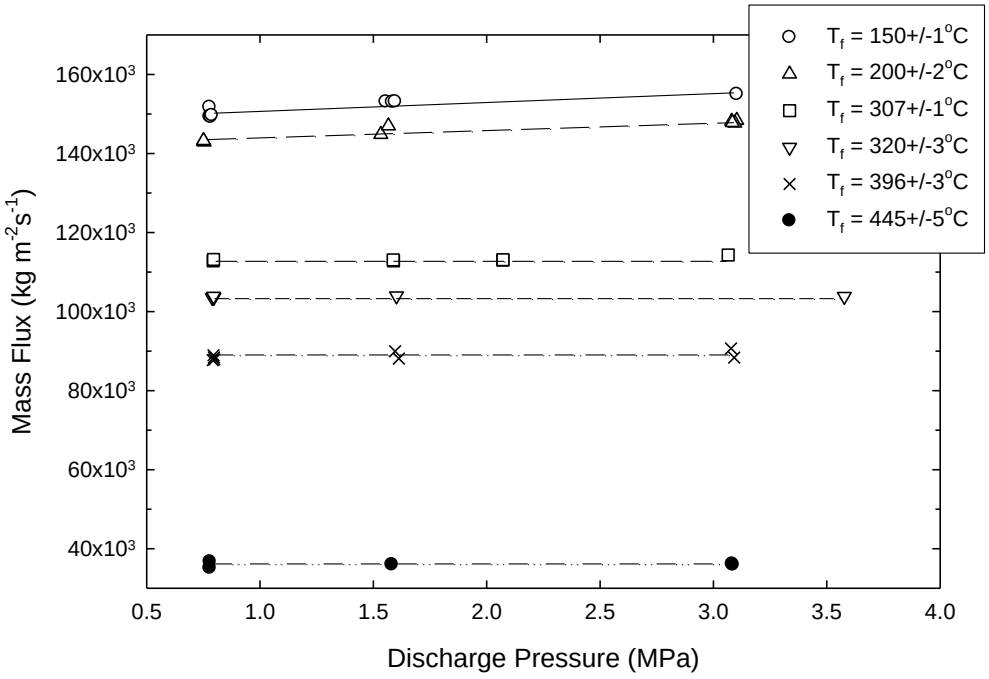

(b)

Figure 4.8 a) Pressure distribution along the test section vs. discharge pressure, b) Mass flux vs. discharge pressure at different temperatures.

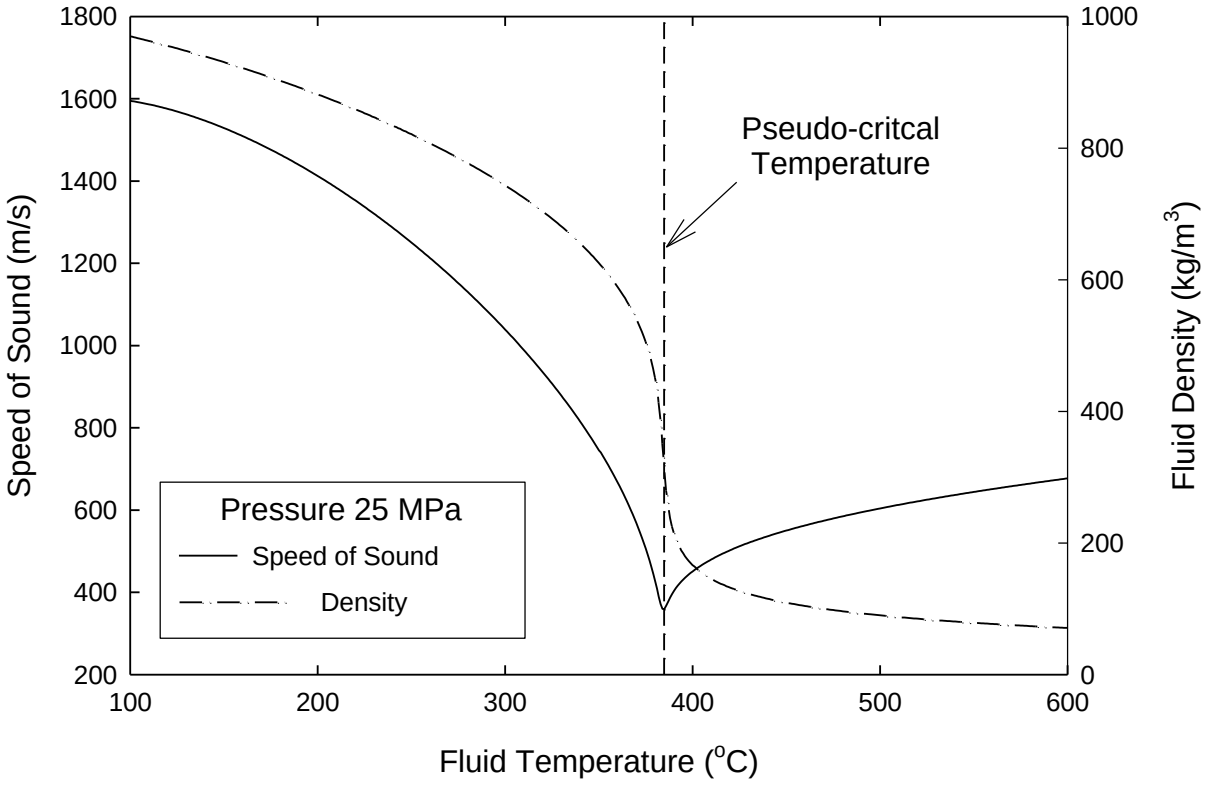

Figure 4.9 Variations of density and speed of sound for water at supercritical pressure.

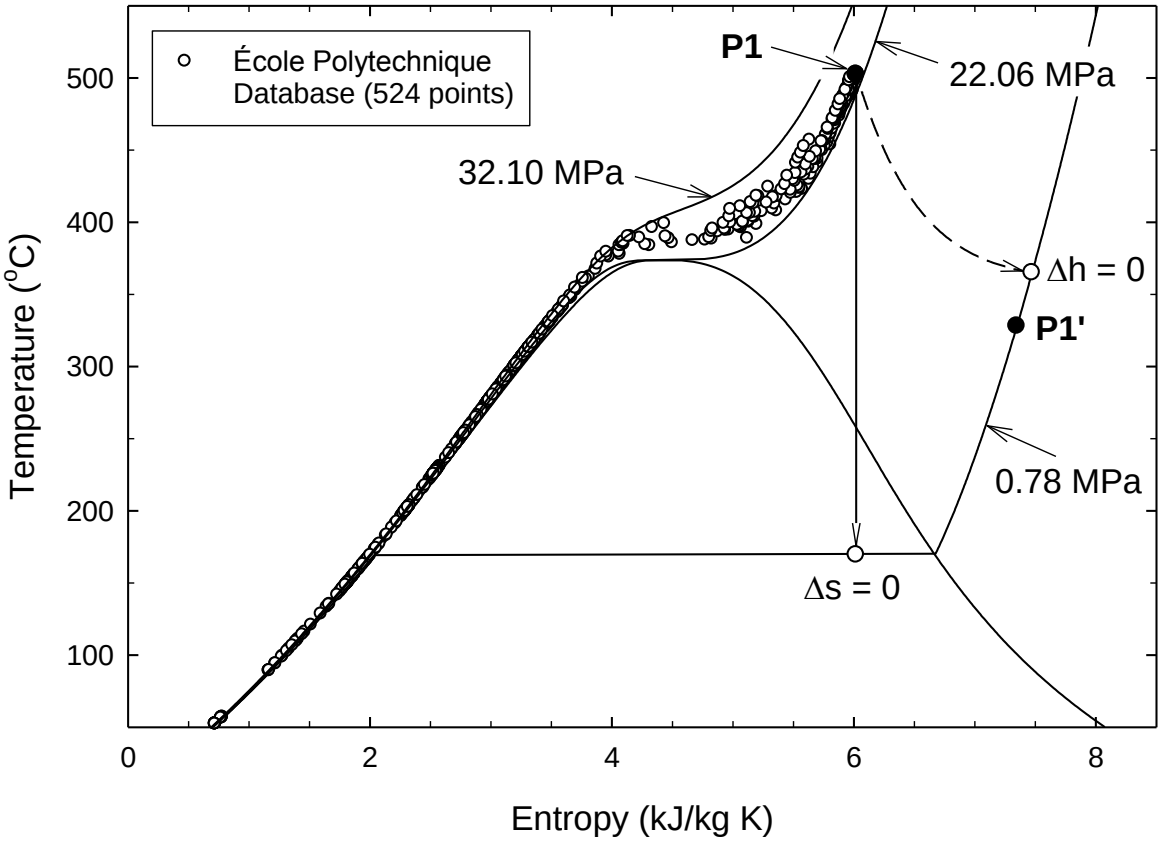

Figure 4.10 Experimental data represented on the T-S diagram.

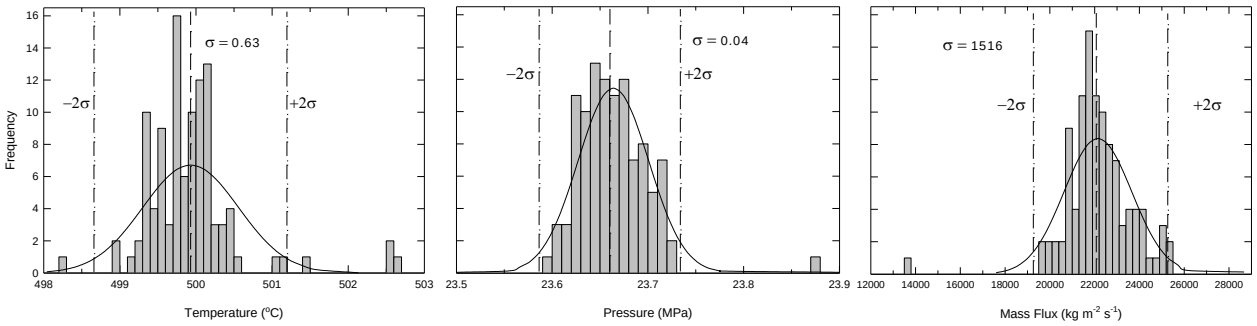

Figure 4.11 Precision of the measurements for Region I (DT_{pc} < -50°C in Figure 4.5.)

Table 4.1 Experimental matrix.

Collected Data Points	Upstream Pressure (MPa)	Upstream Temperature (^{o}C)	Discharge Pressure (MPa)
230	22.0 – 23.0	52 – 491	0.1 – 3.6
247	23.0 – 26.0	52 – 502	0.1 – 3.6
47	26.0 – 32.1	52 – 456	0.7 – 3.6

Table 4.2 Precision of measurements in three different experimental regions.

Flow Variable	Standard Deviation σ		
	Region I	Region II	Region III
	$DT_{pc} <$ -50^{o}C	-50^{o}C $\leq DT_{pc} \leq$ 50^{o}C	50^{o}C $> DT_{pc}$
Temperature (^{o}C)	0.63	2.15	1.14
Pressure (MPa)	0.04	0.30	0.08
Mass Flux$\times 10^{3}$ (kg m^{-2} s^{-1})	1.52	4.22	2.42
Thermal Power (kW)	0.80	1.75	1.30

CHAPTER 5 COMPLEMENTARY RESULTS OF CHOKING FLOW EXPERIMENTS

After the publication of the paper presented in Chapter 4, the choking flow experimental program was continued. Consequently, additional experimental points are added to the initial data bank. Therefore, in this section, the analysis discussed in Chapter 4 will be extended. In particular, the discussion about experimental data will be addressed to those physical aspects that may concern the behaviour of different models used to predict choking flows. Moreover, the evolutions of experimental parameters continuously collected during long periods are also studied and used to analyse the repeatability of the experiments and the quality of the data. Within this framework, the estimation of heater element surface temperature estimations are compared with the measured values.

5.1 Choking flow complementary results

Before starting to perform the experiments, the main objective was to obtain mass flow rate data for flow pressures ranging from 22 *MPa* to 24 *MPa* and the flow temperatures over critical values. Furthermore, we have decided to broaden the flow range to obtain a complete perspective of choking flow of water at supercritical pressures.

During the research work presented in this thesis, 545 steady state choking flow data points of water at supercritical pressures are obtained for flow pressures ranging from 22.1 *MPa* to 32.1 *MPa*, flow temperatures ranging from 50°*C* to 502°*C* and for discharge pressures from 0.1 *MPa* to 3.6 *MPa*. As mentioned before, raw data points are averaged by considering sets containing a minimum of 100 points collected for a period of 10 *s* with 100 *ms* sampling rate. Figure 5.1 shows the treated data plotted on temperature entropy diagram while Figure 5.2 shows the mass flux as a function of DT_{pc}. These figures present the data obtained for supercritical water pressures by covering a wide range of both subcritical and supercritical temperatures.

In general, it is found that the upstream temperature is the dominant factor on mass flow rate and the effect of the upstream pressure is always less than 10% for temperatures away from the pseudo-critical temperatures. Close to the pseudo-critical temperatures, it is difficult to carry out a similar analysis because all thermo-physical parameters change quite fast and affect the mass

flux. Moreover, it is found that the increase in the upstream temperature decreases the mass flux. However, for $DT_{pc} < 50°C$ the mass flux decreases at lower pace.

Before start comparing the predictions of the models with the data, it is important to show the experimental fluid behaviour observed just after the expansion. As it is shown in Figure 4.10 in Chapter 4, measured expansion flow conditions are neither isentropic nor isenthalpic; they are between the two. A more detailed version of Figure 4.10 is shown in Figure 5.1 where three different upstream conditions are analysed. Table 5.1 summarizes the measured values of pressures and temperatures for each data point used to produce the information shown in Figure 5.1. From this figure, it is clear that for high inlet flow temperatures, superheated steam downstream flow conditions are observed. Note that in this figure, diamond symbols correspond to the measured discharge flow conditions. Thus, the primed states in the figure represent the measured downstream flow values, which correspond to their respective flow states (unprimed) prevailing upstream of the orifice (for detailed information see Table 5.1). However, it must be pointed out that for states 3, it is impossible to determine experimentally the exact thermo-physical location of the discharge condition, because the fluid is in the two-phase flow zone. It is obvious that this flow state must be located somewhere on the thick red line.

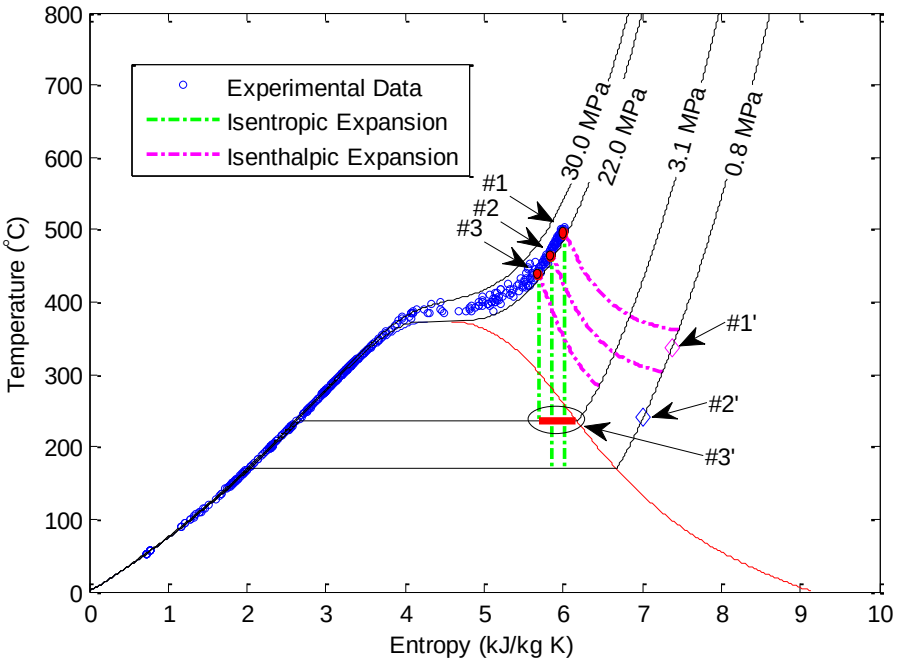

Figure 5.1 Flow discharge for different supercritical flow conditions.

Table 5.1 Experimental fluid states shown in Figure 5.1.

State #	Upstream pressure (*MPa*)	Upstream temperature (°*C*)	Discharge pressure (*MPa*)	Discharge temperature (°C)
1	23.66	499.93	7.80	337.26
2	23.94	470.16	7.80	240.26
3	23.89	444.18	30.82	235.36 (saturation temperature)

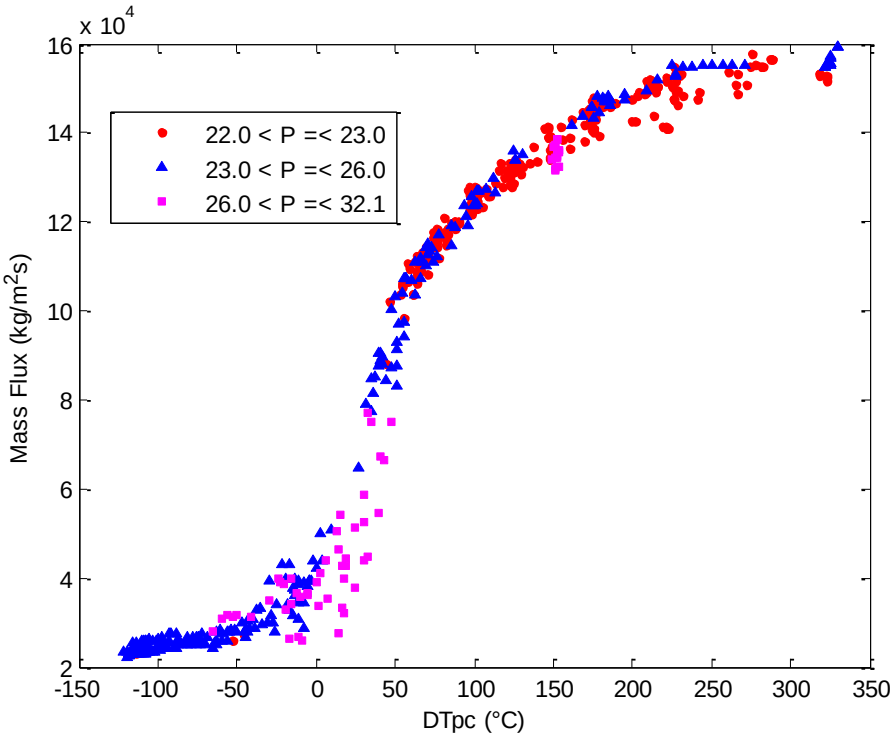

Figure 5.2 Mass flux as a function of DT_{pc}.

Table 5.2 summarizes the measured pressures and temperatures for each data point presented in Figure 5.2. In fact, several other data points are collected during the continuous saving mode that

will be explained later. However, since these points are obtained for studying the repeatability of the experimental conditions, they are not included in Figure 5.2.

Table 5.2 Experimental matrix used to obtain complementary results.

Collected data points	Upstream pressure (MPa)	Upstream temperature (^oC)	Discharge pressure (MPa)
230	22.0 – 23.0	52 – 491	0.1 – 3.6
247	23.0 – 26.0	52 – 502	0.1 – 3.6
68	26.0 – 32.1	52 – 456	0.7 – 3.6

As mentioned above and according to the results shown in Figure 5.1, the behavior of our data seems to indicate that the expansion of supercritical water through a sharp orifice (Figure 1.1) is neither isentropic (reversible) nor isenthalpic (completely irreversible). Nevertheless, most models used to predict flow conditions that can bring about the occurrence of choking flow, consider that the flow undergoes an isentropic process. To this aim, and to better understand our observations and their implication in the modeling approach, we have plotted two limited cases: reversible isentropic flow expansions shown in Figure 5.3a and completely irreversible isenthalpic expansions shown in Figure 5.3b. It must be pointed out that these figures cover a wide range of flow conditions for experiments carried out with constant upstream and downstream flow pressures of 23.8 *MPa* and 0.8 *MPa*, respectively. A similar behavior also applies to other flow conditions used along the actual experimental research program.

As can be observed, for a temperature range varying from a pseudo-critical value (see Equation 4.2) of 384°*C* up to a maximum of 502°*C* achieved during the experiments, depending on the type of process (i.e., $\Delta s = 0$ or $\Delta h = 0$), the flow expansion can be divided in three distinctive regions. Figure 5.3a shows that for a reversible process, it is very difficult if not impossible to experimentally determine the outlet fluid thermodynamic state. In fact, from 384°*C* to up to 502°*C*, Region I in this figure, delimits a two-phase flow zone that necessitates measured values of steam qualities.

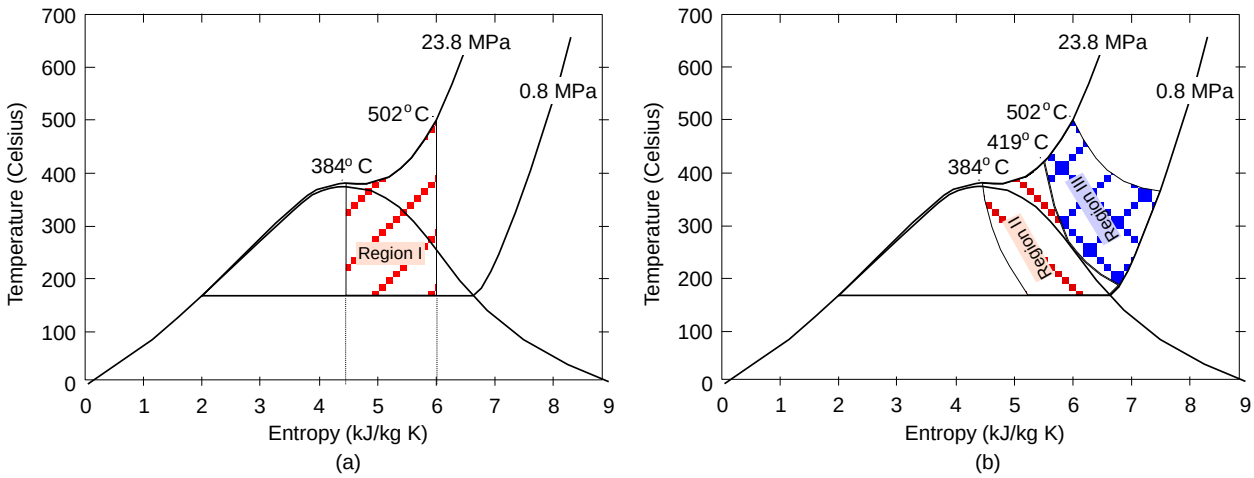

Figure 5.3 a) Isentropic flow expansion, b) Isenthalpic flow expansion.

In turn, if the expansion is assumed completely irreversible, Figure 5.3b indicates the existence of two distinctive regions. For inlet flow temperatures from 384°*C* to up to 419°*C*, most of the outlet fluid is also located inside a two-phase zone (Region II), which requires experimental quality values of the flow. Instead, for inlet flow temperatures from 419°*C* to up to 502°*C*, the Region III in Figure 5.3b shows a zone where we are able to fully characterize the flow as function of both measured temperatures and pressures. Note that the thermodynamic states explicitly shown in Figure 5.1 belong to the Region III of Figure 5.3b; nevertheless, their measured values seem to correspond to a partial irreversible expansion. This observation constitutes a key experimental fact that should be taken into account for further modeling work.

5.2 Comparison of the predictions of the choking flow models with data

In this section, the predictions obtained by using different choking flow models are compared with our experimental data. It is important to mention that limited available choking flow data obtained with sharp edged nozzles at supercritical pressures in the literature were already compared with our experimental data in Chapter 4. Since not only the ranges of the available data in the literature are limited but also they have high dispersion near pseudo-critical temperatures, they are not included for comparing them with model predictions. The following models have been selected to compare their predictions with our data: HEM and M-HEM [96-98], Bernoulli [97] and the polytropic [13] models. Note that they have already been presented in

Section 1.6. As discussed in the literature review (Section 1.6 in Chapter 1), most of them have been developed for treating flows at subcritical conditions, considering two-phase flows or superheated steam as an ideal gas. It is obvious that the application of any of these models to supercritical water flows requires variables such as steam quality, slip ratio between the phases, local throat pressure, etc., which in most cases are impossible to be experimentally determined. Therefore, even though the model predictions can be satisfactory, some care should be taken because they do not necessarily satisfy the physics that controls the choking flow phenomenon.

5.2.1 Homogeneous equilibrium and modified-homogeneous equilibrium model

Note that for clarity purposes, the equation of the HEM is once again repeated in this section. Hence, the critical mass flux is given by:

$$G_c(HEM) = \frac{\left[2\left(h_o - (1-x_E)h_{lE} - x_E h_{gE}\right)\right]^{1/2}}{(1-x_E)v_{lE} + x_E v_{gE}} \tag{5.1}$$

Recently, this equation was modified [96] into a similar one, known as the Modified-Homogeneous Equilibrium Model (M-HEM) which is written as:

$$G_c = \left[\frac{2\left(h_0 - (1-x_E)h_{lE} - x_E h_{gE}\right)}{\frac{C}{\bar{\rho}^2} + \left((1-x_E)v_{lE} + x_E v_{gE}\right)^2}\right]^{1/2} \tag{5.2}$$

where subscript *l* and *g* refer to liquid and vapor phases determined at the critical plane (i.e., at the throat), respectively. Furthermore, h_o and $\bar{\rho}$ are the enthalpy and the volumetric mass determined at flow stagnation conditions, respectively. Both models consider that the fluid expands isentropically. The principal difference between Equations (5.1) and (5.2) consists of a coefficient, *C*, that is introduced to take into account local flow resistance (for sharp edged nozzles, the authors [96] suggest using C=0.6). It is apparent that these models require an appropriate value of the steam quality. To this aim, the authors [96] have proposed to estimate it as follows:

$$x = \frac{s_o - s_l}{s_g - s_l} \tag{5.3}$$

with the entropies estimated at the critical plane by assuming that the discharge follows an isentropic process. It is apparent that the estimation of this quality necessitates knowledge of the location where choking flow occurs (i.e., the critical plane), as well the corresponding thermodynamic properties at this location.

To compare the predictions of these models with the present data set, the use of this quality is physically meaningful only when the flow undergoes an expansion that corresponds to a partial zone of Region I shown in Figure 5.3a (i.e., two-phase mixture zone). In these cases, pressure and temperature are dependent variables. Thus, the quality is determined by iteratively searching a critical plane pressure that provides the maximum value of Equations (5.1) and (5.2) (i.e., dG_c/dp=0) while keeping the entropy constant. In turn, for superheated steam both temperatures and pressures can independently change; therefore, two methods are used to determine the thermo physical properties at the critical plane. The same procedure used before for the two-phase zone is applied or the pressure and temperature prevailing in the critical plane is calculated by assuming that superheated steam (or supercritical fluid) behaves like an ideal gas at choking flow conditions (Ma=1) using Equations (5.4) and (5.5) [21]:

$$\frac{T_c}{T_o} = \frac{2}{\gamma + 1} \tag{5.4}$$

and

$$\frac{P_c}{P_o} = \left(\frac{2}{\gamma + 1} \right)^{\gamma/\gamma - 1} \tag{5.5}$$

However, it must be pointed out that for superheated steam, the isentropic coefficient γ is not necessarily constant. For different inlet fluid pressures and two values of inlet fluid temperatures (for temperatures over critical value of water where the supercritical fluid is considered to behave like an ideal gas) Figure 5.4 and Figure 5.5 are obtained using equation (1.5) and they show the variations of the isentropic expansion coefficient as function of the fluid pressure. Hence,

Equations (5.4) and (5.5) can be used with the appropriate value of γ to determine the fluid conditions prevailing in the critical plane (i.e., that maximizes the mass flow rate). Nevertheless, it is important to mention that, for upstream flow conditions close to the two-phase region, where the important portion of the expansion occurs in the wet region, the isentropic expansion coefficient presented in Figure 5.4 and Figure 5.5 cannot be used. Therefore, one must be very careful to estimate critical plane thermo-physical conditions using Equations (5.4) and (5.5) close to two-phase zone. In this study, since very large inlet flow temperatures are covered (i.e., both subcritical and supercritical temperatures), the critical mass fluxes predicted always using the first method (dG_c/dp=0) are presented. As a result, a comparison of the estimated critical mass fluxes obtained with the HEM and M-HEM models with the experimental data are shown in Figure 5.6. It is apparent that for DT_{pc} lower than 75°C, the M-HEM model with a local resistance coefficient C = 0.6 (suggested by Chen et. al. [100]) is able to follow the experimental trends very well. It is interesting to observe that this model is also able to catch the flow transition occurring around DT_{pc} = 0°C. In turn, the HEM slightly over predicts the data.

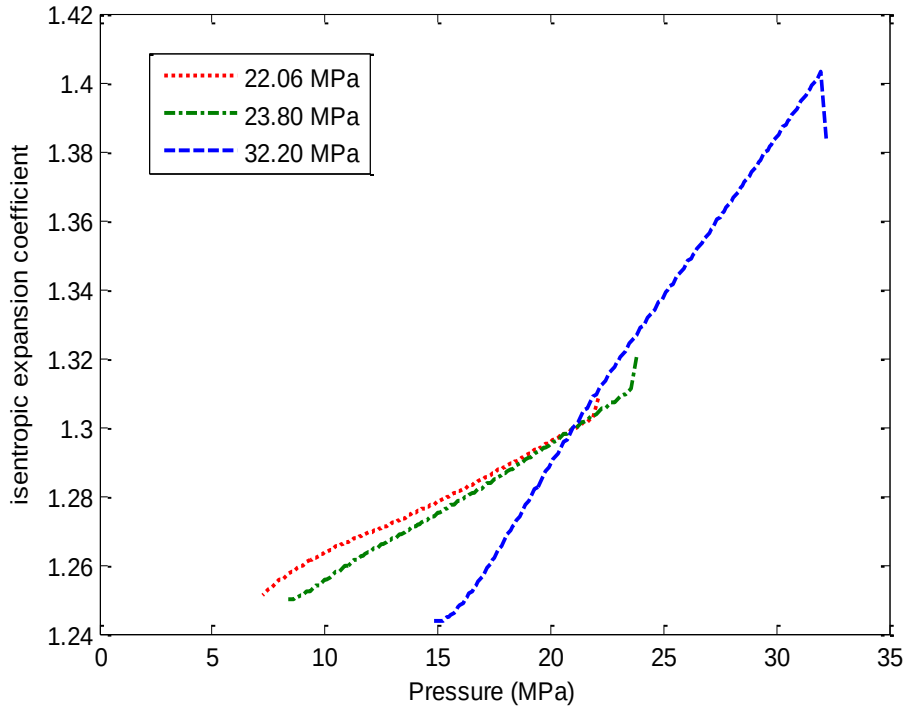

Figure 5.4 Isentropic expansion coefficient for different upstream flow pressures at 450°C.

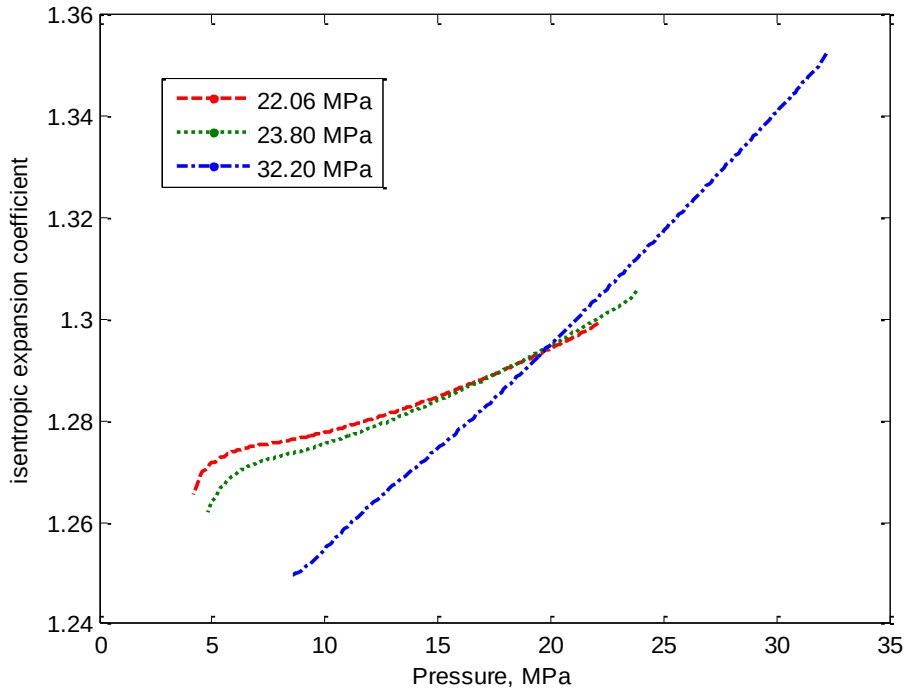

Figure 5.5 Isentropic expansion coefficient for different upstream flow pressures at 500°*C*.

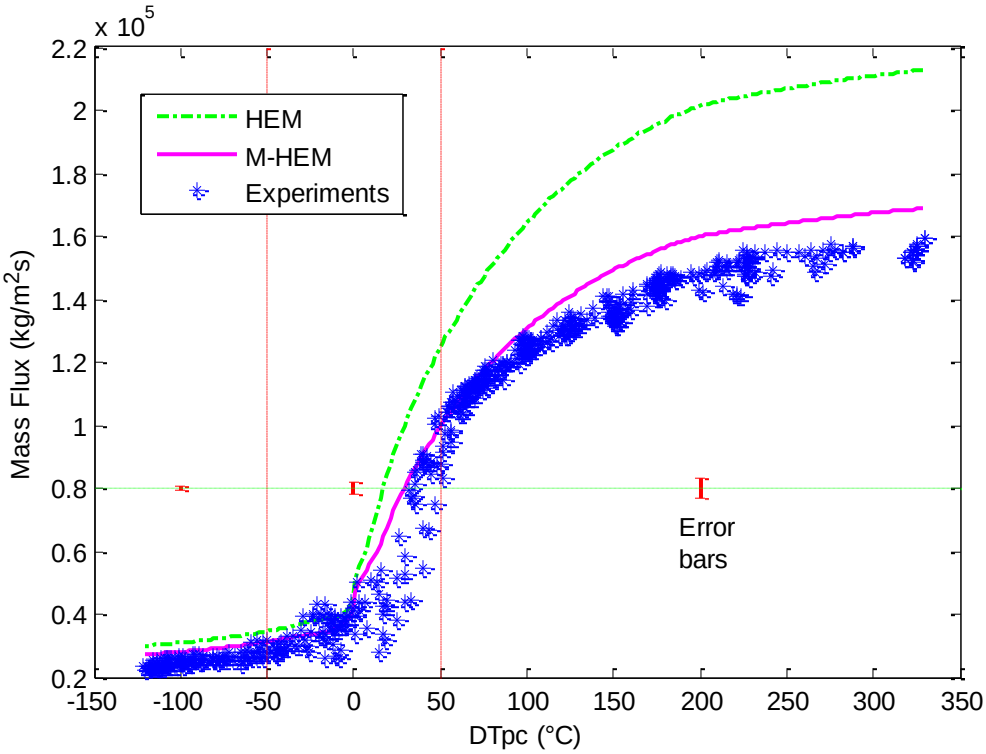

Figure 5.6 Comparison of HEM and M-HEM (C = 0.6) with experimental data at P_o=24 *MPa*.

It is important to mention that for superheated steam conditions at the discharge of the nozzle; the latter method (isentropic expansion coefficient obtained from Figure 5.4 and Figure 5.5) is also used to determine the flow conditions at the critical plane. In this case, M-HEM is able to predict critical mass fluxes reasonably well. Nevertheless, for subcritical inlet flow conditions (i.e., $DT_{pc} > 50°C$) the predictions are not able to follow the data. For the same region, the HEM model always over predicts the data using latter method (constant γ) to calculate the critical plane conditions. These results provide a good indication that the expansion cannot be considered as completely reversible. In fact, the use of constant C in the M-HEM accounts for some tendency toward equilibrium due to a partial momentum transferred by friction.

Later, we have modified the local resistance factor proposed by Chen et al. [100] since that factor was suggested for sharp edged nozzle diameters of 1.41 *mm*, however in this study, the experiments are performed with 1 *mm* nozzle ID. The M-HEM predictions using C=0.8 for flow pressure of 24 *MPa* are presented in Figure 5.7.

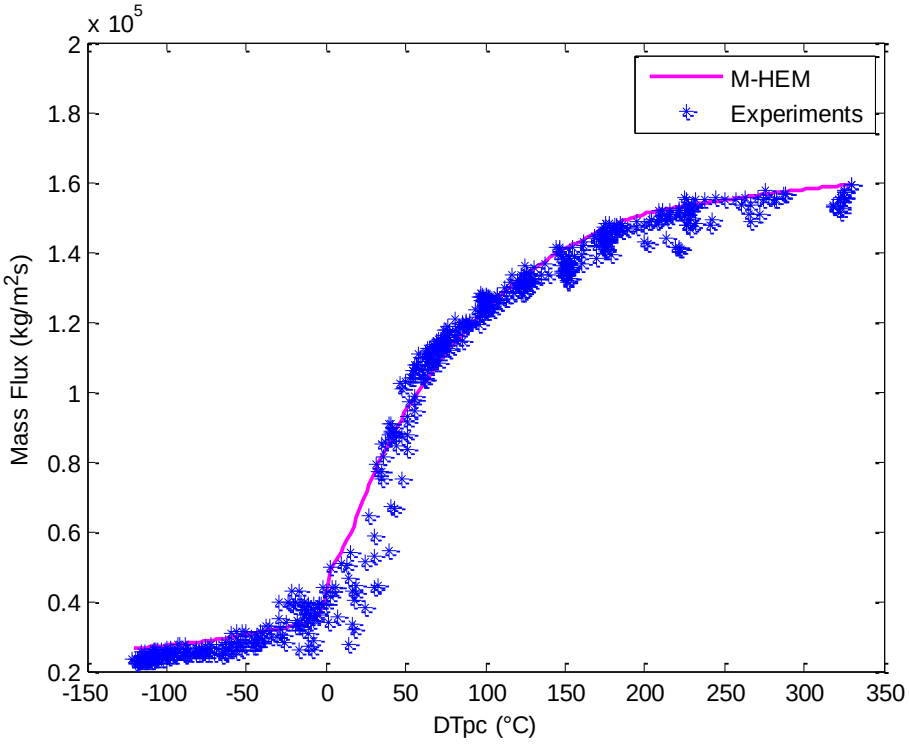

Figure 5.7 Comparison of M-HEM (C = 0.8) with experimental data at P_o=24 *MPa*.

As seen, an excellent fit is obtained for both subcritical and supercritical flow temperatures. Therefore, we suggest to use C=0.8 to estimate the mass fluxes for 1 *mm* ID sharp edged nozzles regardless of flow state (choked or not) at supercritical pressures.

5.2.2 Bernoulli equation

As mentioned before, predictions obtained with Bernoulli's model are also compared with the data. This model, already discussed in Section 1.6, is rewritten as:

$$G_c = C_d \sqrt{2\rho\left(P_o - P_d\right)} \tag{5.6}$$

Figure 5.8 shows the results obtained for two different values of the C_d coefficient required by this model (i.e., C_d=0.4 and C_d= 0.7) for flow pressure of 24 *MPa*.

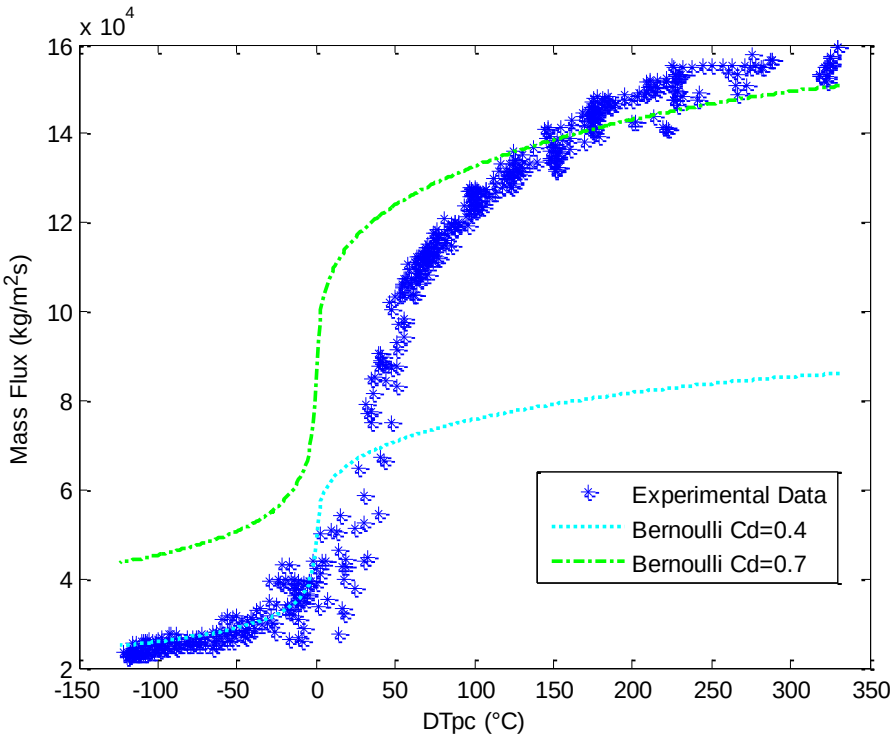

Figure 5.8 Comparison of the prediction obtained Bernoulli's equation with experimental data at P_o=24 *MPa*; P_d=0.8 *MPa*.

In general, Bernoulli's equation seems to estimate mass fluxes at both subcritical (DT_{pc} > 150°C) and supercritical (DT_{pc} < 25°C) flow conditions. Nevertheless, this figure clearly indicates that

for $DT_{pc} > 150°C$, a value of C_d=0.7 produces quite good mass flux predictions, which is not necessarily the case for the lower value of this coefficient. Instead, for $DT_{pc} < 25°C$ this behavior is reversed in such a way that C_d=0.4 seems to be a good choice for predicting critical mass flux in the supercritical region. This comparison seems to indicate that Bernoulli's model is not appropriate to handle both subcritical and supercritical flow conditions using a single value for the C_d coefficient.

5.2.3 Polytropic expansion approach

In this section, the predictions of new modelling approach that was presented in Section 1.6.1 are given. Based on the experimental observations discussed concerning the results presented in Figure 5.1 and Figure 5.3, the model should capture the fact that the flow expansion is neither reversible nor completely irreversible. Figure 5.9 shows the comparison of the predictions obtained with this model assuming both isentropic ($n=\gamma$) and isothermal (n=1) flow expansions. Note that for ideal gases an isothermal process corresponds to dh=0.

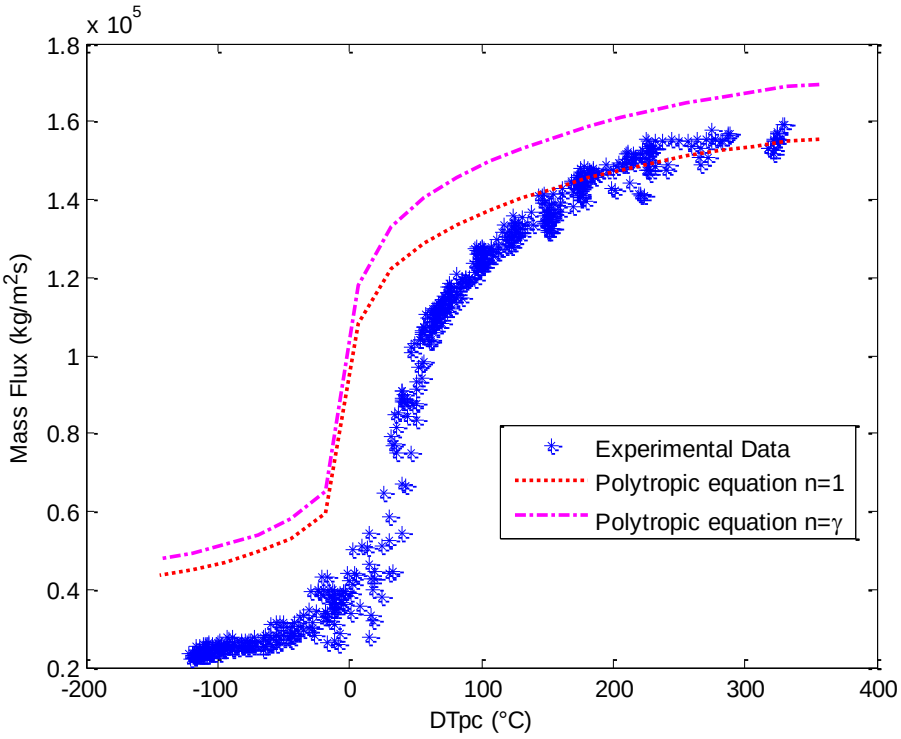

Figure 5.9 Comparison of the prediction obtained with the polytropic equation with experimental data for γ=1.30, P_o=24 *MPa*.

The maximum mass flux is obtained according to the procedure already explained for the HEM and M-HEM (i.e., $dG_c/dp=0$). It is apparent that the polytropic approach seems to follow the trend of the experimental data. However, in general, it over predicts the data. Only about $DT_{pc} > 150°C$, the isenthalpic expansion ($n=1$) is able to predict the mass fluxes where the flow is not choked. For higher values of the fluid temperature ($DT_{pc} < 150°C$), neither the use of a reversible nor the use of a completely irreversible expansion coefficient is able to catch the experimental results. These predictions provide a solid argument about the validity of the experimental observations presented in Figure 5.1. Even though the proposed model over predicts the data, it has similar trends compared with the experimental data. Therefore, a new parameter that will take into account a local resistance factor (similar to M-HEM) should be implemented to increase the accuracy of this approach.

As summary, the M-HEM model with the local resistance factor C equal to 0.8 is the most suitable model to estimate the mass fluxes at supercritical conditions for 1 *mm* ID sharp edged nozzles. After performing additional experiments with different orifice geometries and sizes, this model can be improved by implementing these parameters into local resistance factor, C.

5.3 Experimental repeatability and overall quality of the data

In addition to the error analyses discussed in Chapter 4, to verify the repeatability of the data, similar experiments are repeated at different dates. Furthermore, data are continuously recorded for long periods while both flow pressure and temperature are increased up to reaching the desired supercritical water conditions. In addition, to validate the measurements of fluid and wall temperatures, a heat balance in conjunction with forced convection heat transfer calculations are also applied to the heater element (Figure 2.4). These procedures, implemented to certify the overall quality of the data, are discussed in the following sections. It must be pointed out that the application of this methodology constitutes part of the QA requirement of the Gen-IV program.

5.3.1 Comparison between continuous collected data sets

To verify data reproducibility, experiments are repeated by applying almost the same inlet and outlet flow conditions used before to obtain the data presented in Chapter 4. Nevertheless, instead of saving groups of 100 samples per data point as explained in Section 4.5, in this case, a continuous data recording is performed for periods of about 30 minutes each. By using the same

sampling rate of 100 *ms*, these experiments contain about 18000 points. Data collected using this methodology for inlet and outlet flow pressures of 24 *MPa* and 0.78 *MPa*, respectively, are compared with the entire set of averaged data in Figure 5.10. It is apparent that in the T-s plane representation, the agreement between these two ways of collecting data is excellent. The scattering observed in the supercritical region is due to the fact that the average data are obtained at different upstream pressures by changing the downstream pressures, as it was explained in Chapter 4. It is obvious that in the subcritical region, the incompressibility of the water smooth down the dispersion of the data.

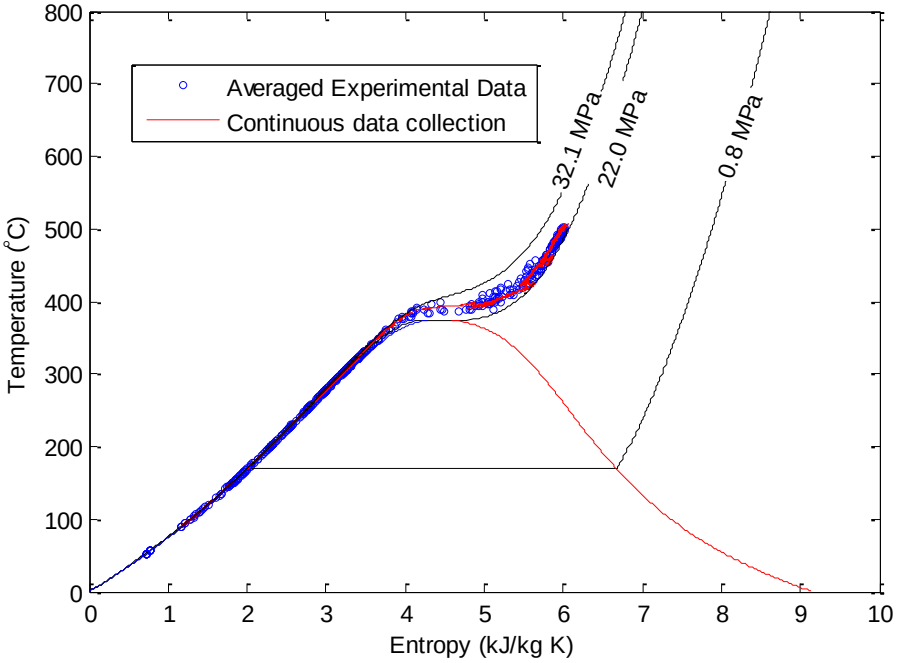

Figure 5.10 Averaged data vs. continuous data collection at supercritical pressures.

In particular, continuously collected data allow us to analyse the dynamic behavior of the supercritical water system. To this aim, a typical continuous experiment is plotted in Figure 5.11. It is important to remember that in Section 4.7, the error analysis is divided into three region as Region I for $DT_{pc} < -50°C$, Region II for $-50°C \leq DT_{pc} \leq 50°C$ and Region III for $50°C > DT_{pc}$. These regions (separated with dashed lines) roughly correspond in Figure 5.11 to the following time scale: Region I for time $2800\ s \leq \tau \leq 3650\ s$, Region II for time $3650\ s \leq \tau \leq 3825\ s$, Region III for time $3825\ s \leq \tau \leq 4580\ s$. Figure 5.11 shows that in order to reach choking flow for water at supercritical conditions, the thermal power applied to the heater element (see Figure

2.2) is increased almost linearly (i.e., Region I). As expected, within this region the bulk fluid temperature measured in the calming chamber (see Figure 2.2), also increases linearly, while the mass flux decreases nonlinearly due to its acceleration (i.e., decrease of the volumetric mass). It is important to remark that the outlet pressure stays almost constant along this region. At about a fluid bulk temperature of about 320°*C*, the maximum wall heater temperature reaches the supercritical value (i.e., about 374°*C*; this temperature is not shown in Figure 5.11) which consequently increases the heat transfer coefficient quite rapidly. At this moment both the fluid bulk temperature and pressure start increasing very rapidly; this is clearly indicated by the changes observed in Region II in Figure 5.11. Hence, to maintain the outlet pressure at the desired value, the thermal power must be rapidly reduced. As has already explained in detail in Chapter 4, the control of the supercritical loop in this region is very cumbersome. In fact, approaching the pseudo-critical temperature from the liquid-like zone provokes major changes on all thermo physical fluid properties.

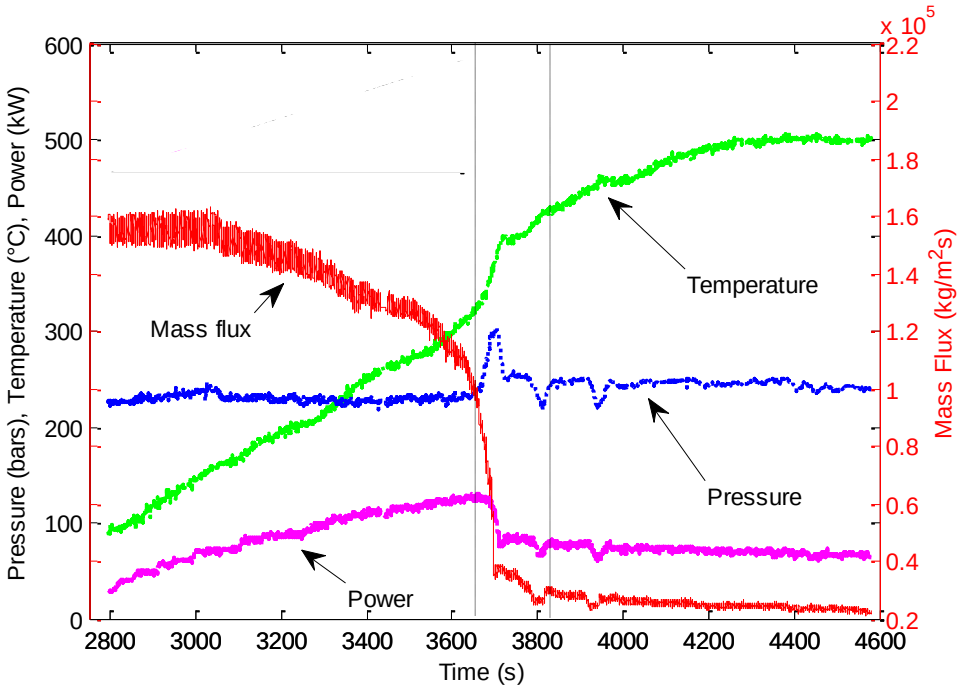

Figure 5.11 Evolution of experimental parameters for continuous data collection.

In particular, in this region the volumetric mass decreases, the heat capacity increases and the speed of sound decreases. After achieving the stabilization of the loop, toward the end of Region II in Figure 5.11, the speed of flow at the orifice plate accelerates and becomes choked.

Therefore, in this region the mass flow rate decreases very fast and reaches almost a stable value afterwards. Figure 5.11 also shows that after achieving choking flow conditions in Region III (i.e., gas-like region), the control of the loop becomes more stable. However, this region is characterized by an important decrease in the fluid heat capacity; thus, convective heat transfer decreases at a relatively high pace where a deteriorated heat transfer regime takes place, consequently an increase in the heater wall surface temperatures are observed. This behavior will be discussed in more detail in the following section. The deterioration of convective heat transfer is partially explained by the fact that even though the bulk fluid temperature continues to increase with decreasing the thermal power, the wall temperature increases much faster (data not shown in Figure 5.11). These results will be also analysed in the following section. In general, Figure 5.11 shows that for such a complex kind of experiment, with the exception of few pressure and temperature fluctuations occurring inside Region II, all key flow variables are measured with relatively low scattering.

Mass fluxes as a function of the pseudo-critical temperature estimated using the equation (4.2) are presented in Figure 5.12 for two similar experiments performed at different days, by covering flow regions given above.

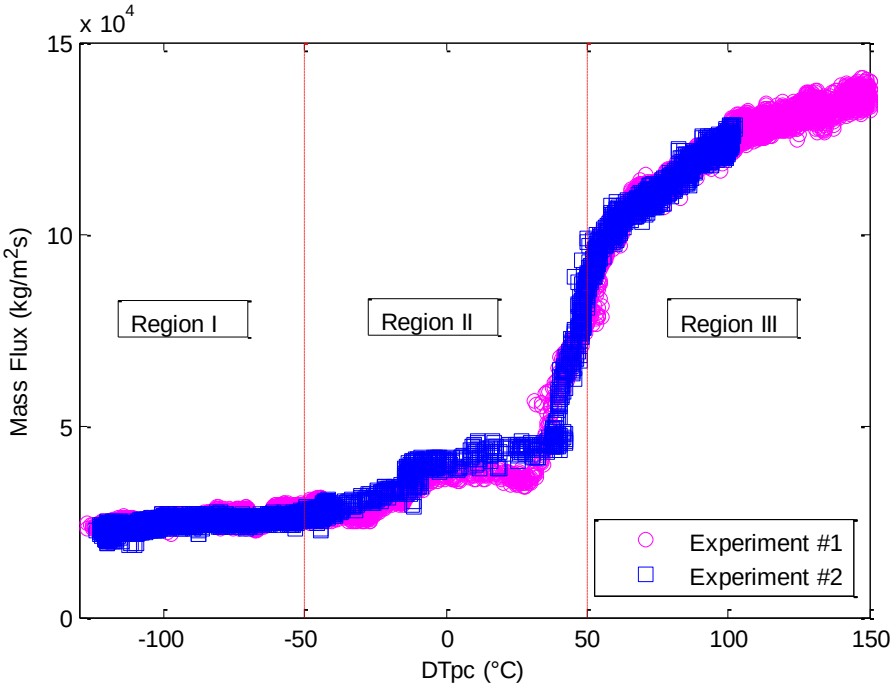

Figure 5.12 Repeatability study.

In Region I, where the flow is observed as choked and at supercritical temperatures, the upstream pressure is 24.0 *MPa* ± 0.3 *MPa* for experiment #1 and 23.7 *MPa* ± 0.3 *MPa* for experiment #2. In Region 3, where the flow is considered not choked and has temperatures lower than the critical temperature, the upstream pressure is 22.8 *MPa* ± 0.2 *MPa* for experiment #1 and 22.7 *MPa* ± 0.3 *MPa* for experiment #2. In all regions, the back pressure is kept constant for both experiments at 0.78 *MPa* ± 0.02 *MPa*. Once again a total collection time of 30 *min* and a sampling time of 100 *ms* are used to collect the data.

Figure 5.12 confirms the excellent reproducibility of the experiments. In particular, for supercritical choking flow conditions, i.e., Region I in the figure, the scattering between the data is less than ± 4.9%. Nevertheless, the scattering increases to up to ± 7.9% in Region II. As explained before, this corresponds to a transition zone where the control of the supercritical loop is extremely difficult. The dispersion in the data decreases with increasing the pseudo-critical temperature in Region III. This is a zone where the fluid is at subcritical conditions and the thermo-physical properties are not significantly affected by the fluid temperature and pressure. In addition to error analyses presented in Chapter 4, the three regions shown in Figure 5.12 are also used to estimate the error margins of the measurements which are summarized in Table 5.3.

Table 5.3 Experimental errors for each flow regions shown in Figure 5.12.

Experimental Region	Upstream pressure (*MPa*)	Upstream temperature (°*C*)	Discharge pressure (*MPa*)	Mass flux (kg/m^2s)
Region I (DT_{pc} < -50°*C*)	0.3 %	0.3 %	0.4 %	4.9 %
Region II (< -50°*C* DT_{pc} < 50°*C*)	1.7 %	0.6 %	0.4 %	7.9 %
Region III (DT_{pc} > 50°*C*)	0.7 %	0.8 %	0.4 %	5.3 %

Furthermore, to determine the region where the flow reaches choking conditions, the average mass flux data collected for an inlet flow pressure of 23 *MPa* and for three values of downstream discharge pressures are presented in Figure 5.13. This figure shows mass fluxes as a function of DT_{pc} calculated using Equations (4.1) and (4.2). The zoomed portion of the data illustrated by the

insert in the same figure clearly shows the region where the flow becomes choked and how the discharge pressure affects the mass flux. It is apparent that for $DT_{pc} > 75°C$ the flow is not choked; the mass flux increases with increasing the discharge pressure. Nevertheless, from the actual data set, it is very difficult to exactly determine the conditions which bring about choking flow. Therefore, we assume that the flow reaches the speed of sound for a DT_{pc} of about $75°C$. Accepting this criterion, Figure 5.13 shows that the flow is completely choked in Region I and II (see Figure 5.12). It must be pointed out that to increase the accuracy on the determination of these limits; it is necessary to further increase the discharge pressure. To this aim we propose to introduce a partial flow blockage far away downstream the orifice in the long discharge line shown in Figure 2.2 and Figure 2.3. This implementation should permit us to repeat similar experiments without over passing maximum operation limits imposed by the medium pressure loop (see Section 2.1).

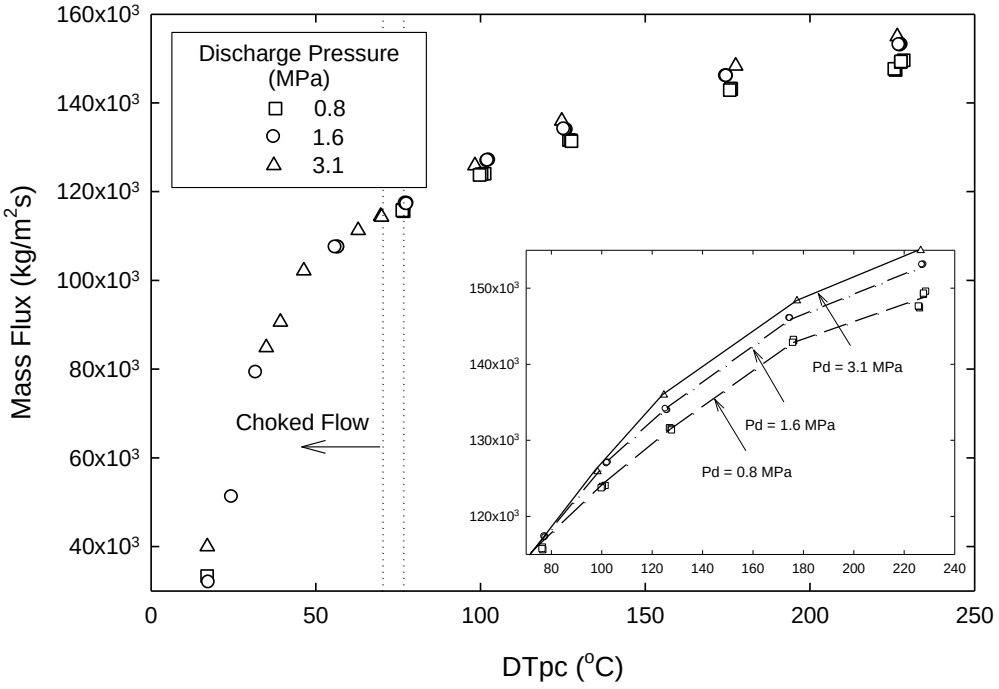

Figure 5.13 Mass flux as a function of DT_{pc} and discharge pressure at 23 *MPa*.

Furthermore, the results presented in Figure 5.13 confirm that in order to determine unambiguously the conditions that could bring about choking flow to occur, the change on the

back flow pressure is mandatory. This observation imposes some doubts on similar choking flow data obtained by other researchers using blowdown type experiments.

5.3.2 Validation of temperature measurements from heat balance and heat transfer calculations

In Section 2.2.3 (Chapter 2) the estimated temperature profiles used for designing the heater element shown in Figure 2.10. However, even though heat fluxes and thermal conductivity of the heater element tubes are selected according to the average temperature of each heater element branch, at the design stage, convective heat transfer coefficient is taken constant along the heater element. In addition, it is also important to mention that Figure 2.10 is obtained for the maximum flow rate that HP pump can supply. In reality, as explained previously, at choking flow conditions the maximum mass flux rate is defined by the flow and it is dependent to flow upstream pressures and temperatures. Consequently, the critical mass flow rate becomes only a function of critical mass flux and orifice diameter. Since in this study, the diameter of the orifice is not changed, critical mass flux also can be expressed as a function of pressures and temperatures.

Before comparing the measured heater element surface temperatures with the estimated heater values, it is obviously necessary to know several other parameters such as, change of the heater element thermal conductivity with temperature and the convection heat transfer coefficient and as well as heat losses. These two items are discussed in the following sections.

5.3.3 Heat losses

The study of heat transfer is not the primary subject of this research since it does not affect directly the choking flow results. Even though the heater element is carefully insulated, there will always be heat losses due to the temperature difference between the heater element surface and the ambient. For this aim, to predict the thermal losses, several thermocouples are inserted in the insulation material as explained before in Section 2.2.3.

In Table 5.4, results of two different experiments that are performed under supercritical conditions at two different days are presented. Since excellent repeatability of the experimental conditions are achieved, only data collected on June 17th, 2013 are used to produce Figure 5.14

and Figure 5.15. In fact, both axial and radial temperature profiles on the heater element for these two experiments come on top of each other.

Table 5.4 Results for two similar experiments performed on different days.

Experiment date	Upstream pressure (*MPa*)	Heater inlet temperature (°*C*)	Heater outlet temperature (^{o}C)	Discharge pressure (*MPa*)	Measured mass flow rate (*kg/s*)	Applied power (*kW*)
30 May 2013	23.92	32.6	498.86	7.83	0.017886	57.34
17 June 2013	24.00	32.3	499.05	7.83	0.017794	58.13

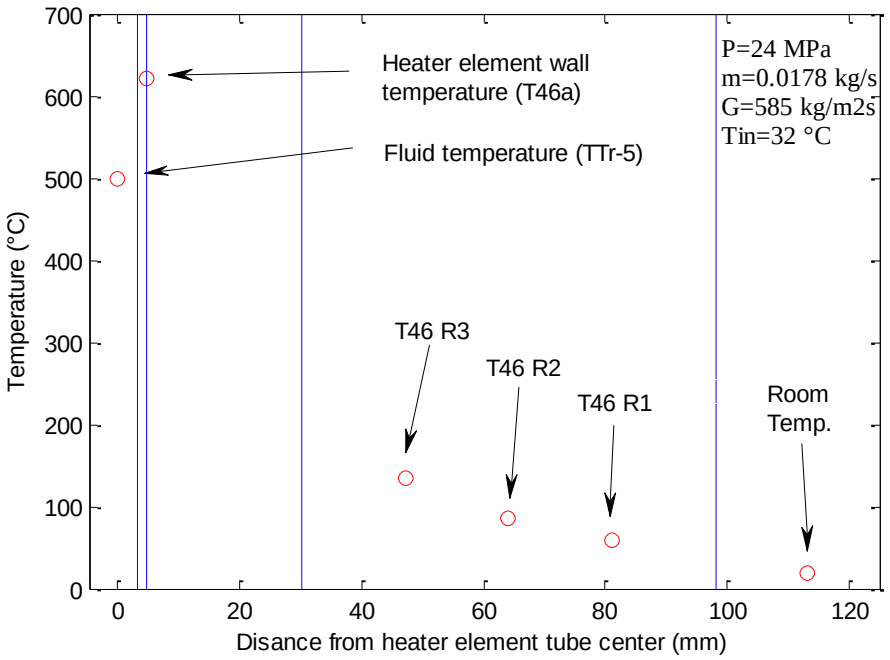

Figure 5.14 Radial temperature at the exit of the heater element.

As a result, Figure 5.14 shows a radial temperature profile obtained by treating data collected from thermocouples TTr-5, T46a, T46 R1, T46 R2, T46 R3 and the room temperature (See Section 2.3.1 and Figure 2.21); further Figure 5.15 shows the axial temperature profile obtained from the spot welded thermocouples on the heater element.

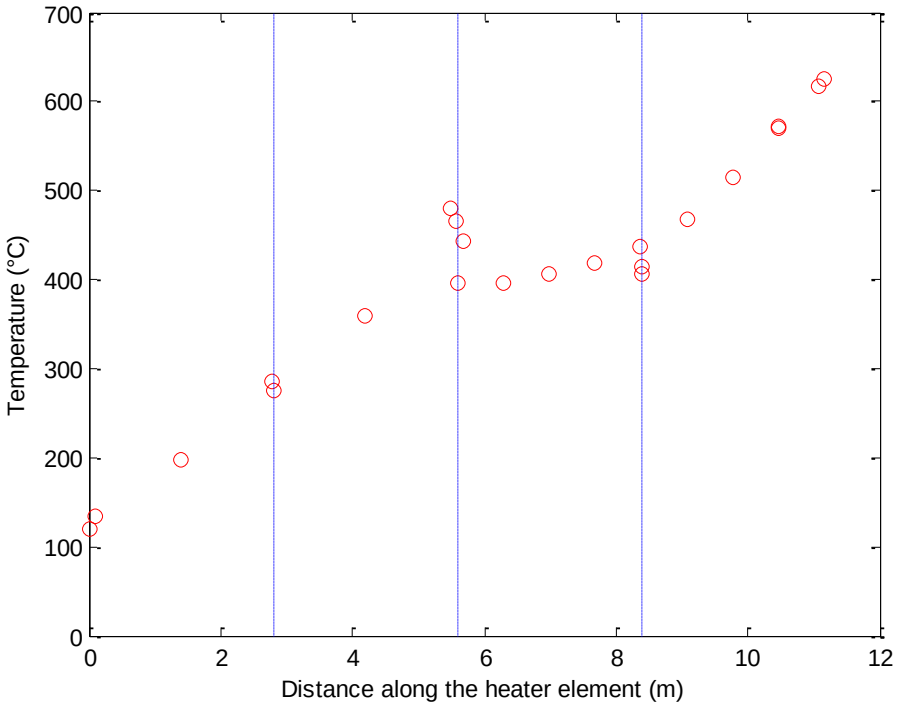

Figure 5.15 Heater element measured surface temperatures.

In Figure 5.14, the first two vertical lines on the left side represent the heater element's inside surface and outside wall surfaces, respectively. The third vertical line corresponds to the interface of Superwool® and Foamglass® thermal insulation materials and the fourth line represents the outside surface of the Foamglass® thermal insulation material.

As explained before, the electrical resistivity of the heater element material changes (increases) with temperature, therefore; the electrical currents passing through each branch of the heater element are not necessarily the same (i.e., electrical current decreases with increasing temperature). Consequently, the applied electrical power tends to decrease in the direction of the flow inside the heater element (i.e., last branch in Figure 2.18 has less thermal heat flux than the first one). For simplicity, to perform the heat transfer calculations, the heat applied to each individual branch of heater element is estimated assuming an average value of the electrical resistivity; then heat flux for each heater element is calculated by taking into account that resistivity. However, in the open literature the electrical resistivity of the Hastelloy C276 is not given for all temperatures [115, 116]; therefore, it is estimated by interpolation.

For the experiment presented in Figure 5.14 and Figure 5.15, it is clear that the applied power and the surface temperature of each heater branch are different and as a result, the heat losses from every branch will be different. However, once again and for simplicity, heat losses are considered evenly distributed all along the heater branches.

Knowing the mass flow rate, the inlet temperature and the outlet fluid temperature that are given in Table 5.4, one can calculate the absorbed energy from the following heat balance equation:

$$\mathrm{Q} = \dot{m}\Delta h \tag{5.7}$$

where Δh is the enthalpy difference of the flow between the inlet and outlet of the heater element and $\dot{m}$ is the measured mass flow rate.

The difference between the measured applied heat and the real heat transfer to the fluid is considered as heat losses. As previously presented in Section 2.3.5, there are two different electrical power measurement systems in the loop. Since a difference is observed between these two devices, the average value of the power is used to calculate heat losses. It is important to mention that, according to equation (5.7) and measured power, between 2 - 7.5% of the applied power is lost depending on the experiment. For the data presented in Table 5.4 only 53.75 kW is absorbed by the fluid. Thus, the applied powers to branch 1 to 4 are found to be 14.04 kW, 13.51 kW, 13.23 kW, and 12.97 kW, respectively.

Actually, the estimated heat losses values seem high, but most of them can be associated to the cooling of the copper clamps. In fact, after preliminary experiments, it is observed that the temperature of the cooper clamps at the bottom side of the heater element (Figure 2.4) were too high. Fans are installed to cool down the copper clamps. These fans also cool the unheated elbows of the heater element (these phenomena will be seen more clearly when the surface temperature profile will be presented in section 5.3.5).

On the other hand, the overall heat transfer between outside surface temperature of the heater element and ambient temperature (i.e., heat losses) are calculated as:

$$Q = \frac{T_{sur} - T_{amb}}{\frac{\ln(r_1 / r_2)}{2\pi L k_1} + \frac{\ln(r_2 / r_3)}{2\pi L k_2} + \frac{1}{2\pi L h_{air}}} \tag{5.8}$$

The maximum estimated value of the heat losses is found to be less than 2%. To determine convective heat transfer to supercritical water, both heat conduction across to tube and an appropriate correlation for the heat transfer coefficients are required. These two items are discussed in the following sections.

5.3.4 Conduction heat transfer coefficient across the wall of heater element

The conduction heat transfer coefficient also changes with temperature along the heater element; it increases with increasing the fluid temperature [115, 116]. Nevertheless, for the purpose of present calculations, this coefficient is considered constant for each branch, but it is varied from one branch to another. The following equation is used to estimate the thermal conductivity of Hastelloy C-276 alloy:

$$k(T) = 0.0171 \times T + 4.975 \tag{5.9}$$

where T is given in Kelvin and conductivity $k(T)$ is in *W/mK*.

5.3.5 Convective heat transfer at supercritical pressures

The estimation of the convective heat transfer coefficient is a real challenge not only for simple tube geometry but also for fuel bundles. Many flow parameters affect this coefficient; some of them increase its value while others can provoke a sudden decrease. In the current study, the flow pressure is always above the critical value, but the temperature of the fluid changes from subcritical to supercritical by passing the critical temperature of the water (i.e., 373.95°*C*). As explained in Section 1.3, drastic changes on the thermo-physical properties of the water occur close to critical or pseudo-critical temperatures. All of these changes on fluid properties make the estimation of the convective heat transfer of supercritical water extremely difficult.

Furthermore, according to Figure 2.3 and Figure 2.18, the flow direction changes along the heater element while the temperature of the fluid continuously increases. Therefore, the fluid can be in downward or upward flow conditions both at subcritical temperatures or supercritical

temperatures. Since the thermal power is increased to reach high temperatures, the location where the transition from subcritical to supercritical temperatures can also shift from upward to downward flow regions. Moreover, when the drastic temperature drop occurs near pseudo-critical temperature (see Figure 1.7), the speed of sound at that pressure reaches a minimum (see Figure 1.8); consequently, for a limited period of time, the outlet pressure of the system increases. Under these conditions, to control the outlet flow variables, the speed of the variable motor drive of the HP pump is adjusted to maintain a desirable flow pressure. All these changes affect not only the convective heat transfer coefficient but also the thermal conduction across the wall of the tube (i.e., important variation of temperatures and heat losses).

The convective heat transfer for the experimental conditions given in Table 5.4 for the data collected on June 17th, 2013 is estimated using the Dittus-Boelter correlation [5] given by:

$$Nu = 0.023 \times \mathrm{Re}^{0.8} \times \mathrm{Pr}^{0.4} \tag{5.10}$$

where the Reynolds and Prandtl numbers are calculated using the bulk temperature of the fluid. To obtain the bulk temperature of the fluid along the heater element, Equation (5.7) is used.

The results of this correlation are presented in Figure 5.16 and Figure 5.17 for both heat transfer coefficient vs. distance from the inlet of the heater element and heat transfer coefficient vs. bulk fluid temperature. To better analyse the results, vertical dotted red lines in Figure 5.16 are used to distinguish the exact locations where the heater element is divided into branches. As previously explained, each leg has 2.794 *m* (110 *in*) long heated section. The flow is downwards direction at the first (inlet) and the third branches and upwards direction at the second and the forth (outlet) branches. It is already mentioned in the literature section that the flow direction may have an effect on the convective heat transfer coefficient. However, since not all the literature studies do not agree how the flow direction affects the convective heat transfer coefficient, especially under supercritical conditions, the Dittus-Boelter correlation is used to estimate the convective heat transfer coefficient without taking into account the effect of flow direction.

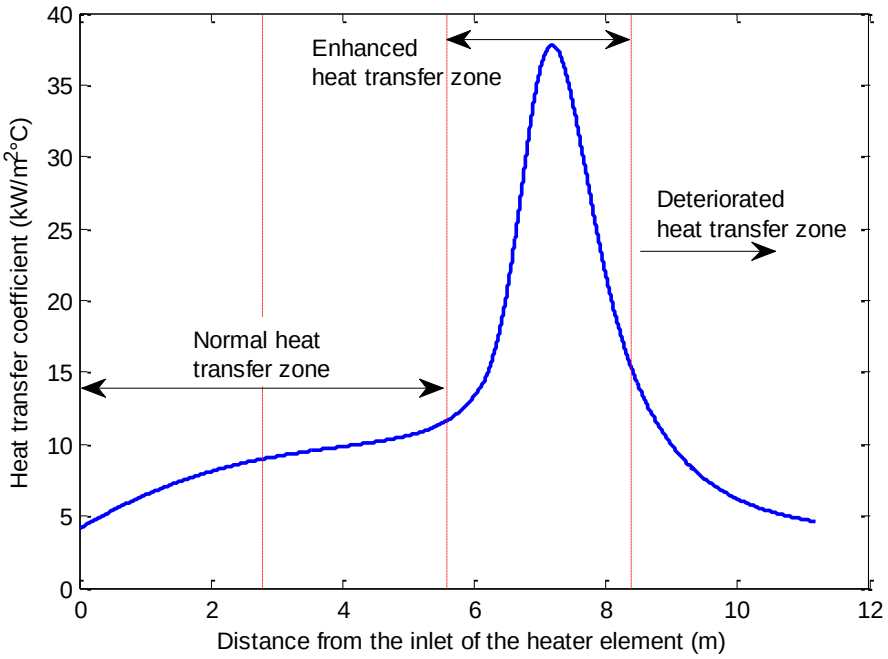

Figure 5.16 Estimated heat transfer coefficient using the Dittus-Boelter equation.

Figure 5.16 clearly shows that the convective heat transfer coefficient predicted by using Dittus-Boelter equation has the following three different regimes: *i*) normal forced convective heat transfer taking place along the first and second branches, *ii*) enhanced forced convective heat transfer occurring along the third branch and *iii*) deteriorated forced convective heat transfer which characterizes the flow in the fourth branch. It must be pointed out that similar results were also obtained by Zoghlami [39]. Even though three regimes are associated with different branches of the heater element in this figure, one must be very careful while using this information since these predictions are obtained using the data given in Table 5.4. If the heater element outlet temperature changes, the locations where different heat transfer regimes occur may shift; therefore depending on the flow conditions, one may not see the deteriorated heat transfer regime at all.

Figure 5.17 shows the forced convective heat transfer coefficient as a function of the bulk fluid temperature. It is clearly seen that the heat transfer coefficient increases quite sharply at the inlet of the third branch of the heater element. i.e., while the flow temperature approaches the pseudo-critical temperature (green dotted line). It reaches a maximum at the pseudo-critical temperature and then decreases drastically with increasing the fluid temperature. For water flows, this effect

seems to be more dominant for flow pressures close to the critical value but it is less dominant for higher pressures. It is important to remark that similar results have been published for water and other fluids [5].

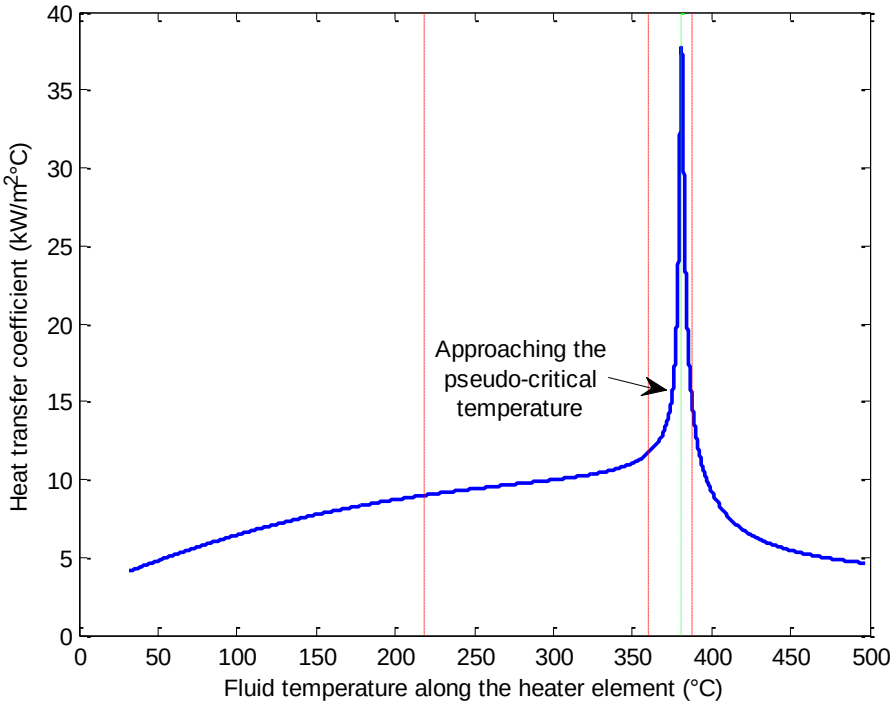

Figure 5.17 Heat transfer coefficient as a function of bulk fluid temperature.

After considering heat losses, as well as the change on the thermal conductivity of Hastelloy C276 and the convective heat transfer coefficient for each branch, the fluid temperature profiles were recalculated. The results are then compared with measured wall temperatures in Figure 5.18. The temperature difference profiles between the heater wall and the bulk fluid temperature are shown in this figure clearly indicate that the heat transfer coefficient increases slowly along the first two branches and reaches a peak in the third branch. Afterwards, a deteriorated heat transfer mode seems to occur; therefore, the difference between the measured surface temperature and the fluid temperature increases along the fourth branch of the heater element.

As mentioned previously, the copper clamps at the bottom of the heater element are cooled with fans to avoid their overheating. Furthermore the elbows on the heater element are not heated;

therefore, when the fluid passes from one branch to another, there is always a temperature drop on the surface of the heater element. This phenomenon is observed (shown in Figure 5.18) from the measurements performed by thermocouples that are spot welded on the wall at both the inlet and outlet sides of each elbow (See Thermocouples T14 and T21a in Figure 2.18).

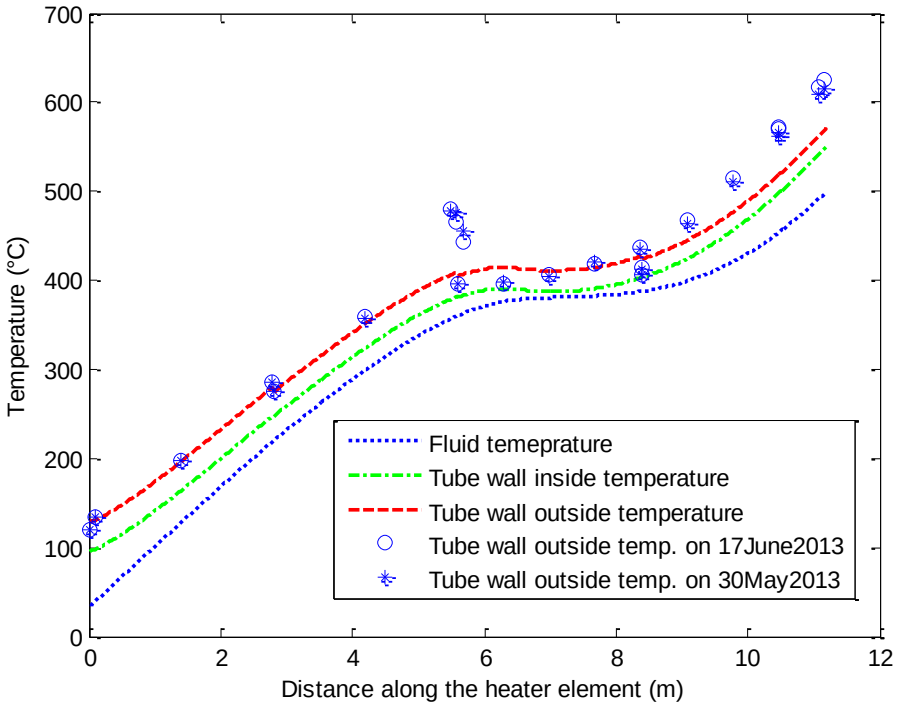

Figure 5.18 Temperature profile along the heater element.

Along each experiment, wall temperature profiles are measured and these values are used to satisfy safety requirements. In general, Figure 5.18 shows that for subcritical flow conditions wall temperature measurements are in good agreement with the estimated surface temperatures. It is obvious that for these cases, the heat transfer coefficient seems to be estimated reasonably well. However, for measured fluid temperatures higher than 400°*C*, not only the wall surface temperatures start deviating from the estimated values but also the temperature differences between the tube surface and fluid increase. This provides a clear indication that for temperatures higher than 400°*C* a deteriorated heat transfer regime is developed and the Dittus-Boelter equation is not able to provide good results.

Another important observation is that when the bulk fluid temperature approaches the pseudo-critical value, just before the enhanced heat transfer regime occurs, the heater element wall surface temperature increases quite fast. It is apparent that this behavior can only be explained by a decrease in the convection heat transfer coefficient; thus, the Dittus-Boelter correlation seems unable to predict this decrease. In principle, the differences between these wall surface measurements can be considered as thermocouple reading error because they are systematic for almost all experimental conditions, but other studies [67] in the literature also observed this behaviour for vertical upward supercritical water flows. Since most of the experiments in this thesis contain subcritical to supercritical transitions in downward flows, they are not compared in detail with other researchers. In the future, the number of the surface temperature measurements in this section of the heater element should be increased to perform other experiments in order to better understand the heat transfer coefficient near pseudo-critical temperatures.

It is important to mention that Figure 5.18 is obtained for a constant flow pressure. However, we know that the flow pressure has important effect on the estimation of convective heat transfer coefficient [5]. Therefore, to better understand the effect of the flow pressure on the convective heat transfer coefficient for water close to pseudo-critical temperature, the estimated heat transfer coefficient by using Dittus-Boelter equation for different fluid pressures and for $500°C$ fluid outlet temperatures are presented in Figure 5.19.

From this figure, it is clear that the highest heat transfer coefficient occurs at fluid pressure close to the critical value. This result is also coherent with the change of isobaric heat capacity of the water for different pressures (See Figure 1.11). Thus, similar to the isobaric heat capacity the location of the maximum heat transfer coefficient changes because the pseudo-critical temperature also changes with pressure. Even though the location of the maximum convective heat transfer coefficient for 32.2 MPa curve is not very clear, it is good to mention that the increase of the pressure shifts the pseud-critical temperature in the heater element. This behaviour provokes the deviation on the locations where the maximum heat transfer occurs in the heater element. At first, over 250 kw/m^2 of convective heat transfer coefficient seems to look very high but the literature review shows that other researchers also observed very high heat transfer coefficients for pressures close to critical values using water [5].

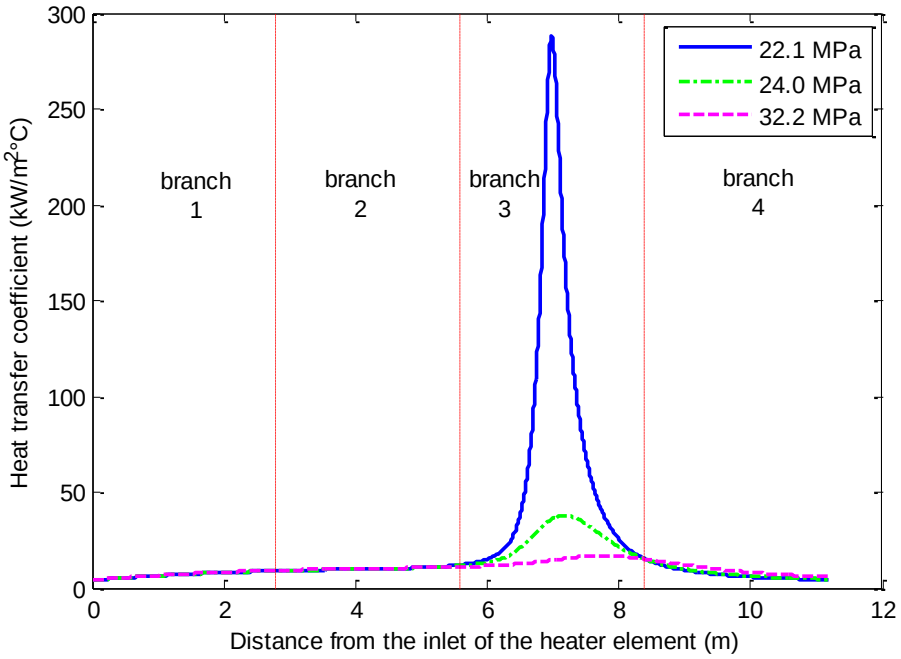

Figure 5.19 Estimated heat transfer coefficient for different flow pressure conditions.

CHAPTER 6 GENERAL DISCUSSION

The objective of this study is to design and construct a supercritical choking flow loop to perform choking flow experiments at flow conditions close to those of future Supercritical Water Cooled Reactors. The choking flow study at supercritical conditions is listed as one of the main research and development activities for SCWR safety area [2, 120, 121]. These data are necessary to design nuclear components and carry out preliminary safety analyses. In the open literature, only three studies exist where the critical flow data of supercritical fluids are presented. The first study is conducted by Lee and Swinnerton [96] with water at supercritical pressures using different type of nozzles. Unfortunately, they only obtained a couple of data points above the critical temperature of water at supercritical pressures, most of their data were obtained at low fluid temperatures. In addition, they were not able to change the discharge pressure; they kept it constant at the atmospheric value for all of the experiments. Therefore, it is impossible to determine whether or not the flow was choked. Lee and Swinnerton proposed a pseudo-critical temperature correlation to define the difference between the pseudo-critical temperature and the upstream flow temperature (DT_{pc}). They used this definition to compare the predictions of the models with their data. Later, Chen et al. [98, 100] have also conducted critical flow experiments at supercritical pressures using sharp and round edged orifices. They used the same DT_{pc} notation proposed by Lee and Swinnerton to compare the model predictions with their experimental results as well as with those obtained by Lee and Swinnerton. However, the data collected with a sharp edged nozzle have a huge dispersion, especially near the pseudo-critical temperatures. Moreover, Chen et al. have also not changed the discharge pressure; therefore, they were not able to determine the exact location where choking flow occurs. The last known study about critical flow at supercritical pressures is conducted by Mignot et al. [26, 103]. However, they performed blowdown type experiments instead of steady state flow ones using both water and carbon dioxide. From the temperature point of view for water flows; their experimental range is very limited (i.e., they have obtained only seven data points).

In this thesis, a very ambitious study is presented. In fact, a new experimental loop is designed and constructed to carry out several experiments by covering a very wide range of temperatures and pressures. In addition, the discharge pressure is changed at will to determine unambiguously whether the flow is choked or not. Furthermore, new correlations to estimate the pseudo-critical temperatures of water and carbon dioxide are proposed. Since the correlation proposed by Lee

and Swinnerton does not satisfy the latest thermo-physical properties of water database [4], we strongly believe that use of the new relationship will help to better understand the physical phenomena. On the other hand, the proposed correlation for carbon dioxide allowed us to compare water and carbon dioxide data by using the same flow representation framework. The fact that, performing choking flow experiments at supercritical flow conditions is quite complex and costly; the new relationships will allow researchers to perform fluid-to-fluid modeling. Such a flow representation can help in reducing the number of the choking flow experiments using water above critical conditions.

After publishing the experimental results presented in Chapter 4, additional experiments are also performed. In particular, the continuous time dependent evolution of several experimental parameters is studied. This procedure, implemented by the first time in our laboratory, permitted us to better characterize the statistical quality of the results. The overall research work is completed by comparing the prediction obtained from different models with the data. In general, it is found that the M-HEM [100] estimates the mass flux of water in 1 *mm* ID sharp nozzles better than the other models.

As a conclusion, along the work performed to fulfill the Ph.D. program requirements, a new laboratory has been constructed, instrumented and commissioned. This facility, unique among North American universities, is used to collect supercritical water data required to design the nuclear reactors that will replace the actual technology by the year of 2040. To this aim, our experiments cover a wide range of flow conditions where experimental information is very scarce or non-existent. It is important to mention that the present research program complies entirely with the Generation-4 objectives as given in [121].

CONCLUSION

In the present thesis, choking flow of water is studied experimentally at supercritical pressures because it constitutes a key parameter for designing safety equipment of future nuclear reactors. To better explain the whole research, we divided the study in to two parts. In the first part, a new supercritical steady-state water flow loop is designed and constructed at the thermal-hydraulic laboratory of École Polytechnique de Montreal. This loop is inter-connected with a medium pressure loop that was already available in the laboratory. Having a separate loop at the discharge of the supercritical loop allowed us to validate the choking flow phenomena. This facility can operate over critical temperatures and pressures with water while the discharge pressure can be changed at will. Up to know, no other water loops, blowdown type or steady-state, are capable of changing discharge pressure. The loop is instrumented with several devices such as pressure transducers, thermocouples, flow meters, control and block valves, etc. The Instrumentation is implemented very attentively and in detail not only to obtain useful data from the experiments but also to safely operate the loop. Before performing experiments, commissioning work of the test facility is completed (such as Hydrostatic Tests) to obtain the certification of Régie du bâtiment du Quebec (RBQ).

To control the loop, a Labview™ program is developed. This program is not only used to collect the data but also ensures the safe operation of the loop by including several trip systems. Since the nature of the experiments is so aggressive and the loop is constructed in an educational building, a special attention is given to safety systems. Even though all of them have redundant system to trip the loop using Labview™ software, electro-mechanical trip systems are also implemented in case of failure in the software. Although all of these tasks made the data acquisition and control program very complex, they are part of the requirements of the GIF IV project.

In the second part of the study, several experiments are performed and 545 mass flux data points are collected for temperatures ranging from 52°*C* to 502°*C* and for pressures from 22.0 *MPa* to 32.2 *MPa* using 1 *mm* ID sharp edged nozzle. The data collected at supercritical flow pressures will be very useful for designing and dimensioning SCWR components (i.e., control and safety equipment, etc.). At the early stages of the experiments, the complex behavior of the loop required several revisions and improvements of the experimental procedure, therefore the data

obtained at this moment are not presented in the thesis. It is also important to mention that other loops in the open literature are not able to come close to the operating conditions of future nuclear reactors. Only one study was able to go up to $454°C$ using water as a working fluid with sharp edged orifice. It had very high scattering in the data especially near critical point where the thermo-physical properties of the fluid change drastically. It is shown at the results section that even though the data available in the literature have the same trend with the data obtained in this study; the present data have much less scattering and cover wider range.

Slight differences are observed between the correlations given in the literature and the latest library of thermo-physical properties of water to estimate the pseudo-critical temperature. Therefore, a new correlation to estimate the pseudo-critical temperature of water is developed in order to compare the data with the existing studies in the literature. Furthermore, the use of DT_{pc} (the difference between the pseudo-critical temperature and the fluid temperature) permitted us to compare mass flux behaviour of water and carbon dioxide, as well. For this purpose, the first time in the literature, we have proposed a correlation to estimate the pseudo-critical temperature of carbon dioxide. Using this correlation, it is observed that for $DT_{pc} < 0°C$ both fluids follow similar trends with almost a constant difference of about 25%. We believe that these two correlations together will be very useful to compare mass fluxes of water and carbon dioxide for different geometry and size nozzles. In this manner, number of costly and difficult critical mass flux of water experiments can be reduced in the future.

In general, it is found that the upstream temperature is the most dominant factor on choking flow rate of water at supercritical pressures. The mass flux decreases with increasing the flow temperature. For temperatures well below the critical value (or pseudo-critical temperature if the pressure is different than the critical pressure) the slope of this decrease is small. However, when the upstream fluid temperature approaches the critical temperature, the slope of the mass flux increases due to the drastic decrease of the fluid density. It is observed that up to a given temperature, the flow seems not to be choked. In this region, the decrease in the speed of sound does not affect the mass flow rate because the flow velocity is much lower than the sound velocity. Therefore, the major contribution to the mass flow rate comes from the change of the fluid density. However, when the fluid temperature approaches the critical value, around $307°C \pm 5°C$, the fluid becomes choked; after this temperature, the velocity of the fluid is determined by the speed of sound at that condition. So the mass flow rate becomes a function of

not only the density but also the speed of sound. Since both the density and the speed of sound decrease rapidly with the fluid temperature approaching the pseudo-critical temperature of the water, a drastic decrease is obtained on the mass flux near pseudo-critical temperatures. For upstream flow temperature higher than the pseudo-critical temperature, the fluid density continues to decrease, but the speed of sound increases. Even through the speed of sound increases, it cannot compensate the decrease in the fluid density and the mass flow rate continues to decrease, but at a much slow pace.

There is a small effect of the upstream pressure differences on the mass flow rate through the nozzle. When the upstream pressure increases, not only the flow velocity but also the density of the flow increases. However, these changes are relatively small compared to the changes due to the temperature differences. As a result, a small increase on the mass flow rate is observed when the upstream pressure is increased. The pressure effect becomes dominant close to the pseudo-critical temperature since the density of the fluid changes very rapidly and becomes less pronounced again for temperatures far up from the pseudo-critical ones.

As a part of this Ph. D. research work, the predictions of the some models were compared with the experimental data. Thus, the estimations of mass flux obtained by using HEM, M-HEM, Bernoulli's equation and polytropic equation are compared with the experimental data. In general, for steam-water flows under subcritical temperature conditions, it is observed that for DT_{pc} >150°*C*, the Bernoulli's equation with a discharge coefficient of C_d=0.7 and polytropic approach with n=1 are able to satisfactorily predict the experimental trends. However, at supercritical temperatures, the discharge coefficient of Bernoulli's equation should be modified to C_d=0.40 to be able to predict the critical mass fluxes. In addition, even though the polytropic approach is able to follow the experimental trend for temperatures around pseudo-critical temperatures and at supercritical temperatures, it lacks accuracy and over predicts the data. On the other hand, HEM and M-HEM are the most appropriate for predicting mass flow rates at supercritical pressures for DT_{pc} < 0°*C* even though HEM slightly over predicts the data. It is good to mention that for DT_{pc} > 0°*C*, the over prediction of the HEM increases with increasing $DT_{pc.}$ However, the M-HEM gives excellent results for all temperatures range using C=0.8 which is different from the value suggested in the literature.

Additional experiments are also performed to analyze the errors and reproducibility of the data. Even though the nature of the experiments is very complex, the collected data are very accurate. Moreover, experiments repeated at different dates have shown a very good repeatability.

In summary, this thesis presents not only new data required for designing future SCWR, but also the study of the capability of some models to predict choking flows. In particular, it is worthy to mention that the data presented in this document cover flow conditions which are not fully described in the open literature. This aspect of the work reinforces its originality as it is confirmed by the fact that the corresponding published paper is now considered as 'Original Research Article' (Journal of Experimental Thermal and Fluid Science, Volume 55, May 2014, Pages 12-20).

Recommendations for future studies

This project is one of the main key research areas of the GIF program. In order to further study the subject, the following important questions have been raised throughout the present thesis and require additional research.

Experimental matrix

It is known that future nuclear reactors will operate around 25 *MPa* with outlet temperatures ranging from 500°*C* up to 625°*C*. In this thesis, the upstream nozzle temperature is increased up to 502°*C* so it will be very useful if temperatures up to 625°*C* are covered in later studies.

Nozzle diameter and geometry

Only a sharp edged orifice is studied during this thesis. The time frame didn't allow us to perform further tests with other nozzles. Other types of nozzles (for example round edged or conic discharge nozzles) should be manufactured to further study the effect of the geometry on choking flows. Also, only 1 *mm* ID nozzle is used for all the tests, therefore, it is recommended to study different ID nozzles. According to the preliminary calculations done using a conservative safety factor, up to 3 *mm* ID nozzles can be used in the facility. For IDs higher than this value, the high pressure pump in the loop will not be able to support enough pressure head to increase the pressure over critical pressure. Moreover, the available thermal power will not be enough to increase the fluid temperatures over critical temperatures. These two equipments can be replaced to study the larger nozzle diameters.

Fluid cleanness and other fluids

De-ionized distilled water is used during this study. At the upstream of the high pressure pump 5 μm glass-fiber filter is installed. This allowed us to remove any solid particles bigger than 5 μm. Extensive literature review showed that the purity of the fluid near critical temperatures affects the thermo-physical properties enormously. We have performed water analyses once a week. However, it would be good practice to perform rigorous chemical analysis of the just before and after each experiments.

At the moment, the supercritical choked flow loop at the thermal-hydraulic laboratory doesn't allow the use of other types of fluids (such as carbon dioxide, Freon etc.), but it would be very

useful if other types of fluids are studied. Since the water's critical parameters are very aggressive, it would be easier to study other types of fluids. As a result, similar studies can be performed and thus, the number of complex and costly water flow experiments can be considerably reduced.

Heat transfer and pressure drop

In this thesis, principally the study of the mass flow rate (or choked flow) of water at supercritical pressures is focused. However, the loop itself is instrumented for performing other experiments (i.e., heat transfer and pressure drop studies). Several thermocouples are placed on the heater element at axial and radial locations. Also, eight pressure taps are located on the test section to measure the pressure drop of water under supercritical conditions in the future. Since the estimation of the heat transfer coefficient and pressure drop at these flow conditions are prime research subjects of future nuclear reactors, it would be very interesting to use the same facility to study these parameters.

Modeling

In this thesis, the predictions obtained with a couple of models are compared with our data. The predictions obtained by using these models show that further work is still necessary to provide more physical foundation that can help us to-obtain a better correlation with the data.

Study of fluid elastic interactions

During this work, a very complex fluid-structure interaction was observed. In fact, when the fluid temperature reaches $500°C$ at pressures higher than the critical value, decreasing the thermal power (when the experiment is completed) provokes a noticeable mechanical displacement of the test section as well as all attached mechanical components (i.e., calming chamber, 2.5 *m* long discharge pipe, elbows, etc.) This noticeable movement is automatically detected and recorded by special motion detection video cameras. To reduce the effect of this complex and not yet well understood phenomena, the mechanical support of the calming chamber was redesigned and manufactured from two strong 12.7 *mm* thick iron retention plates. After several new tests, we have observed that the problem seems to be deteriorated with this modification implemented in the loop. This drawback was already presented and discussed in detail during the AECL-SCWR workshop held in Toronto. Currently, we are studying this particular behaviour; we have solid arguments to believe that it is triggered by a sudden momentum unbalance associated by a rapid

change in fluid density. This observation may have an important impact for designing future SCWR's and must be further analysed to design safety equipment of future reactors.

REFERENCES

[1] U.S. Energy Information Administration, "International Energy Outlook 2013," U.S. Department of Energy, Washington, DC DOE/EIA-0484, 2013.

[2] K. P. Boyle, D. Brady, D. Guzonas, H. Khartabil, L. Leung, J. Lo, S. Quinn, S. Suppiah, and W. Zheng, "Canada's generation IV national program - overview," presented at the 4th International Symposium on Supercritical Water-Cooled Reactors, Heidelberg, Germany, 2009.

[3] I. Pioro and R. Duffey, "Supercritical Water-Cooled Nuclear Reactor Concepts: Review and Status," pp. 23-43, 2007.

[4] E. Lemmon, M. L. Huber, and M. O. McLinden, *NIST Standard Reference Database 23: Reference Fluid Thermodynamic and Transport Properties - REFPROP*, 2010.

[5] I. L. Pioro and R. B. Duffey, *Heat Transfer and Hydraulic Resistance at Supercritical Pressures in Power Engineering Applications*. Three Park Avenue, New York: American Society of Mechanical Engineers, 2008.

[6] Y. Oka, S. Koshizuka, Y. Ishiwatari, and A. Yamaji, *Super Light Water Reactors and Super Fast Reactors: Supercritical-Pressure Light Water Cooled Reactors*: Springer, 2010.

[7] S. Kakaç, *Boilers, Evaporators, and Condensers*: Wiley, 1991.

[8] J. Starflinger, N. Aksan, D. Bittermann, L. Heikinheimo, C. Maraczy, G. Rimpault, and T. Schulenberg, "Roadmap for supercritical-water-cooled reactor RD in Europe," in *Global 2003: Atoms for Prosperity: Updating Eisenhower's Global Vision for Nuclear Energy, November 16, 2003 - November 20, 2003*, New Orleans, LA, United states, 2003, pp. 1137-1142.

[9] Y.Y. Bae, L.K.H. Leung, J.A. Lycklama À Nijeholt, M. Andreani, T. Schulenberg, J. Starflinger, Y. Ishiwatari, Y. Oka, H. Mori, and K. Ezato, "Status of ongoing research on scwr thermal-hydraulics and safety," presented at the GIF Symposium, Paris, France, 2009.

[10] I. L. Pioro and R. B. Duffey, "Experimental heat transfer in supercritical water flowing inside channels (survey)," *Nuclear Engineering and Design*, vol. 235, pp. 2407-2430, 2005.

[11] M. Chatharaju, "Computational study of critical flow discharge in supercritical water cooled reactors," Master of Applied Science, Engineering Physics, McMaster University, Hamilton, Ontario, Canada, 2011

[12] R. B. Duffey and I. L. Pioro, "Experimental heat transfer of supercritical carbon dioxide flowing inside channels (survey)," *Nuclear Engineering and Design*, vol. 235, pp. 913-924, 2005.

[13] A. Hidouche, A. Muftuoglu, and A. Teyssedou, "Comparative study of different flow models used to predict critical flow conditions of supercritical fluids," presented at the The 5th Int. Sym. SCWR (ISSCWR-5), Vancouver, British Columbia, Canada, 2011.

[14] A. Muftuoglu and A. Teyssedou, "Design of a supercritical choking flow facility," presented at the UNENE R&D Workshop 2011, Toronto, Ontario, Canada, 2011.

[15] A. Muftuoglu and A. Teyssedou, "Experimental study of water flow at supercritical pressures," presented at the 34th Annual Conference of Canadian Nuclear Society/ 37th Annual CNS/CNA Student Conference, Toronto, Ontario, Canada, 2013.

[16] A. Muftuoglu and A. Teyssedou, "Experimental study of abrupt discharge of water at supercritical conditions," *Experimental Thermal and Fluid Science*, vol. 55, pp. 12-20, 2014.

[17] R. T. Lahey and F. J. Moody, *The thermal-hydraulics of a boiling water nuclear reactor*: American Nuclear Society, 1993.

[18] J. E. A. John and T. G. Keith, *Gas Dynamics*: Pearson Prentice Hall, 2006.

[19] F. J. Moody, *Introduction to unsteady thermofluid mechanics*: Wiley, 1990.

[20] B. R. Munson, D. F. Young, and T. H. Okiishi, *Fundamentals of fluid mechanics*: Wiley, 1998.

[21] F. M. White, *Fluid Mechanics*: McGraw-Hill Higher Education, 2008.

[22] V. L. Streeter, *Fluid Mechanics*: McGraw-Hill, 1966.

[23] M. J. Moran and H. N. Shapiro, *Fundamentals of engineering thermodynamics*: Wiley, 1988.

[24] M. L. Corradini, "Transport phenomena in supercritical fluids in Gen-IV reactor designs," *Nuclear Technology*, vol. 167, pp. 145-156, 2009.

[25] X. Cheng and T. Schulenberg, "Heat transfer at supercritcal pressures - literature review and application to an HPLWR," Institut fur Kern und energietechnik, Karlsruhe2001.

[26] G. P. H. Mignot, "Experimental investigation of critical flow of supercritical carbon dioxide," 3327979 Ph.D., The University of Wisconsin - Madison, United States -- Wisconsin, 2008.

[27] A. R. C. Duarte and C. M. M. Duarte, *Current Trends of Supercritical Fluid Technology in Pharmaceutical, Nutraceutical and Food Processing Industries*: Bentham Science Publishers, 2009.

[28] I. Pioro and S. Mokry, "Thermophysical Properties at Critical and Supercritical Pressures," 2011.

[29] A. R. Imre, U. K. Deiters, T. Kraska, and I. Tiselj, "The pseudocritical regions for supercritical water," *Nuclear Engineering and Design*, vol. 252, pp. 179-183, 2012.

[30] V. V. Brazhkin, Y. D. Fomin, A. G. Lyapin, V. N. Ryzhov, and K. Trachenko, "Universal crossover of liquid dynamics in supercritical region," *Jetp Letters*, vol. 95, pp. 164-169, Apr 2012.

[31] V. V. Brazhkin, Y. D. Fomin, A. G. Lyapin, V. N. Ryzhov, and K. Trachenko, "Two liquid states of matter: A dynamic line on a phase diagram," *Physical Review E*, vol. 85, Mar 2012.

[32] V. V. Brazhkin, A. G. Lyapin, V. N. Ryzhov, K. Trachenko, Y. D. Fomin, and E. N. Tsiok, "Where is the supercritical fluid on the phase diagram?," *Physics-Uspekhi,* vol. 55, pp. 1061-1079, 2012.

[33] J. I. Frenkel, *Kinetic Theory of Liquids*: Clarendon Press, 1947.

[34] V. V. Brazhkin, Y. D. Fomin, A. G. Lyapin, V. N. Ryzhov, and E. N. Tsiok, "Widom line for the liquid-gas transition in Lennard-Jones system," *Journal of Physical Chemistry B,* vol. 115, pp. 14112-14115, 2011.

[35] V. A. Kurganov, Y. A. Zeigarnik, and I. V. Maslakova, "Heat transfer and hydraulic resistance of supercritical-pressure coolants. Part I: Specifics of thermophysical properties of supercritical pressure fluids and turbulent heat transfer under heating conditions in round tubes (state of the art)," *International Journal of Heat and Mass Transfer,* vol. 55, pp. 3061-3075, 2012.

[36] V. A. Kurganov, Y. A. Zeigarnik, and I. V. Maslakova, "Heat transfer and hydraulic resistance of supercritical-pressure coolants. Part II: Experimental data on hydraulic resistance and averaged turbulent flow structure of supercritical pressure fluids during heating in round tubes under normal and deteriorated heat transfer conditions," *International Journal of Heat and Mass Transfer,* vol. 58, pp. 152-167, 2013.

[37] B. V. Dyadyakin and A. S. Popov, "Heat transfer and thermal resistance of tight seven-rod bundle cooled with water flow at supercritical pressures," *Transactions of VTI,* pp. 244-253, 1977.

[38] G. K. Filonenko, "Hydraulic resistance in pipes," *Toploenergetika,* vol. 1, pp. p. 40-44, 1954.

[39] S. Zoghlami, "Analyse du transfert de chaleur et de la perte de pression pour des écoulements supercritiques dans le réacteur CANDU-SCWR," Master's thesis, École Polytechnique de Montréal, 2013.

[40] V. A. Grabezhnaya and P. L. Kirillov, "Heat Transfer in Pipes and Rod Bundles During Flow of Supercritical-Pressure Water," *Atomic Energy,* vol. 96, pp. 358-364, 2004/05/01 2004.

[41] K. W. Seo, M. H. Kim, M. H. Anderson, and M. L. Corradini, "Heat transfer in a supercritical fluid: Classification of heat transfer regimes," *Nuclear Technology,* vol. 154, pp. 335-349, 2006.

[42] H. S. Swenson, J. R. Carver, and C. R. Kakarala, "Heat Transfer to Supercritical Water in Smooth-Bore Tubes," *Journal of Heat Transfer,* vol. 87, pp. 477-483, 1965.

[43] K. Yamagata, K. Nishikawa, S. Hasegawa, T. Fujii, and S. Yoshida, "Forced convective heat transfer to supercritical water flowing in tubes," *International Journal of Heat and Mass Transfer,* vol. 15, pp. 2575-2593, 1972.

[44] Bishop A, Sandberg R, and Tong L., "Forced convection heat transfer to water at near-critical temperatures and supercritical pressures," *International Chemical Engineering Meeting*, London, England, 1965.

[45] Y. V. Vikrev and V. A. Lokshin, "An experimental study of temperature conditions in horizontal steam generator tubes at supercritical pressure," *Thermal Engineering,* vol. 11(1), pp. 105-109, 1964.

[46] G. A. Adebiyi and W. B. Hall, "Experimental investigation of heat transfer to supercritical pressure carbon dioxide in a horizontal pipe," *International Journal of Heat and Mass Transfer,* vol. 19, pp. 715-720, 1976.

[47] M. Bazargan, D. Fraser, and V. Chatoorgan, "Effect of Buoyancy on Heat Transfer in Supercritical Water Flow in a Horizontal Round Tube," *Journal of Heat Transfer,* vol. 127, pp. 897-902, 2005.

[48] B. S. Petukhov, A. F. Polyakof, V. A. Kuleshov, and Y. L. Sheckter, "Turbulent flow and heat transfer in horizontal tubes with substantial influence of thermal gravitational forces," in *Proceeding of 5th international Heat Transfer Conference*, Tokyo, 1974.

[49] J. Licht, M. Anderson, and M. Corradini, "Heat transfer to water at supercritical pressures in a circular and square annular flow geometry," *International Journal of Heat and Fluid Flow,* vol. 29, pp. 156-166, 2008.

[50] J. D. Jackson and W. B. Hall, "Forced convection heat transfer to fluids at supercritical pressure," *Institution of Mechanical Engineers, Conference Publications,* vol. 2, pp. 563-611, 1979.

[51] M. J. Watts and C. T. Chou, "Mixed convection heat transfer to supercritical pressure water," in *Proceedings of the 7th International Heat Transfer Conference*, Munich, Germany, 1982, pp. 495-500.

[52] B. S. Petukhov, E. A. Kransnoshchekov, and V. S. Protopopov, "An investigation of heat transfer to fluids flowing in pipes under supercritical conditions," in *Proceedings of the 1961–1962 Heat Transfer Conference on International Development in Heat Transfer*, New York, 1961, pp. 569-578.

[53] J. Licht, M. Anderson, and M. Corradini, "Heat transfer and fluid flow characteristics in supercritical pressure water," *Journal of Heat Transfer,* vol. 131, pp. 072502-1 to 072502-14, 2009.

[54] Z. Yang, Q. Bi, H. Wang, G. Wu, and R. Hu, "Experiment of heat transfer to supercritical water flowing in vertical annular channels," *Journal of Heat Transfer,* vol. 135, pp. 042504-1 to 042504-9, 2013.

[55] V. A. Silin, V. A. Voznesensky, and A. M. Afrov, "The light-water integral reactor with natural circulation of the coolant at supercritical pressure B-500 Skdi," *Nuclear Engineering and Design,* vol. 144, pp. 327-336, 1993.

[56] D. C. Groeneveld, S. Tavoularis, P. Raogudla, S. K. Yang, and L. K. H. Leung, "Analytical and experimental program of supercritical heat transfer research at the University of Ottawa," *Nuclear Engineering and Technology,* vol. 40, pp. 107-116, 2008.

[57] G. Richards, G. D. Harvel, I. L. Pioro, A. S. Shelegov, and P. L. Kirillov, "Heat transfer profiles of a vertical, bare, 7-element bundle cooled with supercritical freon R-12," *Nuclear Engineering and Design,* vol. 264, pp. 246-256, 2013.

[58] I. L. Pioro, H. F. Khartabil, and R. B. Duffey, "Heat transfer to supercritical fluids flowing in channels—empirical correlations (survey)," *Nuclear Engineering and Design,* vol. 230, pp. 69-91, 2004.

[59] W. H. McAdams, J. N. Addoms, and W. E. Kennel, *Heat transfer to superheated steam at high pressure*. Michigan: Argonne National Laboratory, 1949.

[60] S. K. Yang and H. F. Khartabil, "Normal and deteriorated meat transfer correlations for supercritical fluids," in *Winter Meeting - American Nuclear Society*, Washington, D.C., United States, 2005, pp. 635-637.

[61] I. L. Pioro and H. F. Khartabil, "Experimental study on heat transfer to supercritical carbon dioxide flowing upward in a vertical tube," presented at the 13th International Conference on Nuclear Engineering (ICONE-13), Beijing, China, 2005.

[62] M. E. Shitsman, "Temperature conditions in tubes at supercritical pressures," *Teploenergetika,* vol. 15, pp. 57-61, 1968.

[63] B. S. Petukhov and A. F. Polyakov, "Boundaries of regimes with "Worsened" heat transfer for supercritical pressure of coolant," *Teplofizika Vysokikh Temperatur,* vol. 12, pp. 221-224, 1974.

[64] B. S. Petukhov, V. S. Protopopov, and V. A. Silin, "Experimental investigation of worsened heat transfer conditions with the turbulent flow of carbon dioxide at supercritical pressure," *Teplofizika Vysokikh Temperatur,* vol. 10, pp. 347-354, 1972.

[65] V. A. Grabezhnaya and P. L. Kirillov, "Heat-transfer degradation boundary in supercritical-pressure flow," *Atomic Energy,* vol. 101, pp. 714-721, 2006.

[66] S. Gupta, E. Saltanov, S. J. Mokry, I. Pioro, L. Trevani, and D. McGillivray, "Developing empirical heat-transfer correlations for supercritical CO2 flowing in vertical bare tubes," *Nuclear Engineering and Design,* vol. 261, pp. 116-131, 2013.

[67] S. Mokry, I. Pioro, A. Farah, K. King, S. Gupta, W. Peiman, and P. Kirillov, "Development of supercritical water heat-transfer correlation for vertical bare tubes," *Nuclear Engineering and Design,* vol. 241, pp. 1126-1136, 2011.

[68] S. J. Mokry, I. L. Pioro, and R. B. Duffey, "Experimental heat transfer to supercritical CO_2 flowing upward in a bare vertical tube," in *Proceedings of SCCO2 Power Cycle Symposium*, Troy, NY, 2009.

[69] M. F. Loewenberg, E. Laurien, A. Class, and T. Schulenberg, "Supercritical water heat transfer in vertical tubes: A look-up table," *Progress in Nuclear Energy,* vol. 50, pp. 532-538, 2008.

[70] J. D. Jackson, "Heat transfer to supercritical pressure fluids. Part 2 - Critical reviews with design recommendations," UK Atomic Energy Autority, Harwell, 1975.

[71] J. M. Locke and D. B. Landrum, "Study of Heat Transfer Correlations for Supercritical Hydrogen in Regenerative Cooling Channels," *Journal of Propulsion and Power,* vol. 24, pp. 94-103, 2008.

[72] H. K. Fauske, "Contribution to the theory of two-phase, one-component critical flow," United States ANL-6633.1, 1962.

[73] E. S. Starkman, V. E. Schrock, K. F. Neusen, and D. L. Maneely, "Expansion of very low quality two-phase fluid through convergent-divergent nozzle," *American Society of Mechanical Engineers - Transactions - Journal of Basic Engineering,* vol. 86, pp. 247-256, 1964.

[74] Y. Kim and D. L. O'Neal, "A comparison of critical flow models for estimating two-phase flow of HCFC22 and HFC134a through short tube orifices," *Int. J. Refrig,* vol. 18, pp. 447-455, 1995.

[75] Henry R.E and F. H.K, "The two-phase critical flow of one-component mixtures in nozzles, orifices and short tubes," *Journal of Heat Transfer,* pp. 179-187, 1971.

[76] M.-S. Chung, "Simulation of SBLOCA based on an Improved Choked Flow Model for RELAP5/MOD3 Code," *Annals of Nuclear Energy,* vol. 32, pp. 913-924, 2005.

[77] V. M. Fthenakis, *Prevention and control of accidental releases of hazardous gases*. New York: Van Nostrand Reinhold, 1993.

[78] F. J. Moody, "Maximum Flow Rate of a Single Component, Two-Phase Mixture," *Journal of Heat Transfer,* vol. 87, pp. 134-141, 1965.

[79] J. A. Trapp and V. H. Ransom, "Choked-flow calculation criterion for nonhomogeneous, nonequilibrium, two-phase flows," *International Journal of Multiphase Flow,* vol. 8, pp. 669-681, 1982.

[80] F. J. Moody, "Maximum two-phase vessel blowdown from pipes," *Journal of Heat Transfer,* vol. 88, pp. 285-295, 1966.

[81] H. K. Fauske, "A theory for predicting pressure gradients for two-phase critical flow," *Nuclear Science and Engineering,* vol. 17, pp. 1-7, 1963.

[82] R. E. Henry, H. K. Fauske, and S. T. McComas, "Two-Phase critical flow at low qualities. Part I. Experimental " *Nuclear Science and Engineering,* vol. 41, pp. 79-91, 1970.

[83] R. E. Henry, H. K. Fauske, and S. T. McComas, "Two-phase critical flow at low qualities. Part II. Analysis," *Nuclear Science and Engineering,* vol. 41, pp. 92-98, 1970.

[84] R. E. Henry, "Two-phase critical discharge of initially saturated or subcooled liquid," *Nuclear Science and Engineering,* vol. 41, pp. 336-342, 1970.

[85] J. J. Schroeder and N. Vuxuan, "Homogeneous non-equilibrium two-phase critical flow model," *Chemical Engineering and Technology,* vol. 10, pp. 420-426, 1987.

[86] D. Abdollahian, J. Healzer, E. Janssen, and C. Amos, "Critical flow data review and analysis," Electric Power Research Institute NP-2192, 1982.

[87] E. Elias and G. S. Lellouche, "Two-phase critical flow," *International Journal of Multiphase Flow,* vol. 20, Supplement 1, pp. 91-168, 1994.

[88] G. B. Wallis, "Critical two-phase flow," *International Journal of Multiphase Flow,* vol. 6, pp. 97-112, 1980.

[89] J. Weisman and A. Tentner, "Models for estimation of critical flow in two-phase systems," *Progress in Nuclear Energy,* vol. 2, pp. 183-197, 1978.

[90] J. L. Xu, T. K. Chen, and X. J. Chen, "Critical flow in convergent-divergent nozzles with cavity nucleation model," *Experimental Thermal and Fluid Science*, vol. 14, pp. 166-173, 1997.

[91] S. W. Kim and H. C. No, "Subcooled water critical pressure and critical flow rate in a safety valve," *International Journal of Heat and Mass Transfer*, vol. 44, pp. 4567-4577, Dec 2001.

[92] S. Levy, "Prediction of two-phase critical flow rate," *Journal of Heat Transfer*, vol. 87, pp. 53-58, 1965.

[93] C. Moon-Hyun, P. Choon-Hyung, and P. Jee-Won, "An experimental investigation of critical flow rates of subcooled water through short pipes with small diameters," *International Communications in Heat and Mass Transfer*, vol. 23, pp. 1053-1064, 1996.

[94] H. J. Richter, "Separated two-phase flow model: Application to critical two-phase flow," *International Journal of Multiphase Flow*, vol. 9, pp. 511-530, 1983.

[95] K. H. Ardron and R. A. Furness, "Study of the critical flow models used in the reactor blowdown analysis," *Nuclear Engineering and Design*, vol. 39, pp. 257-266, 1976.

[96] D. H. Lee and D. Swinnerton, "Evaluation of critical flow for supercritical steam-water," United Kingdom NP-3086, 1983.

[97] Y. Chen, C. Yang, S. Zhang, M. Zhao, and K. Du, "An Experimental Study of critical flow of water under subcritical and supercritical pressures," presented at the 4th International Symposium on Supercritical Water-Cooled Reactors, Heidelberg, Germany, 2009.

[98] Y. Chen, C. Yang, S. Zhang, M. Zhao, K. Du, and X. Cheng, "Experimental study of critical flow of water at supercritical pressure," *Frontiers of Energy and Power Engineering in China*, vol. 3, pp. 175-180, 2009.

[99] Y. Chen, M. Zhao, C. Yang, K. Bi, K. Du, and S. Zhang, "Critical flow of water under supercritical pressures," in *14th International Heat Transfer Conference*, Washington, DC, United states, 2010, pp. 319-326.

[100] Y. Chen, M. Zhao, C. Yang, K. Bi, K. Du, and S. Zhang, "Research on critical flow of water under supercritical pressures in nozzles," *Journal of Energy and Power Engineering*, vol. 6, pp. 201-208, 2012.

[101] B. Gebbeken and R. Eggers, "Blowdown of carbon dioxide from initially supercritical conditions," *Journal of Loss Prevention in the Process Industries*, vol. 9, pp. 285-293, 1996.

[102] G. Mignot, M. Anderson, and M. Corradini, "Initial study of supercritical fluid blowdown," *Fusion Science and Technology*, vol. 47, pp. 574-578, 2005.

[103] G. Mignot, M. Anderson, and M. Corradini, "Critical flow experiment and analysis for supercritical fluid," *Nuclear Engineering and Technology*, vol. 40, pp. 133-138, 2008.

[104] G. P. Mignot, M. H. Anderson, and M. L. Corradini, "Measurement of supercritical CO2 critical flow: Effects of L/D and surface roughness," *Nuclear Engineering and Design*, vol. 239, pp. 949-955, 2009.

[105] A. M. C. Chan and I. G. Elphick, "Critical two-phase flow in a short converging nozzle," *International Journal of Transport Phenomena*, vol. 4, pp. 109-118, 2001.

[106] F. D'Auria and P. Vigni, "Two-phase critical flow models," Committee on the Safety of Nuclear Installations (CSNI), Roma No.49, 1980.

[107] J. C. Lin, G. E. Gruen, and W. J. Quapp, "Critical flow in small nozzles for saturated and subcooled water at high pressure," presented at the ASME winter annual meeting, Chicago, IL, USA, 1980.

[108] A.R. Imre, U.K. Deiters, T. Kraska, and I. Tiselj, "Theoretical investigation of sudden vaporization and water hmaaber in SCWR during loss of coolant accidents," *Nuclear Engineering and Design*, vol. 252, pp. 179-183, 2012.

[109] H. J. Yoon, "Two-phase choking flow at low pressure and low quality," Ph.D. Thesis, Purdue University, West Lafayette, Indiana, United States 2004.

[110] H. J. Yoon, M. Ishii, and S. T. Revankar, "Choking flow modeling with mechanical and thermal non-equilibrium," *International Journal of Heat and Mass Transfer*, vol. 49, pp. 171-186, 2006.

[111] H. S. Isbin, H. K. Fauske, M. Petrick, C. H. Robbins, R. V. Smith, S. A. Szawlewicz, and F. R. Zaloudek, "Critical flow phenomena in two-phase mixtures and their relationships to nuclear safety," presented at the 3rd United Nations International Conference on the Peaceful Uses of Atomic Energy, Geneva, Swirtzerland, 1964.

[112] F. R. Zaloudek, "Steam-water critical flow from high pressure systems. Interim report," General Electric Co., Richland, WA, United States. Hanford Atomic Products Operation, Washington, DC, United States HW-80535-RD, 1964.

[113] B. Spindler and M. Pellissier, "Assessment of TRAC-PF1/MOD1 Version 14. 3 using separate effects critical flow and blowdown experiments," Nuclear Regulatory Commission, Washington, DC (USA). Office of Nuclear Regulatory Research; CEA Centre d'Etudes Nucleaires de Grenoble, 38 (France), Washington, DC , United States NUREG/IA-0023-Vol.2, 1990.

[114] R. E. Henry and H. K. Fauske, "The two-phase critical flow of one-component mixtures in nozzles, orifices, and short tubes," *Transactions of the ASME. Series C, Journal of Heat Transfer*, vol. 93, pp. 179-87, 1971.

[115] I. Haynes International. (2013). *Hastelloy ® C-276 alloy Information*. Available: http://www.haynesintl.com/c276hastelloyalloy.htm

[116] H. T. Metals. (2013). *Hastelloy C-276 technical data*. Available: http://www.hightempmetals.com/techdata/hitempHastC276data.php

[117] R. B. Bird, W. E. Stewart, and E. N. Lightfoot, *Transport Phenomena*: Wiley, 2007.

[118] N. Y. Hydraulic Institute, "Pipe Friction Manual," 3 ed, 1961.

[119] OMEGA. (2013). *Revised Thermocouple Reference Tables*. Available: http://www.omega.ca/temperature/Z/pdf/z204-206.pdf

[120] H. F. Khartabil, R. B. Duffey, N. Spinks, and W. Diamond, "The pressure-tube concept of generation IV Supercritical Water-Cooled Reactor (SCWR): Overview and status," in

American Nuclear Society - International Congress on Advances in Nuclear Power Plants 2005, ICAPP'05, May 15, 2005 - May 19, 2005, Seoul, Korea, Republic of, 2005, pp. 2824-2830.

[121] U.S. Nuclear Energy Research Advisory Committee and the Generation IV International Forum, "A Technology Roadmap for Generation IV Nuclear Energy Systems," 2002.

APPENDIXES

APPENDIX 1 –Certification of the RBQ

Régie du bâtiment Québec

Direction des opérations et des appareils sous pression
Division des services techniques des appareils sous pression

Le 18 octobre 2012

Monsieur Thierry Lafrance,ing.
Évaluation, gestion, conception et installation
Projets de recherche clé en main
École Polytechnique de Montréal
2500, chemin de Polytechnique
Montréal (Québec) H3T 1J4

Référence: N/D ASP2012-011

Objet : Demande de mesures différentes (appareils sous pression)
Laboratoire de thermo hydraulique
Pavillon principal, local B277.1
2500 chemin de Polytechnique, Montréal

Monsieur,

La présente fait suite à votre demande reçue le 5 octobre 2012, concernant l'installation expérimentale d'une série d'accessoires pour le laboratoire de thermo hydraulique au pavillon principal, local B277.1, 2500 chemin de Polytechnique à Montréal.

Nous vous informons de la décision de la Régie du bâtiment du Québec prise lors de la réunion du Comité des mesures différentes du 12 octobre 2012 et suite à l'étude des informations complémentaires reçues le 5 octobre 2012.

CONTEXTE
Ces accessoires font partie d'une installation expérimentale pour le laboratoire de thermo hydraulique au pavillon principal, local B277.1, 2500 chemin de Polytechnique à Montréal. Cette installation se situe entre une chaudière et un ballon de vapeur existants, possédant chacun un numéro Canadien d'enregistrement (CRN). Elle vient donc modifier une installation existante.

Sujet : Installation composée d'accessoires sous pression non enregistrés

PROBLÉMATIQUE
L'installation est réalisée dans le cadre d'un projet de recherche subventionné par le conseil de recherches en sciences naturelles et en génie du Canada. Seule la section d'essais, qui n'est pas sujette à l'approbation par la RBQ, subira une évolution en fonction des résultats issus des expériences. Cette installation sera utilisée au maximum 50h/an pour les cinq prochaines années. L'installation, lorsqu'elle n'est pas en opération, incluant la boucle de production et d'extraction de chaleur, est entreposée avec une légère pression positive d'Azote afin d'éviter la corrosion des éléments en Acier au carbone. Le professeur Alberto Teyssedou, expert dans le domaine, supervise en tout temps l'opération de l'installation.

Montréal
545, boul. Crémazie Est, 7e étage
Montréal (Québec) H2M 2V2
Téléphone : (514) 864-8400
Télécopieur : (514) 873-0829

PROPOSITION DU REQUÉRANT

Les aspects scientifiques sont pris en charge par le professeur Alberto Teyssedou et le design ainsi que tous les calculs reliés au code ASME sont réalisés par l'ingénieur spécialisé en haute pression Stephen Schneller. L'installation couverte par cette demande ne comporte aucun appareil sous pression mais bien une série d'accessoires. La mise en œuvre, incluant la fabrication, l'achat de biens et services ainsi que l'installation, est sous la supervision de l'ingénieur Thierry Lafrance. Nous avons installé un mur de protection pour la salle de contrôle et nous avons installé un blindage d'acier tout autour des accessoires soumis à la haute pression et à la haute température. Nous avons également installé une série de caméras afin de pouvoir intervenir rapidement en cas d'anomalies sur les éléments sensibles de l'installation ainsi que sur la porte d'entrée du secteur. Les essais se dérouleront de soir et de nuit non seulement pour la question de disponibilité énergétique, mais aussi pour nous permettre de restreindre l'accès au secteur entourant le laboratoire. La porte d'accès au secteur entourant le laboratoire sera verrouillée et un écriteau explicite empêchera l'accès.

DÉCISION

La Régie du bâtiment accepte la proposition du requérant en vertu de l'article 26 de la Loi sur les appareils sous pression (L.R.Q., chapitre A-20.01) avec les conditions supplémentaires suivantes:

- L'acceptation de l'installation est faite sur une base unique pour une installation expérimentale, dans le cadre prévu pour l'acceptation spécifique à la présente mesure différente ;
- Toute modification à cette installation doit être déclarée à la Régie du bâtiment du Québec, excluant celle concernant la section d'essais (Test Section);
- Les mesures de sécurité pendant les expériences au laboratoire doivent être respectées à la lettre et en tout temps.
- Il ne doit pas y avoir de contre-indication de la part de l'assureur du propriétaire.

Les documents suivants fournis par le requérant font partie intégrante de la demande :

- **Formulaire de demande de mesures différentes** – M. Thierry Lafrance ing, projets de recherche clé en main, École Polytechnique de Montréal, 2500, chemin de Polytechnique, Montréal, Québec, datée du 5 octobre 2012.

- **Courriel – Documentations complémentaires** de M. Thierry Lafrance ing, projets de recherche clé en main, École Polytechnique de Montréal, 2500, chemin de Polytechnique, Montréal, Québec, à M. Aziz Khssassi ing. RBQ, DAPS du 5 octobre 2012 à 10 :48.

- **Courriel – Documentations complémentaires** de M. Claude Durocher, Vice-président, Dunor, 1955 boulevard Sant-Elzéar Ouest, Laval, Québec à M. Aziz Khssassi ing. RBQ, DAPS du 5 octobre 2012 à 13 :58.

- **Courriel** – de M. Thierry Lafrance ing., projet de recherche clé en main, École Polytechnique de Montréal, 2500, chemin de Polytechnique, Montréal, Québec à Madame Madiha Kotb, ing. RBQ – DASP du 27 septembre 2012 à 17:16.

Cette décision est prise sous réserve des informations contenues dans votre demande et n'est applicable que pour celle-ci.

Il est à noter que cette décision ne dispense pas le requérant d'obtenir toute autre autorisation ou condition requise par toute loi ou tout règlement qui s'applique à cette installation.

Pour tous renseignements supplémentaires concernant ce dossier, veuillez communiquer avec madame Kotb au numéro de téléphone suivant : (514) 873-6536.

Veuillez agréer, Monsieur, nos salutations les meilleures.

Madiha Kotb, M. ing.
Comité des mesures différentes – Montréal
Division des services techniques des appareils sous pression

c.c.: Myriam St-Georges, ing. – RBQ
Aziz Khassasi, ing. – RBQ
Blagovest Levitchansky, ing. – RBQ

APPENDIX 2 – Pressure transducer calibrations

High pressure transducer calibrations

a) PTr-1

Honeywell

0.1 %/o FS

2080 Arlingate Lane
Columbus, Ohio 43228 U.S.A.
Phone: 614-850-5000
Toll free: 800-848-6564
Fax: 614-850-1111
www.honeywell.com/sensotec
sensotec.service@honeywell.com

CE

CERTIFICATE OF CALIBRATION

Product Identification

Product Type:	PRESSURE	Customer Name:	N/A
Model:	TJE	Customer PO:	N/A
Serial No.*:	1372491	Order Code:	AP122DR,1A,2A,5B,6A
Part No.:	060-CS96729206508	Instrument Serial No.:	N/A

* A letter at the end of the serial number indicates the associated bridge.

Product Specifications

Capacity:	5000psia		Supply:	+/-15 OR 26-32 VDC Vdc
Calibrated At:	5000.00psia		Amplifier Output:	0-5 Vdc
Direction / Type:	Pressure	Absolute	Electrical Leakage:	∞ MegΩ

Wiring Code

AMP#12,6-COND,6-PIN,SHN,±15 OR 26-32 VDC

+/-15 VDC SUPPLY	PIN	+26-32 VDC SUPPLY
(+)SUPPLY	A	(+)SUPPLY
(-)OUTPUT/SUPPLY COM.	B	(-)OUTPUT
(-)SUPPLY	C	SUPPLY RETURN
(+)OUTPUT	D	(+)OUTPUT
SHUNT CAL 1	E	SHUNT CAL 1
SHUNT CAL 2	F	SHUNT CAL 2

001-0333-12

This unit has been calibrated using standards whose accuracies are traceable to the National Institute of Standards and Technology (NIST). Units are calibrated based upon ANSI/NCSL Z540 on equipment whose accuracies are within a 4:1 ratio unless otherwise indicated. Reported values may be scaled due to limitations of test equipment such as dead weight increments or local barometric pressure. This certificate of calibration shall not be reproduced in any form, except in full, without the expressed written consent of Honeywell. If you have any questions concerning this certificate of calibration, please call our service department at (614) 850-5000.

Derek W. Drabenstadt, Quality Manager

PRINT DATE: 1/18/2012

Certificate No
1372491-001

Document No. 086-1000-09

Calibration Data

Input Resistance: N/A
Output Resistance: N/A
Calibration Factor: 5.0004V
Operator(s): John Knore
Calibration Date: 01/18/2012
Calibration Procedure: 072-FP75-23, Rev A, Date 09/23/2010

% Capacity	Load (psia)	Raw (V)	Normalized (V)
0	0.00	0.0140	0.0000
50	2500.00	2.5140	2.5000
100	5000.00	5.0134	4.9994
50	2500.00	2.5168	2.5028
0	0.00	0.0139	-0.0001

Shunt Calibration Data

Line No.	Shunt Resistor	Shunt Sense	Zero	Shunt Zero	Shunt Cal	Shunt Cal. Capacity
1	INTΩ	N/A	N/A	N/A	3.9835 V	N/A

Calibration Standards

NIST Traceable #	Inst. ID#	Description	Model	Cal Date	Date Due
3452110	100161	DEADWEIGHT TESTER H2O	TM-TQ-150	08/20/2009	08/20/2012
4132773	7241230	DECADE RESISTOR	0-10M OHMS	05/07/2010	05/07/2012
5305693	200088	DIGITAL MULTIMETER	34401A	07/14/2011	07/14/2012

Environmental Data

Temperature: 74 °F
Humidity: 17 %RH
Pressure: 14.34 psiA

Certificate No
1372491-001

b) Px-1

Honeywell

2080 Arlingate Lane
Columbus, Ohio 43228 U.S.A.
Phone: 614-850-5000
Toll free: 800-848-6564
Fax: 614-850-1111
www.honeywell.com/sensotec
sensotec.service@honeywell.com

CE

CERTIFICATE OF CALIBRATION

Product Identification

Product Type:	PRESSURE	Customer Name:	N/A
Model:	TJE	Customer PO:	N/A
Serial No.*:	1371378	Order Code:	AP122DR,1A,2A,5B,6A
Part No.:	060-CS96729206508	Instrument Serial No.:	N/A

* A letter at the end of the serial number indicates the associated bridge.

Product Specifications

Capacity:	5000psia		Supply:	+/-15 OR 26-32 VDC Vdc
Calibrated At:	5000.00psia		Amplifier Output:	0-5 Vdc
Direction / Type:	Pressure	Absolute	Electrical Leakage:	∞ MegΩ

Wiring Code

AMP#12,6-COND,6-PIN,SHN,±15 OR 26-32 VDC

+/-15 VDC SUPPLY	PIN	+26-32 VDC SUPPLY
(+)SUPPLY	A	(+)SUPPLY
(-)OUTPUT/SUPPLY COM.	B	(-)OUTPUT
(-)SUPPLY	C	SUPPLY RETURN
(+)OUTPUT	D	(+)OUTPUT
SHUNT CAL 1	E	SHUNT CAL 1
SHUNT CAL 2	F	SHUNT CAL 2

001-0393-12

This unit has been calibrated using standards whose accuracies are traceable to the National Institute of Standards and Technology (NIST). Units are calibrated based upon ANSI/NCSL Z540 on equipment whose accuracies are within a 4:1 ratio unless otherwise indicated. Reported values may be scaled due to limitations of test equipment such as dead weight increments or local barometric pressure. This certificate of calibration shall not be reproduced in any form, except in full, without the expressed written consent of Honeywell. If you have any questions concerning this certificate of calibration, please call our service department at (614) 850-5000.

Derek W. Drabenstadt, Quality Manager

PRINT DATE: 12/30/2011

Certificate No

1371378-001

Document No. 086-1000-09

Calibration Data

Input Resistance: N/A
Output Resistance: N/A

Calibration Factor: 5.0032V
Operator(s): John Knore
Calibration Date: 12/30/2011

Calibration Procedure: 072-FP75-23, Rev A, Date 09/23/2010

% Capacity	Load (psia)	Raw (V)	Normalized (V)
0	0.00	0.0157	0.0000
50	2500.00	2.5181	2.5024
100	5000.00	5.0180	5.0023
50	2500.00	2.5210	2.5053
0	0.00	0.0166	0.0009

Shunt Calibration Data

Line No.	Shunt Resistor	Shunt Sense	Zero	Shunt Zero	Shunt Cal	Shunt Cal. Capacity
1	INTΩ	N/A	N/A	N/A	4.0006 V	N/A

Calibration Standards

NIST Traceable #	Inst. ID#	Description	Model	Cal Date	Date Due
3452110	100161	DEADWEIGHT TESTER H2O	TM-TQ-150	08/20/2009	08/20/2012
4132773	7241230	DECADE RESISTOR	0-10M OHMS	05/07/2010	05/07/2012
5305693	200088	DIGITAL MULTIMETER	34401A	07/14/2011	07/14/2012

Environmental Data

Temperature: 72 °F
Humidity: 23 %RH
Pressure: 14.19 psiA

Certificate No
1371378-001

PRINT DATE: 12/30/2011

Document No. 086-1000-09

c) Px-3

Honeywell

2080 Arlingate Lane
Columbus, Ohio 43228 U.S.A.
Phone: 614-850-5000
Toll free: 800-848-6564
Fax: 614-850-1111
www.honeywell.com/sensotec
sensotec.service@honeywell.com

CE

CERTIFICATE OF CALIBRATION

Product Identification

Product Type:	PRESSURE	Customer Name:	N/A
Model:	TJE	Customer PO:	N/A
Serial No.*:	1364591	Order Code:	AP122DN,1A,2A,5B,6A
Part No.:	060-5567-03TJA	Instrument Serial No.:	N/A

* A letter at the end of the serial number indicates the associated bridge

Product Specifications

Capacity:	3000psia		Supply:	+/-15 OR 26-32 VDC Vdc
Calibrated At:	3000.00psia		Amplifier Output:	0-5 Vdc
Direction / Type:	Pressure	Absolute	Electrical Leakage:	∞ MegΩ

Wiring Code

AMP#12,6-COND,6-PIN,SHN,±15 OR 26-32 VDC

+/-15 VDC SUPPLY	PIN	+26-32 VDC SUPPLY
(+)SUPPLY	A	(+)SUPPLY
(-)OUTPUT/SUPPLY COM.	B	(-)OUTPUT
(-)SUPPLY	C	SUPPLY RETURN
(+)OUTPUT	D	(+)OUTPUT
SHUNT CAL 1	E	SHUNT CAL 1
SHUNT CAL 2	F	SHUNT CAL 2

001-0333-12

This unit has been calibrated using standards whose accuracies are traceable to the National Institute of Standards and Technology (NIST). Units are calibrated based upon ANSI/NCSL Z540 on equipment whose accuracies are within a 4:1 ratio unless otherwise indicated. Reported values may be scaled due to limitations of test equipment such as dead weight increments or local barometric pressure. This certificate of calibration shall not be reproduced in any form, except in full, without the expressed written consent of Honeywell. If you have any questions concerning this certificate of calibration, please call our service department at (614) 850-5000.

Derek W. Drabenstadt, Quality Manager

PRINT DATE: 12/14/2011

Certificate No

1364591-001

Document No. 086-1000-09

Calibration Data

Input Resistance: N/A
Output Resistance: N/A

Calibration Factor: 5.0007V
Operator(s): John Knore
Calibration Date: 12/14/2011

Calibration Procedure: 072-FP75-23, Rev A, Date 09/23/2010

% Capacity	Load (psia)	Raw (V)	Normalized (V)
0	0.00	0.0245	0.0000
50	1500.00	2.5246	2.5001
100	3000.00	5.0248	5.0003
50	1500.00	2.5269	2.5024
0	0.00	0.0248	0.0003

Shunt Calibration Data

Line No.	Shunt Resistor	Shunt Sense	Zero	Shunt Zero	Shunt Cal	Shunt Cal. Capacity
1	INTΩ	N/A	N/A	N/A	4.0038 V	N/A

Calibration Standards

NIST Traceable #	Inst. ID#	Description	Model	Cal Date	Date Due
3452110	100161	DEADWEIGHT TESTER H2O	TM-TQ-150	08/20/2009	08/20/2012
4132773	7241230	DECADE RESISTOR	0-10M OHMS	05/07/2010	05/07/2012
5305693	200088	DIGITAL MULTIMETER	34401A	07/14/2011	07/14/2012

Environmental Data

Temperature: 72 °F
Humidity: 21 %RH
Pressure: 14.44 psiA

Certificate No
1364591-001

PRINT DATE: 12/14/2011

Document No. 086-1000-09

Low Pressure transducers calibration tables

Table A1a. Calibration of existing pressure transducers.

Pressure Transducer SN 141143 (750 Psi abs)			
Calibrator (Psi abs)	Transducer Response (Volts)	Transducer Response (Psi abs)	Estimated Error (%)
Tests #1			
0	0.0976	-0.02	NA
400.00	2.7640	399.94	0.015
350.00	2.4300	349.84	0.046
300.00	2.0960	299.74	0.087
250.00	1.7630	249.79	0.084
200.00	1.4299	199.825	0.088
150.00	1.0967	149.845	0.103
100.00	0.7634	99.85	0.150
50.00	0.4305	49.915	0.170
0.00	0.0972	-0.08	NA
Tests #2			
0.00	0.0984	0.42	NA
50.00	0.43	50.325	0.650
100.00	0.7621	99.975	-0.025

150.00	1.0958	150.03	0.020
200.00	1.4278	199.83	-0.085
250.00	1.7617	249.915	-0.034
300.00	2.0940	299.76	-0.080
350.00	2.4270	349.71	-0.083
400.00	2.7600	399.66	-0.085
350.00	2.4260	349.56	-0.126
300.00	2.0930	299.61	-0.130
250.00	1.7605	249.735	-0.106
200.00	1.4272	199.74	-0.130
150.00	1.0937	149.715	-0.190
100.00	0.7606	99.75	-0.250
50.00	0.4275	49.785	-0.430
0.00	0.0946	-0.15	NA

Table A1b. Calibration of existing pressure transducers.

Pressure Transducer SN 270097 (750 Psi abs)			
Calibrator (Psi abs)	Transducer Response (Volts)	Transducer Response (Psi abs)	Estimated Error (%)
Tests #1			
0	0.0976	-0.02	NA
400.00	2.7670	400.39	-0.097
350.00	2.4340	350.44	-0.126
300.00	2.1000	300.34	-0.113
250.00	1.7655	250.165	-0.066
200.00	1.4315	200.065	-0.032
150.00	1.0978	150.01	-0.007
100.00	0.7643	99.985	0.015
50.00	0.4309	49.975	0.050
0.00	0.0978	0.01	NA
Tests #2			
0.00	0.0986	0.13	NA
50.00	0.43	50.14	0.280
100.00	0.7654	100.15	0.150

150.00	1.0987	150.145	0.097
200.00	1.4323	200.185	0.093
250.00	1.7661	250.255	0.102
300.00	2.0990	300.19	0.063
350.00	2.4320	350.14	0.040
400.00	2.7670	400.39	0.097
350.00	2.4330	350.29	0.083
300.00	2.0990	300.19	0.063
250.00	1.7654	250.15	0.060
200.00	1.4317	200.095	0.047
150.00	1.0981	150.055	0.037
100.00	0.7645	100.015	0.015
50.00	0.4312	50.02	0.040
0.00	0.0980	0.04	NA

APPENDIX 3 – Control valve calibrations

Table A2a. Calibration data of control valve CV-1

Generated Loop Current with Circuit of Fig. B1 (*mA*)	Valve Opening (%)	Air Pressure in Valve Actuator (*Psig*)
4.000	0.0	0.1
5.605	10.4	9.2
7.212	20.5	9.7
8.803	30.4	10.0
10.403	40.4	10.9
12.044	50.6	11.4
13.620	60.4	11.9
15.206	70.3	12.5
16.791	80.1	13.1
18.404	90.1	13.9
20.02	99.9	20.2
4.002	0.0	0.1

APPENDIX 4 – Data acquisition and control program

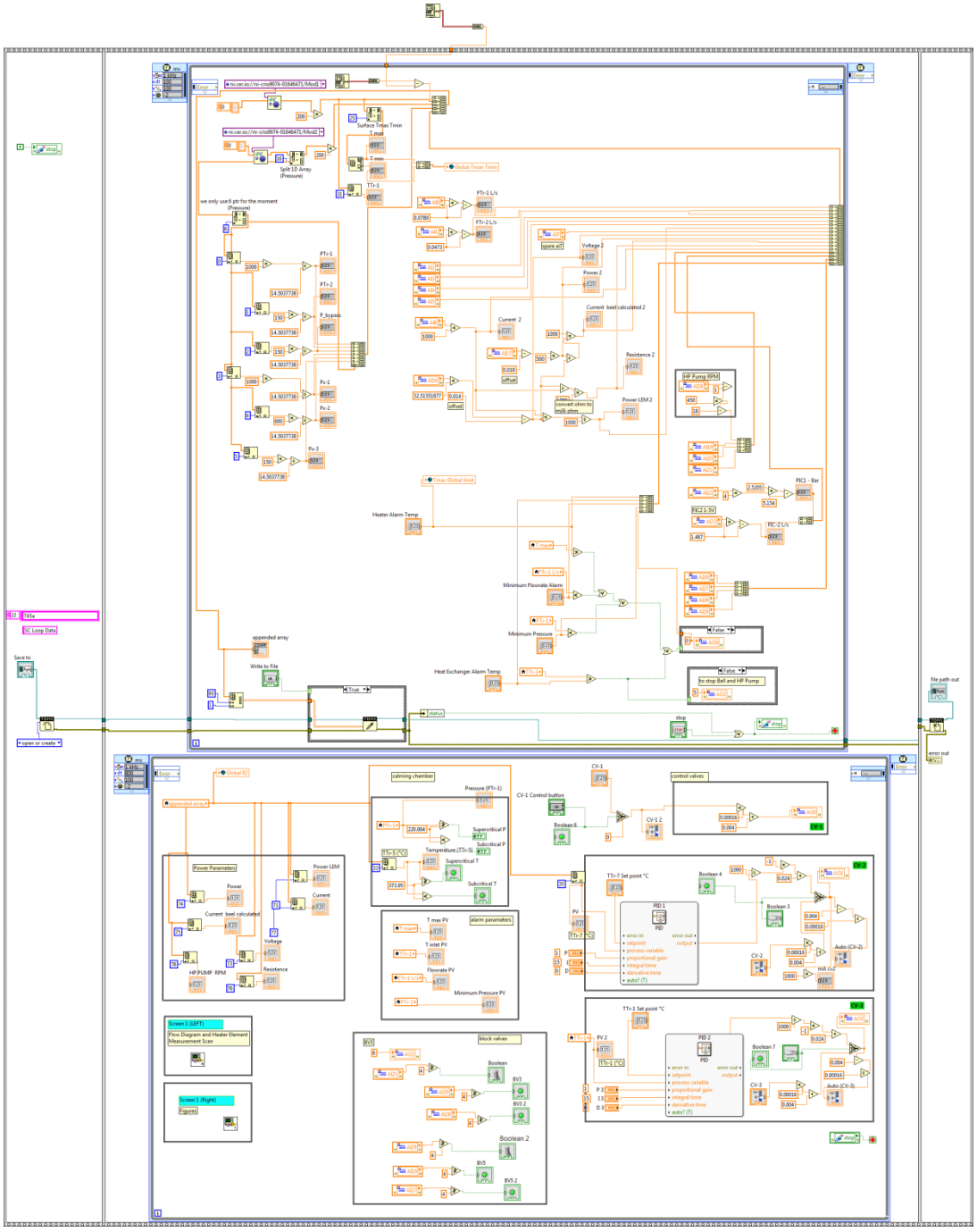

Figure 6.1 Data acquisition and control-1.

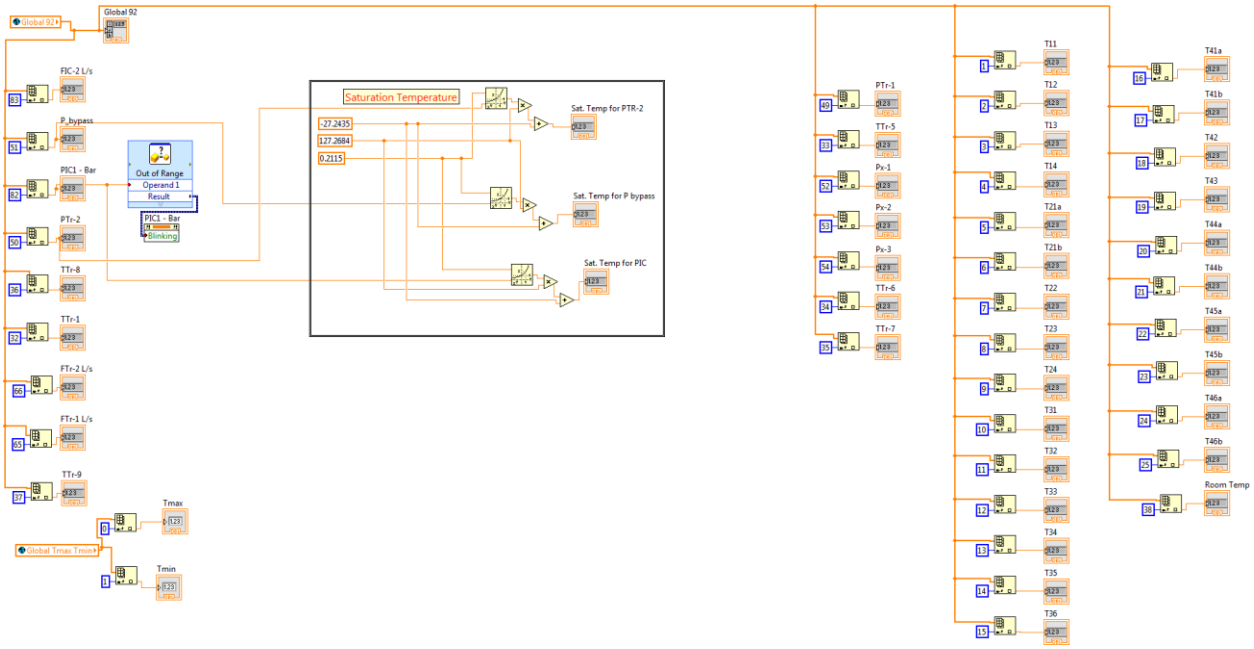

Figure 6.2 Data acquisition and control-2.

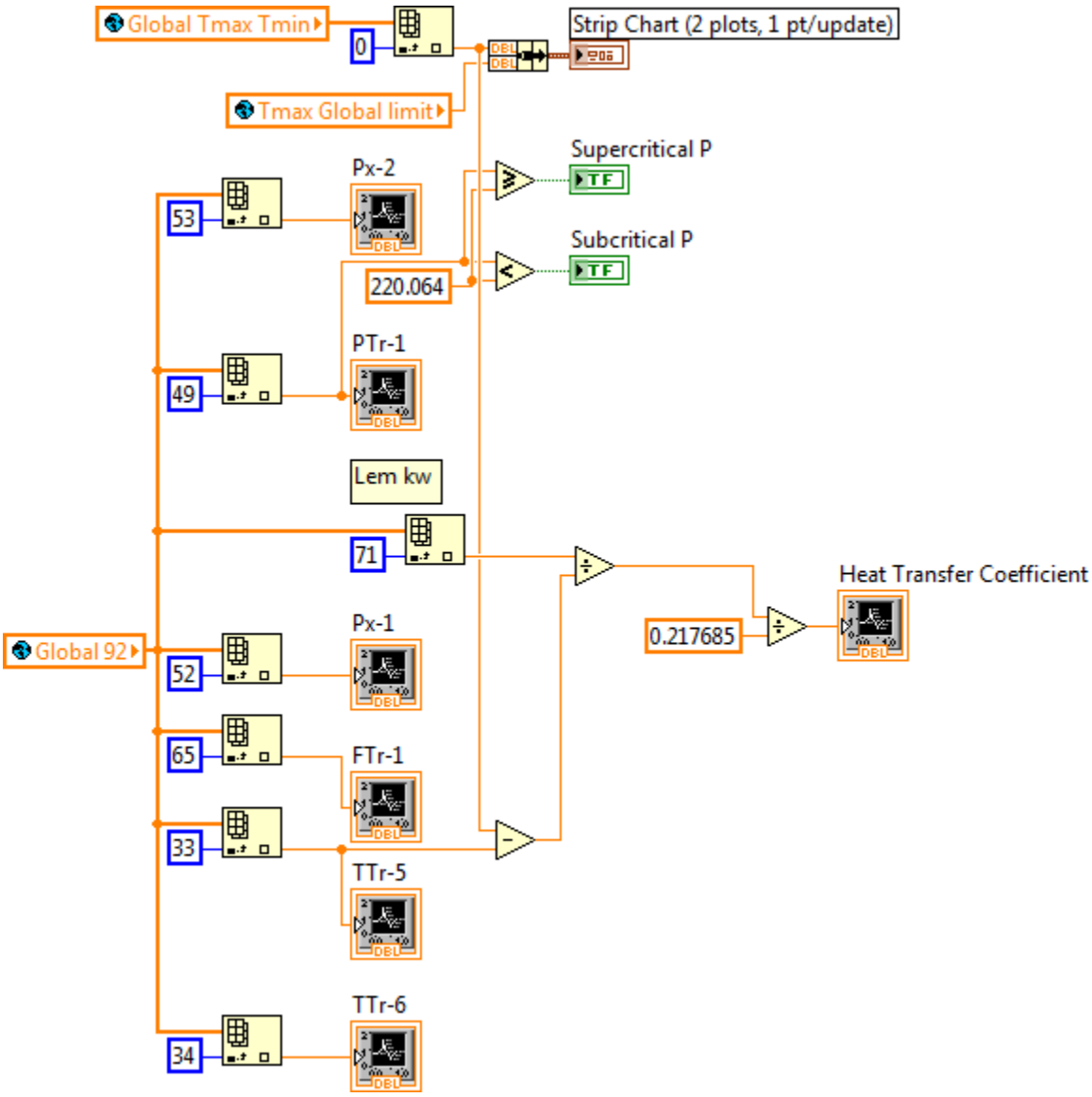

Figure 6.3 Data acquisition and control-3.

APPENDIX 5 – Drawings of the test section

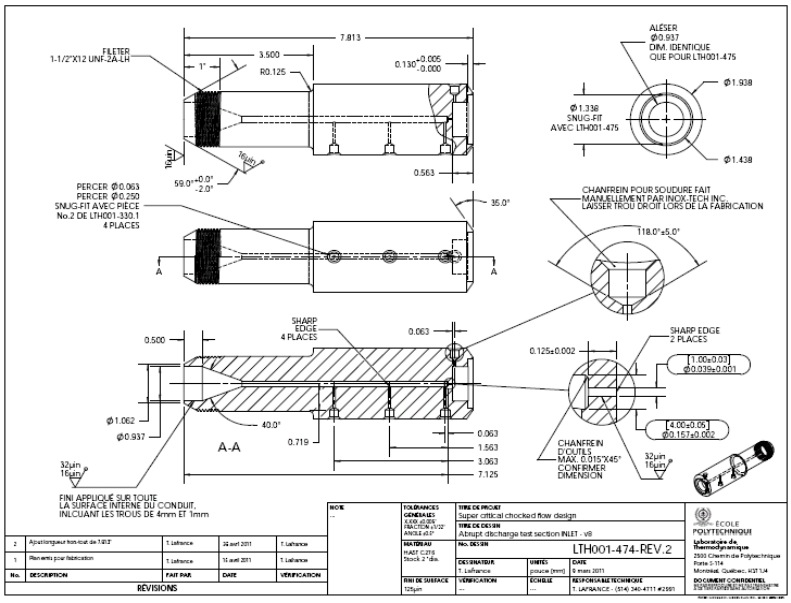

Figure A4a - Test section - inlet portion.

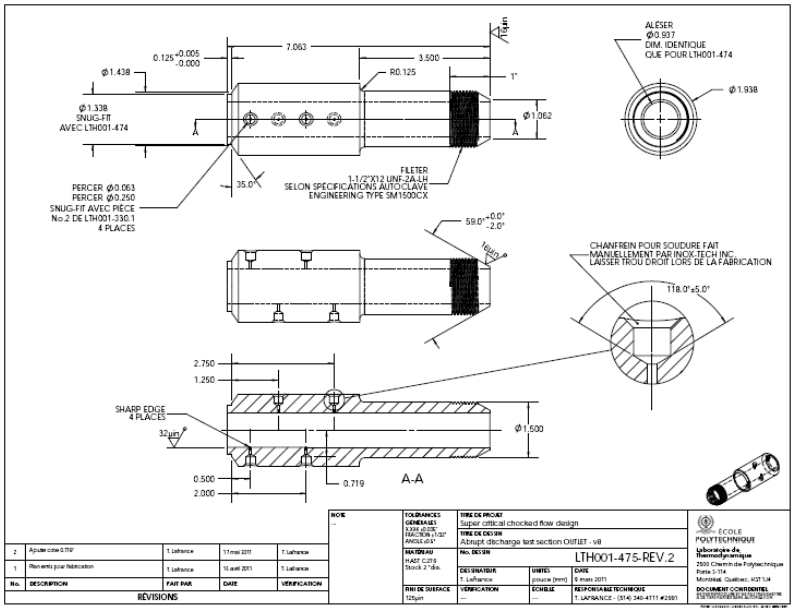

Figure A4b - Test section - outlet portion.

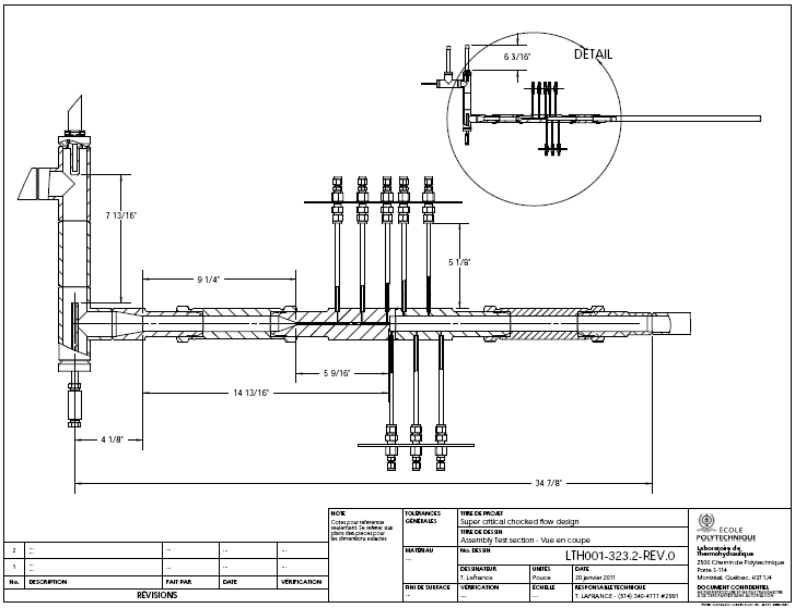

Figure A4c - Test section assembly with pressure lines and calming chamber.

APPENDIX 6 – Loop operation checklist

Item Number	Supercritical Water Loop Checklist	Check Box
1	NOTIFY 4946 OF POWER USAGE IF NECESSARY	
	Instrumentation and control preparation	
2	DAS computer ON	
3	Observation cameras' computer ON	
4	Observation cameras' power supply ON	
5	DAS and HP pump 600V safety switch ON	
6	Thermocouple panel switch ON	
7	Instrumentation panel ON	
8	DAS panel ON	
9	Placard on laboratory entrance door INSTALL	
10	Flashing beacon on laboratory entrance door ON	
11	Laboratory entrance door LOCK	
12	Pit padlock REMOVE	
13	De-Icer OPERATING (winter only)	
14	Check gas ventilation fan (must be ON) (in control room)	
15	Emergency Stop Button PULL OUT	
16	Vanne de delastage CLOSED	
17	Beel flowrate alarm switch ON	
18	Flow rate selector CV-2b	
19	HP pump Start Enable switch DOWN	
20	Steam drum pressurizer buttons PULL OUT	
21	Choke valve potentiometer FULLY CLOCKWISE (open position)	
22	Beel power potentiometer FULLY COUNTERCLOCKWISE (0kW)	
23	BV3 switch CLOSE	
24	BV5 switch CLOSE	
25	Parameter lock switch DOWN	
26	Power cord plugged properly VERIFY	
27	Master switch ON	
28	Panel controllers switches (6) ON	
29	S2 valve position ON (condenser mode)	
30	Steam drum thermometer Min-Max RESET	
31	Steam drum water level 15-36 INCHES (see filling the steam drum if necessary)	
32	Pressure transducer PURGE (see Purging the pressure transducer)	
33	HP Pump needle valve CLOSE	
34	Main cooling water valve FULLY OPEN	
35	Air conditioning SET AT 68°F	

36	Main Pumps (2) cooling valves 50-100% OPEN	
37	Heat exchangers cooling water valve OPEN	
38	a)Small valve Fully OPEN	
39	b)Big valve PARTIALLY OPEN	
40	Steam drum 600V safety switch ON	
41	Steam drum Control switch ON	
42	Steam drum circuit #1 AUTO	
43	Steam drum circuit #2 AUTO	
44	Main pumps 600V safety switch ON	
45	Main pumps selector BOTH	
46	Large pre-heater 600V safety switch ON	
47	Large pre-heater control switch ON	
48	Small pre-heater 600V safety switch ON	
49	Small Pre-heater control switch ON	
50	Compressed air valves (2) ON	
51	Steam drum nitrogen filling valve CLOSE	
52	Dampener pressure VERIFY	
53	Manual bypass valve 50% OPEN	
54	Main valve FULLY OPEN (VERTICAL LINE)	
55	HP pump's drive Ethernet connections CHECK	
56	LABVIEW control and data acquisition system program RUN	
57	GEOVISION observation camera program RUN	
58	LEM 120V switch ON	
59	LEM, LPF fans, Heater elements fans (15) running VERIFY	
60	LPF controller ready VERIFY	
61	Bypass pressure VERIFY	
62	PTr-2 Pressure VERIFY	
	LOOP OPERATION	
63	BV3 OPEN/VERIFY	
64	Globe valve at the upstream of the heat exchangers OPEN	
65	Main circulation pump valve OPEN 14-15%(FOR 0.4lt/s FLOW)	
66	Pressure and Sub-cooling Controllers ADJUST	
67	Large preheater PURGE	
68	HP pump drive padlock REMOVE	
69	Beel 600v safety switch padlock REMOVE	
70	Main loop pressure and cavitation risk VERIFY	
71	Main Pumps ON	
72	FIC-2 flowrate VERIFY	
73	HP pump drive unit switch ON	
74	HP pump Start Enable switch UP	
75	HP pump motor speed SET 400 RPM	

76	HP pump START	
77	LABVIEW motor RPM and drive controller RPM match CHECK	
78	FTr-1 flowrate VERIFY	
79	Heating Protection Circuit START	
80	Steam drum RESET	
81	Steam drum heating elements BOTH ON	
82	Pre-heaters (2) ADJUST AND START	
83	Main pumps subcooling (T1-T2) ADJUST TO APPROX 30°C	
84	Medium pressure loop pressure ADJUST	
85	Subcooling temperature ADJUST DEPENDING ON THE STEAM DRUM TEMP	
86	HP Loop pressure INCREASE GRADUALLY	
87	HP loop pressure WAIT UNTIL DESIRED VALUE IS REACHED	
88	Beel rectifier fans ON	
89	Beel power potentiometer set at 0kW VERIFY	
90	Beel 600V safety switch ON	
91	Beel Limitrol RESET	
92	Beel NI-alarm circuit RESET	
93	Beel ON	
94	Beel power ADJUST AS NEEDED	
95	PTr-1 CHECK WHILE INCREASING POWER	
96	Check TTr-5, if desired value is reached, START LOGGING DATA AS NEEDED	
	STOPING THE LOOP	
97	Beel power ADJUST TO 0kW	
98	Beel OFF	
99	Steam drum's heater Elements BOTH OFF	
100	Pre-heaters (2) OFF	
101	Heating protection circuit STOP	
102	HP pump drive unit OFF	
103	HP pump Start Enable switch DOWN	
104	Main pumps STOP	
105	BV3 CLOSE	
106	LEM 120V switch OFF	
107	Beel 600V safety switch OFF	
108	Beel rectifier fans OFF	
109	Observation camera power supply OFF	
110	GEOVISION observation camera program QUIT	
111	Main pumps 600v safety switch OFF	
112	Large pre-heater 600V safety switch OFF	
113	Small pre-heater 600V safety switch OFF	
114	Steam drum 600V safety switch OFF	

115	Beel 600V safety switch LOCK	
116	HP pump drive switch LOCK	
117	Pit LOCK	
118	Flashing beacon light on laboratory entrance door OFF	
119	Placard on laboratory entrance door REMOVE	
120	Heat exchanger valve CLOSE PARTIALLY	
121	Turn off main cooling valve little bit and wait until the T2 gets less than 100°C, then close it completely	

Next day

122	Heat exchanger valve CLOSE FULLY	
123	Air conditioning OFF	
124	Loop nitrogen pressure ADJUST 1.5-1.6 BAR	

Purging the pressure transducer	
Take distillated water from the water drum to purge (see Purging Procedure)	
Be sure that all the desired pressure line valves are open	

Filling the steam drum	
Manual valves between the steam drum and the pump (2) OPEN	
Filling pump 600V safety switch ON	
Filling pump ON	
Steam drum level WAIT UNTIL DESIRED VALUE IS REACHED	
Filling pump OFF	
Manual valves between the steam drum and the pump (2) PROMPTLY CLOSE	
Filling pump 600V safety switch OFF	

MODERATE EMERGENCY PROCEDURE
Heating power protection circuit STOP
HP pump STOP
HP pump Start Enable switch DOWN
Main pumps OFF IF NECESSARY

WAIT IN THE CONTROL ROOM UNTIL LOOP PRESSURE DROP TO A SAFE VALUE

MAJOR EMERGENCY PROCEDURE
Emergency Stop Button PRESS
Main pumps OFF IF NECESSARY
Beel 600v safety switch OFF
WAIT IN THE CONTROL ROOM UNTIL LOOP PRESSURE DROP TO A SAFE VALUE
AVOID CUTTING THE CONTROL PANEL POWER
NOTIFY SECURITY OF MASSIVE STEAM RELEASE (4444)